Geochronology and Petrogenesis of Hadean to Paleoarchean Mafic and Felsic Crust from the Northeastern Superior Province, Canada

Christian Sole

Thesis submitted to the University of Ottawa
in partial fulfillment of the requirements for the
M.Sc. degree in Earth Sciences

Department of Earth and Environmental Sciences
Faculty of Science
University of Ottawa

Abstract

The first billion years of our planet's history is almost devoid of geological records and this scarcity of Eoarchean/Hadean rocks and minerals greatly limits our understanding of how and when the first crust formed on Earth. The Nuvvuagittuq Greenstone Belt (NGB), located in the Hudson Bay terrane of the Northeastern Superior Province, may host the oldest preserved rocks on Earth. It is locally intruded in its southwestern corner by rare 3.76 Ga trondhjemite bands which impose a minimum age for the NGB, but its dominant lithology, a mafic cummingtonite-amphibolite called the Ujaraaluk unit, displays isotopic evidence suggesting it may represent a rare remnant of Hadean mafic crust as old as 4.3 Ga. However, this proposed Hadean age for the NGB has been heavily debated for more than a decade. As potentially the only remnant of crust formed within the first 500 million years of Earth's history, the NGB could have important implications on our knowledge of the first terrestrial crust. In order to impose tighter geochronological constraints on the NGB, here we present U-Pb zircon and ^{147}Sm-^{143}Nd whole rock data for gneissic gabbro sills that intrude the Ujaraaluk unit as well as U-Pb data for zircons from intruding and surrounding granitoids. A new strategy of sampling for the gneissic gabbros targeted the most evolved plagioclase-rich zones and amphibole-rich cumulative rocks to better constrain their age of magmatic differentiation. The most evolved parts of the sills were also sampled because they are the most likely to contain igneous zircon or baddeleyite that could constrain their crystallization age. Zircons from two compositionally evolved gneissic gabbros yielded U-Pb ages between 2.7 and 2.6 Ga consistent with the timing of Neoarchean metamorphism in the region. A plagioclase-rich layer found within the gabbro sills yielded zircons defining a U-Pb Concordia upper intercept age of 2789 Ma, but their texture and Th/U ratios are more consistent with recrystallization of zircon subsequent to the breakdown of an older Zr-bearing phase and therefore do not constrain the age of emplacement of

the sills. However, a ^{147}Sm-^{143}Nd isochron for the gneissic gabbros, including the newly identified plagioclase-rich evolved zone and hornblende-rich cumulative rock, yielded an isochron age of 4151 ± 290 (MSWD = 9, n = 6) interpreted as the timing of magmatic differentiation of the sills. This 4.1 Ga age thus strongly supports the previously proposed Hadean age for the NGB. New zircon U-Pb data reported here for plutonic trondhjemites found in the central and eastern parts surrounding the NGB suggests that the extent of the ~3.8 Ga Eoarchean felsic magmatism is greater than previously thought. New zircon trace element and oxygen isotope data for a series of granitoids surrounding and locally intruding the NGB previously dated at 3.76 Ga, 3.66 Ga, 3.51 Ga and 3.35 Ga provide a better understanding of the petrogenetic processes responsible for early felsic crust production. Zircons from the 3.76 Ga, 3.66 Ga and 3.35 Ga granitoids are characterized by rare earth element trends typical of unaltered igneous zircons. However, zircons from the 3.51 Ga magmatic event display unusual rare earth element patterns, with a striking positive Eu-anomaly, suggesting that they may have experienced some type of post-magmatic alteration. Zircon $\delta^{18}O$ values appear to have slightly increased over time with the zircons from the oldest 3.76 Ga trondhjemites displaying mean $\delta^{18}O$ values within the mantle zircon field and the younger Paleoarchean granitoids progressively deviating from the mantle zircon field to reach a mean zircon $\delta^{18}O$ value of 6.58‰ at 3.35 Ga. This suggests that the 3.76 Ga trondhjemites were derived from an unaltered crustal source, whereas the ≤3.66 Ga granitoids were derived from a supracrustal source that had experienced some degree of low-temperature hydrothermal alteration. This trend of mantle-like zircon $\delta^{18}O$ values preserved in the first evolved crust, which deviate towards higher zircon $\delta^{18}O$ values in successive felsic magmatic events, has also been observed in other Hadean and Eoarchean terranes indicating that similar processes may have operated on a global scale during the production and evolution of early continental crust.

Résumé

Le premier milliard d'années d'histoire de notre planète est presque dépourvu d'enregistrements géologiques et la rareté de roches et minéraux éoarchéens/hadéens limite grandement notre compréhension de quand et comment la première croûte terrestre s'est formée. La ceinture de roches vertes de Nuvvuagittuq (NGB), située dans le terrane de la baie d'Hudson de la Province de Nord-est du Supérieur, présente potentiellement les plus anciennes roches préservées sur Terre. Des minces intrusions trondhjémitiques datées à 3.76 Ga et trouvées dans la partie sud-ouest de la ceinture impose un âge minimum pour la NGB, mais sa lithologie dominante, une amphibolite mafique à cummingtonite appelée l'unité Ujaraaluk, présente des compositions isotopiques qui suggèrent qu'elle pourrait représenter un morceau de croûte mafique hadéenne aussi vieille que 4.3 Ga. Cependant, cet âge hadéen proposé pour la NGB a été fortement débattu pendant plus d'une décennie. En tant que le seul vestige de croûte potentiellement formé au cours des 500 premiers millions d'années de l'histoire de la Terre, la NGB pourrait avoir des implications importantes sur nos connaissances au sujet de la première croûte terrestre. Afin d'imposer des contraintes géochronologiques plus strictes sur la NGB, nous présentons ici des données U-Pb sur des zircons et des données ^{147}Sm-^{143}Nd de roches totales sur des sills de gabbro gneissiques qui sont en intrusion dans l'unité Ujaraaluk, ainsi que des données U-Pb sur des zircons provenant de granitoïdes intrusifs et environnants. Une nouvelle stratégie d'échantillonnage pour les gabbros gneissiques a ciblé les zones les plus évoluées riches en plagioclase et les roches cumulatives riches en amphiboles pour mieux contraindre leur âge de différenciation magmatique. Les parties les plus évoluées des sills ont également été échantillonnées car elles sont les plus susceptibles de contenir des zircons ou baddeleyites ignés qui pourraient contraindre l'âge de cristallisation des sills. Les zircons de deux gabbros gneissiques ayant une composition chimique plus évoluée ont donné des

âges U-Pb entre 2.7 et 2.6 Ga, ce qui correspond avec l'âge du métamorphisme régional néoarchéen. Des zircons provenant d'une couche riche en plagioclase trouvée dans les sills a donné un âge pour l'intercepte supérieur Concordia U-Pb de 2789 Ma. Par contre, leurs textures et leurs rapports Th/U sont plus cohérents avec la recristallisation du zircon suite à la dissolution d'une phase plus ancienne contenant du Zr et donc ne contraint pas l'âge de mise en place des sills. Cependant, une isochrone ^{147}Sm-^{143}Nd pour les gabbros gneissiques, comprenant la zone évoluée riche en plagioclase et la roche cumulative riche en hornblende, a donné un âge de 4151 ± 290 (MSWD = 9, n = 6) interprété comme le moment de différenciation magmatique des sills. Cet âge de 4.1 Ga appuie donc fortement l'âge hadéen proposé précédemment pour la NGB. Les nouvelles données U-Pb rapportées ici pour les zircons des trondhjémites plutoniques entourant la NGB au centre et à l'est suggèrent que l'épisode magmatique felsique éoarchéen de ~3.8 Ga est plus important qu'on ne le pensait auparavant. De nouvelles données d'éléments traces et d'isotopes d'oxygène des zircons provenant d'une série de granitoïdes entourant et localement en intrusions dans la NGB datées à 3.76 Ga, 3.66 Ga, 3.51 Ga et 3.35 Ga permettent de mieux comprendre les processus pétrogénétiques responsables de la production de croûte felsique précoce. Les zircons des granitoïdes âgés de 3.76 Ga, 3.66 Ga et 3.35 Ga sont caractérisés par des profils d'éléments des terres rares typiques des zircons ignés non-altérés. Cependant, les zircons de l'événement magmatique à 3.51 Ga présentent des profils d'éléments des terres rares inhabituels, avec une anomalie positive en Eu notable, ce qui suggère qu'ils pourraient avoir subi un certain type d'altération post-magmatique. Les valeurs en $\delta^{18}O$ des zircons semblent avoir légèrement augmenté avec le temps. Les zircons des trondhjémites les plus anciennes à 3.76 Ga montrent des valeurs moyennes de $\delta^{18}O$ dans le champ de zircon du manteau et les granitoïdes paléoarchéens plus jeunes s'écartent progressivement du champ de zircon du manteau pour atteindre une valeur

moyenne en $\delta^{18}O$ de 6.58‰ à 3.35 Ga. Cela suggère que les trondhjémites à 3.76 Ga proviennent d'une source crustale non-altérée, alors que les granitoïdes ≤3.66 Ga proviennent d'une source supracrustale qui a subi un certain degré d'altération hydrothermale à basse température. Cette tendance où les zircons préservés dans la première croûte évoluée passent de valeurs en $\delta^{18}O$ correspondant au champ de zircon du manteau, pour ensuite s'écarter vers des valeurs plus élevées en $\delta^{18}O$ lors d'événements magmatiques felsiques successifs, a également été observée dans d'autres terranes hadéennes et éoarchéennes indiquant que des processus similaires auraient pu opérer à l'échelle globale lors de la production et de l'évolution de la croûte continentale précoce.

Acknowledgements

I would first like to thank my supervisor, Dr. Jonathan O'Neil, for all of his support and guidance over the years. You have helped develop my passion for research ever since you took me as a student during my third year of undergraduate studies. Since then, I have been extremely fortunate to perform field work, lab work and present my research nationally and internationally under your supervision. I am eternally grateful for all of these opportunities, for everything you have taught me, and for our many years of playing volleyball together. Double Spike will forever be known as Garnet B champions.

I would also like to thank Dr. Hanika Rizo for all of her support. From start to finish, you have been an integral part of this project and I am forever thankful for your constant guidance and encouragement over the years.

A special thank you goes out to the Pituvik Landholding Corporation of Inukjuak for all of their logistical work enabling us to conduct field work for this project. Field work was funded in part thanks to the Northern Scientific Training Program. Additional funding was provided by an Ontario Graduate Scholarship.

Thank you to all of the laboratory personnel that helped make this project a reality. To Alain Mauviel (uOttawa), for his help making thin sections and preparing sample mounts. To Lilianne Pagé (uOttawa), for her assistance conducting major element geochemical analyses and for providing detailed explanations of the analytical procedure. To Samuel Morfin (uOttawa), for his assistance with REE LA-ICP-MS analyses and for providing detailed explanations of the analytical procedure. To Richard Stern and Robert Dokken (uAlberta), for their help preparing sample mounts and conducting zircon oxygen isotope SIMS analyses. To Rolando Lastra (NRCan), for his assistance in the use of the selFrag. To Shuangquan Zhang (Carleton U), for his assistance during TIMS analyses. To Joshua Davies (UQAM), for his help with the Wilfley water table and for providing scientific feedback. To Jean-Louis Paquette (LMV), for his assistance in LA-ICP-MS U-Pb data collection, preparing sample mounts and for providing scientific feedback. To Glenn Poirier (uOttawa), for his help with the SEM.

I would also like to thank past and present graduate students in the Ottawa-Carleton Early Earth Research group: Dan Stepner, Benjamin Wasilewski, Janick Flageole, Ayesha Landon-Browne, Alexandre Rouleau, Andréane Dupuis-Mitchell, Victor Garcia, Sarah Mount and Daniel

Peters. Thank you for your assistance in the lab, for providing me with scientific feedback and for some well-deserved social time.

To all of the undergraduate and graduate students, professors and faculty staff that I have had the chance to interact with over the past seven years here at the University of Ottawa, thank you for making my BSc and MSc degrees such an unforgettable experience.

Finally, I cannot thank my family and friends enough for all their love and support. I am constantly reminded of how extremely lucky I am to be surrounded with what is most important in life. This journey would not have been possible without you.

Table of Contents

List of Figures

List of Tables

Chapter 1

Introduction

The Hadean (4568 to 4000 Ma) and the Eoarchean (4000 to 3600 Ma) are the two earliest periods of the geological time scale. However, only few Hadean to Eoarchean terranes are preserved worldwide leaving the first one billion years of Earth's history almost devoid of geological records. Hadean detrital zircons up to ~4.4 Ga (Wilde et al., 2001), known as the Jack Hills zircons, have been widely used to study the early Earth but their host rock has been destroyed, limiting the information they provide about the early crust. Pre-3.6 Ga rocks are preserved in rare terranes including the 3.66 Ga Ancient Gneiss Complex, Swaziland (Compston and Kröner, 1988; Kröner, 2007), the 3.73 Ga Narryer terrane, Australia (Nutman et al., 1991; Wilde and Spaggiari, 2007), the 3.85 Ga Napier Complex, Antarctica (Black et al., 1986; Kusiak et al., 2013), the 3.85 Ga Itsaq Gneiss Complex, Greenland (Baadsgaard et al., 1984; Nutman et al., 1996; Nutman and Friend, 2009), the 3.87 Ga Saglek-Hebron Complex, Canada (Vezinet et al., 2018; Wasilewski et al., *submitted*), the 3.89 Ga Anshan area, China (Song et al., 1996; Wu et al., 2008), the 4.03 Ga Acasta Gneiss Complex, Canada (Bowring and Williams, 1999; Reimink et al., 2016) and the 3.76 to 4.28 Ga Nuvvuagittuq Greenstone Belt, Canada (Cates and Mojzsis, 2007; O'Neil et al., 2008, 2012). Because of the paucity of the earliest rock records, the geological processes that operated shortly after the Earth's formation are still relatively poorly constrained. Many major questions such as when did plate tectonics start, when did life start, when and how did the first crust form and many more are still heavily debated to this day. Tighter age constraints and a better comprehension of the petrogenetic processes that formed these scarce Hadean and Eoarchean terranes may hold the clues needed to answer some of these unresolved questions.

Located in northern Quebec, Canada, the Nuvvuagittuq Greenstone Belt (NGB) is mostly comprised of mafic-ultramafic lithologies that are surrounded and locally intruded by multiple generations of granitoids. The NGB is at least 3.76 Ga as defined by U-Pb zircon ages in thin

trondhjemitic bands that have been found intruding the southwestern part of the belt (e.g. Augland and David, 2015; Cates and Mojzsis, 2007; Darling et al., 2013; O'Neil et al., 2013; Simard et al., 2003). However, some isotopic evidence suggests that the dominant lithology in the NGB, a heterogeneous cummingtonite-amphibolite termed the "Ujaraaluk unit", could be as old as 4.3 Ga which would make it the oldest rock preserved on Earth (O'Neil et al., 2008, 2012). The interpretation of the Ujaraaluk unit's isotopic composition remains highly debated though and the proposed Hadean age for the Nuvvuagittuq Greenstone Belt has been questioned (e.g. Augland and David, 2015; Caro et al., 2017; Cates et al., 2013; Guitreau et al., 2013; Roth et al., 2013). Nevertheless, the NGB and surrounding rocks are the oldest from the Superior Craton and represent a unique window into the formation and evolution of the primitive crust. As potentially the oldest rocks on Earth, better constraints on the exact age of the NGB have major implications on important geological questions regarding Earth's earliest crust.

In Chapter 2, we focus on improving the geochronological constraints on the Nuvvuagittuq Greenstone Belt. New U-Pb zircon and ^{147}Sm-^{143}Nd whole rock isotope analyses are presented for fine-grained gneissic gabbro sills that intrude the Ujaraaluk unit. The intrusive nature of these gabbro sills is used to establish a minimum age for the Ujaraaluk unit and the NGB. In Chapter 3, we present new U-Pb data on zircons from felsic rocks in the NGB area as well as new zircon rare earth element (REE) and oxygen isotope analyses for the multiple generations of granitoids surrounding the NGB. These analyses build on previous zircon U-Pb and Hf isotope data published by O'Neil et al. (2013) to give a more detailed insight on the petrogenetic processes responsible for the formation of these granitoids.

References

Augland, L. E., & David, J. (2015). Protocrustal evolution of the Nuvvuagittuq Supracrustal Belt as determined by high precision zircon Lu-Hf and U-Pb isotope data. Earth and Planetary Science Letters, 428, 162–171.

Baadsgaard, H., Nutman, A. P., Bridgwater, D., Rosing, M., McGregor, V. R., & Allaart, J. H. (1984). The zircon geochronology of the Akilia association and Isua supracrustal belt, West Greenland. Earth and Planetary Science Letters, 68(2), 221–228.

Black, L. P., Sheraton, J. W., & James, P. R. (1986). Late Archaean granites of the Napier Complex, Enderby Land, Antarctica: a comparison of Rb-Sr, Sm-Nd and U-Pb isotopic systematics in a complex terrain. Precambrian Research, 32, 343–368.

Bowring, S. A., & Williams, I. S. (1999). Priscoan (4.00-4.03 Ga) orthogneisses from northwestern Canada. Contributions to Mineralogy and Petrology, 134(1), 3–16.

Caro, G., Morino, P., Mojzsis, S. J., Cates, N. L., & Bleeker, W. (2017). Sluggish Hadean geodynamics: Evidence from coupled ^{146,147}Sm–^{142,143}Nd systematics in Eoarchean supracrustal rocks of the Inukjuak domain (Québec). Earth and Planetary Science Letters, 457, 23–37.

Cates, N. L., & Mojzsis, S. J. (2007). Pre-3750 Ma supracrustal rocks from the Nuvvuagittuq supracrustal belt, northern Québec. Earth and Planetary Science Letters, 255(1–2), 9–21.

Cates, N. L., Ziegler, K., Schmitt, A. K., & Mojzsis, S. J. (2013). Reduced, reused and recycled: Detrital zircons define a maximum age for the Eoarchean (ca. 3750-3780Ma) Nuvvuagittuq Supracrustal Belt, Québec (Canada). Earth and Planetary Science Letters, 362, 283–293.

Compston, W., & Kröner, A. (1988). Multiple zircon growth within early Archaean tonalitic gneiss from the Ancient Gneiss Complex, Swaziland. Earth and Planetary Science Letters, 87(1–2), 13–28.

Darling, J. R., Moser, D. E., Heaman, L. M., Davis, W. J., O'Neil, J., & Carlson, R. (2013). Eoarchean to neoarchean evolution of the Nuvvuagittuq Supracrustal belt: New insights from U-Pb zircon geochronology. American Journal of Science, 313(9), 844–876.

Guitreau, M., Blichert-Toft, J., Mojzsis, S. J., Roth, A. S. G., & Bourdon, B. (2013). A legacy of Hadean silicate differentiation inferred from Hf isotopes in Eoarchean rocks of the Nuvvuagittuq supracrustal belt (Québec, Canada). Earth and Planetary Science Letters, 362, 171–181.

Kröner, A. (2007). The Ancient Gneiss Complex of Swaziland and Environs: Record of Early Archean Crustal Evolution in Southern Africa. In M. J. van Kranendonk, R. H. Smithies, & V. C. Bennett (Eds.), Earth's Oldest Rocks, Developments in Precambrian Geology, 15, Amsterdam: Elsevier, pp. 465–480.

Kusiak, M. A., Whitehouse, M. J., Wilde, S. A., Dunkley, D. J., Menneken, M., Nemchin, A. A., & Clark, C. (2013). Changes in zircon chemistry during archean UHT metamorphism in the Napier Complex, Antarctica. American Journal of Science, 313(9), 933–967.

Nutman, A. P., Friend, C. R. L., & Paxton, S. (2009). Detrital zircon sedimentary provenance ages for the Eoarchaean Isua supracrustal belt southern West Greenland: Juxtaposition of an imbricated ca. 3700 Ma juvenile arc against an older complex with 3920-3760 Ma components. Precambrian Research, 172(3–4), 212–233.

Nutman, A. P., Kinny, P. D., Compston, W., & Williams, I. S. (1991). SHRIMP U-Pb zircon geochronology of the Narryer Gneiss Complex, Western Australia. Precambrian Research, 52, 275–300.

Nutman, A. P., McGregor, V. R., Friend, C. R. L., Bennett, V. C., & Kinny, P. D. (1996). The Itsaq Gneiss Complex of southern West Greenland; the world's most extensive record of early crustal evolution (3900-3600 Ma). Precambrian Research, 78(1-3 Special Issue), 1–39.

O'Neil, J., Boyet, M., Carlson, R. W., & Paquette, J. L. (2013). Half a billion years of reworking of Hadean mafic crust to produce the Nuvvuagittuq Eoarchean felsic crust. Earth and Planetary Science Letters, 379, 13–25.

O'Neil, J., Carlson, R. W., Francis, D., & Stevenson, R. K. (2008). Neodymium-142 evidence for hadean mafic crust. Science, 321(5897), 1828–1831.

O'Neil, J., Carlson, R. W., Paquette, J. L., & Francis, D. (2012). Formation age and metamorphic history of the Nuvvuagittuq Greenstone Belt. Precambrian Research, 220–221, 23–44.

Reimink, J. R., Chacko, T., Stern, R. A., & Heaman, L. M. (2016). The birth of a cratonic nucleus: Lithogeochemical evolution of the 4.02-2.94 Ga Acasta Gneiss Complex. Precambrian Research, 281, 453–472.

Roth, A. S. G., Bourdon, B., Mojzsis, S. J., Touboul, M., Sprung, P., Guitreau, M., & Blichert-Toft, J. (2013). Inherited ^{142}Nd anomalies in Eoarchean protoliths. Earth and Planetary Science Letters, 361, 50–57.

Simard, M., Parent, M., David, J., & Sharma, K. N. M. (2003). Géologie de la région de la rivière Innuksuac (34K et 34L). Ministère des Ressources naturelles, Québec; RG 2002-10, 46 pages.

Song, B., Nutman, A. P., Liu, D., & Wu, J. (1996). 3800 to 2500 Ma crustal evolution in the Anshan area of Liaoning Province, northeastern China. Precambrian Research, 78(1–3), 79–94.

Vezinet, A., Pearson, D. G., Thomassot, E., Stern, R. A., Sarkar, C., Luo, Y., & Fisher, C. M. (2018). Hydrothermally-altered mafic crust as source for early Earth TTG: Pb/Hf/O isotope and trace element evidence in zircon from TTG of the Eoarchean Saglek Block, N. Labrador. Earth and Planetary Science Letters, 503, 95–107.

Wasilewski, B., O'Neil, J., Rizo, H., & Paquette, J.-L. (Submitted). Petrogeochemistry, geochronology and crustal evolution of the Saglek-Hebron Complex (Northern Labrador).

Wilde, S. A., & Spaggiari, C. (2007). The Narryer Terrane, Western Australia: A Review. In M. J. van Kranendonk, R. H. Smithies, & V. C. Bennett (Eds.), Earth's Oldest Rocks, Developments in Precambrian Geology, 15, Amsterdam: Elsevier, pp. 275–304.

Wilde, S. A., Valley, J. W., Peck, W. H., & Graham, C. M. (2001). Evidence from detrital zircons for the existence of continental crust and oceans on the Earth 4.4 Gyr ago. Nature, 409(6817), 175–178.

Wu, F. Y., Zhang, Y. Bin, Yang, J. H., Xie, L. W., & Yang, Y. H. (2008). Zircon U-Pb and Hf isotopic constraints on the Early Archean crustal evolution in Anshan of the North China Craton. Precambrian Research, 167(3–4), 339–362.

Chapter 2

New time constraints on mafic intrusions from the Nuvvuagittuq Greenstone Belt, Canada: Evidence for the oldest rocks on Earth

2.1 Introduction

Our ability to study how and when the first crust formed is heavily impaired by the lack of early geological records. Rare Hadean detrital zircons have been found in the Jack Hills conglomerate of the Yilgarn Craton in western Australia (Wilde et al., 2001), a sandstone in the Barberton Greenstone Belt of the Kaapvaal Craton in southern Africa (Byerly et al., 2018), and few individual xenocrysts from the Sao Francisco Craton in Brazil (Paquette et al., 2015), as well as the Cathaysia Block (Xing et al., 2014) and the North Qinling orogenic belt of China (Wang et al., 2007). However, the host rocks of these zircons have been eroded away. Beside the 4.03 Ga tonalitic gneiss found within the Acasta Gneiss Complex in Canada (Bowring and Williams, 1999; Reimink et al., 2016), preserved terrestrial rocks of undisputed age appear to be non-existent in the Hadean. Therefore, many questions still remain regarding the composition and the petrogenesis of the Earth's primordial crust. Moreover, studies on the early crust often focus on the evolved felsic rocks, which constitute most Archean terranes. This is also in part due to the fact that felsic rocks commonly host zircons that can often provide robust and precise geochronological constraints. However, granitoids are mostly formed through second stage melting of a mafic precursor rather than direct melting from the mantle and likely do not represent primordial crust. Mafic and ultramafic rocks can however be challenging to date because they usually do not contain zircons and the complex thermal history that characterizes most Archean cratons commonly disturbs long-lived isotopic systems applied at the whole rock scale leading to less precise and often equivocal ages. Nevertheless, since the first crust that formed on Earth was likely mafic in nature (e.g. Carlson et al., 2019), efforts to better constrain the age of the oldest mafic/ultramafic rocks can provide important insight into the formation of the Earth's primitive crust.

Over the last decade, the Nuvvuagittuq Greenstone Belt (NGB), located in northern Quebec, Canada, has been the object of scientific debate regarding its age (see O'Neil et al., 2019 for review) as it could represent a unique remnant of Hadean mafic crust. The NGB hosts a variety of mafic-ultramafic lithologies but is dominated by a heterogeneous mafic cummingtonite-amphibolite termed the "Ujaraaluk unit". Small intrusive trondhjemitic bands set a minimum age of 3.76 Ga for the NGB, but ^{142}Nd isotopic evidence suggests that the Ujaraaluk unit is as old as 4.3 Ga (O'Neil et al., 2008, 2012, 2019). This age has been challenged (e.g. Augland and David, 2015; Caro et al., 2017; Cates et al., 2013; Guitreau et al., 2013; Roth et al., 2013), but if correct, these would be the oldest rocks preserved on Earth and represent a potential remnant of Earth's primordial mafic crust. Determining the exact age of the NGB is therefore crucial. The petrology and geochemistry of the NGB rocks have been used to constrain the tectonic settings operating at the time of their formation (Turner et al., 2014; O'Neil et al., 2016, 2019). Micro structures and filaments preserved in banded iron formations have also been used by Dodd et al. (2017) as evidence for early life recorded in the NGB. Whether the NGB rocks are Eoarchean or Hadean in age thus has important implications for our understanding of some of the first geological processes to have operated shortly after Earth's formation 4.568 billion years ago (Bouvier and Wadhwa, 2010).

Efforts to obtain U-Pb ages on zircon in the Ujaraaluk unit have yielded Neoarchean ages consistent with regional metamorphism (Darling et al., 2013) and long-lived isotopic systems such as ^{147}Sm-^{143}Nd and ^{176}Lu-^{176}Hf have shown evidence of post-magmatic disturbance in the Ujaraaluk unit (O'Neil et al., 2012, 2013). The Ujaraaluk unit is however intruded by large differentiated gabbro sills whose geochemical and isotopic compositions appear to be less affected by post-magmatic processes (O'Neil et al., 2011, 2012). Previous geochemical studies have shown

that these large mafic intrusions are chemically differentiated (O'Neil et al., 2012) and careful sampling of the most evolved (perhaps zircon/baddeleyite-bearing) and pyroxene-rich cumulative portions of these sills can offer a unique opportunity to further constrain the age of the NGB.

In this chapter, we present new U-Pb and ^{147}Sm-^{143}Nd data for a series of samples from these gabbro sills that were specifically targeted to date the timing of their magmatic differentiation. We then use initial Nd isotopic compositions to discuss about potential sources for the mafic lithologies found in the NGB.

2.2 Geological Setting

2.2.1 Geology of the Nuvvuagittuq Greenstone Belt

The Nuvvuagittuq Greenstone Belt is located in the Tikkerutuk Domain of the Northeastern Superior Province (NESP) along the eastern shoreline of the Hudson Bay in northern Quebec, Canada (Figure 2.1). Early work suggested that the NESP was mostly comprised of granulite-grade granitoids (Card and Ciesielski, 1986; Percival et al., 1992; Stevenson, 1968). However, detailed regional mapping has shown that the NESP is mostly comprised of Neoarchean plutonic suites in which thin remnants of amphibolite- to granulite-grade greenstone belts can be traced along strike (Leclair, 2005; Percival and Card, 1994; Percival et al., 1995, 1996, 1997). The NESP was originally separated into multiple lithotectonic domains based on different lithological assemblages displaying large linear positive and negative aeromagnetic anomalies (Percival et al., 1992). Since then, further mapping and isotopic work has shown that the NESP can be divided into two isotopically distinct terranes: the Arnaud River terrane to the east and the Hudson Bay terrane to the west (Boily et al., 2009) (Figure 2.1). The Arnaud River terrane is characterized by granitoids younger than 2.88 Ga with juvenile Nd isotopic compositions yielding depleted mantle

model ages (T_{DM}) <3.0 Ga. In contrast, the Hudson Bay terrane is composed of Neoarchean granitoids that intrude remnants of a reworked Meso- to Eoarchean craton. These Meso- to Eoarchean tonalite-trondhjemite-granodiorite (TTG) and greenstone belt remnants are defined by T_{DM} ages as old as 4.4 Ga and inherited zircon core ages older than 3.0 Ga (Boily et al., 2009; O'Neil et al., 2012). The Hudson Bay terrane is thus considered as representing the cratonic nucleus of the NESP onto which the more juvenile Arnaud River terrane was juxtaposed (Percival and Skulski, 2000; Percival et al., 2012).

The NGB, located 30 km south of Inukjuak, Quebec, comprises the oldest rocks from the Hudson Bay terrane. It is a ~10 km^2 volcano-sedimentary sequence dominated by mafic and ultramafic rocks with subordinate chemical sedimentary rocks (Figure 2.1). The NGB is surrounded by multiple generations of Eoarchean to Mesoarchean TTG dated at ~3760 Ma, ~3660 Ma, ~3510 Ma, ~3350 Ma and ~2990 Ma (Cates and Mojzsis, 2009; David et al., 2009; Macquistan, 2020; O'Neil et al., 2013). Rare trondhjemite bands intruding the southwestern corner of the belt yield U-Pb zircon ages of ~3760 Ma (Augland and David, 2015; Cates and Mojzsis, 2007; Darling et al., 2013; David et al., 2009; O'Neil et al., 2013; Simard et al., 2003) and a Neoarchean pegmatite also intrudes the NGB (David et al., 2009).

The NGB has undergone multiple phases of deformation producing a tight isoclinal south-closing synform refolded into a large-scale north-closing synform (Nadeau, 2003; O'Neil et al., 2007; Simard et al., 2003). The NGB also experienced at least two metamorphic events (Cates and Mojzsis, 2009): a ~3.6 Ga event coeval with the emplacement age of 3.6 Ga bordering tonalites and a ~2.7 Ga event as evidenced by Sm-Nd ages of garnet growth in the Ujaraaluk unit (O'Neil et al., 2012), U-Pb metamorphic overgrowth ages in zircons from the trondhjemite band (Cates and Mojzsis, 2009; David et al., 2009) as well as U-Pb ages of metamorphic zircons found in both

the Ujaraaluk unit (Darling et al., 2013) and gneissic gabbro sills (Darling et al., 2013; David et al., 2009; O'Neil et al., 2012). This Neoarchean peak-metamorphic event reached temperatures of ~650°C corresponding to upper amphibolite facies metamorphism (Cates and Mojzsis, 2009).

The predominant lithology found across the NGB was described as a lithological unit called the Ujaraaluk unit. These heterogeneous gneissic mafic rocks consist of varying proportions of cummingtonite + biotite + quartz + plagioclase ± garnet ± anthophyllite ± cordierite. In the southwest corner of the NGB, massive aphanitic greenstones composed of chlorite + epidote + actinolite + plagioclase ± quartz exhibit the same geochemical characteristics as the Ujaraaluk unit and are thus thought to be a lower metamorphic grade equivalent of the same lithology (O'Neil et al., 2007, 2011). The Ujaraaluk unit has been interpreted as representing a package of hydrothermally altered mafic pyroclastic rocks that were deposited in a submarine volcanic environment (O'Neil et al., 2011). The Ujaraaluk rocks have been subdivided into three distinct geochemical groups mainly based on different Al/Ti ratios and trace element compositions (O'Neil et al., 2011). The high-Ti Ujaraaluk rocks are geochemically similar to tholeiitic basalts, whereas the low-Ti Ujaraaluk rocks, further subdivided into depleted low-Ti and enriched low-Ti groups, share compositional affinities with boninitic and calc-alkaline mafic rocks. The three compositionally distinct Ujaraaluk groups also follow a chemostratigraphy in the NGB with the high-Ti tholeiitic rocks interpreted to be at the base of the sequence and the depleted low-Ti boninitic and enriched low-Ti calc-alkaline rocks representing the top of the sequence (O'Neil et al., 2011). This stratigraphy is quite similar to the one observed in modern subduction zones and thus the Ujaraaluk unit may have been formed through episodic subduction initiation environments (Turner et al., 2014; O'Neil et al. 2016).

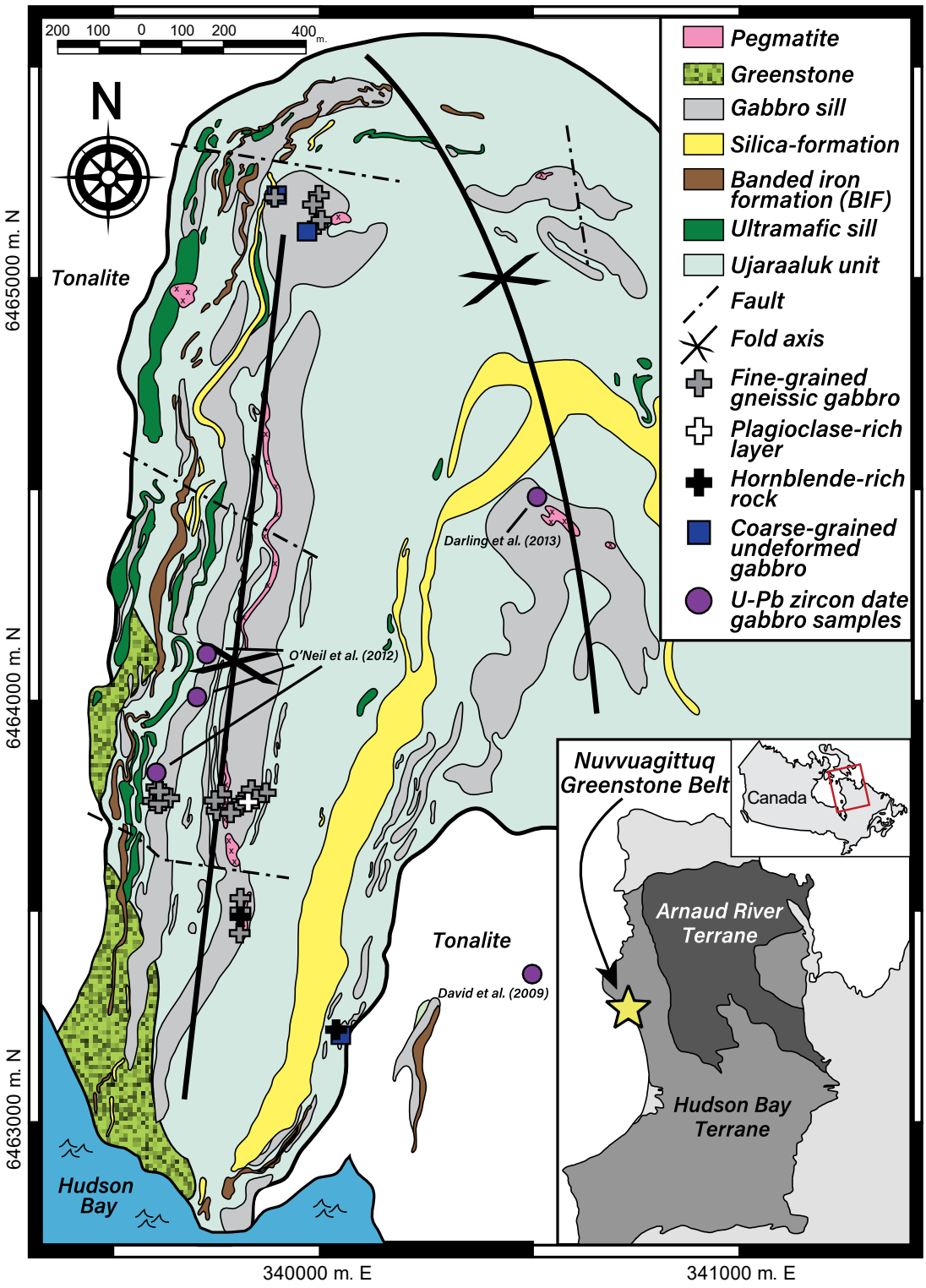

Figure 2.1: Regional map of the Northeastern Superior Province and geological map of the Nuvvuagittuq Greenstone Belt modified from O'Neil et al. (2012). Coordinates are in UTM zone 18, NAD27. Gabbro samples collected in this study are represented by the grey, white and black plusses and blue squares. Locations of gabbro samples with previously reported U-Pb dates discussed in Section 2.5.1.1 (Darling et al., 2013; David et al., 2009; O'Neil et al., 2012) are represented by the purple circles.

Within the Ujaraaluk unit lie ultramafic bodies that can be observed as discontinuous "boudins" for up to a few hundreds of meters following stratigraphy (Figure 2.1). These serpentinized metaperidotites are also divided into similar geochemical groups as the Ujaraaluk unit and follow the same chemostratigraphy, which has led to the interpretation that they represent ultramafic cumulates cogenetic to the mafic Ujaraaluk rocks (O'Neil et al., 2007, 2011, 2012, 2019).

The Ujaraaluk unit is intruded by fine-grained hornblende-plagioclase metagabbroic sills displaying a prominent gneissic texture. They mainly occur as two 40–100 m wide sills that can be continuously traced for up to 2 km along the NGB (Figure 2.1). These gabbro sills generally have a similar mafic composition to the Ujaraaluk rocks but with higher Ca contents, which is reflected in their mineralogy as their dominant amphibole is hornblende rather than cummingtonite. They display rare earth element (REE) profiles that vary from relatively flat to slightly light rare earth element (LREE)-enriched and are thus interpreted to be differentiated sills (O'Neil et al., 2012). A ^{147}Sm-^{143}Nd isochron on these fine-grained gneissic gabbro sills yielded an age of 4115 ± 100 Ma (MSWD = 4.8; n = 13) (O'Neil et al., 2012).

The NGB is also intruded by undeformed metagabbros with a coarse-grained texture. These undeformed gabbroic intrusions are compositionally similar to the gneissic gabbroic sills but mostly display relatively flat REE profiles. Based on the textural difference with the gneissic gabbro sills, the coarse-grained gabbros have been interpreted to represent a younger series of mafic intrusions (O'Neil et al., 2012; 2019). David et al. (2009) obtained an age of 2693 ± 3 Ma on zircons from one of the coarse-grained gabbros, but they interpreted these as metamorphic zircons based on their radial-sector zoning textures. An internal Sm-Nd isochron on mineral separates yielded a similar age of 2719 ± 100 Ma (O'Neil et al., 2012) and whole rock ^{147}Sm-^{143}Nd

and ^{176}Lu-^{176}Hf isochrons on a suite of coarse-grained gabbro samples gave ages of 2867 ± 210 Ma (Benn, 2018) and a 2741 ± 100 Ma (Plakholm, 2019) respectively, consistent with a younger Neoarchean emplacement age.

2.2.2 Age of the Nuvvuagittuq Greenstone Belt

There is a consensus in the scientific community that the belt is at least Eoarchean in age, but some isotopic evidence suggests it could have been formed in the Hadean. A short overview of the different arguments for an Eoarchean age and a Hadean age for the NGB is presented here, but a complete review can be found in O'Neil et al. (2019).

As the NGB dominantly comprises mafic to ultramafic rocks, most zircon U-Pb geochronological constraints come from scarce trondhjemitic bands intruding the southwest corner of the belt. Zircons from these trondhjemitic bands have been dated in many studies (Augland and David, 2015; Cates and Mojzsis, 2007; Darling et al., 2013; David et al., 2009; O'Neil et al., 2013; Simard et al., 2003), yielding an average age of ~3.77 Ga. The intrusive nature of these trondhjemitic bands thus imposes a minimum Eoarchean age on the NGB. However, the discovery of variations in ^{142}Nd/^{144}Nd ratios in rocks from the Ujaraaluk unit was used as evidence for an older Hadean age for the belt (O'Neil et al., 2008, 2012). Deviations in μ^{142}Nd,

$$\text{where } \left(\mu^{142}Nd = \frac{^{142}Nd/^{144}Nd_{sample} - ^{142}Nd/^{144}Nd_{terrestrial\ standard}}{^{142}Nd/^{144}Nd_{terrestrial\ standard}} \times 10^{6} \right),$$

can only be produced by Sm-Nd fractionation in the first 500 million years of Earth's history given the half-life of 103 million years of the parent isotope ^{146}Sm (Marks et al., 2014). The large variation in μ^{142}Nd values and the positive correlation between the μ^{142}Nd values and the Sm/Nd

ratios found in a suite of differentiated rocks from the Ujaraaluk unit was interpreted by O'Neil et al., (2008, 2012, 2019) as representing an isochron yielding a crystallization age of 4313^{+23}_{-27} Ma, which would make the Nuvvuagittuq rocks the oldest on Earth. This Hadean age is further supported by the 4.1 Ga ^{147}Sm-^{143}Nd isochron age obtained from the gneissic gabbro sills that intrude the Ujaraaluk unit, thus imposing a minimum age on the latter (O'Neil et al., 2012).

Nevertheless, the proposed Hadean age for the NGB is highly debated. The correlation between μ^{142}Nd anomalies and Sm/Nd ratios present in the Ujaraaluk unit has also been interpreted as a result of mixing between an Eoarchean superchondritic mantle-derived melt and an ancient LREE-enriched mantle component formed ca.4500 Ma (Roth et al., 2013). However, others have shown that the Sm-Nd isotopic compositions for both the long-lived and short-lived systems are not consistent with such mixing scenario (O'Neil et al., 2019). Some authors also argued that the long-lived ^{147}Sm-^{143}Nd and ^{176}Lu-^{176}Hf isotopic systems support an Eoarchean age for the Ujaraaluk unit (Guitreau et al., 2013; Roth et al., 2013), although is has been demonstrated that these long-lived isotope systems in the Ujaraaluk unit may have been disturbed at the whole rock scale by post-magmatic processes and are thus not representative of their igneous crystallization age (O'Neil et al., 2012, 2013).

Cates et al. (2013) suggested a maximum age of ~3780 Ma for the NGB based on the oldest zircons retrieved from a fuchsitic quartzite found within the Ujaraaluk unit that they interpreted as detrital in origin. According to this geological interpretation, this would provide a maximum age for the NGB mafic volcanic sequence. However, Darling et al. (2013) noted that the zircon ages and chemical compositions in this fuchsitic quartzite were comparable to those found in the trondhjemite bands and therefore concluded that the fuchsitic rocks are highly metasomatized

felsic intrusive rocks rather than detrital in nature. They suggest that the fuchsitic quartz-rich rocks only place a minimum emplacement age on the NGB.

The precise age of the NGB may remain equivocal until a Hadean zircon is found. It is well accepted that the ^{142}Nd anomalies found in the Ujaraaluk unit implies that the genesis of the NGB required a Hadean component (Caro et al., 2017; O'Neil et al., 2008, 2012; Roth et al., 2013). However, as potentially the oldest rocks preserved on our planet, further work must be done to better constrain the exact age of the NGB.

2.3 Methods

2.3.1 Whole rock major and trace elements

A total of 30 mafic samples were collected from the Nuvvuagittuq Greenstone Belt during the summer of 2017. This includes 27 samples from the gneissic gabbro sills (24 homogeneous fine-grained gabbros, one plagioclase-rich layer and two hornblende-rich samples) and three samples from the coarse-grained undeformed gabbro intrusions. An additional two fine-grained gabbros were sampled from the neighbouring Ukaliq Supracrustal Belt (USB) located a few kilometers northeast of the NGB. These gabbroic samples display the same mineralogical composition and fabric as the gneissic gabbro sills from the NGB. The full list of samples with GPS coordinates can be found in Table A.1. Polished thin sections were made for all 32 samples in order to make detailed petrographic descriptions. All samples were cut free of weathered surfaces and secondary veins before being crushed using a steel jaw crusher and further grinded in a ceramic pulveriser to produce a fine powder for geochemical analyses.

Major element concentrations for all 32 mafic samples were analyzed by X-ray Fluorescence (XRF) on a Rigaku Supermini200 WDXRF spectrometer at the X-ray Core Facility

Laboratories at the University of Ottawa. Powdered samples were fused using a flux made in-house (79/21 $Li_2B_4O_7/LiBO_2$) and combined with 80 mg of LiBr non-wetting agent to produce glass disks (sample/flux ratio of ~1:7). Standards used for mafic calibration curves were: UB-N, UM-2, MRG-1, PM-s, BCR-2, WS-E, SY-3, BHVO-2, BM, AN-G, BCR-032 and PC-1016. Standards SY-3, MRG-1 and BCR-032 were used for drift correction and BHVO-2 was used as a mafic check to validate results. Accuracy and precision were determined by multiple measurements of the MRG-1 standard. Accuracies were <5% for SiO_2, Al_2O_3, Fe_2O_3, MnO, MgO, CaO, TiO_2; 10% for Na_2O, K_2O and >20% for P_2O_5. Precisions were <5% for SiO_2, Al_2O_3, Fe_2O_3, MgO, CaO, TiO_2 and between 5–10% for MnO, Na_2O, K_2O and P_2O_5.

All samples were analyzed for trace element concentrations on an Agilent 8800 QQQ Triple-Quadrupole inductively coupled plasma mass spectrometer (ICP-MS) at the Geochemistry Core Facility Laboratories at the University of Ottawa. Approximately 100 mg of powdered sample was dissolved in closed Savillex beakers using a 1:5 HNO_3-HF mixture and placed on a hot plate at 125°C for four days. Savillex beakers were then opened and left on a hot plate until complete evaporation. Samples were re-dissolved in closed beakers with 6M HCl and placed on a hot plate at 125°C for two days. Two drops of boric acid were added to each beaker before evaporation to help dissolve any fluorides that may have formed during the initial HF dissolution. After evaporation, each sample was re-dissolved in 5 ml of 7M HNO_3 and left on a hot plate overnight in preparation for dilution. Once completely dissolved, an additional 35 ml of 7M HNO_3 was added to each solution. For each sample, an aliquot of 1 ml of this main solution was taken to which 11 ml of 0.01M HNO_3 with traces of HF was added. Each solution was doped with 2 ppb In to monitor for possible instrumental drift during the analyses. Dissolved samples ready for analysis on the ICP-MS resulted in solution 0.65 M HNO_3 and corresponded to dilution factors of

~4000. Rock standards BHVO-2, BCR-2 and BIR-1a were dissolved and prepared following the same protocol and analysed multiple times to determine accuracies and precisions. The BHVO-2 standard was used as an internal standard whereas BCR-2 and BIR-1a were considered as unknowns to validate the results. Accuracies were better than 5% for the REE, Sc, V, Co, Ni, Cu, Zn, Ga, Rb, Sr, Y, Zr, Nb, Cs, Ba, Hf; between 5–10% for Cr, Ta, Pb, Th, U and >15% for Ge. Precisions were obtained from repeated measurements of the BHVO-2 standard and were between 1–10% on the REE, Sc, V, Cr, Co, Ni, Cu, Zn, Ga, Rb, Sr, Y, Zr, Nb, Cs, Ba, Hf, Ta, Pb, U and between 10–20% for Ge and Th.

2.3.2 Whole rock Sm-Nd isotope analyses

A total of eight samples were analyzed for whole rock ^{147}Sm-^{143}Nd isotope analyses. Six gneissic gabbro samples from the NGB were selected including four fine-grained homogeneous gabbros, the plagioclase-rich layer and one hornblende-rich sample. Two fine-grained gabbros collected in the Ukaliq belt were also analyzed. Sample preparation for isotopic analyses was performed in the Advanced Research Complex clean laboratory of the Department of Earth and Environmental Sciences at the University of Ottawa. Between 25 and 80 mg of powdered sample was dissolved for each sample. A spike enriched in ^{150}Nd and ^{149}Sm was added to the samples prior to dissolution in order to measure the Sm and Nd concentrations by isotope dilution. Sample and spike weights are presented in Table 2.1. The dissolution procedure was the same as the one described in Section 2.3.1 for the whole-rock trace element analyses.

After the digestion, samples were dissolved in 2 ml of 2M HCl and centrifuged before being loaded onto primary columns filled with 200–400 mesh AG50W-X8 cation exchange resin for LREE extraction. Sm and Nd were then separated from the LREE fractions using columns

filled with 300 mg of Eichrom Ln-Spec resin 50–100 µm. The complete primary and Ln-Spec column protocols can be found in Table A.2.

Table 2.1: Sample and spike weights for whole rock ^{147}Sm-^{143}Nd isotope analyses. Abbreviations: Plag = Plagioclase, Hbl = Hornblende.

Sample	Lithology	Location	Sample Weight (g)	Spike Weight (g)	Spike Number
PC-612	Gneissic gabbro	Nuvvuagittuq	0.02539	0.06397	DTM 16-1-116
PC-613	Gneissic gabbro	Nuvvuagittuq	0.07780	0.06330	DTM 16-1-116
PC-618	Plag-rich layer	Nuvvuagittuq	0.05402	0.06103	DTM 16-1-116
PC-628	Gneissic gabbro	Nuvvuagittuq	0.08004	0.06980	DTM 16-1-116
PC-630	Gneissic gabbro	Nuvvuagittuq	0.07866	0.06797	DTM 16-1-116
PC-635	Hbl-rich rock	Nuvvuagittuq	0.05105	0.06609	DTM 16-1-116
UK-001	Gneissic gabbro	Ukaliq	0.02625	0.04826	DTM 16-1-116
UK-003	Gneissic gabbro	Ukaliq	0.05412	0.06751	DTM 16-1-116

Sm and Nd isotopic compositions were measured using double rhenium (Re) filaments on a Thermo-Fisher Triton thermal ionisation mass spectrometer (TIMS) at the Isotope Geochemistry and Geochronology Research Centre (IGGRC) at Carleton University in Ottawa. Sm and Nd fractions were dissolved in 1 µl of 2.5M HCl and loaded onto outgassed Re filaments. For Nd analyses, data was measured statically on a double filament assembly, using seven Faraday cups. ^{143}Nd, ^{144}Nd, ^{145}Nd, ^{146}Nd, ^{148}Nd and ^{150}Nd were monitored as well as ^{147}Sm for correction of isobaric interferences. Nd analyses consisted of 140 ratios at 8 second integration time. Instrumental mass bias fractionation was corrected using an exponential law and a $^{146}Nd/^{144}Nd = 0.7219$. Repeated measurements of the JNdi-1 standard yielded an average $^{143}Nd/^{144}Nd$ ratio of 0.512103 ± 0.000005 (n = 5). Although this value overlaps within error with the accepted value of Tanaka et al. (2000) of 0.512115 ± 0.000007, all $^{143}Nd/^{144}Nd$ results were normalized to the JNdi-1 value of 0.512115. Sm analyses consisted of 100 ratios at 8 second integration time. ^{147}Sm, ^{148}Sm, ^{149}Sm, ^{150}Sm, ^{152}Sm and ^{154}Sm were monitored along with ^{146}Nd and ^{155}Gd for correction

of isobaric interferences. Sm isotopic ratios were corrected for mass fractionation to $^{147}Sm/^{152}Sm = 0.56081$. Errors on Sm/Nd ratios determined by isotopic dilution are 0.5%.

^{147}Sm-^{143}Nd isochrons were generated using the Isoplot/Ex v.4.15 software package (Ludwig, 2012). $\varepsilon^{143}Nd$ values were calculated using the CHUR values of $^{143}Nd/^{144}Nd = 0.512630$ and $^{147}Sm/^{144}Nd = 0.1960$ (Bouvier et al., 2008).

2.3.3 Zircon U-Pb geochronology

Three samples from the NGB gneissic gabbros, including two samples that appeared compositionally more evolved (PC-601 and PC-602) and the plagioclase-rich layer found within the gabbro sills (PC-618), were selected and processed in order to separate potential baddeleyites or zircons. PC-618 was disaggregated using a selFrag at CanmetMINING Natural Resources Canada in Ottawa. Small blocks of the sample were repeatedly broken up using 150 high voltage discharges (200 kV) at a frequency of 3 Hz in a vessel with a working electrode gap of 40 mm. PC-601 and PC-602 were crushed using more conventional methods such as a steel jaw crusher followed by a disk pulveriser. All three samples were sieved to separate the fraction below 250 μm and then ran through a Wilfley water table with a 5–7° inclination in order to isolate the heavy mineral separates. The heavy mineral fraction of sample PC-618 was further separated though heavy liquid and Frantz magnetic separation. Seventy-five zircons were recovered for PC-618 and between 100–120 zircons were picked for PC-601 and PC-602 in order to minimize the chance of missing a zircon population representing 5% of the total population (Vermeesch, 2004).

Zircons were mounted on an epoxy resin and then polished to expose grain centers prior to U-Th-Pb isotope analyses on a Thermo Scientific Element XR ICP-MS coupled with a Resonetics M50E 193 nm excimer laser ablation (LA) system at the Laboratoire Magmas et Volcans (LMV)

in Clermont-Ferrand, France. A laser spot size of 20 µm at a repetition rate of 3 Hz and a fluency of 2.5 J/cm^2 was used for all three samples. Single analyses consisted of 30 s of background measurement with the laser off, 60 s of zircon ablation and a 30 s delay to wash out the previous sample in preparation for the next analysis. The full analytical protocol for isotope dating with LA-ICP-MS is described in detail in Hurai et al. (2010), Paquette et al. (2014) and Mullen et al. (2018) and additional information on the instrument settings for this session is available in Table A.3. U-Pb fractionation during laser sampling and instrumental mass discrimination was corrected by standard bracketing of repeated measurements of the GJ-1 zircon (Jackson et al., 2004) (Figure A.1). The 91500 zircon reference material (Wiedenbeck et al., 1995) was also measured repeatedly and treated as an unknown to independently control the reproducibility and accuracy of the corrections (Figure A.2). Data reduction was performed using the GLITTER® software package from Macquarie Research Ltd (van Achterbergh et al., 2001). Data was not corrected for common Pb, but ^{204}Pb was monitored to discard any analyses that contained common Pb. Analyses that were >20% discordant were discarded from the age calculation.

Weighted mean ^{206}Pb/^{207}Pb ages and Concordia diagrams were generated using the Isoplot/Ex v.2.49 software package (Ludwig, 2001). Following LA-ICP-MS analyses, all three mounts were carbon coated before cathodoluminescence (CL) imaging at the Microanalysis Laboratory at the University of Ottawa. A JEOL 6610LV scanning electron microscope (SEM) equipped with a Gatan MINI-CL and backscattered electron (BSE) detectors was used to ensure no important internal zoning was missed during laser ablation work.

2.4 Results

2.4.1 Field observations and petrography

Two texturally different gabbro intrusions were found in the Nuvvuagittuq Greenstone Belt: a finer-grained gabbro displaying a pronounced gneissic fabric (Figure 2.2A) and a coarser-grained undeformed gabbro (Figure 2.2B). The gneissic gabbros are present as kilometer-scale continuous sills intruding the older Ujaraaluk unit whereas the coarse-grained undeformed gabbros are found locally intruding the gneissic gabbros (Figure 2.2C) as well as the other supracrustal lithologies in the NGB such as the Ujaraaluk unit and the chemical sedimentary rocks. The strong fabric of these fine-grained gabbros is often defined by thin, alternating sub-centimeter-scale plagioclase-rich bands and hornblende-rich bands (Figure 2.2A). However, these large sills also display meter-scale plagioclase-rich layers (Figure 2.2D) and hornblende-rich rocks (Figure 2.2E) that may be more reflective of variations in the primary mineralogical composition within the sills. These larger scale hornblende-rich and plagioclase-rich zones were specifically targeted as they potentially were formed through magmatic differentiation of these large gabbroic intrusions. Fine-grained gabbros with a similar fabric as those in the NGB were also observed in the nearby Ukaliq Supracrustal Belt.

The gneissic gabbros are composed of fine to medium-grained hornblende + plagioclase + quartz ± biotite ± cummingtonite (Figure 2.3A). The fabric exhibited in these gabbros is defined by the alignment of hornblende ± biotite ± cummingtonite grains (Figure 2.3A). The hornblende and biotite is sometimes locally replaced by chlorite and epidote whereas the plagioclase grains display minor to heavy sericite alteration. Mineral proportions vary within the sills. The plagioclase-rich zones consist of ~50% very fine-grained plagioclase that is heavily altered to sericite (Figure 2.3B). In comparison, the hornblende-rich rocks are composed almost entirely of

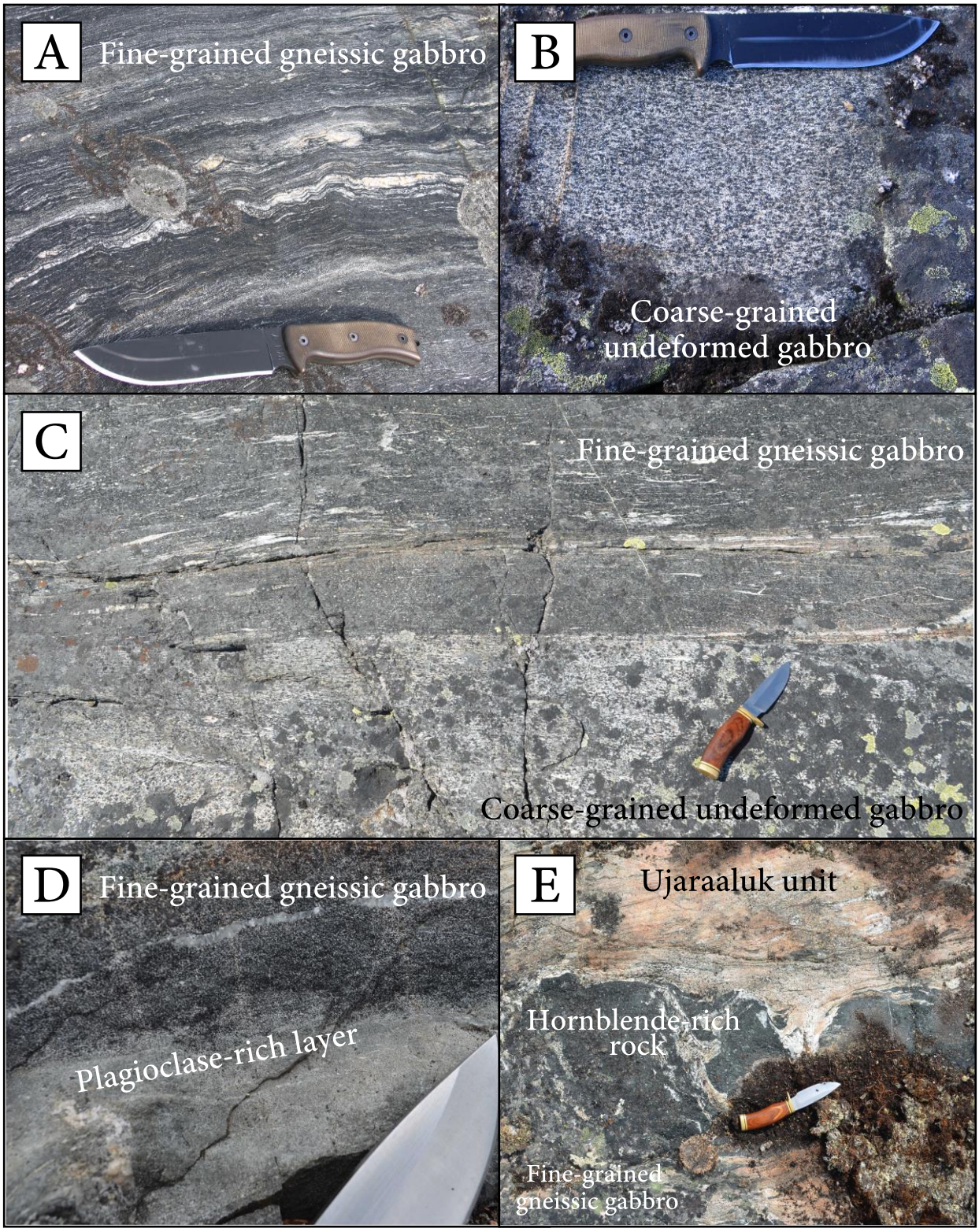

Figure 2.2: Field pictures of the NGB gabbros. A) Fine-grained gneissic gabbro. B) Coarse-grained undeformed gabbro. C) Contact between the fine-grained gneissic gabbro and coarse-grained undeformed gabbro. D) Plagioclase-rich layer within the fine-grained gneissic gabbro. E) Hornblende-rich rock at the contact of the Ujaraaluk unit and the fine-grained gneissic gabbro.

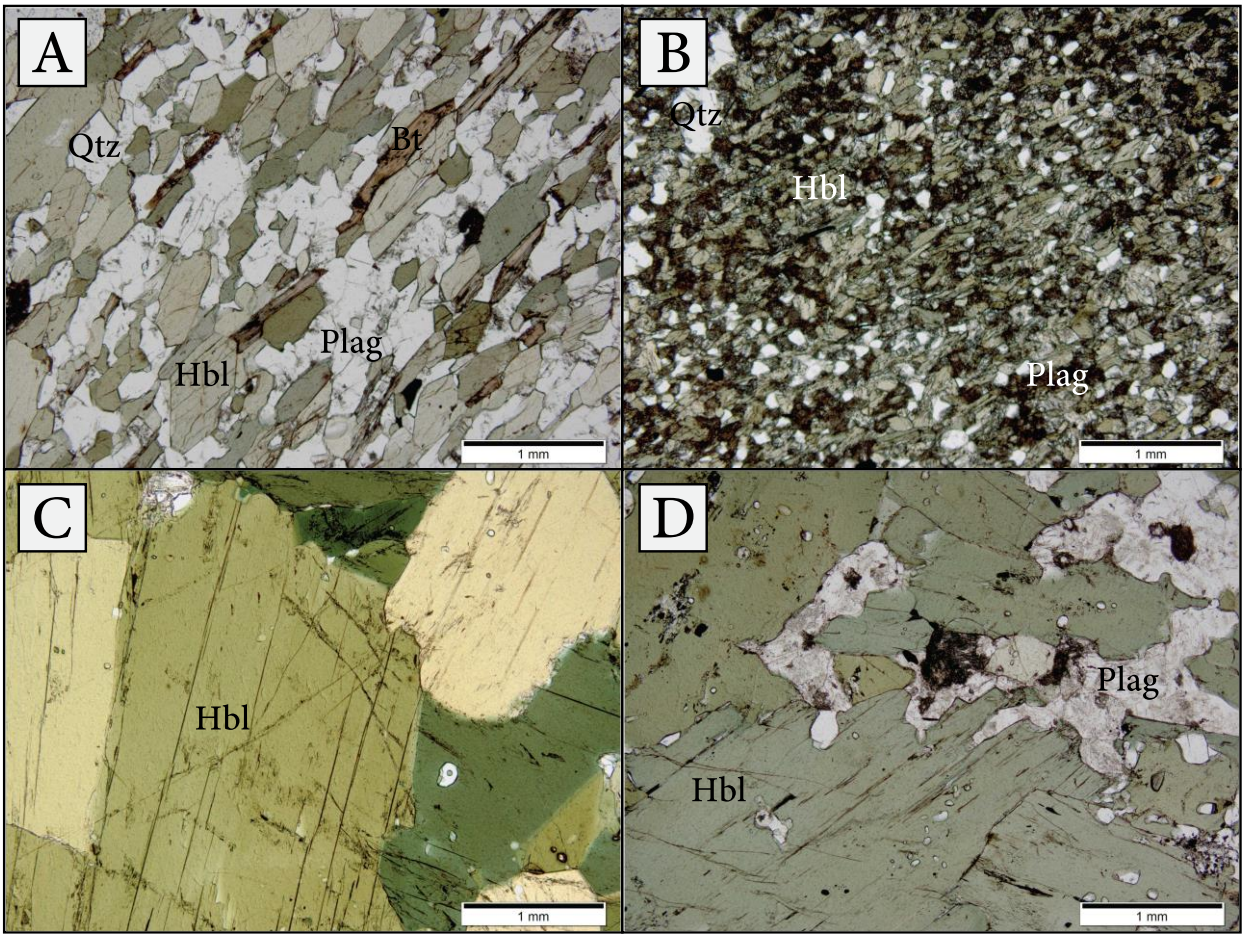

Figure 2.3: Microphotographs of the NGB gabbros under plain-polarized light at 5x magnification. A) Fine-grained gneissic gabbro (PC-607); B) Plagioclase-rich layer (PC-618); C) Hornblende-rich rock (PC-635); D) Coarse-grained undeformed gabbro (PC-633). Abbreviations: Hbl = Hornblende; Plag = Plagioclase; Qtz = Quartz; Bt = Biotite.

very coarse hornblende with subordinate plagioclase that is highly altered to sericite (Figure 2.3C). Mineral abundances for the more homogeneous fine-grained gneissic gabbro samples mostly vary between 50% to 70% hornblende and 20% to 40% plagioclase.

The undeformed coarse-grained gabbros have a similar mineralogy to the fine-grained gneissic gabbros and are composed of hornblende + plagioclase ± quartz (Figure 2.3D). The hornblende and plagioclase abundances are mostly 60% to 70% and 30% to 40%, respectively. However, as opposed to the fine-grained gabbros, no mineral alignment or fabric is observed in

these coarse-grained gabbros (Figure 2.3D). These gabbros are also homogeneous at the outcrop scale and do not display hornblende or plagioclase-rich zones such as those observed within the gneissic sills.

2.4.2 Geochemistry

Major and trace element compositions of all gneissic gabbro samples analyzed in this study are presented in Table A.4. The compositions of three undeformed coarse-grained gabbro samples analyzed here are also found in Table A.4 for comparison and are described in more detail in Benn (2018).

The fine-grained gneissic gabbros now exhibit a metamorphic paragenesis but their CIPW normative mineralogy mostly consists of gabbro to olivine gabbro compositions (Figure 2.4). The hornblende-rich samples exhibit a higher proportion of normative pyroxene and fall into the gabbroic melanosome compositional field, whereas the sample from the plagioclase-rich layer contains some of the most normative plagioclase content (Figure 2.4). The whole-rock major element composition of the gneissic gabbros is generally basaltic with SiO_2 content ranging from 45 to 56 wt.% and MgO content ranging from 3 to 16 wt.%, which decreases slightly with increasing SiO_2 contents (Figure 2.5A). The two hornblende-rich samples are compositionally distinct in terms of SiO_2-MgO and display either low SiO_2 (PC-635; 45 wt.%) or high MgO (PC-604; 16 wt.%) compared to the other gneissic gabbros. The plagioclase-rich sample (PC-618) displays lower MgO (5 wt.%) and higher SiO_2 (53 wt.%) content than most gneissic gabbros. The plagioclase-rich sample PC-618 also displays one of the lowest Mg# (Mg# = 53.8) compared to most other gabbros ranging in Mg# from 62.3 to 54.8. CaO content for the fine-grained gneissic gabbros ranges from 6 to 13 wt.% which slightly decreases with increasing SiO_2 content (Figure

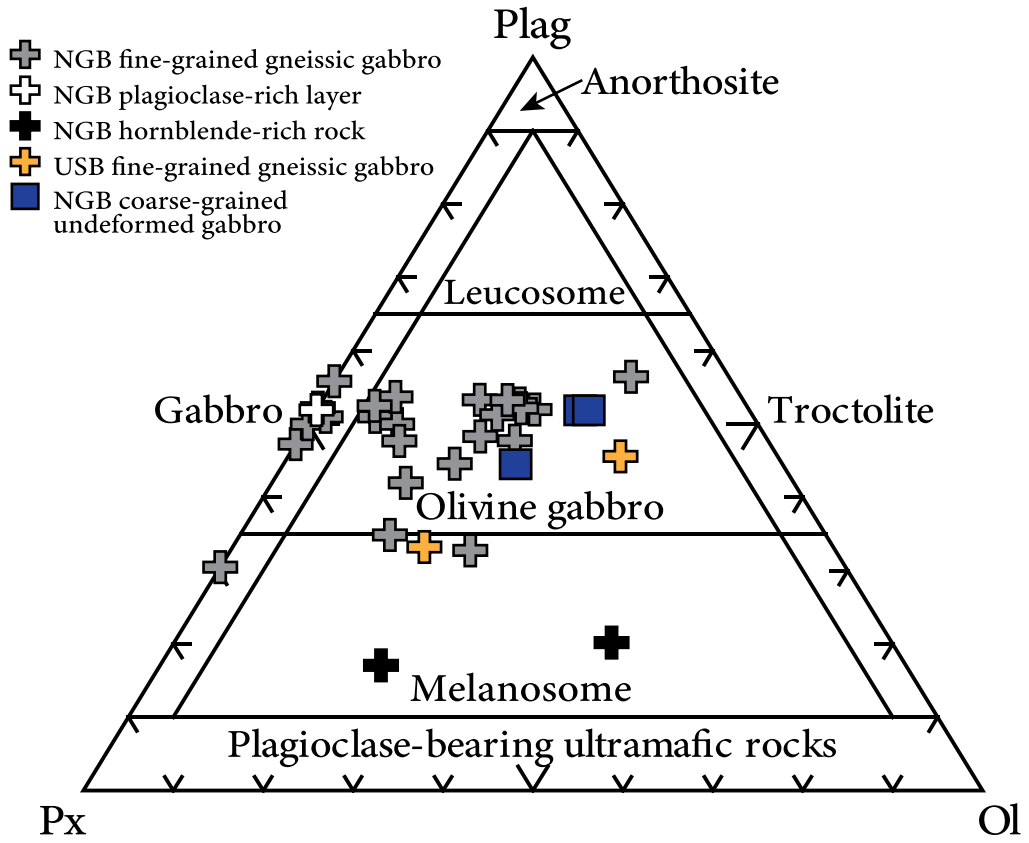

Figure 2.4: Plag-Px-Ol CIPW normative mineralogy ternary diagram (Le Maître, 2002) for the NGB and USB gabbros. Abbreviations: Plag = Plagioclase; Px = Pyroxene; Ol = Olivine. Symbols: Grey plusses = NGB fine-grained gneissic gabbros; White plus = NGB plagioclase-rich layer; Black plusses = NGB hornblende-rich rocks; Orange plusses = USB fine-grained gneissic gabbros; Blue squares = NGB coarse-grained undeformed gabbros.

2.5B). The hornblende-rich samples have CaO concentrations (~11.5 wt.%) that are higher than most homogeneous gabbro samples (<10 wt.%). The plagioclase-rich sample also displays high CaO content (11.5 wt.%). Al_2O_3 content for the homogeneous gneissic gabbros and the plagioclase-rich layer mostly range from 15 to 17 wt.% and shows no correlation with SiO_2 content (Figure 2.5C). The hornblende-rich samples have the lowest Al_2O_3 of all gneissic gabbro samples (<10 wt.%). TiO_2 concentrations for the gneissic gabbros are all <1 wt.% and slightly decrease with increasing SiO_2 content (Figure 2.5D). The hornblende-rich samples show one of the highest (PC-635; 0.99 wt.%) and the lowest (PC-604; 0.32 wt.%) TiO_2 contents of all gabbro samples.

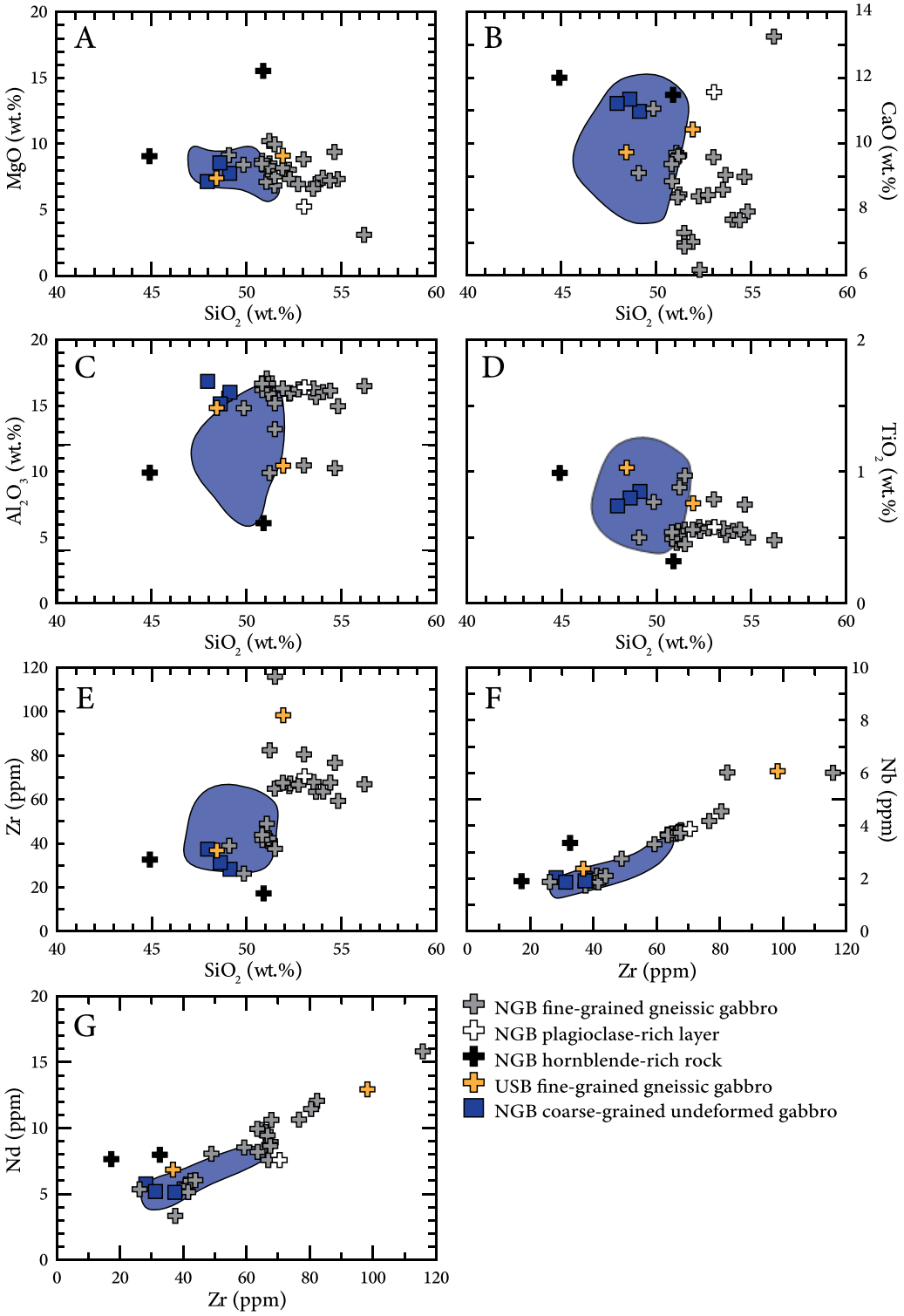

Figure 2.5: Major and trace element compositions of the NGB and USB gabbros. A-E) Selected major and trace element concentrations vs. SiO_2. F-G) Selected trace element concentrations vs. Zr. Shaded blue areas represent NGB coarse-grained undeformed gabbro compositions reported in O'Neil et al. (2007) and Benn (2018). Same symbols as in Figure 2.4.

Incompatible trace elements such as Zr display a positive correlation with increasing SiO_2 content in the gneissic gabbros (Figure 2.5E). This positive correlation also exists when high field strength elements (HFSE) such as Nb and LREE such as Nd are compared to Zr (Figure 2.5F-G). The hornblende-rich samples generally show the lowest concentrations in incompatible trace elements whereas the plagioclase-rich layer displays some of the highest concentrations in incompatible trace elements of all gneissic gabbro samples.

The gneissic gabbros exhibit flat to LREE-enriched chondrite-normalized REE patterns with no to small negative Eu anomalies (Figure 2.6A). The plagioclase-rich sample displays a LREE-enriched pattern while the two hornblende-rich samples display different La/Sm ratios. Sample PC-604 displays a LREE-enriched pattern whereas PC-635 exhibits a flat to slightly LREE-depleted profile (Figure 2.6A). Contrasting with the range of LREE enrichment of the gneissic fine-grained gabbros, all coarse-grained undeformed gabbros display homogeneous flat REE profiles (Figure 2.6B).

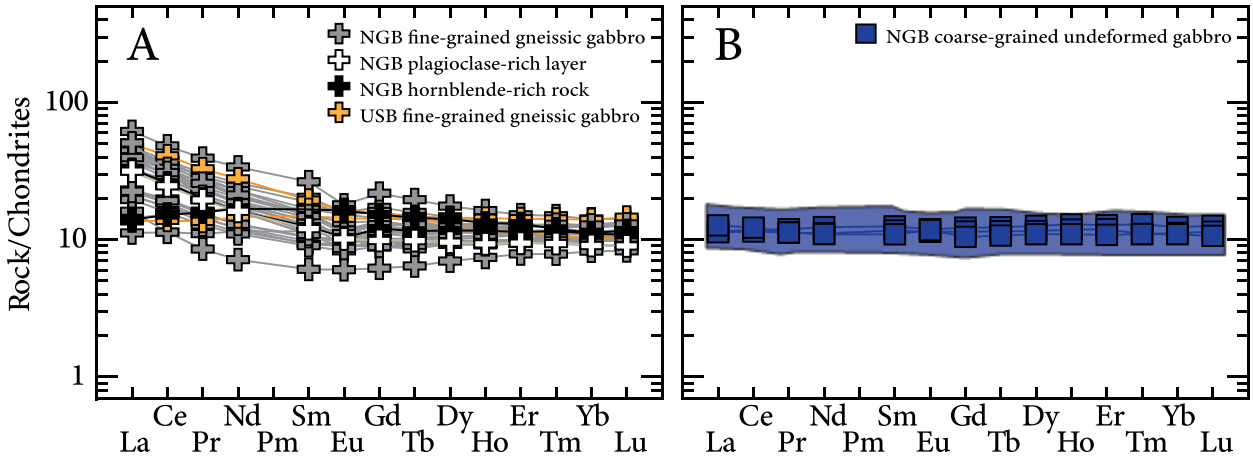

Figure 2.6: Chondrite-normalized REE profiles of the gabbro samples. A) NGB and USB fine-grained gneissic gabbros and associated plagioclase-rich layer and hornblende-rich rocks. B) NGB coarse-grained undeformed gabbros. Normalized after Sun and McDonough (1989). Shaded blue areas represent NGB coarse-grained undeformed gabbro compositions reported in O'Neil et al. (2007) and Benn (2018). Same symbols as in Figure 2.4.

2.4.3 Zircon U-Pb isotope data

Between 70–100 zircons from two compositionally evolved fine-grained gneissic gabbros (PC-601 and PC-602) and from the plagioclase-rich layer (PC-618) were analyzed by LA-ICP-MS for U-Pb geochronology. Data for all individual zircons is available in Table A.5. CL images of representative zircons for each sample can be found in Figure 2.7 and the Concordia diagrams for each sample are shown in Figure 2.8.

Zircons from PC-601 are small (50–80 µm), rounded, multi-faceted, transparent grains. They are generally inclusion-free, have a low to moderate degree of fracturing, and have homogeneously dark or mottled features under CL imaging (Figure 2.7A). Uranium concentrations mostly range from 500–700 ppm with an average Th/U ratio of 0.20 ± 0.01 (2σ-mean). These zircons represent a single population yielding a Concordia age of 2669 ± 2 Ma ($MSWD_{(C+E)}$ = 0.90, n = 74) (Figure 2.8A).

PC-602 contains zircons that are similar to those found in PC-601. They are small (40–70 µm), multi-faceted, transparent, rounded, mostly inclusion-free, have a low to moderate degree of fracturing and have homogeneously dark or mottled features in CL (Figure 2.7B). Zircons in PC-602 also have similar Th/U ratios with an average of 0.16 ± 0.05 (2σ-mean), but with higher U concentrations that mostly range between 800–1100 ppm. The Concordia diagram for PC-602 yields an upper intercept age of 2648 ± 9 Ma (MSWD = 2.2, n = 62) and the most concordant zircons yield a weighted mean $^{207}Pb/^{206}Pb$ age of 2626 ± 9 Ma (MSWD = 1.05, n = 33) (Figure 2.8B). It is worth noting that two larger grains (80–100 µm) displayed subhedral prismatic shapes and bright CL zoned cores that were surrounded by a dark homogeneous rim. Both of these zircons, however, contained common-Pb and these analyses were rejected.

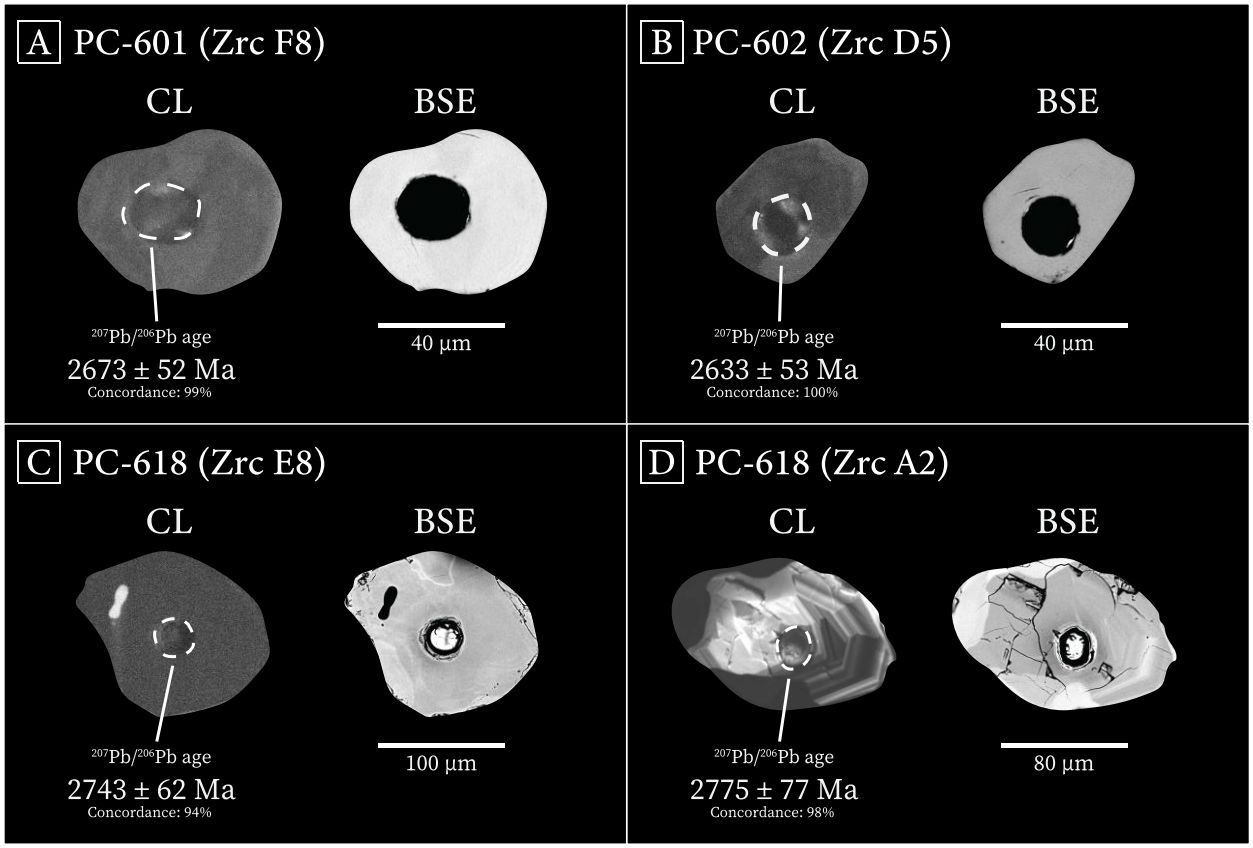

Figure 2.7: CL and BSE images of representative zircons from two compositionally evolved fine-grained gneissic gabbros (PC-601 and PC-602) and the plagioclase-rich layer (PC-618). U-Pb analysis spot is highlighted by the white dashed circle. A) Sample PC-601, zircon #F8 displaying dark mottled features; B) Sample PC-602, zircon #D5 displaying dark mottled feature; C) Sample PC-618, zircon #E8 displaying no observable features other than an inclusion; D) Sample PC-618, zircon #A2 displaying oscillatory zoning and a small dark rim. Abbreviations: Zrc = Zircon; CL = Cathodoluminescence; BSE = Back-scattered electron.

Zircons from the plagioclase-rich layer PC-618 are larger (100–200 µm) and display a rounded to anhedral prismatic shape. They exhibit a low to moderate degree of fracturing and contain a few inclusions. Most of the zircons have homogeneously dark or mottled features in CL (Figure 2.7C), but a dozen grains display oscillatory and sector zoning (Figure 2.7D). All zircons have low U concentrations with an average of 50 ppm. However, the zircons that display oscillatory and sector zoning have lower Th/U ratios with an average of 0.009 ± 0.005 (2σ-mean) compared to the dark unzoned zircons which have higher Th/U ratios with an average of 0.74 ± 0. (2σ-mean). Most of the zoned zircons yield a Concordia age of 2766 ± 12 Ma (MSWD $_{(C+E)}$ = 1.6,

n = 12) (Figure 2.8C), whereas the homogeneously dark unzoned zircons yield a statistically similar upper intercept age of 2789 ± 19 Ma (MSWD = 2.5, n = 53) (Figure 2.8C).

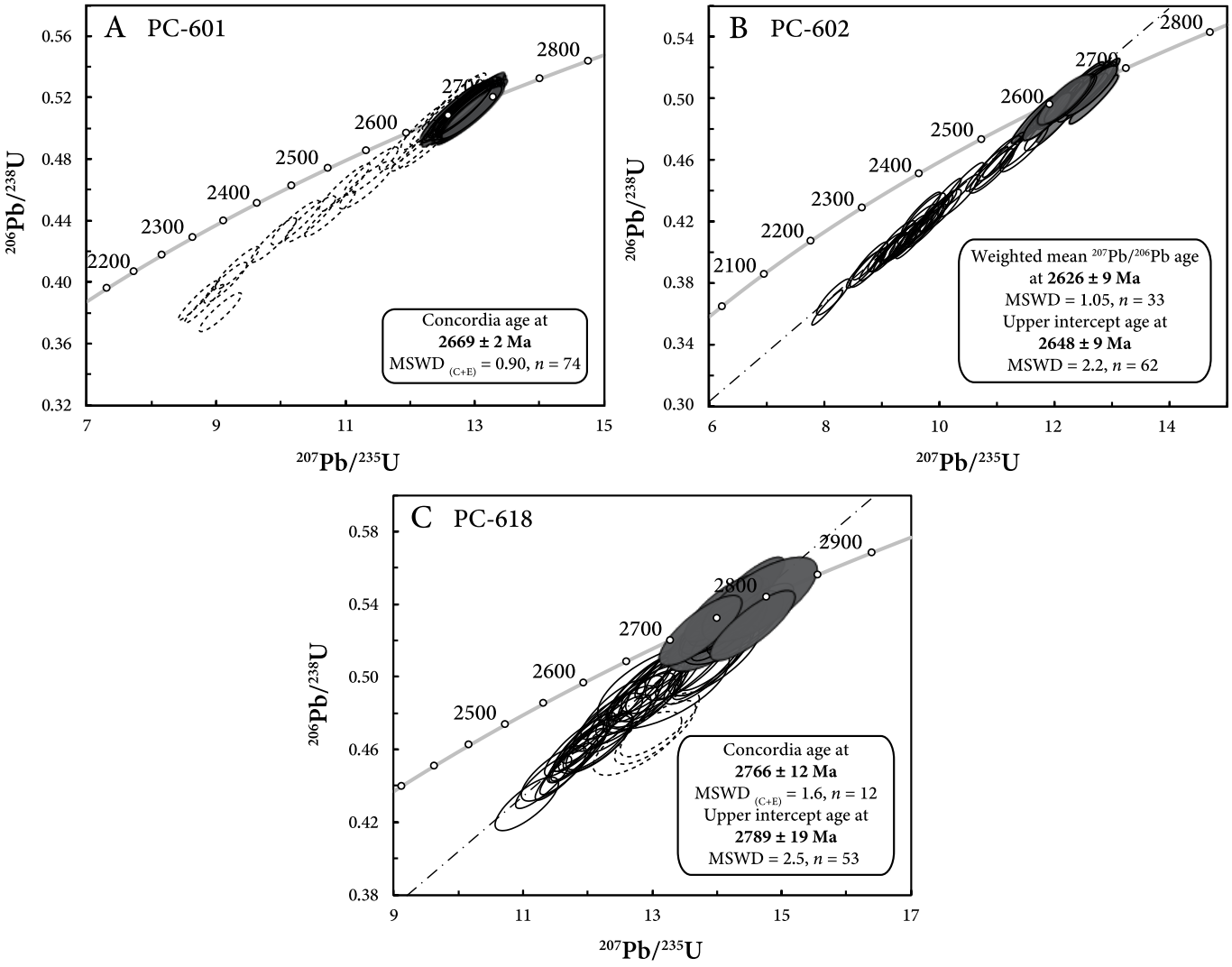

Figure 2.8: Concordia diagrams of two compositionally evolved fine-grained gneissic gabbros (PC-601 and PC-602) and plagioclase-rich layer (PC-618). A) PC-601; B) PC-602; C) PC-618. The dotted ellipses represent zircons that were not included in the age calculation. The dark grey-filled ellipses represent zircons used in the calculation of the weighted mean $^{207}Pb/^{206}Pb$ age and Concordia age in B) and C), respectively, and open ellipses represent zircons used to calculate the upper intercept age.

2.4.4 ^{147}Sm–^{143}Nd isotope data

A new sampling strategy targeted the most evolved portions and cumulative parts in the fine-grained gneissic gabbro sills in order to better constrain their age of magmatic differentiation. Samples were carefully selected based on their petrology and whole-rock geochemical compositions. Therefore, the plagioclase-rich layer sample (PC-618) and hornblende-rich sample (PC-635) were analyzed for their Sm-Nd isotopic composition as well as four fine-grained gneissic gabbro samples showing a compositional range, including one sample with a flat REE profile and three with varying degrees of LREE-enrichment. Additionally, two fine-grained gneissic gabbro samples from the nearby Ukaliq Supracrustal Belt (USB) were analyzed for comparison with the NGB gabbros. The Sm-Nd isotopic data for all eight samples can be found in Table 2.2.

$^{147}Sm/^{144}Nd$ ratios for the NGB samples range in value from 0.1454 to 0.1984 with the plagioclase-rich and the amphibole-rich samples displaying the lowest and highest $^{147}Sm/^{144}Nd$ ratios, respectively. Present-day $^{143}Nd/^{144}Nd$ ratios for all six NGB samples range from 0.511287 to 0.512741. The Nd model T_{DM} ages for all NGB samples range from 4.0 to 4.3 Ga except for the hornblende-rich sample yielding a T_{DM} age of 4.5 Ga, although this sample has a slightly suprachondritic $^{147}Sm/^{144}Nd$. An isochron including all analyzed gabbroic samples from the NGB yields an age of 4151 ± 290 Ma (MSWD = 9, n = 6) with an initial $^{143}Nd/^{144}Nd$ ratio of 0.507269 ± 0.000040 corresponding to an initial $\varepsilon^{143}Nd$ value of +0.6 ± 0.8 (Figure 2.9). The two USB fine-grained gneissic gabbro samples, UK-001 and UK-003, display $^{147}Sm/^{144}Nd$ ratios of 0.1399 and 0.2005 and present-day $^{143}Nd/^{144}Nd$ ratios of 0.511137 and 0.512809, respectively. Both Ukaliq samples also have T_{DM} ages of 4.0 and 4.1 Ga and display a similar Sm/Nd vs. $^{143}Nd/^{144}Nd$ trend as the NGB gabbros, defining a 2-point isochron with an age of 4163 ± 83 Ma and an initial $\varepsilon^{143}Nd$ value of +1.1.

Table 2.2: Sm-Nd isotope data of the NGB and USB fine-grained gneissic gabbros. Nd and Sm concentrations were determined by isotope dilution. 2σ errors for the $^{143}Nd/^{144}Nd$ ratios are in the last decimal place. Errors for the $^{147}Sm/^{144}Nd$ ratios are 0.5%. εNd values for all NGB and USB gabbro samples were calculated at the isochron age of 4151 Ma using the CHUR values of $^{143}Nd/^{144}Nd = 0.512630$ and $^{147}Sm/^{144}Nd = 0.1960$ (Bouvier et al., 2008). Abbreviations: GG = Fine-grained gneissic gabbro; Plag-GG = Plagioclase-rich layer; Hbl-GG = Hornblende-rich rock.

Sample	Lithology	Location	Nd (ppm)	Sm (ppm)	$^{147}Sm/^{144}Nd$	$^{143}Nd/^{144}Nd \pm 2\sigma$	εNd (4151 Ma)	T_{DM}
PC-612	GG	NGB	15.62	3.93	0.1522	0.511411 ± 5	-0.2	4.3
PC-613	GG	NGB	5.23	1.39	0.1611	0.511726 ± 4	1.1	4.1
PC-618	Plag-GG	NGB	7.46	1.79	0.1454	0.511287 ± 4	1.0	4.1
PC-628	GG	NGB	5.23	1.71	0.1978	0.512741 ± 4	1.2	4.0
PC-630	GG	NGB	5.02	1.35	0.1627	0.511750 ± 4	0.7	4.2
PC-635	Hbl-GG	NGB	7.81	2.56	0.1984	0.512693 ± 4	-0.1	4.5
UK-001	GG	USB	12.86	2.98	0.1399	0.511137 ± 5	1.0	4.1
UK-003	GG	USB	6.61	2.19	0.2005	0.512809 ± 5	1.1	4.0

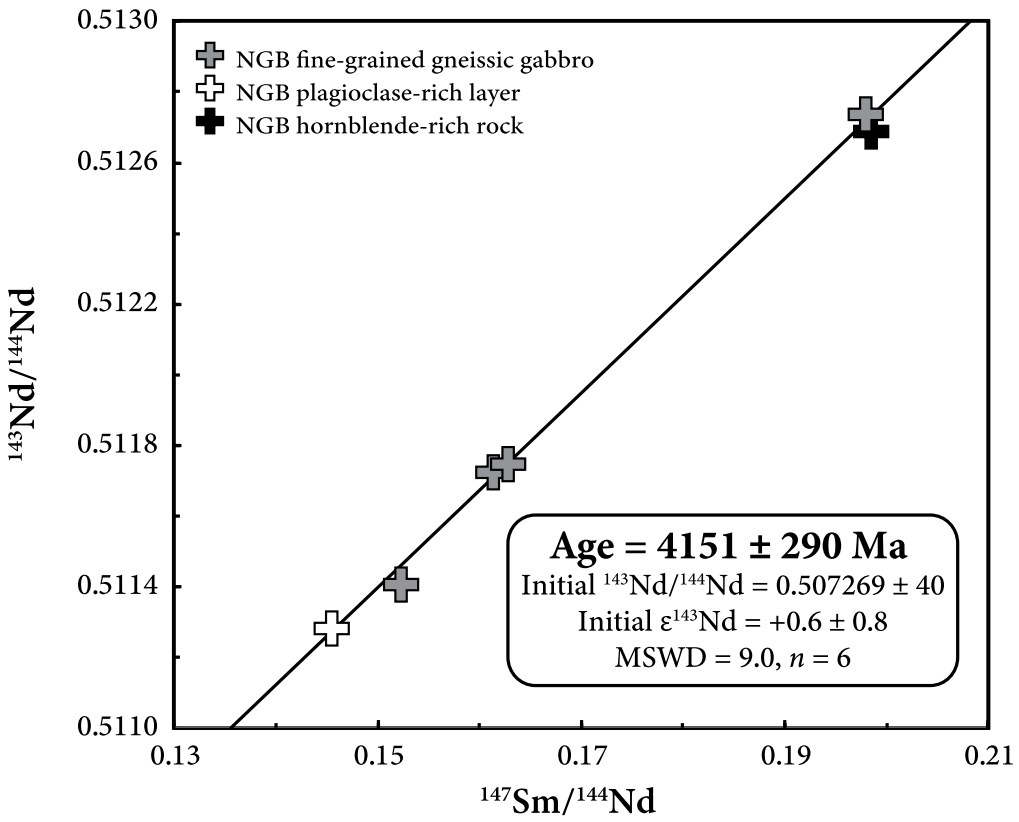

Figure 2.9: $^{147}Sm/^{144}Nd$ vs. $^{143}Nd/^{144}Nd$ isochron diagram of the NGB fine-grained gneissic gabbros, plagioclase-rich layer and hornblende-rich rock. Same symbols as in Figure 2.4.

2.5 Discussion

2.5.1 Age of gabbro sills and implication for the Nuvvuagittuq Greenstone Belt

2.5.1.1 Zircon U-Pb geochronology constraints

One of the main challenges for determining a precise and robust age for the NGB is that it is dominated by mafic and ultramafic rocks which are difficult to date using the well established U-Pb geochronology methods on zircons. Because of the lack of zircon-bearing lithologies within the NGB volcanic sequence, age constraints provided by conventional U-Pb geochronology rely on the geological relationship interpretation of rare felsic zircon-bearing rocks to the NGB supracrustal assemblage. The oldest zircon U-Pb ages in the NGB are from a few 20-50 cm wide trondhjemitic bands found in the southwestern corner of the belt that have been dated at ~3.77 Ga (Augland and David, 2015; Cates and Mojzsis, 2007; Darling et al., 2013; David et al., 2009; O'Neil et al., 2013). Although most studies have interpreted these trondhjemitic bands as intruding the NGB, which would impose a minimum age for the belt (e.g. Cates and Mojzsis, 2007; O'Neil et al., 2013), some authors have argued that these trondhjemitic bands were deposited as felsic tuffs within the NGB (e.g. Augland and David, 2015; David et al., 2009), in which case would provide the age of formation of the NGB volcanic assemblage. A few zircons found in a fuchsitic quartz-rich rock has led Cates et al. (2013) to propose a maximum age of 3780 Ma for the NGB, but this geochronological constraint relies on their interpretation that the fuchsitic quartz-rich rock is detrital in nature. This contrasts with the interpretation of Darling et al. (2013) who argue that the fuchsitic quartz-rich rock has a metasomatic origin. This highlights the challenge of precisely dating the oldest supracrustal rocks, which are commonly deformed and metamorphosed, and for which the geological relationships are often not the subject of scientific consensus.

With the absence of igneous zircon in the oldest Ujaraaluk volcanic unit, the large differentiated gabbro sills, especially their compositionally evolved parts, represent the best candidates to obtain an igneous U-Pb age on zircon or baddeleyite which would impose a minimum age for the Ujaraaluk unit. Three samples from the differentiated gabbro sills were specifically targeted for this purpose and identified as the most promising samples to contain primary zircon or baddeleyite. U-Pb zircon analyses for the plagioclase-rich sample (PC-618) and both compositionally evolved gneissic gabbros (PC-601 and PC-602) yielded Neoarchean ages of 2789 Ma, 2669 Ma and 2626 Ma, respectively (Figure 2.8). These newly reported ages are similar to the ~2690 Ma age that had been previously published for the gabbroic intrusions in the NGB (Darling et al., 2013; David et al., 2009; O'Neil et al., 2012), but span more than 150 million years, suggesting that Neoarchean zircon growth in the NGB gabbros was more protracted than previously thought. It is important to note that all three gabbro samples analyzed for U-Pb ages in this study were collected from the two continuous fine-grained gneissic gabbro sills in the western part of the belt (Figure 2.1). In contrast, the gabbros analyzed by David et al. (2009) and Darling et al. (2013) were both collected near the axis of the synform in the middle of the belt (Figure 2.1). Their samples are described as being a coarse to medium-grained homogeneous gabbro and are likely from the distinct generation of younger undeformed gabbroic intrusions that yielded the 2867 ± 210 Ma ^{147}Sm-^{143}Nd isochron (Benn, 2018). Comparing zircon morphological and chemical characteristics as well as U-Pb ages between the fine-grained gneissic gabbro sills and the coarse-grained undeformed gabbro intrusions should thus be made with caution.

Zircons from PC-601 yielded a Concordia age of 2669 ± 2 Ma which is comparable within uncertainty to the mean ^{207}Pb/^{206}Pb age obtained by O'Neil et al. (2012) in a fine-grained gneissic gabbro. The age obtained for sample PC-602 is slightly younger however, yielding an upper

intercept age of 2648 ± 9 Ma and a mean $^{207}Pb/^{206}Pb$ age of 2626 ± 9 Ma for its most concordant zircons. Nevertheless, the upper intercept age of PC-602 still yields a comparable U-Pb age within uncertainty to that of PC-601 and the data of O'Neil et al. (2012). The apparent younger age of PC-602 may just reflect the selection of different grains to include in the age calculation. The zircon analyses for PC-602 are also more discordant which may be partly due to their very high U concentrations (>900 ppm), resulting in a larger extent of Pb-loss. Regardless of the slight age differences, both PC-601 and PC-602 contain small (~60 µm), multi-faceted, rounded zircons with dark homogeneous CL emissions that are typical of zircon formed during metamorphism in mafic rocks under sub-solidus conditions (e.g. Corfu et al., 2003; Rubatto, 2017 and references therein). Their metamorphic origin is also supported by their high U concentrations (avg. >600 ppm) and low Th/U ratios (avg. 0.18), which are similar values to the data of O'Neil et al. (2012). In comparison, zircons retrieved from the coarse-grained undeformed gabbro samples of David et al. (2009) and Darling et al. (2013) are larger in size (~100 µm) with sector and fir-tree zoning and have much lower U concentrations (avg. 82 ppm) and higher Th/U ratios (avg. 0.35), more typical of igneous zircons. We therefore interpret the U-Pb zircon ages for samples PC-601 and PC-602 to likely represent metamorphic ages rather than constraining the age of emplacement of the gneissic gabbro sills.

Baddeleyite (ZrO_2) has gained significant attention in recent years as being a reliable accessory mineral for dating the emplacement age of mafic dykes and sills (e.g. Heaman & LeCheminant, 1993; Peng et al., 2011; Silveira et al., 2013; Söderlund et al., 2005; 2013) because it tends to be enriched in U (up to thousands of ppm) and has virtually no initial Pb making it ideal for U-Pb geochronology. It was first reported by Keil and Friker (1974) that baddeleyite crystallizes as a primary accessory phase in the late-stage differentiates of gabbroic magmas. The

plagioclase-rich layer sample (PC-618) found within the gneissic gabbros (Figure 2.2D) was chosen for U-Pb geochronology because it is believed to represent a late-stage differentiate of gabbroic magma and therefore has the best chance of containing igneous baddeleyite. However, no baddeleyites were recovered in PC-618 but its noticeably different zircon texture, chemistry and U-Pb ages compared to PC-601 and PC-602 may hint towards the breakdown of baddeleyite and subsequent zircon crystallization during metamorphism.

Baddeleyite is often readily converted to polycrystalline zircon during the initial stages of metamorphism because excess silica causes the following reaction to occur: ZrO_2 (baddeleyite) + SiO_2 = $ZrSiO_4$ (zircon) (Davidson & van Breemen, 1988; Heaman & LeCheminant, 1993). U-Pb dating of this polycrystalline zircon has been shown to record the timing of baddeleyite breakdown and therefore yields ages that may be up to a few tens of million years older than the timing of peak metamorphism (Söderlund et al., 2008). The 2789 ± 19 Ma upper intercept age of PC-618 could therefore be recording the timing of baddeleyite breakdown prior to peak metamorphism at ~2.7 Ga. This would explain the ~100 Ma older ages obtained for the zircons of PC-618 compared to the U-Pb ages of the metamorphic zircon found in PC-601 and PC-602 and those previously reported in the NGB gabbros (David et al., 2009; Darling et al., 2013; O'Neil et al., 2012).

The zircon chemistry of PC-618 also provides further evidence supporting the interpretation that these represent polycrystalline zircon which formed following the breakdown of baddeleyite. Baddeleyite characteristically has very low Th contents (often <20 ppm) and therefore low Th/U ratios (<0.05) (Heaman and LeCheminant, 1993). The zircons in PC-618 showing homogeneous dark CL textures have average Th and U contents of 39 and 47 ppm, respectively, corresponding to higher Th/U ratios (avg. 0.74). These elevated Th/U ratios make it difficult to determine if they were truly formed by the breakdown of igneous baddeleyite.

However, Söderlund et al. (2008) noted that there is a distinctively higher amount of Th in polycrystalline zircon in comparison to its baddeleyite precursor. Given the small U concentrations in the homogeneous dark CL zircons of PC-618, an increase in Th content during the breakdown of baddeleyite could account for their abnormally higher Th/U ratios. In contrast, the zircons in PC-618 displaying oscillatory and sector zoning have very low Th contents (avg. 0.31 ppm) and correspondingly very low Th/U ratios (avg. 0.009). Complete dissolution of igneous baddeleyite to recrystallize metamorphic polycrystalline zircon could produce such chemical characteristics. In order to confirm that the zircons in PC-618 were formed by the breakdown or dissolution of igneous baddeleyite, further chemical mapping of these zircons would be needed to identify if any potential relict baddeleyite remains.

Nevertheless, these newly reported zircon U-Pb ages for the gneissic gabbros are consistent with processes occurring during the regional metamorphism at ~2.7 Ga and do not provide timing constraints on the emplacement of the gabbro sills.

2.5.1.2 Whole-rock Sm-Nd isotopic constraints

Since no igneous zircons or baddeleyites are present, or at least survived, in the differentiated gabbro sills, we must rely on other isotope systems to constrain their emplacement age. Long-lived isotopic systems must however be used with caution in Archean terrains that have been subjected to complex protracted thermal histories. Isotopic systems, such as ^{147}Sm-^{143}Nd, can be disturbed by several post-magmatic processes that would affect the Sm/Nd ratio or reset the Nd isotopic compositions, even partially, of the studied samples.

The Ujaraaluk unit is presumed to be the oldest lithology in the NGB. It is interpreted as being a package of mafic volcanic rocks intruded by younger gabbroic sills and trondhjemitic

intrusions. Both long-lived ^{147}Sm-^{143}Nd and ^{176}Lu-^{176}Hf isotopic systems in the Ujaraaluk unit have been disturbed to a certain extent and whole-rock isochrons yielded imprecise ages varying between 3.7 and 2.5 Ga, depending on if the Ujaraaluk unit is considered as a whole or if the distinct geochemical groups within the Ujaraaluk unit are considered individually (O'Neil et al., 2012, 2013). While the long-lived isotopic systems seem to have been perturbed in the Ujaraaluk unit, the relatively low scatter on the ^{147}Sm-^{143}Nd isochron for the fine-grained gneissic gabbro sills suggested that the ^{147}Sm-^{143}Nd system may have been better preserved in these intrusive rocks compared to the extrusive Ujaraaluk unit (O'Neil et al., 2012). A series of samples from the fine-grained gabbro sills yielded an isochron age of 4115 ± 100 Ma (MSWD = 4.8). If this is interpreted as their crystallization age, the NGB fine-grained gabbro sills would represent rare Hadean rocks preserved on Earth and their intrusive nature would impose a minimum age on the Ujaraaluk unit. However, the significance of the ^{147}Sm-^{143}Nd isotopic composition in these gabbro sills has often been overlooked in models proposing that the NGB is not Hadean and rather disregarded as being the result of mixing with an undefined LREE-enriched Hadean reservoir (e.g. Caro et al., 2017; Guitreau et al., 2013; Roth et al., 2013).

Because these fine-grained gabbro sills appear to be magmatically differentiated, the new sampling strategy implemented here targeted the most evolved plagioclase-rich zones interpreted as residual liquids, and pyroxene-rich (now metamorphosed to amphibolites) cumulative portions of the sills. Applying the ^{147}Sm-^{143}Nd isotopic system to this combination of evolved, homogenous and cumulative gabbro samples would in fact be the best equivalent to an internal isochron, which can constrain the timing of primary magmatic differentiation within the gabbro sills. The ^{147}Sm-^{143}Nd isochron including these newly analyzed plagioclase-rich evolved and hornblende-rich cumulative gabbros yielded an age of 4151 ± 290 Ma (MSWD = 9, n = 6) (Figure 2.9).

It could be argued that the $^{147}Sm/^{144}Nd$ vs. $^{143}Nd/^{144}Nd$ correlation defined by the gabbro samples is indicative of mixing between two reservoirs, in which case the age obtained from the slope of this correlation would have no geochronological significance. In fact, interaction with an Hadean enriched component has been proposed to explain the ^{142}Nd isotopic composition of the NGB Ujaraaluk unit. Roth et al. (2013) suggested that the $^{142}Nd/^{144}Nd$-Sm/Nd correlation in the Ujaraaluk unit represents a mixing line, rather than an isochron, between a superchondritic mantle-derived melt and either a Hadean crust or an enriched mantle component formed at ca.4500 Ma. Similarly, Caro et al. (2017) proposed that the ^{142}Nd composition of the Ujaraaluk unit could be inherited through metasomatic enrichment of their mantle source. Despite the fact that it was concluded by O'Neil et al. (2019) that such mixing did not occur for the Ujaraaluk unit based on their geochemical and coupled ^{143}Nd-^{142}Nd isotopic compositions, it is worth closely assessing if a plausible mixing scenario could have affected the isotopic composition of the gabbro sills.

Figure 2.10 shows the difference between an isochron that is geochronologically meaningful and mixing between a REE-enriched reservoir and a REE-depleted reservoir. In the case of an isochron (Figure 2.10A and B), all co-genetic samples have the same $^{143}Nd/^{144}Nd$ at the time of their formation at 4.1 Ga (t = 0) (Figure 2.10A). The samples define a correlation in the present-day and its slope corresponds to the age of the sample suite (Figure 2.10B). Figures 2.10C and D illustrate a suite of samples with isotopic compositions that are the result of mixing at 3.77 Ga (t = 0) between two compositionally distinct reservoirs (Figure 2.10C). This suite of samples will evolve isotopically for 3.77 billion years (Figure 2.10D) to display today the same correlation as the 4.1 Ga isochron of Figure 2.10B, although the slope of this mixing line has no geochronological meaning. In a mixing scenario, the initial isotopic compositions of the different samples will not be the same (as shown on Figure 2.10C) and commonly display a correlation with

their Nd concentrations resulting from the mixing between two reservoirs with distinct Nd concentrations and isotopic compositions.

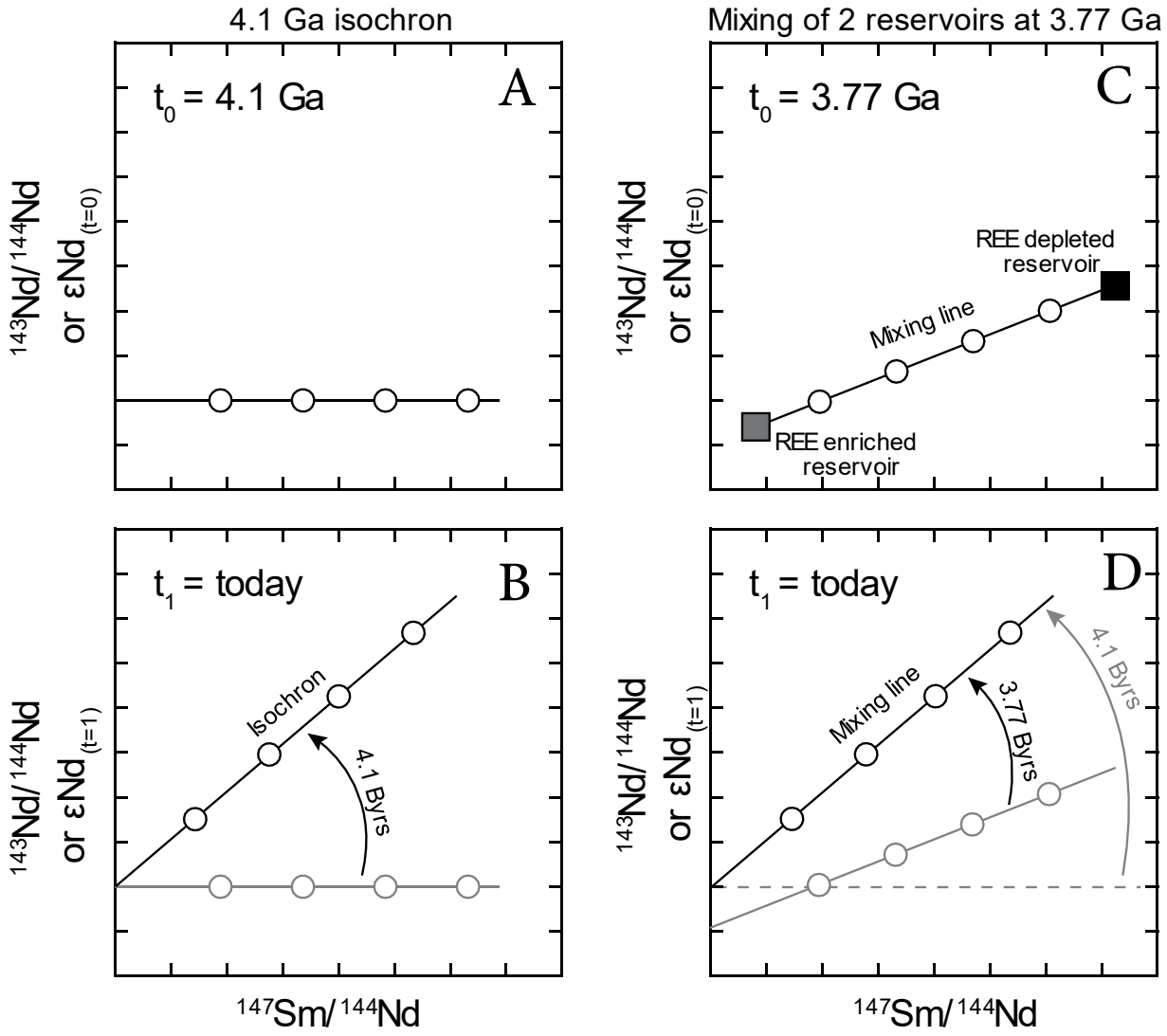

Figure 2.10: Schematic showing the evolution of a 4.1 Ga ^{147}Sm-^{143}Nd isochron versus the evolution of mixing of two reservoirs at 3.77 Ga. A-B) Evolution of cogenetic samples producing a slope equivalent to an isochron with an age of 4.1 Ga. C-D) Evolution of mixing of two reservoirs at 3.77 Ga to produce isotopic compositions with a similar slope to that of a 4.1 Ga isochron. In this scenario, the slope however has no geochronological significance.

Figure 2.11A shows the εNd values of the gneissic gabbro samples calculated at 4151 Ma (the age of the isochron of Figure 2.9) against their Nd concentration. No correlation is observed and despite some minor scatter, all samples display εNd values at 4151 Ma within error of the initial εNd value of +0.6 ± 0.8 obtained from the isochron diagram. If the correlation of Figure 2.9 represents a mixing line rather than an isochron, the timing of that mixing event would most likely be at 3.77 Ga, as proposed by the studies arguing that the NGB does not host Hadean rocks (e.g. Caro et al., 2017; Cates et al., 2013; Guitreau et al., 2013, Roth et al., 2013). Figure 2.11B shows that no clearly defined correlation with Nd concentrations is found when the εNd values of the gneissic gabbros are calculated at 3770 Ma. Sample PC-612 displays an initial εNd value slightly below the initial εNd values for the other fine-grained homogeneous gabbro samples and one could argue that Figure 2.11B shows a broad correlation, but this weak correlation in mainly caused by this one sample. Sample PC-612 also has the highest LREE concentration among all 24 fine-grained gabbro samples collected for this study. This could suggest that its LREE-enrichment and Nd isotopic composition are not primary, which would perhaps support a mixing model. However, if this sample is not considered, the isochron age is still the same within error and becomes 4091 ± 270 Ma with an MSWD = 4.4.

Figure 2.12 shows a correlation between the gneissic gabbros $\varepsilon^{143}Nd$ values calculated at 3.77 Ga and their $^{147}Sm/^{144}Nd$ ratios, including samples previously analyzed by O'Neil et al. (2012). This positive correlation is to be expected if the gabbros are 4.1 billion years old, as their $^{143}Nd/^{144}Nd$ ratios would have evolved between 4.1 and 3.77 Ga. Alternatively, a positive correlation could also be produced if their isotopic composition is the result of mixing at 3.77 Ga, as illustrated in Figure 2.10. In a mixing scenario, the enriched component is however expected to lie on the low Sm/Nd side of the regression (Figure 2.10C). It is therefore possible to put isotopic

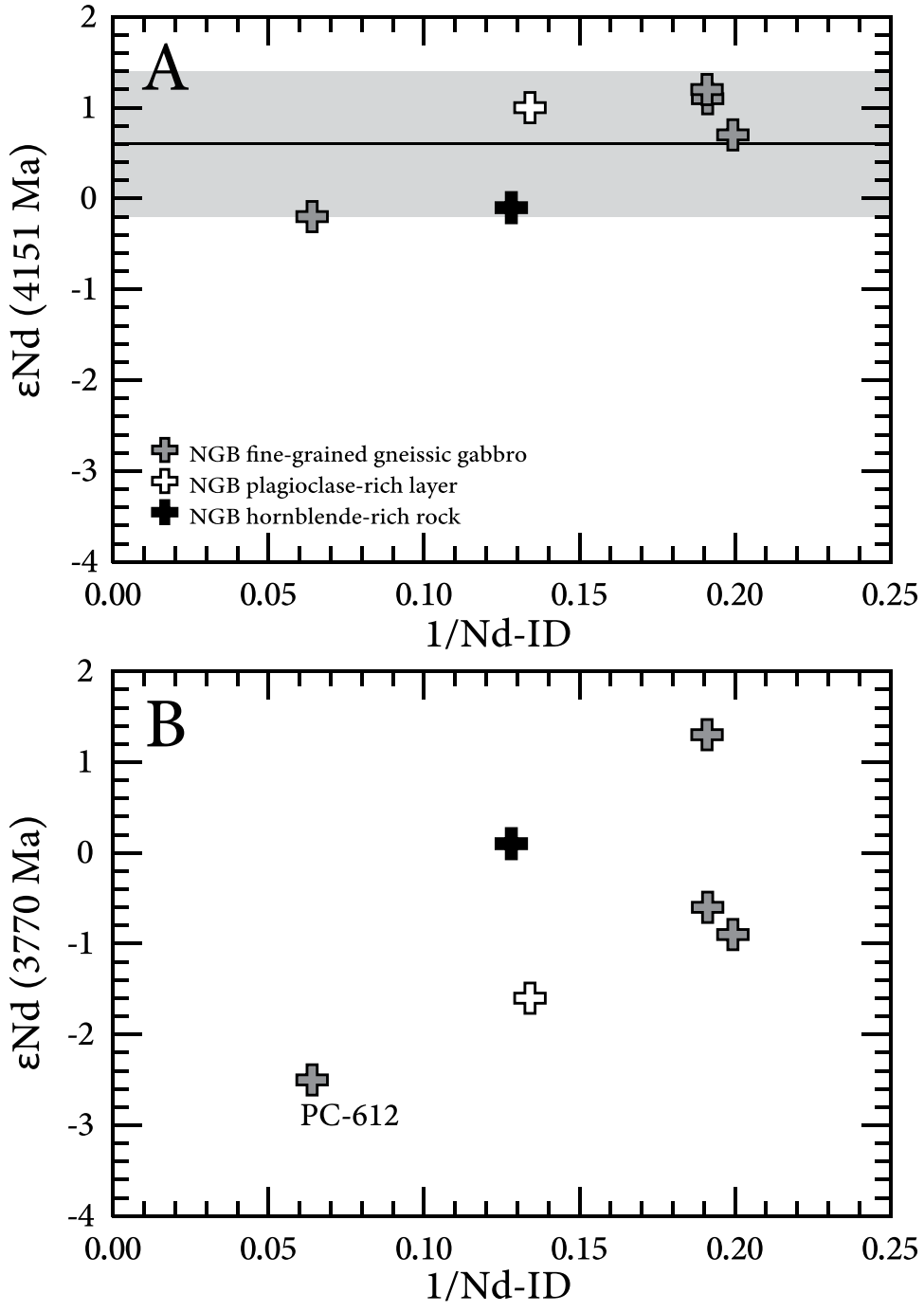

Figure 2.11: Initial εNd values vs. 1/Nd plots. A) Initial εNd values of the NGB fine-grained gneissic gabbros calculated at an age of 4151 Ma. Black line and grey box represent the average initial εNd value of +0.6 ± 0.8 obtained from the isochron diagram (Figure 2.9). B) Initial εNd values of the NGB fine-grained gneissic gabbros, calculated at an age of 3770 Ma. Nd concentrations were determined by isotope dilution (ID) (Table 2.2). Same symbols as in Figure 2.4.

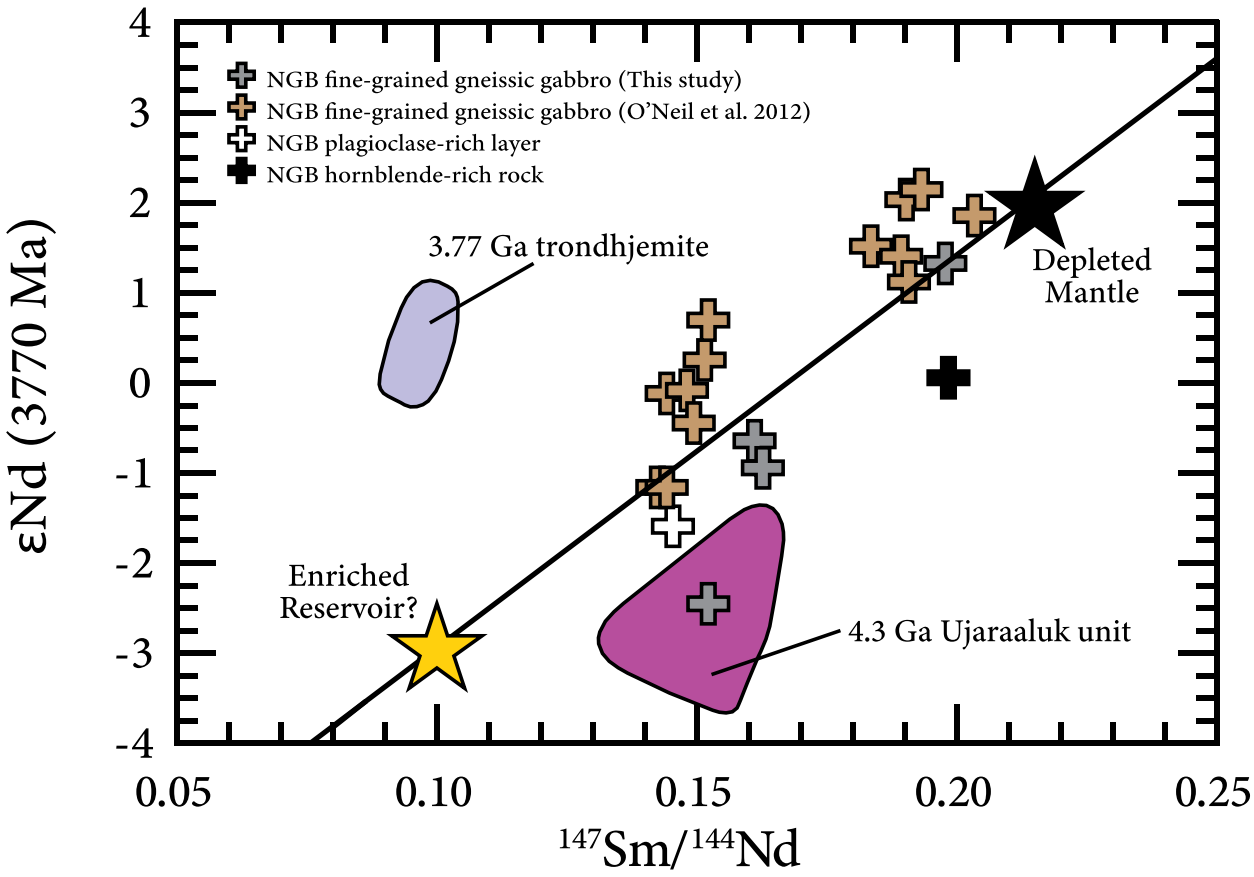

Figure 2.12: Initial εNd values vs. $^{147}Sm/^{144}Nd$ plot of the NGB fine-grained gneissic gabbros, Ujaraaluk unit and trondhjemite bands calculated at an age of 3770 Ma. Same symbols as in Figure 2.4. Additional symbols: Brown plusses = fine-grained gneissic gabbros from O'Neil et al. (2012); Yellow star = Hypothetical Enriched Reservoir; Black star = Depleted Mantle. Black line is a linear regressions running through the gneissic gabbro samples. Data for the NGB fine-grained gneissic gabbros (brown plusses) as well as the 4.3 Ga enriched Ujaraaluk unit and 3.77 Ga trondhjemite band compositional fields are from O'Neil et al. (2012) and references therein.

constraints on the potential enriched source or contaminants that would be involved in a mixing scenario. Figure 2.12 shows the different enriched lithologies of the NGB that could represent such enriched end-member. The 3.77 Ga trondhjemite bands that locally intrude the NGB, and sometimes found within the gabbro sills, could be a potential source contaminant, but their isotopic composition plot well off the regression line that is defined by the gneissic gabbro isotopic compositions (Figure 2.12). The enriched Ujaraaluk also appear not to be a suitable enriched end-member, as they display lower εNd values than the gabbros at comparable $^{147}Sm/^{144}Nd$ and do not

lie on the gabbro regression line. Only the gabbro sample PC-612 displays a similar εNd value to the enriched Ujaraaluk unit, which is also the gabbro sample with the isotopic composition that is the most diverging from the other gabbro samples, as previously discussed.

Although the possibility of this $^{143}Nd/^{144}Nd$–$^{147}Sm/^{144}Nd$ correlation representing a mixing line cannot be completely discounted for, our potential source contaminants mixing model suggests that it is unlikely. In order to account for the differentiated, unfractionated and intermediate isotopic compositions observed in the fine-grained gneissic gabbros, only an unknown evolved source (yellow star on Figure 2.12) could be responsible for the isotopically differentiated compositions of the fine-grained gneissic gabbros. Even if this unknown enriched reservoir existed as Hadean crust or enriched mantle, different degrees of mixing with a Hadean LREE-enriched reservoir would be unlikely to produce and preserve the mineralogy difference between the samples analyzed here that are interpreted as the result of magmatic fractionation. A regression through sample PC-618 and PC-635 only, which are the plagioclase-rich and hornblende-rich samples respectively, yields an age of 4006 ± 91 Ma. Both samples have in fact similar Nd concentrations. The fact that the same $^{147}Sm/^{144}Nd$ vs. $^{143}Nd/^{144}Nd$ correlation, or isochron, is preserved between samples interpreted as an evolved residual liquid and a cumulate, produced by magmatic differentiation of the sills, argues against mixing between compositionally distinct reservoirs. To produce the range of isotopic compositions measured in the gneissic gabbros, different degrees of mixing would have had to occur, which at the outcrop-scale is quite improbable.

As previously mentioned, this correlation is interpreted as being equivalent to an internal isochron with plagioclase-rich samples having low $^{147}Sm/^{144}Nd$ and isotopically unradiogenic compositions as well as hornblende-rich samples that display more radiogenic isotopic

compositions and higher Sm/Nd ratios. We therefore suggest that this ^{147}Sm-^{143}Nd internal isochron constrains the timing of magmatic differentiation within the fine-grained gneissic gabbro sills. The age obtained here for the new suite of differentiated samples overlaps the age of 4115 ± 100 Ma previously obtained by O'Neil et al. (2012). A combination of both data sets yields an isochron age of 4114 ± 140 Ma (MSWD = 14, n = 19) with an initial $^{143}Nd/^{144}Nd$ ratio of 0.507359 ± 0.000021 corresponding to an initial εNd value of +1.5 ± 0.4 (Figure 2.13). This more targeted approach provides strong evidence that the age of magmatic differentiation of the gneissic gabbro sills is constrained to 4.1 Ga.

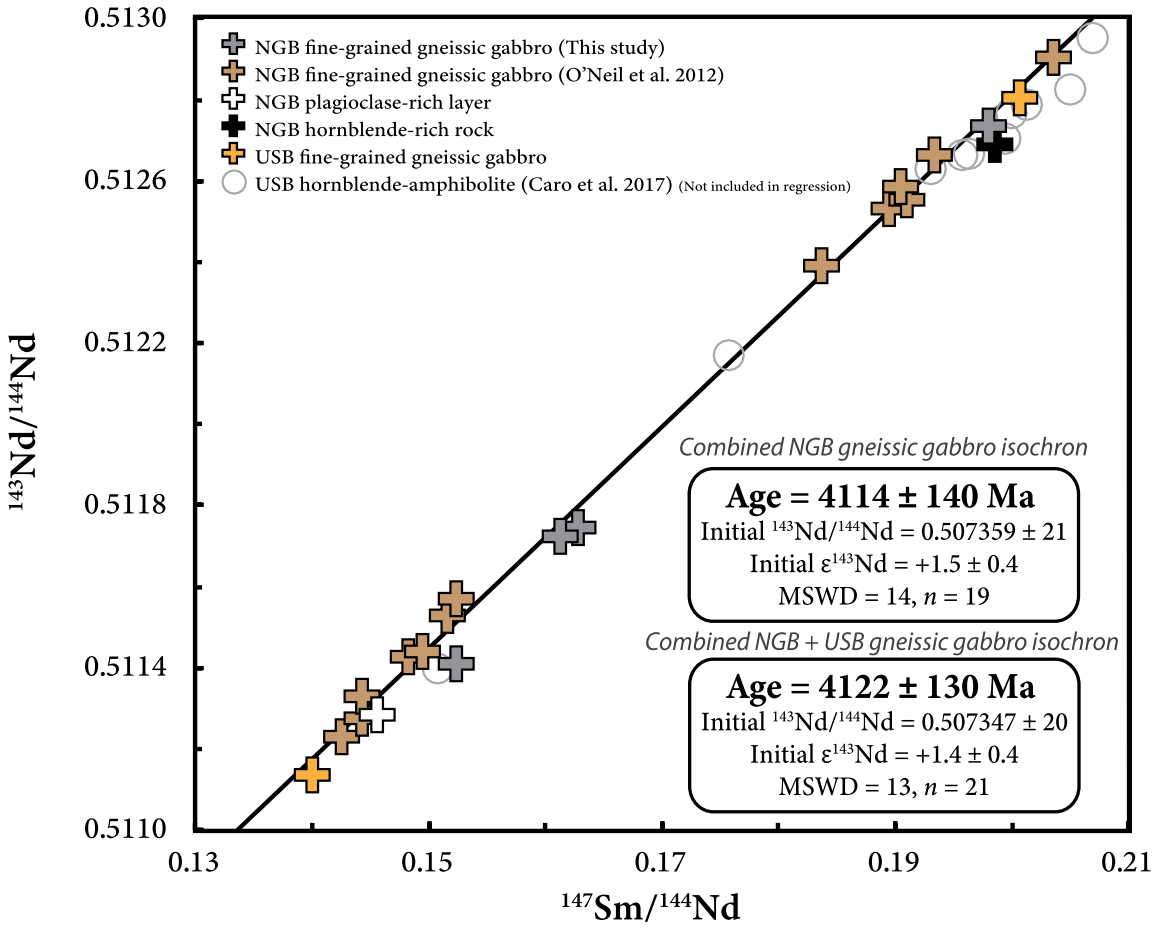

Figure 2.13: $^{147}Sm/^{144}Nd$ vs. $^{143}Nd/^{144}Nd$ isochron diagram for the NGB and USB fine-grained gneissic gabbros. Same symbols as in Figure 2.4. Additional symbols: Brown plusses = fine-grained gneissic gabbro data from O'Neil et al. (2012); Grey circles = USB enriched and tholeiitic hornblende-amphibolite data from Caro et al. (2017), not included in regression.

2.5.2 Evidence for Hadean magmatism in the Northeastern Superior Province

The ^{147}Sm-^{143}Nd isotopic composition of the fine-grained gabbroic sills suggests the preservation of Hadean rocks in the NGB. Similar gabbroic rocks are found in a small enclave mostly composed of mafic and ultramafic lithologies referred to as the Ukaliq Supracrustal Belt (USB), located a few kilometers northeast of the NGB. Caro et al. (2017) noted that the USB mafic and ultramafic rocks shared some geochemical similarities with the NGB Ujaraaluk unit and suggested that the mafic hornblende-plagioclase amphibolites in the USB could represent a less altered version of the Ujaraaluk unit and therefore better reflect primary characteristics of their parental magmas. They divided the amphibolites into tholeiitic, boninitic, transitional and enriched geochemical groups, similarly to the NGB Ujaraaluk unit. Detailed petrological and geochemical comparison between the NGB and the USB is difficult due to the limited exposure of the USB mostly consisting of ultramafic rocks, but one striking difference is the lack of cummingtonite-amphibolites in the USB that are so dominant in the NGB. During the fieldwork we conducted on the USB, only rare thin occurrences of cummingtonite-amphibolites were found. A single amphibolite sample was classified as "enriched amphibolite" by Caro et al. (2017), whereas the "enriched Ujaraaluk unit" is the most prominent geochemical group in the NGB. The USB "boninitic amphibolites" also have distinctively lower Al/Ti ratios compared to the NGB "boninitic Ujaraaluk" rocks, for which the high Al/Ti ratio is their most distinctive geochemical feature. The USB "tholeiitic amphibolites" share geochemical affinities with the NGB "tholeiitic Ujaraaluk unit", but O'Neil et al. (2019) noted that most USB amphibolites are actually mineralogically, texturally, and compositionally more similar to the NGB fine-grained gneissic gabbro sills rather than the Ujaraaluk unit. They also suggested that the USB enriched and tholeiitic amphibolites could be equivalent to the more differentiated and unfractionated portions of the

NGB mafic sills. In fact, the Ukaliq samples considered by Caro et al. (2017) as the "best preserved" samples yielded a scattered isochron with an age of 3963 ± 250 Ma (MSWD = 613). If only the tholeiitic and enriched amphibolites are considered (the samples we interpret as equivalent to the differentiated fine-grained gabbros), the age of the regression becomes 4052 ± 310 Ma, yet Caro et al. (2017) interpreted the age of emplacement of the Ukaliq rocks at 3.75 Ga.

Two hornblende-plagioclase amphibolite samples from Ukaliq were analyzed for their ^{147}Sm-^{143}Nd compositions in this study. Both samples are petrologically similar to the NGB fine-grained gneissic gabbros and display a wide range of Sm/Nd ratios which would be consistent with different degrees of differentiation. Although a two-point isochron may not be as statistically robust, a regression line through both USB data points from this study yields a ^{147}Sm-^{143}Nd age of 4163 ± 83 Ma, overlapping with the age of 4114 ± 140 Ma defined by the whole suite of NGB gabbros. Both USB amphibolites analyzed here have ^{147}Sm-^{143}Nd isotopic compositions comparable to the NGB fine-grained gneissic gabbros. They cover the full range of $^{147}Sm/^{144}Nd$ ratios measured in the NGB gabbros and also plot on the same best-fit regression line (Figure 2.13). When the NGB and USB gabbroic samples are combined, the ^{147}Sm-^{143}Nd isochron yields an age of 4122 ± 130 Ma (MSWD = 13, n = 21) with an initial $^{143}/^{144}Nd$ ratio of 0.507347 ± 0.000020 corresponding to an initial $\varepsilon^{143}Nd$ value of +1.4 ± 0.4 (Figure 2.13). Figure 2.13 also shows that the USB samples classified as tholeiitic and enriched amphibolites by Caro et al. (2017) follow the same $^{147}Sm/^{144}Nd$ vs. $^{143}Nd/^{144}Nd$ trend as the NGB fine-grained gneissic gabbro sills. This may suggest that the Hadean mafic magmatic event that we propose was recorded by the Nuvvuagittuq fine-grained gneissic gabbro sills was also preserved in the Ukaliq Supracrustal Belt, and thus in a larger extent of the Northeastern Superior Province.

2.5.3 Mantle evolution in the Nuvvuagittuq Greenstone Belt

Approximately 1.5 billion years of mafic magmatism is preserved in the NGB including the ~4.3 Ga Ujaraaluk unit and its cogenetic ultramafic cumulates (O'Neil et al., 2008, 2012), the 4.1 Ga fine-grained gneissic gabbros (O'Neil et al., 2012, this study) and the ~2.8 Ga coarse-grained undeformed gabbros (Benn, 2018; Plakholm, 2019). These multiple generations of mantle-derived mafic rocks present a unique opportunity to gain an insight on the early mantle evolution during the Hadean and Archean eons. O'Neil et al. (2012) have shown that the long-lived ^{147}Sm-^{143}Nd isotopic system has been partially disturbed in the Ujaraaluk unit, but they identified a suite of least disturbed samples defining an isochron yielding an age of 4.32 Ga with an initial εNd of +0.5. The long-lived Nd isotopic composition of the Ujaraaluk unit should however be used with caution to asses the isotopic composition of their source. Nevertheless, both the Ujaraaluk unit and fine-grained gneissic gabbros yield initial ε^{143}Nd values that are consistent with a source compositionally similar to the depleted mantle at 4.3 Ga and 4.1 Ga, respectively. This contrasts with the coarse-grained undeformed gabbros exhibiting a lower ε^{143}Nd compared to the depleted mantle at ~2.8 Ga (Figure 2.14). Interestingly, the fine-grained gneissic gabbros and coarse-grained undeformed gabbros display similar initial ε^{143}Nd values of $+1.4 \pm 0.4$ and $+1.1 \pm 0.3$, respectively, despite their nearly 1.3 billion year age difference.

If both generations of gabbros were derived from a common mantle source, this source would have been produced from an early depletion event to evolve to slightly radiogenic εNd compared to CHUR by 4.1 Ga, to then evolve with a near chondritic Sm/Nd ratio for over 1 billion (Figure 2.14). A similar trend is found in the Archean Saglek-Hebron Complex in northern Labrador, where multiple generations of mantle-derived rocks exhibit comparable initial εNd values between +1.7 and +1.8 for over 800 million years, between ~3.5 Ga and ~2.7 Ga (Flageole,

2019). If both generations of Nuvvuagittuq gabbros are rather derived from distinct mantle sources, the εNd value of +1.1 at 2.8 Ga of the undeformed gabbros would suggest a slightly suprachondritic mantle source, yet not as depleted as the "normal" depleted mantle. Their flat LREE profiles also argue against an enriched mantle source.

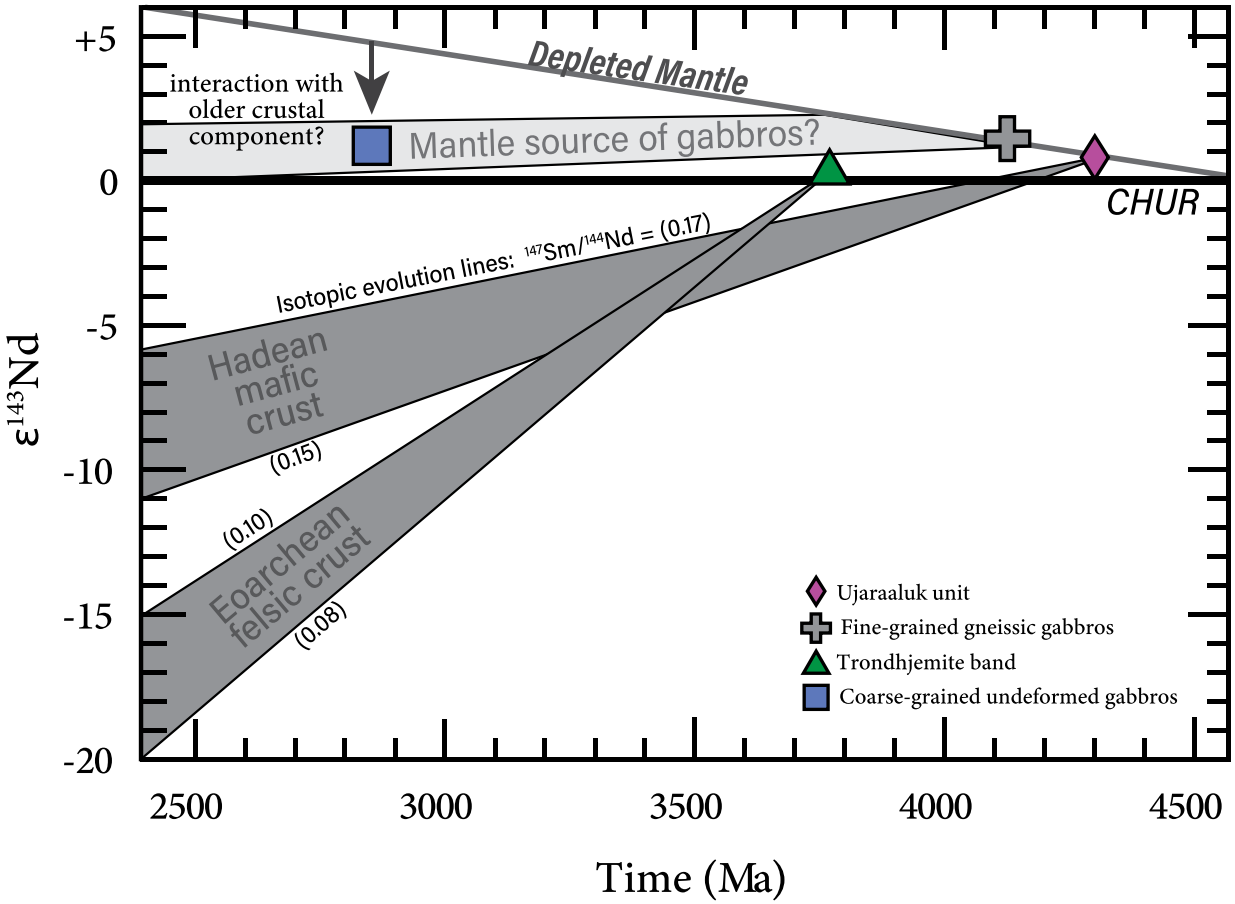

Figure 2.14: Initial $\varepsilon^{143}Nd$ values of the NGB Ujaraaluk unit, fine-grained gneissic gabbros, trondhjemite band and coarse-grained undeformed gabbros vs. Time (Ma). Age and $\varepsilon^{143}Nd$ values for the Ujaraaluk unit and trondhjemite band are from O'Neil et al. (2012), age and $\varepsilon^{143}Nd$ value for the coarse-grained undeformed gabbros are from Benn (2018) and age and $\varepsilon^{143}Nd$ value of the NGB fine-grained gneissic gabbros are from Figure 2.13. Light grey area represents a hypothetical $^{147}Sm/^{144}Nd$ isotopic evolution line if the NGB fine-grained gneissic gabbros and coarse-grained undeformed gabbros share a similar mantle source. Dark grey areas represent average $^{147}Sm/^{144}Nd$ isotopic evolution lines ranging from 0.17 to 0.15 for the Ujaraaluk unit (Hadean mafic crust) and from 0.10 to 0.08 for the trondhjemite band (Eoarchean felsic crust) (O'Neil et al., 2012). Abbreviation: CHUR = Chondritic Uniform Reservoir. Symbols: Purple diamond = Ujaraaluk unit; Grey plus = Fine-grained gneissic gabbros; Green triangle = Trondhjemite band; Blue square = Coarse-grained undeformed gabbros.

Alternatively, the involvement of an older crustal component in the source of the Neoarchean undeformed gabbros could account for their unradiogenic εNd value relative to the depleted mantle. This scenario is supported by the observation that these Neoarchean coarse-grained gabbros have much older T_{DM} ages between 3.3 and 4.5 Ga, compared to their crystallization of 2.8 Ga (Benn, 2018). If the interaction with an older crustal component is responsible for the isotopic composition of the coarse-grained undeformed gabbros, it had to exhibit low εNd values by the time of emplacement of the undeformed gabbros to account for their initial $\varepsilon^{143}Nd$ value of +1.1 at 2.8 Ga. Two potential candidates arise in this scenario: the 4.3 Ga Ujaraaluk unit and the Eo-to Paleoarchean TTGs surrounding and locally intruding the NGB (Figure 2.14). The Neoarchean gabbros are commonly intruding the Ujaraaluk unit which could represent a source contaminant given its estimated low εNd of -5 to -9 at 2.8 Ga (Figure 2.14), but it is unlikely that gabbroic magmas assimilated significant amounts of mafic crust given the higher temperature required to remelt basaltic crust. However, Glazner et al. (1991) observed a possible interaction of mantle-derived basaltic magmas and pre-existing mafic continental crust in the Pisgah and Amboy craters in southern California. The possibility of interaction with the mafic Ujaraaluk unit therefore cannot be discarded. However, given the similar Nd concentrations of the most enriched Ujaraaluk and the undeformed gabbros, it would require at least 25-30% mixing to account for the difference between the Nd isotopic composition of the depleted mantle at 2.8 Ga and the εNd value of +1.1 of the coarse-grained gabbros (assuming respective Nd concentrations of 7 ppm and 10 ppm for the undeformed gabbros and Ujaraaluk, and $\varepsilon Nd_{(2.8Ga)}$ value of -7 for the Ujaraaluk unit). Future ^{142}Nd analyses in the coarse-grained undeformed gabbros could help provide further evidence supporting or opposing the Ujaraaluk unit as the potential source contaminant.

Silicic crust has much lower solidus temperatures and commonly higher Nd concentrations in comparison to mafic crust and the low initial εNd of the undeformed gabbros relative to the depleted mantle could suggest the involvement of felsic crust as a source contaminant. By 2.8 Ga, the Nuvvuagittuq Eoarchean TTG would have evolved to low εNd values between -11 and -14 (Figure 2.14) and it would only require between 10 and 15% mixing between the gabbroic magma and the Eoarchean TTG to lower the εNd of the undeformed gabbro to +1.1, assuming they were derived from the depleted mantle and considering Nd concentration of 15-20 ppm for the TTG. However, the coarse-grained gabbros display relatively flat REE profiles (Figure 2.6B; see also Benn, 2018) which supports limited involvement, if any, of a LREE-enriched Eoarchean TTG as the source contaminant. Even if it is difficult to constrain the exact source contaminant, the low initial εNd values and deficits in ^{142}Nd measured in a number of Neoarchean TTGs from the Hudson Bay terrane (Boily et al., 2009; O'Neil and Carlson, 2017) suggest that an early enriched crustal reservoir was involved in the stabilization of the Northeastern Superior Province and could potentially have affected the initial isotopic composition of the Nuvvuagittuq Neoarchean undeformed gabbros.

2.6 Conclusion

As potentially the oldest rocks on Earth, confirming the Hadean age of the Nuvvuagittuq Greenstone Belt has significant implications on understanding some of the first geological processes to have operated on Earth. Although it is at least Eoarchean, the disagreement on the exact age of the NGB has been ongoing for nearly a decade. The intrusive nature of the fine-grained gneissic gabbro sills and the fact that they exhibit limited geochemical and isotopic disturbance potentially makes them ideal rocks to firmly constrain the minimum age of the NGB.

Zircons retrieved from two compositionally evolved gneissic gabbros and from a plagioclase-rich evolved layer within the gneissic gabbros yielded Neoarchean ages between ~2.6 and ~2.8 Ga. These zircon ages are however more consistent to be reflective of the regional metamorphism or may be recording the breakdown of primary igneous baddeleyites to form polycrystalline zircon. Nonetheless, the zircon U-Pb ages recorded in the gneissic gabbro sills do not constrain their emplacement age. However, a new sampling strategy targeting petrologically distinct portions of the fine-grained gabbros, interpreted to represent the most evolved liquids and cumulate portions formed through igneous differentiation within the large sills, yielded an Sm-Nd isochron age of 4.15 Ga. The identical age obtained when only the hornblende-rich and plagioclase-rich samples are considered, equivalent to an internal isochron, strongly supports that it represents the age of magmatic differentiation rather than an artefact from mixing with an unknown Hadean enriched reservoir. The Nuvvuagittuq fine-grained gabbro sills would therefore represent rare Hadean rocks preserved on Earth. The comparable Nd isotopic compositions exhibited by gabbroic rocks from the nearby Ukaliq Supracrustal Belt hints at the fact that a larger extent of Hadean crust may be preserved in the Hudson Bay terrane of the Northeastern Superior Province.

References

Augland, L. E., & David, J. (2015). Protocrustal evolution of the Nuvvuagittuq Supracrustal Belt as determined by high precision zircon Lu-Hf and U-Pb isotope data. Earth and Planetary Science Letters, 428, 162–171.

Benn, D. (2018). An Isotopic and Geochemical comparison of gabbro sills from the Nuvvuagittuq Greenstone Belt, Northern Quebec. BSc Thesis: University of Ottawa, 43 p.

Boily, M., Leclair, A., Maurice, C., Bédard, J. H., & David, J. (2009). Paleo- to Mesoarchean basement recycling and terrane definition in the Northeastern Superior Province, Québec, Canada. Precambrian Research, 168(1–2), 23–44.

Bouvier, A., Vervoort, J. D., & Patchett, P. J. (2008). The Lu-Hf and Sm-Nd isotopic composition of CHUR: Constraints from unequilibrated chondrites and implications for the bulk composition of terrestrial planets. Earth and Planetary Science Letters, 273(1–2), 48–57.

Bouvier, A., & Wadhwa, M. (2010). The age of the Solar System redefined by the oldest Pb-b age of a meteoritic inclusion. Nature Geoscience, 3(9), 637–641.

Bowring, S. A., & Williams, I. S. (1999). Priscoan (4.00-4.03 Ga) orthogneisses from northwestern Canada. Contributions to Mineralogy and Petrology, 134(1), 3–16.

Byerly, B. L., Lowe, D. R., Drabon, N., Coble, M. A., Burns, D. H., & Byerly, G. R. (2018). Hadean zircon from a 3.3 Ga sandstone, Barberton greenstone belt, South Africa. Geology, 46(11), 967–970.

Card, K. D., & Ciesielski, A. (1986). DNAG #1; Subdivisions of the Superior Province of the Canadian Shield. Geoscience Canada, 13(1), 5–13.

Carlson, R. W., Garçon, M., O'Neil, J., Reimink, J., & Rizo, H. (2019). The nature of Earth's first crust. Chemical Geology, 530, 119321.

Caro, G., Morino, P., Mojzsis, S. J., Cates, N. L., & Bleeker, W. (2017). Sluggish Hadean geodynamics: Evidence from coupled $^{146,147}Sm$–$^{142,143}Nd$ systematics in Eoarchean supracrustal rocks of the Inukjuak domain (Québec). Earth and Planetary Science Letters, 457, 23–37.

Cates, N. L., & Mojzsis, S. J. (2007). Pre-3750 Ma supracrustal rocks from the Nuvvuagittuq supracrustal belt, northern Québec. Earth and Planetary Science Letters, 255(1–2), 9–21.

Cates, N. L., & Mojzsis, S. J. (2009). Metamorphic zircon, trace elements and Neoarchean metamorphism in the ca. 3.75 Ga Nuvvuagittuq supracrustal belt, Québec (Canada). Chemical Geology, 261(1–2), 99–114.

Cates, N. L., Ziegler, K., Schmitt, A. K., & Mojzsis, S. J. (2013). Reduced, reused and recycled: Detrital zircons define a maximum age for the Eoarchean (ca. 3750-3780Ma) Nuvvuagittuq Supracrustal Belt, Québec (Canada). Earth and Planetary Science Letters, 362, 283–293.

Corfu, F., Hanchar, J. M., Hoskin, P. W. O., & Kinny, P. (2003). Atlas of zircon textures. In J. M. Hanchar, & P. W. O. Hoskin (Eds.), Zircon, Reviews in Mineralogy and Geochemistry, 53, Mineralogical Society of America, Washington, D.C., pp. 469–500.

Darling, J. R., Moser, D. E., Heaman, L. M., Davis, W. J., O'Neil, J., & Carlson, R. (2013). Eoarchean to neoarchean evolution of the Nuvvuagittuq Supracrustal belt: New insights from U-Pb zircon geochronology. American Journal of Science, 313(9), 844–876.

David, J., Godin, L., Stevenson, R., O'Neil, J., & Francis, D. (2009). U-Pb ages (3.8-2.7 Ga) and Nd isotope data from the newly identified Eoarchean Nuvvuagittuq supracrustal belt, superior Craton, Canada. Bulletin of the Geological Society of America, 121(1–2), 150–163.

Davidson, A., & Van Breemen, O. (1988). Baddeleyite-zircon relationships in coronitic metagabbro, Grenville Province, Ontario: implications for geochronology. Contributions to Mineralogy and Petrology, 100, 291–299.

Dodd, M. S., Papineau, D., Grenne, T., Slack, J. F., Rittner, M., Pirajno, F., O'Neil, J., & Little, C. T. S. (2017). Evidence for early life in Earth's oldest hydrothermal vent precipitates. Nature, 543(7643), 60–64.

Flageole, J. (2019). Sm-Nd Isotopic Composition of Mantle-Derived Rocks from the Saglek-Hebron Gneiss Complex, Northern Labrador. MSc Thesis: University of Ottawa, 112 p.

Glazner, A. F., Farmer, G. L., Hughes, W. T., Wooden, J. L., & Pickthorn, W. (1991). Contamination of basaltic magma by mafic crust at Amboy and Pisgah craters, Mojave Desert, California. Journal of Geophysical Research, 96(B8), 13673–13691.

Guitreau, M., Blichert-Toft, J., Mojzsis, S. J., Roth, A. S. G., & Bourdon, B. (2013). A legacy of Hadean silicate differentiation inferred from Hf isotopes in Eoarchean rocks of the Nuvvuagittuq supracrustal belt (Québec, Canada). Earth and Planetary Science Letters, 362, 171–181.

Heaman, L. M., & LeCheminant, A. N. (1993). Paragenesis and U-Pb systematics of baddeleyite (ZrO2). Chemical Geology, 110(1–3), 95–126.

Hurai, V., Paquette, J.-L., Huraiova, M., & Konecny, P. (2010). Age of deep crustal magmatic chambers in the intra-Carpathian back-arc basin inferred from LA-ICPMS U-Th-Pb dating of zircon and monazite from igneous xenoliths in alkali basalts. Journal of Volcanology and Geothermal Research, 198, 275–287.

Jackson, S. E., Pearson, N. J., Griffin, W. L., & Belousova, E. A. (2004). The application of laser ablation-inductively coupled plasma-mass spectrometry to in situ U-Pb zircon geochronology. Chemical Geology, 211(1–2), 47–69.

Keil, K., & Fricker, P. E. (1974). Baddeleyite (ZrO2) in Gabbroic Rocks from Axel Heiberg Island, Canadian Arctic Archipelago. American Mineralogist, 59(3–4), 249–253.

Leclair, A.D. (2005). Géologie du nord-est de la Province du Supérieur, Québec. Ministère des Ressources naturelles et de la Faune, DV 2004-04, 19 pages, 1 carte (échelle 1:750 000).

Le Maître, R. W. (2002). Igneous Rocks: A Classification and Glossary of Terms (2nd Edition). New York: Cambridge University Press.

Ludwig, K. R. (2012). User's Manual for Isoplot Version 3.75–4.15: A Geochronological Toolkit for Microsoft Excel. Berkeley Geochronological Center, Special Publication (Vol. 5).

Ludwig, K. R. (2001). Isoplot/Ex, version 2.49. A Geochronological Toolkit for Microsoft Excel. Berkeley Geochronological Center, Special Publication, 55 p.

Macquistan, M. (2020). New constraints on the crustal evolution of the Northeastern Superior Province revealed by U-Pb-Hf on zircons from Paleo to Mesoarchean granitoids. BSc Thesis: University of Ottawa, 36 p.

Marks, N. E., Borg, L. E., Hutcheon, I. D., Jacobsen, B., & Clayton, R. N. (2014). Samarium-neodymium chronology and rubidium-strontium systematics of an Allende calcium-aluminum-rich inclusion with implications for 146Sm half-life. Earth and Planetary Science Letters, 405(1777), 15–24.

Mullen, E. K., Paquette, J. L., Tepper, J. H., & McCallum, I. S. (2018). Temporal and spatial evolution of Northern Cascade Arc magmatism revealed by LA–ICP–MS U–Pb zircon dating. Canadian Journal of Earth Sciences, 55(5), 443–462.

Nadeau, P. (2003). Structural investigation of the Porpoise Cove area, Northeastern Superior Province, Northern Quebec. MSc Thesis: Simon Fraser University, 95 p.

O'Neil, J., Boyet, M., Carlson, R. W., & Paquette, J. L. (2013). Half a billion years of reworking of Hadean mafic crust to produce the Nuvvuagittuq Eoarchean felsic crust. Earth and Planetary Science Letters, 379, 13–25.

O'Neil, J., & Carlson, R. W. (2017). Building Archean cratons from Hadean mafic crust. Science, 355(6330), 1199–1202.

O'Neil, J., Carlson, R. W., Francis, D., & Stevenson, R. K. (2008). Neodymium-142 evidence for hadean mafic crust. Science, 321(5897), 1828–1831.

O'Neil, J., Carlson, R. W., Papineau, D., Levine, E. Y., & Francis, D. (2019). The Nuvvuagittuq Greenstone Belt: A Glimpse of Earth's earliest crust. In M. J. Van Kranendonk, V. C. Bennett, & J. E. Hoffmann (Eds.), Earth's Oldest Rocks. Amsterdam: Elsevier, pp. 349–374.

O'Neil, J., Carlson, R. W., Paquette, J. L., & Francis, D. (2012). Formation age and metamorphic history of the Nuvvuagittuq Greenstone Belt. Precambrian Research, 220–221, 23–44.

O'Neil, J., Francis, D., & Carlson, R. W. (2011). Implications of the Nuvvuagittuq Greenstone Belt for the Formation of Earth's Early Crust. Journal of Petrology, 52(5), 985–1009.

O'Neil, J., Maurice, C., Stevenson, R. K., Larocque, J., Cloquet, C., David, J., & Francis, D. (2007). The Geology of the 3.8 Ga Nuvvuagittuq (Porpoise Cove) Greenstone Belt, Northeastern Superior Province, Canada. In M. J. van Kranendonk, R. H. Smithies, & V. C. Bennett (Eds.), Earth's Oldest Rocks, Developments in Precambrian Geology, 15, Amsterdam: Elsevier, pp. 219–250.

O'Neil, J., Rizo, H., Boyet, M., Carlson, R. W., & Rosing, M. T. (2016). Geochemistry and Nd isotopic characteristics of Earth's Hadean mantle and primitive crust. Earth and Planetary Science Letters, 442, 194–205.

Paquette, J.-L., Barbosa, J. S. F., Rohais, S., Cruz, S. C. P., Goncalves, P., Peucat, J. J., Leal, A. B. M., Santos-Pinto, M., & Martin, H. (2015). The geological roots of South America: 4.1Ga and 3.7Ga zircon crystals discovered in N.E. Brazil and N.W. Argentina. Precambrian Research, 271, 49–55.

Paquette, J.-L., Piro, J.-L., Devidal, J.-L., Bosse, V., Didier, A., Sannac, S., & Abdelnour, Y. (2014). Sensitivity Enhancement in LA-ICP-MS by N2 Addition to Carrier Gas: Application to Radiometric Dating of U-Th-Bearing Minerals. Agilent ICP-MS Journal, 58, 4–5.

Peng, P., Bleeker, W., Ernst, R. E., Söderlund, U., & McNicoll, V. (2011). U-Pb baddeleyite ages, distribution and geochemistry of 925Ma mafic dykes and 900Ma sills in the North China craton: Evidence for a Neoproterozoic mantle plume. Lithos, 127(1–2), 210–221.

Percival, J. A., & Card, K.D. (1994). Geology, Lac Minto - Rivière aux Feuilles. Geological Survey of Canada; Map 1854A, scale 1/500 000.

Percival, J. A., Mortensen, J. K., Stern, R. A., Card, K. D., & Begin, N. J. (1992). Giant granulite terranes of northeastern Superior Province: the Ashuanipi complex and Minto block. Canadian Journal of Earth Sciences, 29(10), 2287–2308.

Percival, J. A., & Skulski, T. (2000). Tectonothermal evolution of the northern Minto block, Superior Province, Quebec, Canada. Canadian Mineralogist, 38(2), 345–378.

Percival, J.A., Skulski, T. & Card, K.D. (1995). Geology, Rivière Kogaluc - Lac Qalluviartuuq region (parts of 34J and 34O). Geological Survey of Canada; Open file 3112.

Percival, J.A., Skulski, T. & Nadeau, L. (1996). Geology, Lac Couture, Quebec. Geological Survey of Canada; Open file 3315.

Percival, J.A., Skulski, T. & Nadeau, L. (1997). Reconnaissance geology of the Pelican - Nantais belt, northeastern Superior province, Quebec. Geological Survey of Canada; Open file 3525.

Percival, J.A., Skulski, T., Sanborn-Barrie, M., Stott, G.M., Leclair, A.D., Corkery, M.T., & Boily, M. (2012). Geology and tectonic evolution of the Superior Province, Canada. In J.A. Percival, F.A. Cook, & R.M. Clowes (Eds.), Tectonic Styles in Canada: The LITHOPROBE Perspective. Geological Association of Canada, Special Paper 49, pp. 321–378.

Plakholm, J. (2019). Lu-Hf isotopic compositions of gabbroic intrusions from the Nuvvuagittuq Greenstone Belt, Quebec. BSc Thesis: Carleton University.

Reimink, J. R., Chacko, T., Stern, R. A., & Heaman, L. M. (2016). The birth of a cratonic nucleus: Lithogeochemical evolution of the 4.02-2.94 Ga Acasta Gneiss Complex. Precambrian Research, 281, 453–472.

Roth, A. S. G., Bourdon, B., Mojzsis, S. J., Touboul, M., Sprung, P., Guitreau, M., & Blichert-Toft, J. (2013). Inherited 142Nd anomalies in Eoarchean protoliths. Earth and Planetary Science Letters, 361, 50–57.

Rubatto, D. (2017). Zircon: The Metamorphic Mineral. Reviews in Mineralogy and Geochemistry, 83(1), 261–295.

Silveira, E. M., Söderlund, U., Oliveira, E. P., Ernst, R. E., & Leal, A. B. M. (2013). First precise U-Pb baddeleyite ages of 1500Ma mafic dykes from the São Francisco Craton, Brazil, and tectonic implications. Lithos, 174, 144–156.

Simard, M., Parent, M., David, J., & Sharma, K. N. M. (2003). Géologie de la région de la rivière Innuksuac (34K et 34L). Ministère des Ressources naturelles, Québec; RG 2002-10, 46 pages.

Söderlund, U., Hellström, F. A., & Kamo, S. L. (2008). Geochronology of high-pressure mafic granulite dykes in SW Sweden: Tracking the P-T-t path of metamorphism using Hf isotopes in zircon and baddeleyite. Journal of Metamorphic Geology, 26(5), 539–560.

Söderlund, U., Ibanez-Mejia, M., El Bahat, A., Ernst, R. E., Ikenne, M., Soulaimani, A., Youbi, N., Cousens, B., El Janati, M., & Hafid, A. (2013). Reply to Comment on "U-Pb baddeleyite ages and geochemistry of dolerite dykes in the Bas-Drâa inlier of the Anti-Atlas of Morocco: Newly identified 1380Ma event in the West African Craton" by André Michard and Dominique Gasquet. In Lithos (Vol. 174, pp. 101–108).

Söderlund, U., Isachsen, C. E., Bylund, G., Heaman, L. M., Patchett, P. J., Vervoort, J. D., & Andersson, U. B. (2005). U-Pb baddeleyite ages and Hf, Nd isotope chemistry constraining repeated mafic magmatism in the Fennoscandian Shield from 1.6 to 0.9 Ga. Contributions to Mineralogy and Petrology, 150(2), 174–194.

Stevenson, I. M. (1968). A geological reconnaissance of Leaf River map-area, New Quebec and Northwest Territories. Geological Survey of Canada; Memoire, 356.

Sun, S. S., & McDonough, W. F. (1989). Chemical and isotopic systematics of oceanic basalts: Implications for mantle composition and processes. Geological Society Special Publication, 42(1), 313–345.

Tanaka, T., Togashi, S., Kamioka, H., Amakawa, H., Kagami, H., Hamamoto, T., Yuhara, M., Orihashi, Y., Yoneda, S., Shimizu, H., Kunimaru, T., Takahashi, K., Yanagi, T., Nakano, T., Fujimaki, H., Shinjo, R., Asahara, Y., Tanimizu, M., & Dragusanu, C. (2000). JNdi-1: A neodymium isotopic reference in consistency with LaJolla neodymium. Chemical Geology, 168(3–4), 279–281.

Turner, S., Rushmer, T., Reagan, M., & Moyen, J. F. (2014). Heading down early on? Start of subduction on earth. Geology, 42(2), 139–142.

van Achterbergh, E., Ryan, C. G., Jackson, S. E., & Griffin, W. L. (2001). Data reduction software for LA-ICP-MS. In P. J. Sylvester (Ed.), Laser Ablation-ICPMS in the Earth Sciences, Mineralogical Association of Canada, 29, pp. 239–243.

Vermeesch, P. (2004). How many grains are needed for a provenance study? Earth and Planetary Science Letters, 224(3–4), 441–451.

Wang, H., Chen, L., Sun, Y., Liu, X., Xu, X., Chen, J., Zhang, H., & Diwu, C. (2007). ~4.1 Ga xenocrystal zircon from Ordovician volcanic rocks in western part of North Qinling Orogenic Belt. Chinese Science Bulletin, 52(21), 3002–3010.

Wiedenbeck, M., Allé, P., Corfu, F., Griffin, W. L., Meier, M., Oberli, F., von Quadt, A., Roddick, J. C., & Spiegel, W. (1995). Three natural zircon standards for U-Th-Pb, Lu-Hf, trace element and REE analyses. Geostandards Newsletter, 19(1), 1–23.

Wilde, S. A., Valley, J. W., Peck, W. H., & Graham, C. M. (2001). Evidence from detrital zircons for the existence of continental crust and oceans on the Earth 4.4 Gyr ago. Nature, 409(6817), 175–178.

Xing, G. F., Wang, X. L., Wan, Y., Chen, Z. H., Jiang, Y., Kitajima, K., Ushikubo, T., & Gopon, P. (2014). Diversity in early crustal evolution: 4100 Ma zircons in the Cathaysia Block of southern China. Scientific Reports, 4(1), 1–8.

Chapter 3

Petrogenesis of the Eoarchean to Paleoarchean felsic crust in the Northeastern Superior Province, Canada: Insights from zircon U-Pb, trace element and oxygen isotope compositions

3.1 Introduction

Archean cratons are dominated by silica-rich rocks from the tonalite-trondhjemite-granodiorite (TTG) series. Nearly 50 years of TTG research have shown that they are likely produced by the melting of garnet-bearing metamafic rocks and that they are geochemically different from modern granitoids, suggesting that they may have formed through petrogenetic processes unique to the Archean (e.g. Moyen and Martin, 2012 and references therein). However, there is very little preserved felsic crust older than 3.5 Ga. The terranes that host these >3.5 TTGs have also commonly undergone complex thermal histories which can hinder our knowledge and understanding of how and when early continental crust formed. Zircon is a common accessory mineral found in TTGs and serves as a great geochronological and petrological tool due to its chemical and physical resistance to high temperature and pressure events. Zircon is commonly analyzed for its U-Pb/Hf/O isotope and trace element compositions which enables us to extract valuable information regarding the conditions under which it crystallized (i.e. Hoskin and Schaltegger, 2003; Valley, 2003). Detailed zircon studies correlate with a better comprehension of TTG petrogenesis and thus provide a more exhaustive understanding of how ancient continents formed and stabilized.

Some of the oldest known TTGs of the Superior Craton are located in the Tikkerutuk domain of the Northeastern Superior Province (NESP), namely around the Nuvvuagittuq Greenstone Belt (NGB) interpreted to be at least 3.77 Ga and potentially as old as 4.3 Ga, which would make it the oldest crustal remnant preserved on Earth (e.g. O'Neil et al., 2019). Because they could represent the oldest rocks on Earth, most studies in the NGB area have focussed on the mafic supracrustal rocks and the chemical sediments within the belt itself. However, multiple generations of granitoids with ages of 3.76 Ga, 3.66 Ga, 3.51 Ga, 3.35 Ga, 2.99 Ga and 2.69 Ga

(Darling et al., 2013; David et al., 2009; Macquistan, 2020; O'Neil et al., 2013) surround and locally intrude the NGB. This episodic felsic magmatism occurring over 1 billion years and covering almost the entire Archean Eon presents a great opportunity to study the evolution and petrogenetic processes responsible for the production of early continental crust.

In this chapter, we present new zircon U-Pb data from trondhjemites intruding or in direct contact with the NGB, as well as from one granitoid sample from the nearby Ukaliq Supracrustal Belt, in order to better constrain the timing of felsic magmatism around the NGB. We also present new trace element compositions and oxygen isotope data for a series of zircons from multiple granitoid generations that have previously been analyzed for their U-Pb and Hf isotope compositions and dated between 3.3 and 3.8 Ga (O'Neil et al., 2013). This zircon data is then used to gain a more detailed insight on the petrogenetic processes that helped formed the multiple generations of granitoids in the area. Finally, we compare our zircon data to those of other Hadean and Archean terranes found across the globe.

3.2 Geological Setting

The Northeastern Superior Province (NESP), located in northern Quebec, Canada, is mostly composed of Neoarchean granitoids including a tonalite-trondhjemite suite, a granodiorite-granite suite and a pyroxene-bearing tonalite-trondhjemite suite (Boily et al., 2009) in which thin remnants of amphibolite- to granulite-grade greenstone belts can be traced along strike (Leclair, 2005; Percival and Card, 1994; Percival et al., 1995, 1996, 1997). Mapping, U/Pb geochronology and Nd isotopic data have suggested that the NESP can be divided into two distinct terranes: the Arnaud River terrane to the east and the Hudson Bay terrane to the west (Boily et al., 2009) (Figure 3.1). The Arnaud River terrane is characterized by juvenile Nd isotopic compositions yielding

depleted-mantle model ages (T_{DM}) <3.0 Ga whereas the Hudson Bay terrane is defined by low Nd isotopic values with T_{DM} ages as old as 4.4 Ga and inherited zircon core ages older than 3.0 Ga (Boily et al., 2009 and references therein; O'Neil et al., 2012; O'Neil and Carlson, 2017). The Hudson Bay terrane has thus been interpreted to represent the nucleus of the NESP (Boily et al., 2009), with evidence for the contribution of older crust in its petrogenesis.

O'Neil and Carlson (2017) have suggested that reworking of a Hadean mafic crust was an important process in the formation of the Neoarchean TTG from the Hudson Bay terrane. This was supported by the fact that tonalites and trondhjemites from the Loup Marin and Favard suites of the NESP yielded deficits in ^{142}Nd compared to the terrestrial Nd standard (O'Neil and Carlson, 2017). Variations in μ^{142}Nd values,

$$\text{where } \left(\mu^{142}Nd = \frac{^{142}Nd/^{144}Nd_{sample} - ^{142}Nd/^{144}Nd_{terrestrial\ standard}}{^{142}Nd/^{144}Nd_{terrestrial\ standard}} \times 10^6 \right),$$

can only be produced by Sm-Nd fractionation in the Hadean, due to the short half-life of the parent isotope (^{146}Sm) of 103 million years (Marks et al., 2014). Given the Neoarchean age of the granitoids from the Hudson Bay terrane, O'Neil and Carlson (2017) attributed their ^{142}Nd deficits (as low as -15) compared to modern terrestrial mantle to the reworking of a much older (>4.2 Ga) Hadean mafic crust. The Nuvvuagittuq Greenstone Belt located in the Tikkerutuk Domain of the Hudson Bay terrane may represent a remnant of this Hadean mafic crust. The dominant lithology of the belt, the Ujaraaluk unit, is interpreted to be a vestige of early mafic primitive oceanic crust (O'Neil et al., 2019). The correlation between μ^{142}Nd and Sm/Nd ratios in the mafic and ultramafic rocks of the Ujaraaluk unit was interpreted to represent an isochron yielding an age of nearly 4.3 Ga (O'Neil et al., 2008, 2012). This Hadean age is further supported by the 4.1 Ga ^{147}Sm-^{143}Nd

isochron age obtained in a pair of gneissic gabbro sills that intrude the Ujaraaluk, which impose a minimum age on the latter (Chapter 2 of this thesis). Despite the fact that the proposed Hadean age for the NGB remains debated (see O'Neil et al., 2019 for review), it is surrounded and locally intruded by TTG as old as 3.77 Ga (Cates and Mojzsis, 2007; Darling et al., 2013; David et al., 2009; O'Neil et al., 2013), representing the oldest felsic rocks from the Superior Province. The NGB area has recorded over 1 billion years of episodic felsic magmatism (Figure 3.1), making this part of the NESP ideal to study the early evolution of the continental crust.

The oldest U-Pb zircon ages in the NESP were obtained from thin, 10-30cm, discontinuous trondhjemitic bands that have only been found in the southwestern most part of the NGB. Due to the lack of zircon-bearing lithologies in the belt, these small trondhjemite bands have been dated extensively in several studies yielding ages from 3751 to 3817 Ma (Augland and David, 2015; Cates and Mojzsis, 2007; Darling et al., 2013; David et al., 2009; O'Neil et al., 2013). These trondhjemitic bands are interpreted as intruding the NGB and thus their mean ~3.76 Ga age is believed to establish a minimum age for the belt (Cates and Mojzsis, 2007; O'Neil et al., 2019).

A plutonic trondhjemite bordering the southern extent of the NGB was also dated at 3.76 Ga. Its exact same age, geochemical composition and Hf isotopic composition to the intruding trondhjemitic bands suggest that both lithologies share a common petrogenesis (O'Neil et al., 2013). Other generations of TTG magmatism in the region include a 3.66 Ga plutonic tonalite which borders the NGB's southern and western limit (David et al., 2009; O'Neil et al., 2013) and a slightly younger 3.51 Ga tonalite part of the Voizel Suite (Simard et al., 2003) is also found in the southern extremity of the NGB (O'Neil et al., 2013). TTGs with similar 3.66 Ga and 3.51 Ga ages have also recently been found surrounding the nearby Ukaliq Supracrustal Belt suggesting that these magmatic events are not only restricted to the surrounding areas of the NGB (Greer et

al., 2020). Younger granitoids surrounding the NGB include a 3.35 Ga plagioclase-quartz-biotite-bearing rock of unknown origin found within the western limb of the NGB that has been termed a "felsic schist" (David et al., 2009; O'Neil et al., 2013) and a 2.99 Ga granodiorite located in the northeastern extremity of the belt (Macquistan, 2020). The youngest felsic magmatic event recorded in the NGB is a 2.69 Ga granitic pegmatite synchronous with the Neoarchean regional metamorphic event (David et al., 2009).

The Eoarchean to Paleoarchean felsic plutonism surrounding the NGB displays typical Archean TTG compositions including a pronounced heavy rare earth element (HREE) depletion indicative of their derivation from a garnet-bearing mafic precursor (Moyen and Martin, 2012). Isotopic studies have suggested that the multiple generations of TTGs surrounding the NGB could be generated by the episodic remelting of a Hadean mafic precursor (O'Neil et al., 2012, 2013). This is supported by the εHf vs. time trend for zircons from Eoarchean to Mesoarchean granitoids (O'Neil et al., 2013), as well as the low $^{142}Nd/^{144}Nd$, compared to the terrestrial Nd standard, of their host TTG (O'Neil et al., 2012). The NGB Ujaraaluk unit and gabbro sills intruding the NGB have the required geochemical and isotopic compositions and are thus the most likely precursor crustal sources of these Eo- to Mesoarchean TTG (O'Neil et al., 2013). This is further supported by melting experiments that have shown that the partial remelting of an Ujaraaluk-like rock produces melts that match the compositions of the NGB tonalites (Adam et al., 2012).

Despite comprising the oldest felsic magmatic rocks in the Superior Province, and some of the oldest evolved rocks on Earth, the multiple generations of granitoids surrounding the NGB remain poorly characterized. Better geochronological constraints and a better understanding of the petrogenesis of these TTGs provide a unique opportunity to help resolve unanswered questions regarding the processes responsible for the generation of early continental crust.

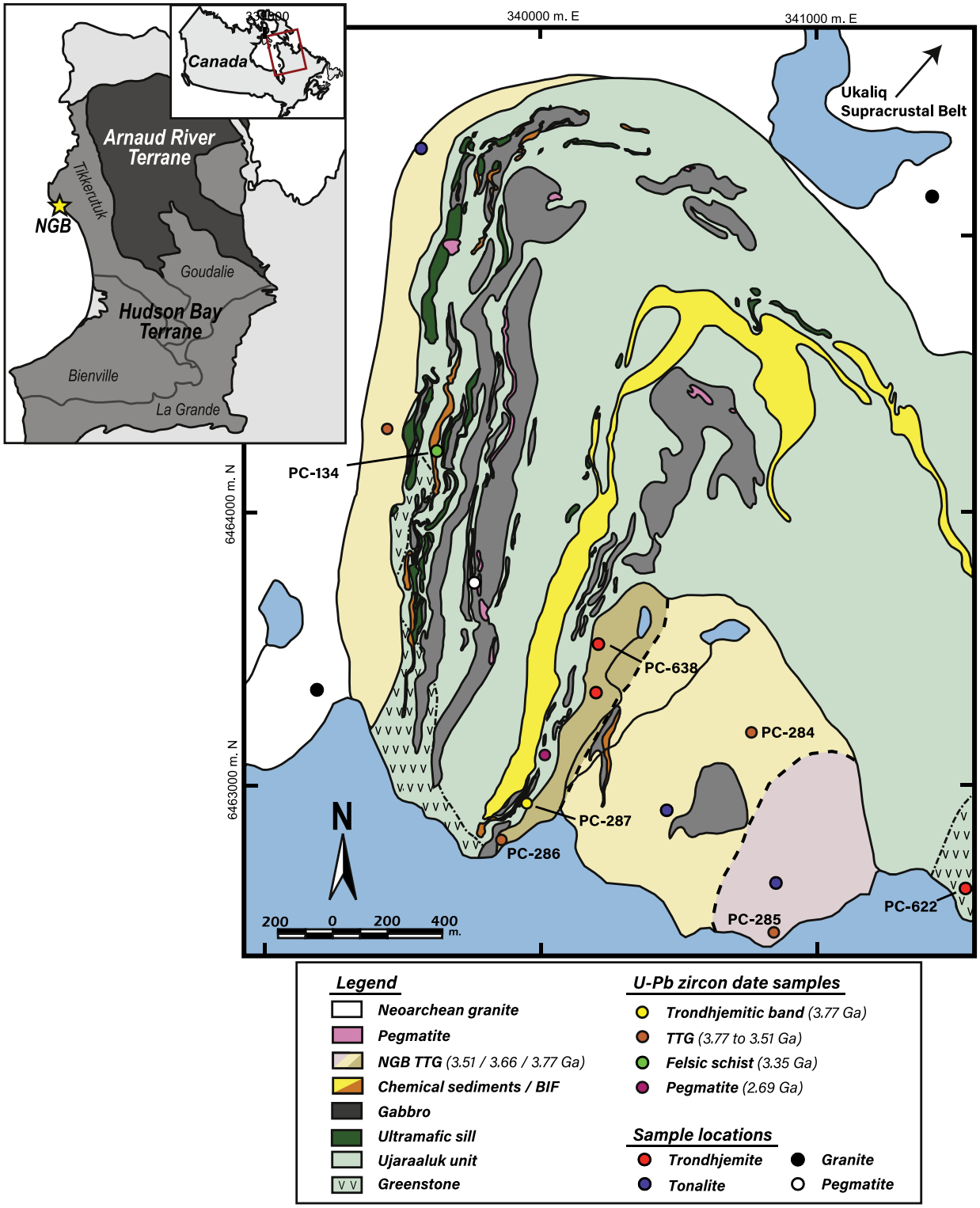

Figure 3.1: Regional map of the Northeastern Superior Province and geological map of the Nuvvuagittuq Greenstone Belt modified from O'Neil et al. (2019). Coordinates are in UTM zone 18, NAD27. Labelled samples are those for which U-Pb dates are available and discussed throughout this chapter. Previous U-Pb date samples are from David et al. (2009) and O'Neil et al. (2013).

3.3 Methods

3.3.1 Whole rock major and trace elements

Ten TTGs surrounding the Nuvvuagittuq Greenstone Belt and one intruding pegmatite were sampled during fieldwork in the summer of 2017. A TTG found intruding hornblende-amphibolites in a nearby region known as the Ukaliq Supracrustal Belt (USB) was also collected. A full list of rock types and their GPS coordinates can be found in Table B.1. All samples were cut free of weathered surfaces and crushed in order to make polished thin sections and fine powders for detailed petrographic descriptions as well as major and trace element analyses.

Major element concentrations for all 12 felsic samples were analyzed by X-ray Fluorescence (XRF) on a Rigaku Supermini200 WDXRF spectrometer at the X-ray Core Facility Laboratories at the University of Ottawa. Powdered samples were fused using a flux made in-house (79/21 $Li_2B_4O_7/LiBO_2$) and combined with 80 mg of LiBr non-wetting agent to produce glass disks (sample/flux ratio of ~1:7). Standards used for felsic calibration curves were: AMH-1, GSP-2, GS-N, AN-G, SY-3, MA-N, OU-3, BCR-032, PC-1016, GPO-16, GPO-17, GPO-18 and MRG-1. Standards SY-3, MRG-1 and BCR-032 were used for drift correction and GSP-2 was used as a felsic check to validate results. Accuracy and precision were determined by multiple measurements of the SY-3 standard. Accuracies were <5% for SiO_2, Al_2O_3, Fe_2O_3, MnO, MgO, CaO, Na_2O, K_2O, P_2O_5 and ~10% for TiO_2. Precisions were <5% for SiO_2, Al_2O_3, Fe_2O_3, MnO, MgO, CaO, Na_2O, K_2O, P_2O_5 and >15% for TiO_2.

Trace element concentrations for all 12 samples were analyzed on an Agilent 8800 QQQ Triple-Quadrupole ICP-MS at the Geochemistry Laboratories at the University of Ottawa. Approximately 100 mg of powdered sample was dissolved in closed Savillex beakers using a 1:5 HNO_3-HF mix and placed on a hot plate at 125°C for four days. Savillex beakers were then opened

and left on a hot plate until complete evaporation. Samples were re-dissolved in 6M HCl and placed on a hot plate at 125°C in closed beakers for two days. Two drops of boric acid were added to each sample before being evaporated to help dissolve any fluorides that may have formed during the initial HF dissolution. In order to ensure total dissolution of refractory phases (i.e. zircon), all samples were re-dissolved in 1ml of 6M HCl and then centrifuged. The supernatant of each sample was set aside whereas the residue containing the undissolved refractory phases was put into a Teflon micro-capsule and then dried on a hot plate. Once completely dry, 100 µl of concentrated HF and 70 µl of concentrated HNO_3 were added into each micro-capsule. The micro-capsules were placed in a high-pressure steel jacketed Parr bomb and left in an oven at 140°C for four days. They were then taken out of the Parr bomb and dried on a hot plate. Once completely dry, 100 µl of 6M HCl was added to each micro-capsule before being placed back into the high-pressure steel jacket Parr bomb and left in an oven at 140°C for two days. The dissolved residues were then combined with their respective supernatant fractions. A drop of boric acid was added to each beaker before being evaporated on a hot plate to help dissolve any fluorides that may have formed during the Parr bomb HF dissolution. Each sample was re-dissolved in 5 ml of 7M HNO_3 and left on a hot plate overnight in preparation for dilution. Once completely dissolved, an additional 35 ml of 7M HNO_3 was added to each solution. An aliquot of 1 ml was taken from each solution and transferred to a separate 15 ml centrifuge tube from which 11 ml of 0.01M HNO3 with traces of HF and In was added to each sample. Once homogenized, samples were ready for analysis on the ICP-MS. Dilution factors were aimed to be 4000 times and calculated by weight. BHVO-2, BCR-2, BIR-1a and GSP-2 standards were analyzed multiple times for accuracies and precisions. The BHVO-2 standard was used to calculate the unknown felsic sample concentrations and BCR-2, BIR-1a and GSP-2 were considered as unknowns to validate the results. Accuracies were <5% for the REE,

Sc, V, Co, Ni, Cu, Zn, Ga, Rb, Sr, Y, Zr, Nb, Cs, Ba, Hf; between 5–10% for Cr, Ta, Pb, Th, U and >15% for Ge. Precisions were obtained from repeated measurements of the BHVO-2 standard and were between 1–10% on the REE, Sc, V, Cr, Co, Ni, Cu, Zn, Ga, Rb, Sr, Y, Zr, Nb, Cs, Ba, Hf, Ta, Pb, U and between 10–20% for Ge and Th.

3.3.2 Zircon trace element analyses

Trace element analyses were performed on zircons from five felsic samples (PC-134, PC-284, PC-285, PC-286 and PC-287) that were previously analyzed by O'Neil et al. (2013) for U-Pb and Hf isotopes. Analyses were conducted on an Agilent 7700x ICP-MS coupled with a Photon Machines Analyte Excite 193 nm excimer laser at the Geochemistry Laboratories at the University of Ottawa. The ICP-MS was operated at 1550 W with a sample depth of 5.2 mm. A carrier gas consisting of high purity He mixed in the cell with an Ar make-up gas at flows of 1 l/min and 0.76 l/min, respectively. Cathodoluminescence (CL) imaging from O'Neil et al. (2013) was used to guide laser work in order to measure trace element concentrations in the same zircon growth zones as previous U-Pb and Hf analyses. A laser spot size of 32 µm at a repetition rate of 10 Hz with a fluence of 4.7 mJ/cm^2 was used for all analyses. Single analyses consisted of 30 s of background measurements, 50 s of ablation and 30 s of flush to prepare for the next analysis. All zircons were analyzed for the following elements: Si, P, Ti, Fe, Y, Zr, La, Ce, Pr, Nd, Sm, Eu, Gd, Tb, Dy, Ho, Er, Tm, Yb, Lu, Hf, Th and U. Detection limits and dwell times for each analyzed element can be found in Table B.2. Primary reference material NIST 612 (Pearce et al., 1997) was used for calibration collectively with an internal standardization using isotope ^{29}Si. Secondary reference materials NIST 610 (Pearce et al., 1997), GSE-1G (Jochum et al., 2005) and zircon 91500 (Wiedenbeck et al., 1995) were used for quality control. The preferred values from GeoRem

(http://georem.mpch-mainz.gwdg.de/) were used for all reference materials. Data reduction was carried out using the GLITTER® software package from Macquarie Research Ltd (van Achterbergh et al., 2001). Time-resolved data for each element was carefully examined for every in-situ analysis in order to determine if any non-zircon inclusions (e.g. apatite, allanite, etc.) were encountered. This allowed for selection and isolation of non-zircon inclusion signal intervals, if permitting.

3.3.3 Zircon oxygen isotope analyses

Oxygen isotope analyses were performed on zircons from the same five felsic samples as for trace element analyses (PC-134, PC-284, PC-285, PC-286 and PC-287). Mount preparation and secondary ion mass spectrometry (SIMS) analyses were carried out at the Canadian Center for Isotopic Microanalysis (CCIM) at the University of Alberta, Canada. Zircons that had previously been analyzed for U-Pb dating and Hf isotopes (O'Neil et al., 2013) as well as trace element concentrations (this study) were extracted from their respective mounts and re-mounted on a single, 25 mm diameter epoxy mount (M1521). Additional zircons picked from the heavy mineral separates of PC-284, PC-285 and PC-286 were also mounted on M1521 as supplementary material. The new epoxy mount was lightly polished using a diamond grit solution to expose grain centers and cleaned with a lab soap solution and de-ionized water. The epoxy mount was sputter coated with 25 nm of high-purity Au prior to scanning electron microscopy (SEM) imaging using a Zeiss EVO MA15 instrument equipped with a high-sensitivity, broadband cathodoluminescence (CL) and backscattered electron (BSE) detectors. Beam conditions were 15 kV with a 3–5 nA sample current. Prior to SIMS analysis, an additional 100 nm of Au was sputter coated onto the mount.

Oxygen isotopes (^{18}O, ^{16}O) in zircon were analyzed using a Cameca IMS 1280 multicollector ion microprobe. A $^{133}Cs^{+}$ primary beam was operated with an impact energy of 20 keV and a beam current of ~2 nA. The ~10 µm diameter probe was rastered (18 x 18 µm) for 30 s prior to acquisition, and then 7 x 7 µm during acquisition, forming analyzed areas ~15 µm across and ~1 µm deep. The normal incidence electron gun was utilized for charge compensation. Negative secondary ions were extracted into the secondary (transfer) column using a –10 kV potential. Transfer conditions included a 122 µm entrance slit, a 5 x 5 mm field aperture, and 100x sample magnification at the field aperture plane. No energy filtering was employed. The mass/charge separated oxygen ions were detected simultaneously in Faraday cups L'2 ($^{16}O^{-}$) and H'2 ($^{18}O^{-}$) at mass resolutions (M/Δm at 10%) of 1950 and 2250, respectively. Secondary ion count rates for $^{16}O^{-}$ and $^{18}O^{-}$ were typically ~2 x 10^{9} and 4 x 10^{6} counts/s utilizing 1010 Ω and 1011 Ω amplifier circuits, respectively. Faraday cup baselines were measured at the start of the analytical session. A single analysis took 240 s, including pre-analysis rastering, automated secondary ion tuning, and 75 s of continuous peak counting.

Instrumental mass fractionation was monitored by repeated analysis of the UAMT1 zircon primary reference material (S0081 with $\delta^{18}O_{VSMOW}$ = +4.87‰; R. Stern, unpublished laser fluorination data, University of Oregon) once after every four unknowns. A secondary reference material, zircon TEM-2 ($\delta^{18}O_{VSMOW}$ = +8.2‰; Black et al., 2004), was also analyzed after every 8 unknowns. The $^{18}O^{-}/^{16}O^{-}$ data set for UAMT1 zircon was processed collectively for one analytical session (n = 59), yielding a standard deviation (SD) of 0.09‰, following correction for systematic within-session drift of +0.4‰. The individual spot uncertainties for the unknowns at 95% confidence for $\delta^{18}O_{VSMOW}$ include errors relating to within-spot counting statistics, between-spot (geometric) effects, and correction for instrumental mass fractionation, with a median of ±0.20‰.

Results for multiple spots on multiple grains of zircon TEM-2 yielded a weighted mean $\delta^{18}O_{VSMOW}$ = +8.11‰ (MSWD = 1.3; n = 25; SD = 0.12‰) which overlaps with the value of Black et al. (2004) (Figure B.1). $\delta^{18}O_{VSMOW}$ was calculated using the following equation:

$$\delta^{18}O_{VSMOW} = (({}^{18}O/{}^{16}O_{SAMPLE})/({}^{18}O/{}^{16}O_{VSMOW}) - 1)$$

where ${}^{18}O/{}^{16}O_{VSMOW}$ = 0.0020052. $\delta^{18}O_{VSMOW}$ values are reported in ‰.

3.3.4 Zircon U-Pb isotope analyses

Three TTGs (PC-622, PC-638 and UK-002) were selected for zircon U-Pb dating. Samples were crushed using a steel jaw crusher followed by a disk pulveriser and then sieved to keep the 250–106 µm size fraction. Heavy mineral fractions were first extracted through heavy liquid separation using methylene iodide. A Frantz magnetic separator with a current of ~20 A and a platform inclination of 20° was then used to remove the magnetic minerals. Approximately 120 zircons were picked and mounted for all three samples. Zircon mounts were polished to expose grain centers and then carbon coated prior to CL imaging at the Microanalysis Laboratory at the University of Ottawa. A JEOL 6610LV SEM equipped with a Gatan MINI-CL and BSE detectors was used to identify internal zircon structures in order to facilitate laser ablation work.

U-Th-Pb isotope analyses were performed on a Thermo Scientific Element XR ICP-MS coupled with a Resonetics M50E 193 nm excimer laser ablation (LA) system at the Laboratoire Magmas et Volcans (LMV) in Clermont-Ferrand, France. A laser spot size of 20–27 µm at a repetition rate of 3 Hz and a fluency of 2.5 J/cm^2 was used for all three samples. Single analyses consisted of 30 s of background measurement with the laser off, 60 s of zircon ablation and a 30 s

delay to wash out the previous sample in preparation for the next analysis. The full analytical protocol for isotope dating with LA-ICP-MS is described in detail in Hurai et al. (2010), Paquette et al. (2014) and Mullen et al. (2018) and additional information on the instrument settings for this session is available in Table B.3. U-Pb fractionation during laser sampling and instrumental mass discrimination was corrected by standard bracketing of repeated measurements of the GJ-1 zircon (Jackson et al., 2004) (Figure B.2). The 91500 zircon reference material (Wiedenbeck et al., 1995) was also measured repeatedly and treated as an unknown to independently control the reproducibility and accuracy of the corrections (Figure B.3). Data reduction was performed using the GLITTER® software package from Macquarie Research Ltd (van Achterbergh et al., 2001). Data was not corrected for common Pb. Analyses that were >20% discordant were discarded from the age calculation. Weighted mean $^{206}Pb/^{207}Pb$ ages and Concordia diagrams were generated using the Isoplot/Ex v.2.49 software package (Ludwig, 2001).

3.4 Results

3.4.1 Petrography and geochemistry

Most felsic intrusive rocks sampled around the NGB have CIPW normative mineralogy compositions consistent with trondhjemite-tonalite-granodiorite and one sample displays a higher normative orthoclase content, plotting in the granite field (Figure 3.2). Despite its comparable normative mineralogy to other NGB TTG, sample PC-648 was classified as a granite due to its similar whole-rock major element composition to the granitic sample PC-642 (detailed further). The felsic sample collected in the USB is classified as a tonalite (Figure 3.2). The NGB trondhjemitic samples are composed of medium to coarse-grained plagioclase + quartz + biotite and display a foliation defined by biotite grains. Mineral abundances are typically 50% plagioclase,

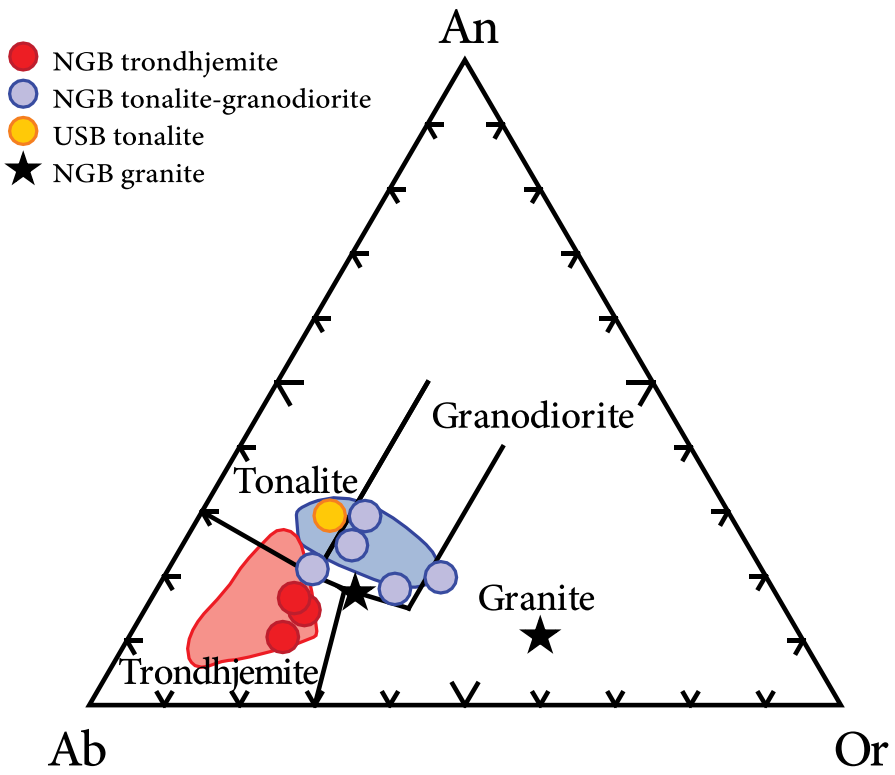

Figure 3.2: Normative An-Ab-Or diagram (Barker, 1979) for the classification of granitoids. Symbols: Red circles = NGB trondhjemites; Blue circles = NGB tonalites-granodiorites; Yellow circle = USB tonalite; Black stars = NGB granites. Shaded areas represent NGB fields for samples defined as trondhjemite (red) and tonalite (blue) by O'Neil et al. (2013).

35–40% quartz and 10–15% biotite (Figure 3.3A). Plagioclase grains exhibit a moderate sericite alteration and chlorite can be found altering the rims of biotite grains. The NGB and USB tonalites-granodiorites are composed of a similar mineralogical assemblage with varying proportions of medium to coarse-grained plagioclase + quartz + biotite ± K-feldspar (Figure 3.3B). Most samples display a slight alignment of biotite grains but PC-623 exhibits a well-developed foliation of biotite. Plagioclase grains exhibit a moderate sericite alteration and chlorite can be found altering the rims of biotite grains. It should be noted that PC-634, sampled to the northwest of the NGB (Figure 3.1), contains hornblende instead of biotite and shows no preferential alignment of its hornblende grains (Figure 3.3C). Furthermore, the hornblende is often altered to chlorite or epidote

and the sample displays extensive sericitization of plagioclase. The granites to the west and north of the NGB are characterized by coarse-grained K-feldspar + quartz + plagioclase ± biotite (Figure 3.3D). The granite sampled to the west of the NGB (PC-642) has a higher abundance of K-feldspar compared to the one sampled to the north (PC-648), which is also reflected in their CIPW norm (Figure 3.2). Biotite grains are often altered to chlorite and plagioclase grains are heavily sericitized. Myrmekites can also be found at the microscopic scale in both samples. The lack of aligned biotite in these granites suggests that they have not been deformed as much as the other granitoids surrounding the NGB.

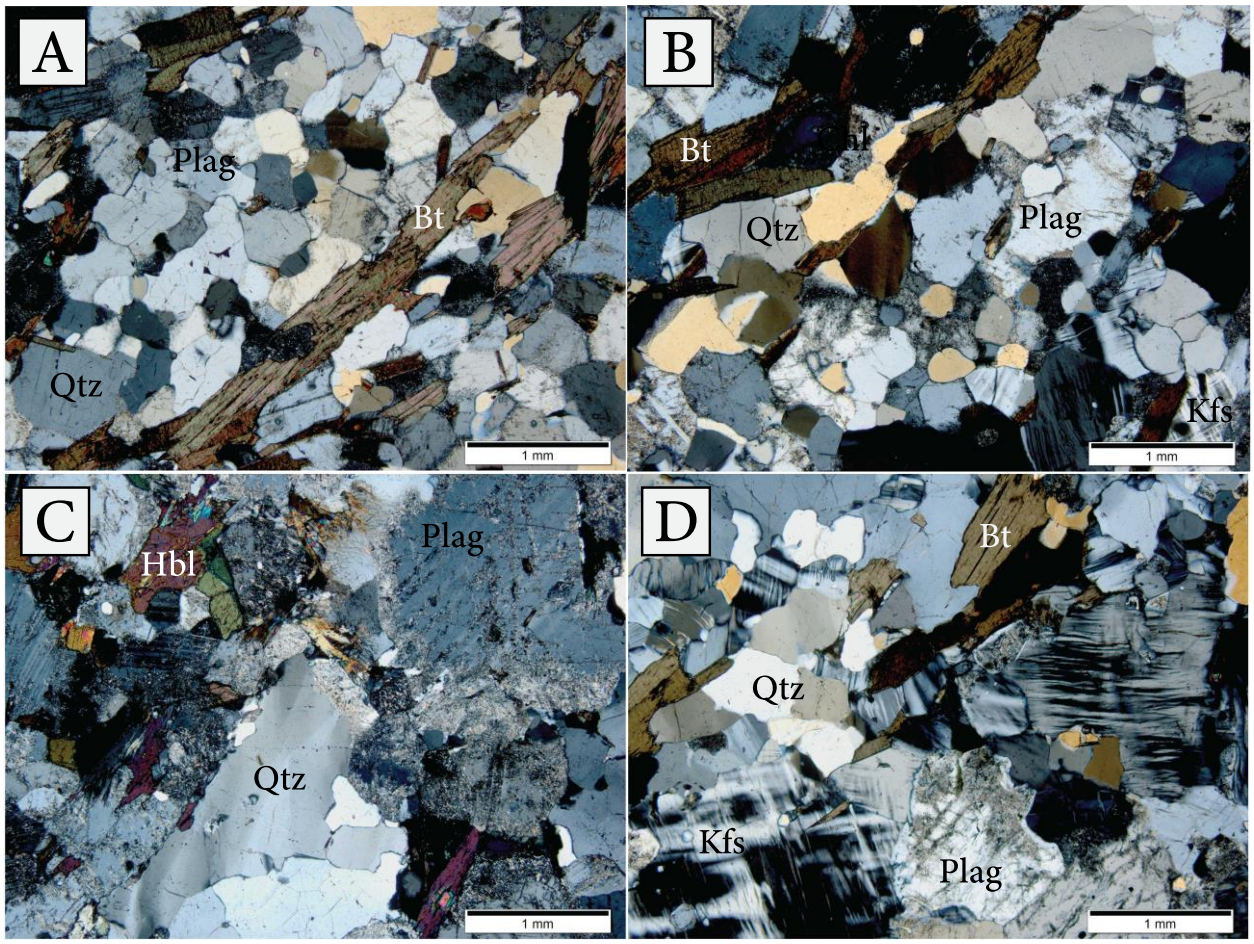

Figure 3.3: Microphotographs of the NGB granitoids under cross-polarized light at 5x magnification. A) Trondhjemite (PC-638); B) Tonalite-granodiorite (PC-625A); C) Tonalite-granodiorite (PC-634); D) Granite (PC-642). Abbreviations : Qtz = Quartz; Plag = Plagioclase; Bt = Biotite; Kfs = K-feldspar; Hbl = Hornblende.

Major and trace element data for the granitoid and pegmatite samples are presented in Table B.4. The granitoids display silica content ranging from 60.3 wt.% to 73.7 wt.% (Figure 3.4A). The granites have the highest SiO_2 values (>72 wt.%) whereas SiO_2 for the TTG mostly range from 65 to 70 wt.%. SiO_2 content increases as MgO decreases for all granitoids (Figure 3.4A). Al_2O_3, Fe_2O_3 and TiO_2 contents generally decrease with decreasing MgO values for all rock types (Figure 3.4B-D). Granites typically have lower Al_2O_3, Fe_2O_3 and TiO_2 contents compared to the trondhjemites and tonalites-granodiorites. CaO content shows no correlation with MgO content but the granites and trondhjemites generally exhibit lower CaO values (<2.4 wt.%) compared to the tonalites-granodiorites (>2.4 wt.%) (Figure 3.4E). There is also no clear trend of increasing alkali values with decreasing MgO content for the trondhjemites and tonalites-granodiorites (Figure 3.4F). However, the granites do have the highest alkali (>7.4 wt.%) and lowest MgO values (<0.5 wt.%) of all granitoid rocks (Figure 3.4F).

Most incompatible trace elements do not show systemic variations with increasing MgO or decreasing SiO_2, except perhaps the La/Yb ratios. When the trondhjemites and tonalites-granodiorites are considered separately, the La/Yb ratio increases with decreasing MgO and increasing SiO_2 content (Figure 3.4G). However, concentrations for compatible trace elements such as Cr, Ni and Co decrease with decreasing MgO for the whole suite of granitoids, with the granitic samples exhibiting the lowest concentrations (Figure 3.4H). When normalized to chondrite, all granitoid samples display a depletion in HREE compared to light rare earth elements (LREE), typical of Archean granitoids (Figure 3.5A). The NGB trondhjemites and UGB tonalite are generally characterized by greater depletion in HREE compared to the NGB tonalites-granodiorites, leading to distinct $(La/Yb)_N$ ratios of 23.4–69.4 and 12.8–29.6 respectively. All TTGs show no to slightly negative Eu anomalies. The two granite samples display contrasting

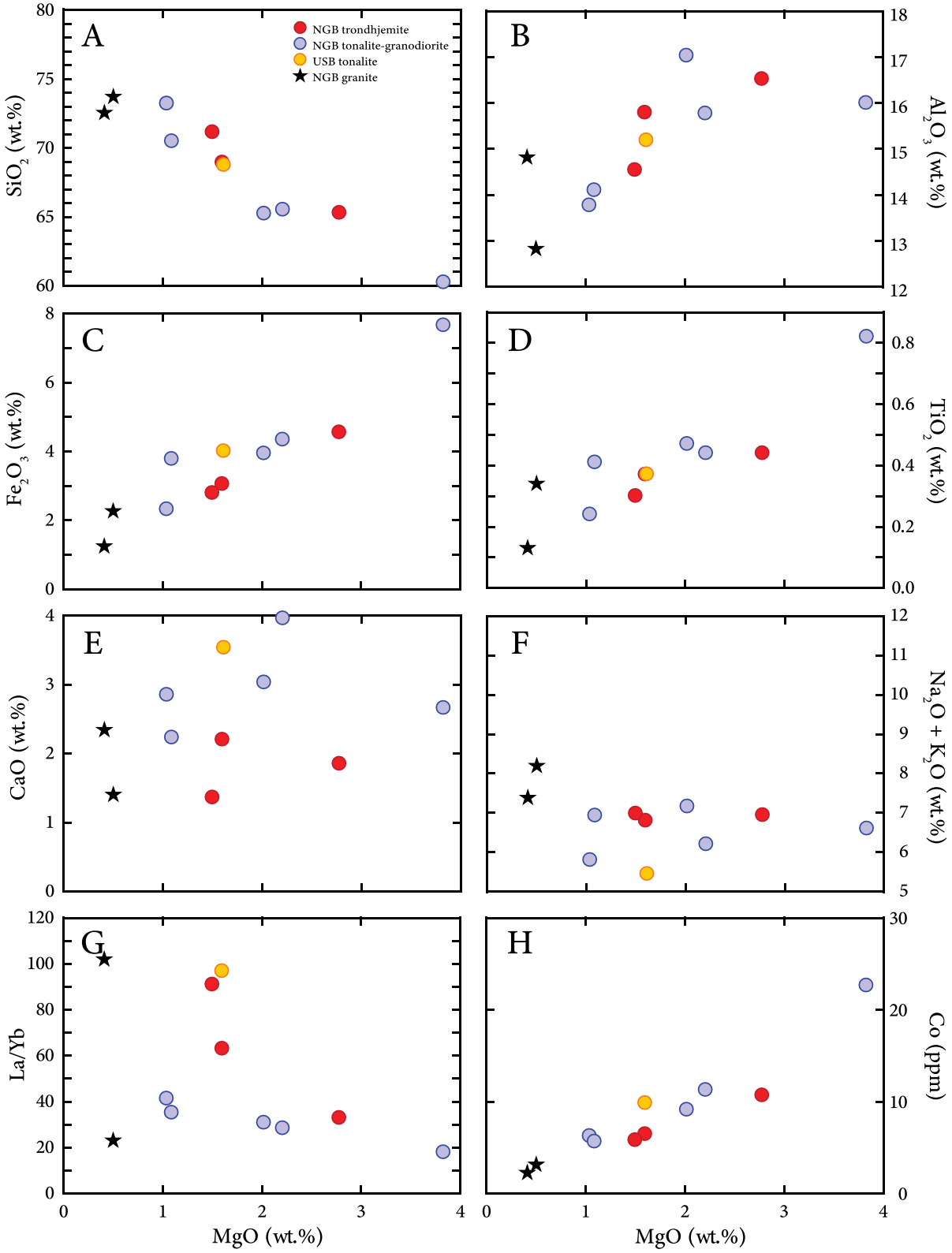

Figure 3.4: Major and trace element compositions of the NGB and USB granitoids. A-H) Selected major and trace element concentrations vs. MgO. Same symbols as in Figure 3.2.

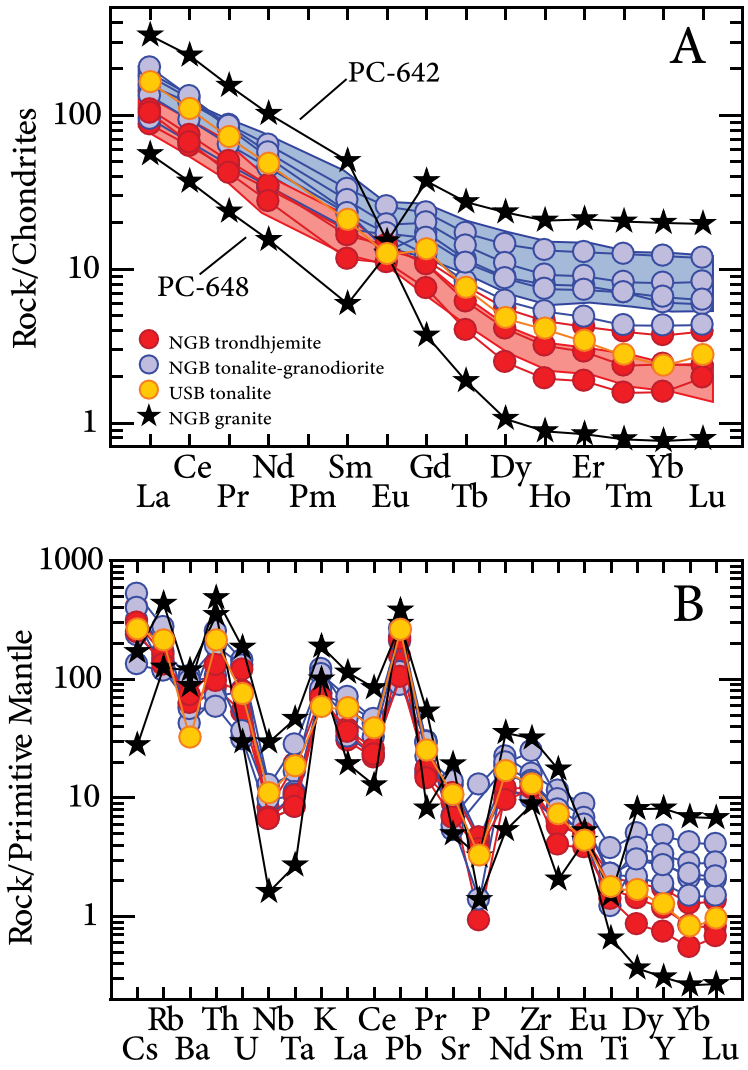

Figure 3.5: Trace element spider diagrams of the NGB and USB granitoids. A) Normalized to chondrites. Shaded areas represent NGB fields for samples defined as trondhjemite (red) and tonalite (blue) by O'Neil et al. (2013). B) Normalized to the primitive mantle. Both diagrams are normalized after Sun and McDonough (1989). Same symbols as in Figure 3.2.

REE patterns. The granite sampled to the west of the NGB (PC-642) has the highest REE concentration of all granitoids with a pronounced negative Eu anomaly, whereas the granite sampled to the north of the NGB (PC-648) has the lowest REE concentration of all granitoids and a pronounced positive Eu anomaly (Figure 3.5A). Sample PC-648 also displays a marked HREE depletion compared to the other granitoid samples. When normalized to the primitive mantle, all

granitoids display typical negative Nb, Ta, and P anomalies as well as a positive Pb anomaly (Figure 3.5B). The NGB tonalites-granodiorites also exhibit a small negative Ti anomaly which is not observed in the NGB trondhjemites and UGB tonalite. The granites display similar anomalies to the TTGs and PC-642 consistently shows a much greater abundance in most trace elements compared to PC-648 (Figure 3.5B).

3.4.2 Zircon U-Pb isotope data

Between 100–120 zircons from the surrounding NGB trondhjemite, a thin trondhjemitic band found in the east of the NGB, and the USB tonalite were analyzed by LA-ICP-MS for U-Pb geochronology. Data for all individual zircons is available in Table B.5. CL images for representative zircons of each sample can be found in Figure 3.6. Ages for all three samples are reported as weighted mean $^{207}Pb/^{206}Pb$ ages using Concordia diagrams (Figure 3.7).

Zircons from both NGB trondhjemitic samples (PC-622 and PC-638) are generally 150 to 300 µm long and exhibit a subhedral prismatic shape with well developed oscillatory zoning (Figure 3.6A-B). They also display low to high degrees of fracturing and contain small inclusions. Zircons from PC-622 and PC-638 have U concentrations that range from 100–200 ppm and Th/U ratios of 0.73 ± 0.04 and 0.67 ± 0.04 (2σ-mean), respectively. These values are consistent with an igneous origin. PC-622 and PC-638 both yield a single age population with statistically undistinguishable ages of 3753 ± 6 Ma (MSWD = 0.34, n = 70) and 3753 ± 5 Ma (MSWD = 0.26, n = 81), respectively (Figure 3.7A-B). It is worth mentioning that a single concordant zircon found in PC-638 with obscured oscillatory zoning (Figure 3.6C) yielded a $^{207}Pb/^{206}Pb$ age of 2734 Ma (Figure 3.7B). Zircons with CL images that could suggest the presence of a core and rim were analyzed for both zones, but no age differences were found between these spatial domains.

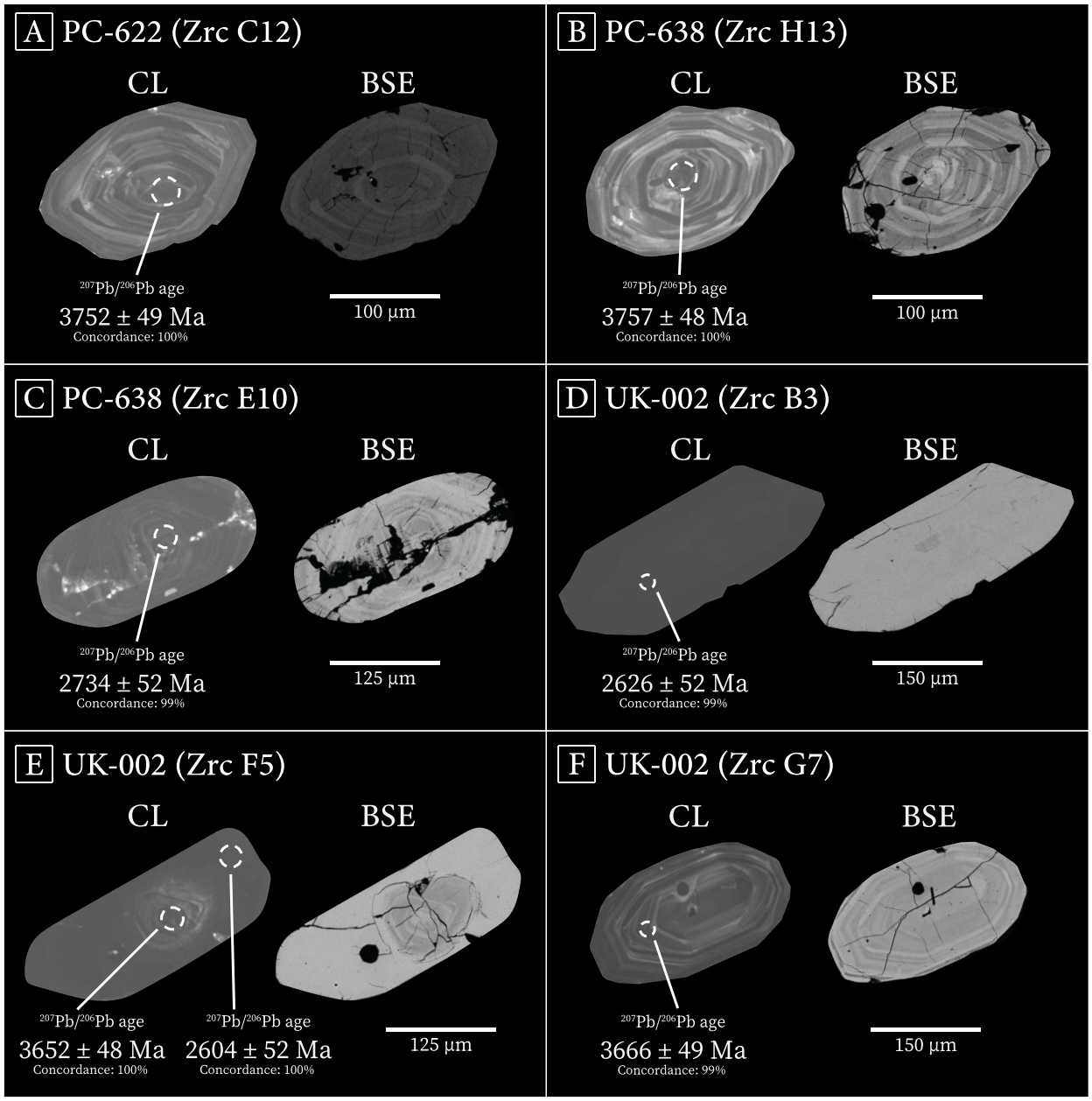

Figure 3.6: CL and BSE images of representative zircons from a thin trondhjemitic band found in the east of the NGB (PC-622), the surrounding NGB trondhjemite (PC-638) and the USB tonalite (UK-002). U-Pb analysis spot is highlighted by the white dashed circle. A) Sample PC-622, zircon #C12 displaying oscillatory zoning; B) Sample PC-638, zircon #H13 displaying oscillatory zoning; C) Sample PC-638, zircon #E10 displaying a dark overprint obscuring its oscillatory zoning; D) Sample UK-002, zircon #B3 displaying no observable features; E) Sample UK-002, zircon F5 displaying a faint zoned core and a dark rim; F) Sample UK-002, zircon G7 displaying oscillatory zoning. Abbreviations: Zrc = Zircon; CL = Cathodoluminescence; BSE = Back-scattered electron.

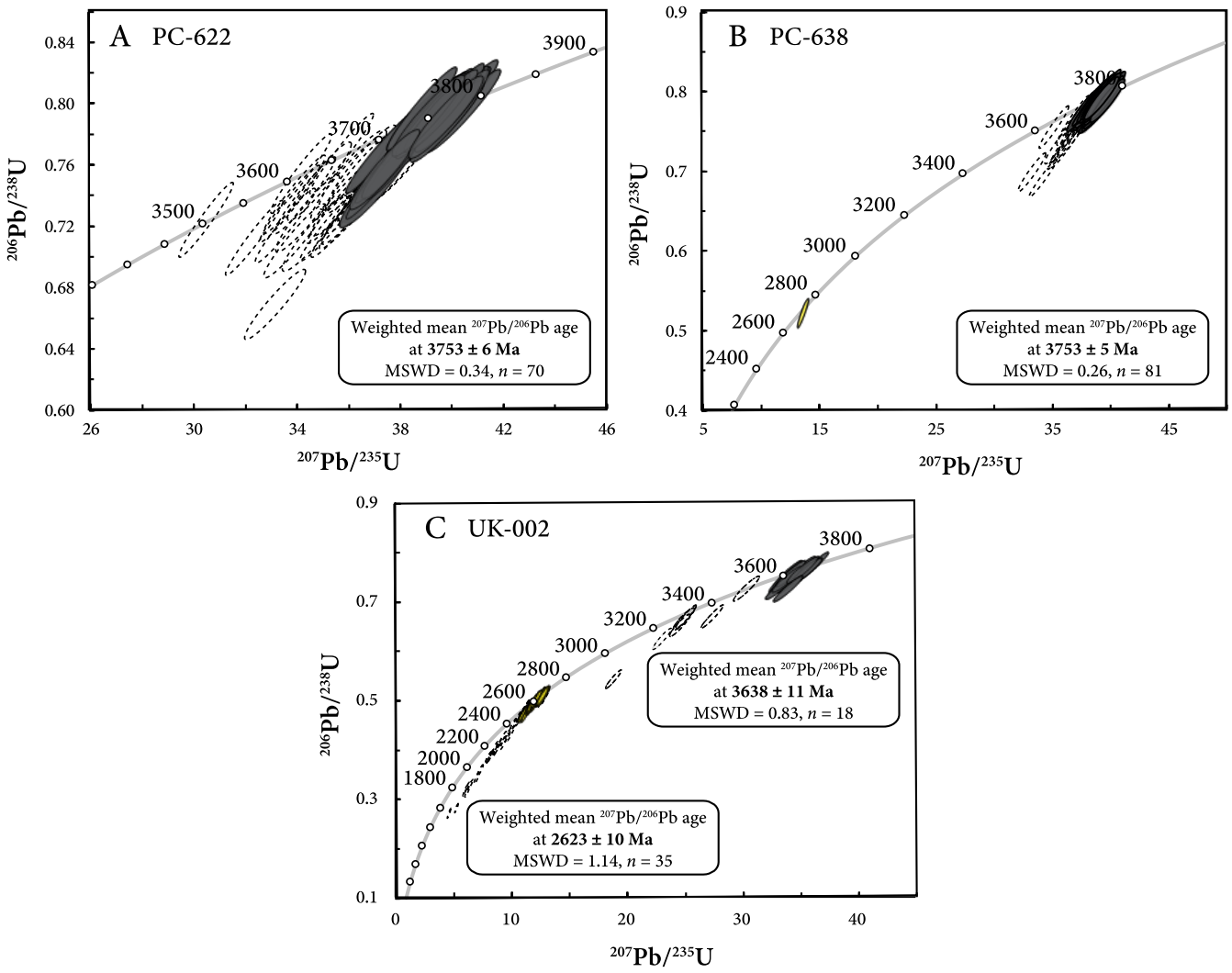

Figure 3.7: Concordia diagrams of two NGB trondhjemitic samples (PC-622 and PC-638) and the USB tonalite (UK-002). A) PC-622; B) PC-638; C) UK-002. The grey ellipses represent oscillatory zoned zircons and cores whereas the yellow ellipses represent zircons and rims with dark CL features. The dotted ellipses represent zircons that were not included in the age calculation.

The tonalite from the Ukaliq Supracrustal Belt (UK-002) contains euhedral prismatic zircons that are generally larger (300 to 400 µm) and exhibit a low to moderate degree of fracturing. Most of the zircons are characterized by dark CL images with no observable features (Figure 3.6D). However, 13 grains display faint cores with oscillatory zoning that are surrounded by a dark CL rim (Figure 3.6E) and four zircons show oscillatory zoning throughout the whole grain (Figure

3.6F). These zoned zircons and cores are characterized by U concentrations ranging between 100–300 ppm and Th/U ratios of 0.70 ± 0.09 (2σ-mean). In comparison, the dark CL zircons and rims have much higher U concentrations (>1000 ppm) and lower Th/U ratios of 0.20 ± 0.01 (2σ-mean).The dark CL grains and rims together yield an age of 2623 ± 10 Ma (MSWD = 1.14, n = 35) whereas the cores and grains displaying oscillatory zoning yield an older age of 3638 ± 11 Ma (n = 18, MSWD = 0.83) (Figure 3.7C).

3.4.3 Zircon trace element and oxygen isotope compositions

A subset of zircons from five granitoids surrounding and locally intruding the NGB that had previously been analyzed for U-Pb and Hf isotope compositions by O'Neil et al. (2013) were selected for trace element and oxygen isotope analyses. Locations of the five granitoids can be found in Figure 3.1 and a short description of these five samples can be found in Table 3.1.

Table 3.1: Summary table of five granitoid samples surrounding and locally intruding the NGB previously analyzed for U-Pb and Hf isotope compositions by O'Neil et al. (2013). Abbreviations: Plag = Plagioclase; Qtz = Quartz; Bt = Biotite.

Sample	Host rock	Age (Ma)	Zircon texture	Average Th/U
PC-134	Plag-Qtz-Bt felsic schist	3353 ± 4	Oscillatory zoning	0.85
PC-284	Tonalite	3657 ± 4	Oscillatory zoning	0.74
PC-285	Tonalite	3508 ± 8	Oscillatory zoning	0.40
PC-286	Trondhjemite	3756 ± 4	Oscillatory zoning	0.71
PC-287	Trondhjemite band	3757 ± 4	Oscillatory zoning	0.58

Between 13 and 20 zircons from each of the five granitoid samples were analyzed for trace element concentrations, with some zircons analyzed multiple times, for a total of 87 measurements. Trace element analyses were carried out on the same spatial domains as those used for U-Pb and Hf isotope compositions by O'Neil et al. (2013). Minimum, maximum and mean trace element

contents as well as Th/U, Ce/Ce*, Eu/Eu*, $(La/Sm)_N$ and $(Lu/Sm)_N$ values for zircons in all five granitoids can be found in Table 3.2. All individual zircon analyses can be found in Table B.6. Because abnormally high P or Fe-Ti concentrations most likely indicate that an inclusion in the zircon (i.e. apatite, allanite, titanite) was partially or fully ablated during analysis, analyses showing high concentrations in P or Fe-Ti were discarded and not included in the minimum/maximum values or in the calculated mean concentrations of Table 3.2. Zircons that were analyzed for potential core and rim spatial domains showed no differences in REE patterns. It is important to note that oscillatory zoning present in these grains is in part responsible for compositional differences amongst zircons from the same sample or within the same zircon.

Chondrite-normalized REE patterns for all zircons are shown in Figure 3.8. Zircons from all samples show similar REE profiles and are characterized by normalized LREE concentrations 2 to 4 orders of magnitude lower than the HREE (avg. $(Lu/Sm)_N$ = 46.8–74.0). All samples have zircons exhibiting positive Ce-anomalies (avg. Ce/Ce* = 8.35–17.6), but with sample PC-285 displaying smaller Ce-anomalies (avg. Ce/Ce* = 1.66). Zircons from all samples show Eu-anomalies with PC-134, PC-284, PC-286 and PC-287 yielding negative Eu-anomalies (avg. Eu/Eu* = 0.17–0.39), whereas zircons from PC-285 show striking positive Eu-anomalies (avg. Eu/Eu* = 3.12) (Figure 3.8). The four samples with negative Eu-anomalies have low P concentrations that generally range between 150–300 ppm as well as Ti and Fe concentrations that are mostly <20 ppm and <100 ppm, respectively. Zircons from PC-285 have notably higher Fe, LREE, and U concentrations compared to the other granitoid samples. The Th/U ratios measured here are consistent with those reported in O'Neil et al. (2013), with Th/U ratios ranging between 0.6 and 0.9 for PC-134, PC-284, PC-286 and PC-287, while Th/U ratios in zircons from PC-285 are slightly lower with an average of 0.47 (Table 3.2).

Table 3.2: Trace element concentrations (ppm) of zircons in five granitoid samples surrounding and locally intruding the NGB. Analyses displaying evidences of inclusions (i.e. high P or Fe-Ti) were not considered in the minimum/maximum values or the calculated means. Ages are from O'Neil et al. (2013). Chondrite normalizing values are from Sun and McDonough (1989).

Sample	**PC-134**			**PC-284**			**PC-285**			**PC-286**			**PC-287**		
Host rock	Felsic schist			Tonalite			Tonalite			Trondhjemite			Trondhjemite band		
Age (Ma)	3353			3657			3508			3756			3757		
Analyses	n = 11			n = 11			n = 15			n = 13			n = 11		
	Min	**Mean**	**Max**	**Min**	**Mean**	**Max**	**Min**	**Mean**	**Max**	**Min**	**Mean**	**Max**	**Min**	**Mean**	**Max**
P	159	247	455	174	286	495	114	270	484	125	181	277	149	254	386
Ti	12.1	17.0	25.6	7.7	10.1	17.4	2.4	13.2	28.9	3.5	5.9	7.9	3.2	9.8	19.1
Fe	25.1	129	326	32.7	88.6	227	153	757	1417	11.9	37.1	194	33.8	94.7	189
Y	660	1092	1889	630	788	989	411	1015	1939	350	522	797	261	500	1059
La	0.09	3.18	8.11	0.05	2.92	14.2	3.39	25.2	54.1	0.04	0.58	3.82	0.04	0.72	2.75
Ce	16.6	26.7	41.5	15.0	31.7	58.6	16.7	104	225	9.66	16.2	22.4	9.96	14.9	25.1
Pr	0.19	1.73	4.69	0.14	1.28	5.23	0.80	12.7	31.9	0.07	0.36	0.97	0.05	0.60	2.20
Nd	2.44	11.2	32.0	2.04	7.73	27.3	2.48	60.4	148	0.95	3.21	5.67	0.52	4.51	15.9
Sm	3.02	8.15	19.2	3.04	5.19	11.5	1.17	16.0	32.5	1.73	3.34	6.45	1.25	3.84	10.6
Eu	0.24	0.90	2.14	0.58	1.15	2.44	1.18	23.5	102	0.48	0.86	2.05	0.29	0.93	2.12
Gd	13.5	28.0	49.4	13.1	17.9	24.8	4.97	31.4	72.3	8.74	13.1	24.4	5.98	13.8	27.1
Tb	4.50	8.53	13.5	4.17	5.45	6.61	2.03	7.86	18.0	2.71	3.94	7.02	1.93	4.09	8.00
Dy	53.3	96.6	165	49.9	66.1	81.1	28.9	90.3	199	28.9	44.0	74.0	21.7	44.7	92.5
Ho	20.3	35.0	62.8	20.9	25.9	33.2	13.1	34.4	72.1	11.0	16.9	26.4	7.88	16.4	34.3
Er	95.0	159	303	106	126	167	63.1	161	316	53.4	82.0	122	41.8	77.8	163
Tm	18.5	31.9	62.1	23.7	27.7	35.1	14.0	33.4	61.6	11.0	17.7	25.6	8.96	16.9	36.4
Yb	167	287	569	231	273	345	146	327	562	106	175	254	92.9	167	357
Lu	31.5	52.7	104	45.4	55.3	73.4	30.9	65.9	106	22.3	37.4	51.0	21.3	34.6	66.6
Hf	6802	9375	10923	7856	8989	9810	8141	9456	10958	8263	9139	10354	8443	10114	11990
Th	44.3	110	311	79.7	140	264	67.6	235	436	46.3	97.1	173	53.8	94.3	130
U	51.9	157	731	95.8	185	385	217	540	829	56.0	113	163	78.0	158	245
Th/U	0.43	0.90	1.21	0.66	0.75	1.03	0.25	0.47	1.34	0.73	0.84	1.06	0.36	0.63	0.86
Ce/Ce*	1.44	8.35	49.3	1.98	12.8	45.8	1.16	1.66	3.03	2.62	17.6	51.1	2.47	15.1	60.2
Eu/Eu*	0.09	0.17	0.33	0.25	0.36	0.44	0.49	3.12	9.89	0.28	0.39	0.50	0.24	0.39	0.52
$(Lu/Sm)_N$	19.5	46.8	69.9	25.9	71.5	96.9	9.9	55.2	237	36.7	74.0	134	24.7	68.7	118
$(La/Sm)_N$	1.05	13.0	86.1	0.52	20.0	116	0.23	1.21	3.23	2.09	24.6	72.8	1.57	20.5	54.7

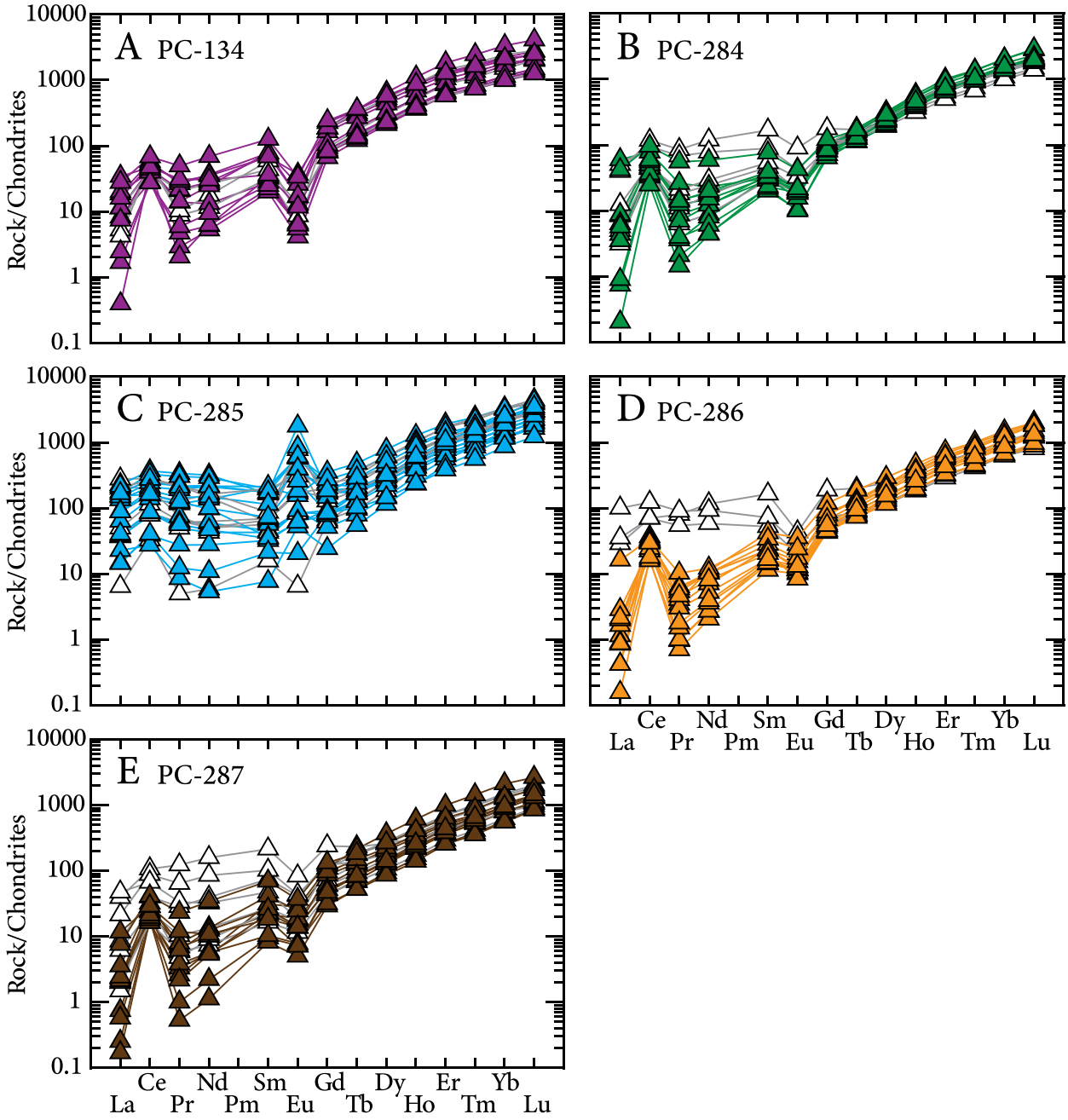

Figure 3.8: Chondrite-normalized zircon REE profiles of five granitoid samples surrounding and locally intruding the NGB. A) PC-134; B) PC-284; C) PC-285; D) PC-286; E) PC-287. Normalized after Sun and McDonough (1989). Symbols: Purple triangles = PC-134 zircons; Green triangles = PC-284 zircons; Blue triangles = PC-285 zircons; Orange triangles = PC-286 zircons; Brown triangles = PC-287 zircons; White triangles = Zircon analyses that were not considered in the minimum/maximum values or mean calculations of Table 3.2.

Between 16 and 64 oxygen isotope analyses, for a total of 203 measurements, were carried out on whole zircon and zircon fragments from all five granitoid rocks. Oxygen isotope analyses were performed on the same spatial domains as those used in previous trace element analyses. Minimum, maximum and mean $\delta^{18}O_{VSMOW}$ values for each sample can be found in Table 3.3. The analysis for one zircon from PC-285 was discarded due to it being significantly lower than all other measured values (+3.59‰ compared to the mean of +5.79‰, n = 40). $\delta^{18}O_{VSMOW}$ values for all individual analyses can be found in Table B.7. The mean zircon $\delta^{18}O_{VSMOW}$ values range from +5.65‰ (PC-287; 3757 Ma) to +6.58‰ (PC-134; 3353 Ma). As was the case with the zircon trace element analyses, zircons from all granitoid samples did not show statistically different $\delta^{18}O_{VSMOW}$ values between potential cores and rims. Zircons from both Eoarchean trondhjemitic samples display similar slightly lower $\delta^{18}O_{VSMOW}$ values (<+5.8‰) compared to the younger tonalite PC-284 and felsic schist PC-134 (>+6.0‰). Zircons from PC-285 yielded an average $\delta^{18}O_{VSMOW}$ value of +5.79‰, but also display a more important variation in $\delta^{18}O_{VSMOW}$ values compared to the other samples, with individual zircons ranging from +5.01‰ to +6.84‰. This sample also shows the most heterogeneous zircon age distribution with an older population yielding an age of 3508 ± 8 Ma, a younger population with a mean $^{207}Pb/^{206}Pb$ age of 3433 ± 7 Ma and a number of zircons with ages younger than 3300 Ma (O'Neil et al., 2013).

Table 3.3: Minimum, maximum and mean zircon $\delta^{18}O_{VSMOW}$ values (‰) in five granitoid samples surrounding and locally intruding the NGB. Ages are from O'Neil et al. (2013).

Sample	**Host rock**	**Age (Ma)**	**Analyses**	**$\delta^{18}O_{VSMOW}$ Values**		
				Minimum	Mean ± 2σ	Maximum
PC-134	Felsic schist	3353	n = 16	6.11	6.58 ± 0.36	6.89
PC-284	Tonalite	3657	n = 64	5.30	6.07 ± 0.49	6.65
PC-285	Tonalite	3508	n = 40	5.01	5.79 ± 0.68	6.84
PC-286	Trondhjemite	3756	n = 49	5.24	5.75 ± 0.31	6.04
PC-287	Trondhjemite band	3757	n = 33	4.99	5.65 ± 0.34	5.94

3.5 Discussion

3.5.1 Extent of the Eoarchean felsic magmatism

The oldest U-Pb zircon ages recorded in the Nuvvuagittuq Greenstone Belt are from small ~3.76 Ga intrusive trondhjemitic bands that have only been found in the southwestern part of the NGB (Figure 3.1; PC-287) (e.g. Augland and David, 2015; Cates and Mojzsis, 2007; Darling et al., 2013; David et al., 2009; O'Neil et al., 2013). A plutonic trondhjemite bordering the southwestern corner of the belt yields a similar 3.76 Ga age (Figure 3.1; PC-286) (O'Neil et al., 2013). Their comparable ages, whole-rock geochemical compositions and zircon Hf isotopic compositions have led O'Neil et al. (2013) to believe that the trondhjemitic bands and plutonic trondhjemite represent the same magmatic event. The plutonic trondhjemite PC-286 was collected less than 2 meters from the contact with the NGB mafic rocks and the extent of the 3.76 Ga trondhjemitic plutonic body was inferred in this part of the NGB solely based on similar geochemical compositions with other samples collected to the northeast of PC-286 (O'Neil et al., 2013). However, no U-Pb ages have yet to confirm this interpretation.

PC-638 was collected towards the northern limit of the 3.76 Ga plutonic trondhjemite inferred from whole-rock geochemical compositions (mainly from the more pronounced HREE depletion that characterized NGB trondhjemitic rocks), in order to better constrain the extent of the 3.76 Ga plutonic trondhjemite (Figure 3.1). The undistinguishable U-Pb age of 3753 ± 5 Ma obtained for PC-638 (Figure 3.7B) confirms that the 3.76 trondhjemitic magmatic event was more important in the NGB and extends to the northeast as previously proposed by O'Neil et al. (2013). A single concordant zircon found in PC-638 yielded a $^{207}Pb/^{206}Pb$ age of 2734 Ma (Figure 3.7B). However, the timing of its age and its obscured oscillatory zoning (Figure 3.6C) suggest that it experienced metamorphic overprinting. A trondhjemitic sample (PC-622) collected in the eastern

part of the NGB (Figure 3.1) also yielded an identical weighted mean zircon U-Pb age of 3753 ± 6 Ma (Figure 3.7A) which marks the first reported finding of an Eoarchean trondhjemite in the eastern portion of the belt. Recently, a 3.76 Ga TTG was also found next to the 3.66 Ga tonalite that borders the western limit of the NGB (Greer et al., 2020). These newly reported U-Pb ages provide further evidence that the extent of the 3.76 Ga magmatic event around the Nuvvuagittuq area of the NESP is more widespread than originally thought and not restricted to the rare fine-grained trondhjemitic bands intruding the NGB.

The Ukaliq Supracrustal Belt, located a few kilometers northeast of the NGB, is a small ~300m x 50m enclave comprising of mafic and ultramafic rocks that may share similar geochemical and isotopic characteristics with some lithologies of the NGB (Caro et al., 2017, Chapter 2 of this thesis). The poor and limited exposure and the lack of cummingtonite-bearing amphibolites in the USB that dominate the NGB make it difficult to establish an unequivocal genetic link between the two belts (O'Neil et al., 2019), but the presence of hornblende-amphibolites in the USB that are mineralogically, texturally, geochemically and isotopically similar to the fine-grained gneissic gabbros of the NGB indicates that both regions preserve Hadean mafic rocks (Chapter 2 of this thesis). Sample UK-002 was collected from a thin felsic band intruding the hornblende-amphibolites in the USB in order to better constrain the age of the USB mafic rocks, similarly to the age constraints provided by the 3.76 Ga trondhjemite bands intruding the NGB gabbros. Zircons from UK-002 yielded a weighted mean U-Pb age of 3638 ± 11 Ma (Figure 3.7C), which confirms a minimum Eoarchean age for the USB gabbroic rocks. A second age population, made up of zircons and zircon rims displaying dark CL features, yielded a weighted mean U-Pb age of 2623 ± 10 Ma (Figure 3.7C), consistent with the timing of regional metamorphism. The ~3.64 Ga age is thus considered as the age of zircon crystallization while the

~2.62 Ga age is considered as the age of metamorphic overprinting. This newly reported ~3.64 Ga age is similar to previously reported ages of 3.60 to 3.45 Ga for tonalitic gneisses surrounding the USB (Caro et al., 2017; Greer et al., 2020) and to the 3.66 Ga NGB tonalites (David et al., 2009; O'Neil et al., 2013). Despite the fact that the whole-rock major element composition and CIPW normative mineralogy for UK-002 is reminiscent of the NGB tonalites (Figure 3.2), its pronounced HREE depletion is similar to the 3.76 Ga NGB trondhjemites (Figure 3.5A). It is therefore difficult to establish if the same ~3.6 Ga felsic magmatic event was recorded in both the NGB and USB or if it represents coeval but distinct magmatic episodes. Nevertheless, this suggests that the extent of the 3.76 Ga trondhjemitic magmatism may only be restricted to the Nuvvuagittuq Greenstone Belt.

3.5.2 Petrogenesis of the Nuvvuagittuq granitoids

Multiple generations of TTGs spanning more than 400 million years found locally intruding and surrounding the Nuvvuagittuq Greenstone Belt present a great opportunity to study the evolution of early felsic crust. These include a 3.76 Ga intrusive and plutonic trondhjemite, a 3.66 Ga and 3.51 Ga tonalite as well as a 3.35 Ga felsic schist (O'Neil et al., 2013). The zircon initial εHf value trend with time for the ≤3.66 Ga granitoids follow a $^{176}Lu/^{177}Hf$ evolution line that is consistent with the derivation of a 4.3–4.4 Ga mafic crust similar in composition to that of the Ujaraaluk unit (O'Neil et al., 2013). However, zircon initial Hf compositions for the 3.76 Ga trondhjemites exhibit slightly more radiogenic Hf isotopic compositions compared to the trend defined by the ≤3.66 Ga granitoids, which could suggest a different protolith. O'Neil et al. (2013) determined that the higher initial εHf zircon values for the 3.76 Ga trondhjemites could be explain

if they were sourced from the melting of a 4.1 Ga mafic rock with a $^{176}Lu/^{177}Hf$ ratio similar to that of the NGB fine-grained gneissic gabbros.

In order to gain a better insight on the petrogenetic processes responsible for multi-generational TTG formation observed in and around the Nuvvuagittuq Greenstone Belt, additional trace element and oxygen isotope analyses were carried out on zircons from the same TTG samples previously analyzed for U-Pb and Hf isotope compositions by O'Neil et al. (2013).

3.5.2.1 Insights from zircon trace element compositions

Zircons from the 3.76 Ga small intrusive trondhjemitic band (PC-287) and plutonic trondhjemite (PC-286), 3.66 Ga tonalite (PC-284) and 3.35 Ga felsic schist (PC-134) all exhibit steeply rising slopes from the LREE to the HREE, a positive Ce-anomaly and a negative Eu-anomaly. These REE profiles are consistent with unaltered igneous zircon where the higher HREE concentrations compared to the LREE can be explained by the fact that the smaller-radii HREE (i.e. Lu^{3+} = 0.977 Å) are more readily able to replace Zr^{4+} (0.84 Å) in the zircon crystal lattice due to their similar ionic radii (Shannon, 1976). The larger radii of the LREE (i.e. La^{3+} = 1.16 Å) makes them less compatible in the zircon crystal lattice. One exception to this is Ce, which can be both trivalent (Ce^{3+}) and tetravalent (Ce^{4+}). Ce^{4+} has an ionic radius of 0.97 Å and is therefore more compatible in zircon. Positive Ce-anomalies are associated with the abundance of Ce^{4+} in the melt which is directly related to the Ce^{4+}/Ce^{3+} ratio. This ratio is a function of oxygen fugacity and therefore a positive Ce-anomaly is associated with crystallization under variable yet relatively oxidized melt conditions (Murali et al., 1983). However, the co-existing Ce-anomaly and Eu-anomaly in unaltered igneous zircons creates an oxygen fugacity paradox. Europium can be divalent (Eu^{2+}) or trivalent (Eu^{3+}). Under oxidizing magma conditions, the high Eu^{3+}/Eu^{2+} ratio

should produce normalized zircon REE patterns with no or reduced Eu-anomaly (e.g. Burnham and Berry, 2012). Nevertheless, this paradox may be explained by the higher affinity of Eu in felspars whose fractionation produces Eu-depleted magmas prior to or during zircon crystallization (Hoskin & Schaltegger, 2003 and references therein). The Eu-anomaly in zircon would thus be an inherited feature from a Eu-depleted melt and may be less sensitive to oxygen fugacity in comparison to Ce. Therefore, the typical igneous zircon REE compositions found in samples PC-134, PC-284, PC-286 and PC-287 indicate that the 3.76 Ga, 3.66 Ga and 3.35 Ga magmatic events in the Nuvvuagittuq Greenstone Belt are all consistent with oxidized melts that experienced plagioclase fractionation prior to or during zircon crystallization. The steeply rising slopes from the LREE to the HREE also imply that the zircons did not crystallize alongside a HREE-bearing mineral phase such as garnet (i.e. Rubatto, 2002). The exact origin of the felsic schist (PC-134) was previously equivocal, but the typical igneous REE trend of its zircons suggests that they crystallized from a melt as previously proposed by O'Neil et al. (2013) rather than from metamorphic fluids (i.e. David et al., 2009).

Figure 3.9 compares the REE compositions of zircons from the NGB granitoids to zircons from other early terranes. The vast majority of Hadean and early Archean zircons compiled here are characterized by a typical magmatic REE trends with steeply rising slopes from the LREE to the HREE, a positive Ce-anomaly and a negative Eu-anomaly (Figure 3.9). With the exception of the 3.5 Ga tonalite (PC-285) (detailed further), zircons from the NGB granitoids display similar REE compositions to Hadean and Eoarchean zircons from the Jack Hills, the Acasta Gneiss Complex, the Itsaq Gneiss Complex and the Saglek-Hebron Complex that have been interpreted as unaltered. This suggests that the NGB zircons, with the possible exception of zircons from PC-285, display relatively pristine compositions that have not been significantly affected by post-

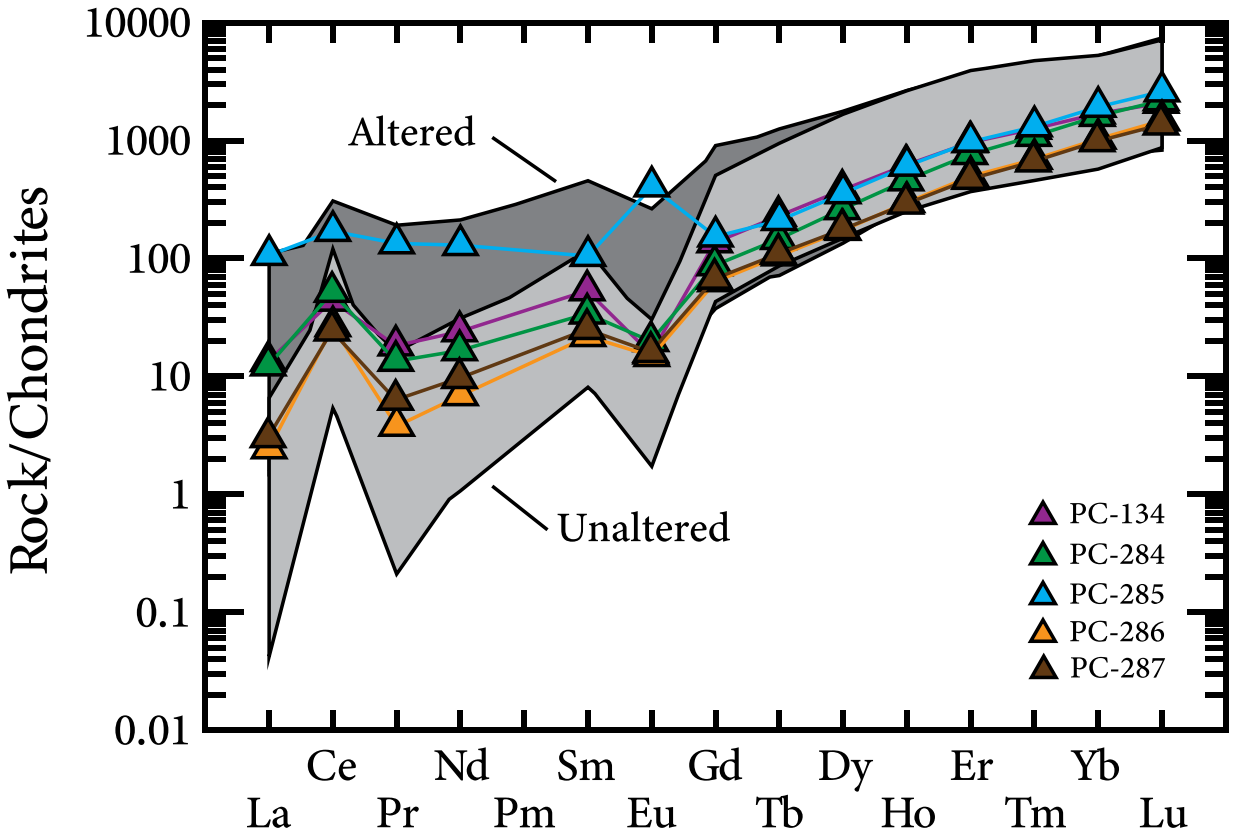

Figure 3.9: Compilation of selected REE analyses from other Hadean and Archean zircons. Dark grey "Altered" and light grey "Unaltered" zircon fields are comprised of zircon REE compositions from the Saglek-Hebron Complex (Vezinet et al., 2018), the Itsaq Gneiss Complex (Whitehouse and Kamber., 2002), the Acasta Gneiss Complex (Reimink et al., 2014) and the Jack Hills zircons (Cavosie et al., 2006; Peck et al., 2001). Trace element concentrations from zircons of the five NGB granitoids are plotted as mean values from Table 3.2. Normalized after Sun and McDonough (1989). Same symbols as in Figure 3.8.

magmatic alteration. It also points to that fact that the petrogenetic conditions controlling crustal zircon chemistry have not changed since the formation of the oldest crustal evolved rocks. It is worth noting that two NGB TTGs, PC-134 and PC-284, have slightly higher La concentrations compared to the "unaltered" zircon field defined by zircons from previous studies (e.g. Cavosie et al., 2006; Reimink et al., 2014; Vezinet et al., 2018; Whitehouse and Kamber, 2002). A subset of the Jack Hills zircons displaying a LREE-enrichment was originally interpreted as derived from a

highly differentiated magma, indicating that evolved continental crust was already present in the Hadean (Peck et al., 2001; Wilde et al., 2001). This "LREE overabundance" has also been found in other zircons such as those in a 3.8 Ga tonalitic gneiss from the Itsaq Gneiss Complex, but zircon/whole rock distribution coefficient modeling demonstrated that a LREE-enrichment in zircon cannot be used to infer original melt composition and rather stems from secondary post-magmatic processes (Whitehouse & Kamber, 2002). Despite the higher La content of zircons from PC-134 and PC-284, both samples still display well-defined magmatic zircon REE patterns and are unlikely to have been affected by LREE-enrichment after their crystallization.

Zircons from sample PC-285 display contrasting REE profiles (Figure 3.8C) compared to the zircons found in the other generations of granitoids studied here, which may indicate a different petrogenetic history for the 3.51 Ga magmatic event bordering the southern limit of the NGB. These zircons display LREE-depletion compared to the HREE, still indicative that the zircons did not crystallize alongside a HREE-bearing mineral phase, but with higher LREE contents compared to the other NGB granitoids (Figure 3.8). The Ce-anomaly in the zircons of PC-285 are only slightly positive, perhaps indicative of crystallization from a more reduced magma, and most zircons show notable positive Eu-anomalies (Figure 3.8C). Higher LREE contents could be due to micro-inclusions of LREE-bearing phases such as apatite and monazite that are commonly found in zircon. However, all zircons from PC-285 display the same relative higher abundance of LREE and it is unlikely that each analysis was effected by LREE inclusions. Moreover, as mentioned in Section 3.4.3, all analyses displaying abnormally high concentrations in P or Fe-Ti indicative of inclusions were discarded and therefore the possibility of mineral inclusions being the cause of the LREE-enrichment in the zircons of PC-285 can be ruled out. Alternatively, higher LREE contents and lower positive Ce-anomalies have historically been associated to hydrothermal zircons (e.g.

Hoskin, 2005) or to some type of alteration process in radiation-damaged regions leading to local LREE-enrichment (e.g. Cavosie et al., 2006). In fact, zircons in PC-285 display REE profiles more similar to the "altered" zircons from other early terranes (Figure 3.9) and tend to plot closer to the hydrothermal zircon field compared to zircons from the other generations of granitoids in the NGB (Figure 3.10). However, the reliability of such discrimination diagrams has been called into question and may not be suitable for every situation (e.g. Fu et al., 2009; Zhong et al., 2018 and references therein). Nevertheless, the LREE-enrichment present in the zircons of PC-285 is most likely related to some type of hydrothermal origin or alteration. However, hydrothermal zircon analyses reported in Hoskin (2005) and zircons labelled as "altered" in other studies (e.g. Bell et al., 2016; Reimink et al., 2020; Vezinet et al., 2018) do not typically display the positive Eu-anomaly that is so prominent in the zircons of PC-285 (Figure 3.8C). Therefore, hydrothermalism or alteration cannot account for all the trace element characteristics of the zircons in PC-285.

Positive Eu-anomalies in zircons have rarely been reported. Such excess in Eu compared to other REE of similar radius could be produced if the magma from which the zircons crystallized was characterized by a pronounced positive Eu-anomaly, but the whole-rock REE profile for PC-285 actually displays a slight negative Eu-anomaly (O'Neil et al., 2013). Zircons with positive Eu-anomalies were reported in a group of zircons from a jadeitite in Guatemala (Yui et al., 2010). These zircons have higher LREE contents, smaller positive Ce-anomalies and pronounced positive Eu-anomalies similar to those observed in the zircons of PC-285. Yui et al. (2010) interpreted these zircon REE patterns as being the result of a reducing fluid leading to plagioclase alteration or decomposition during zircon formation allowing for excess Eu to be incorporated into the zircon crystal lattice. The interpretation that the Guatemalan jadeitite zircons crystallized from such hydrothermal fluids was further supported by their sub- to anhedral form, a lack of oscillatory

zoning, presence of fluid inclusions and very low Th/U ratios of <0.005 (Yui et al., 2010). Although the zircons from PC-285 share similarities to the Guatemalan jadeitite zircons in terms of REE compositions, they display euhedral forms, have oscillatory zoning and average Th/U ratios of 0.47 which are all more consistent with magmatic zircons. Nevertheless, textural and compositional characteristics of hydrothermal zircons seem to have a large discrepancy and definitive features have yet to be established (e.g. Hoskin and Schaltegger, 2003; Schaltegger, 2007).

Regardless of their origin, the zircons in PC-285 most likely experienced some type of alteration, as indicated by their elevated LREE contents, as well as plagioclase breakdown during zircon crystallization to account for their positive Eu-anomaly. Elevated calcium contents in zircon have been used as an alteration indicator because Ca^{2+} is incompatible in the zircon crystal lattice (i.e. Rayner et al., 2005). Additional Ca analyses in the zircons of PC-285 may help determine their degree of alteration in order to establish if any reliable petrogenetic information can be inferred from their chemical compositions. Recently, it has been discovered that ~3.5 Ga magmatism may be more widespread than previously thought in the surrounding areas of Nuvvuagittuq and Ukaliq (Greer et al., 2020). Further trace element analyses in zircons from other 3.5 Ga TTGs in the region may help uncover if the zircon REE compositions of PC-285 are the result of local alteration processes or are consistent with specific petrogenetic processes that affected the entirety of the Voizel Suite.

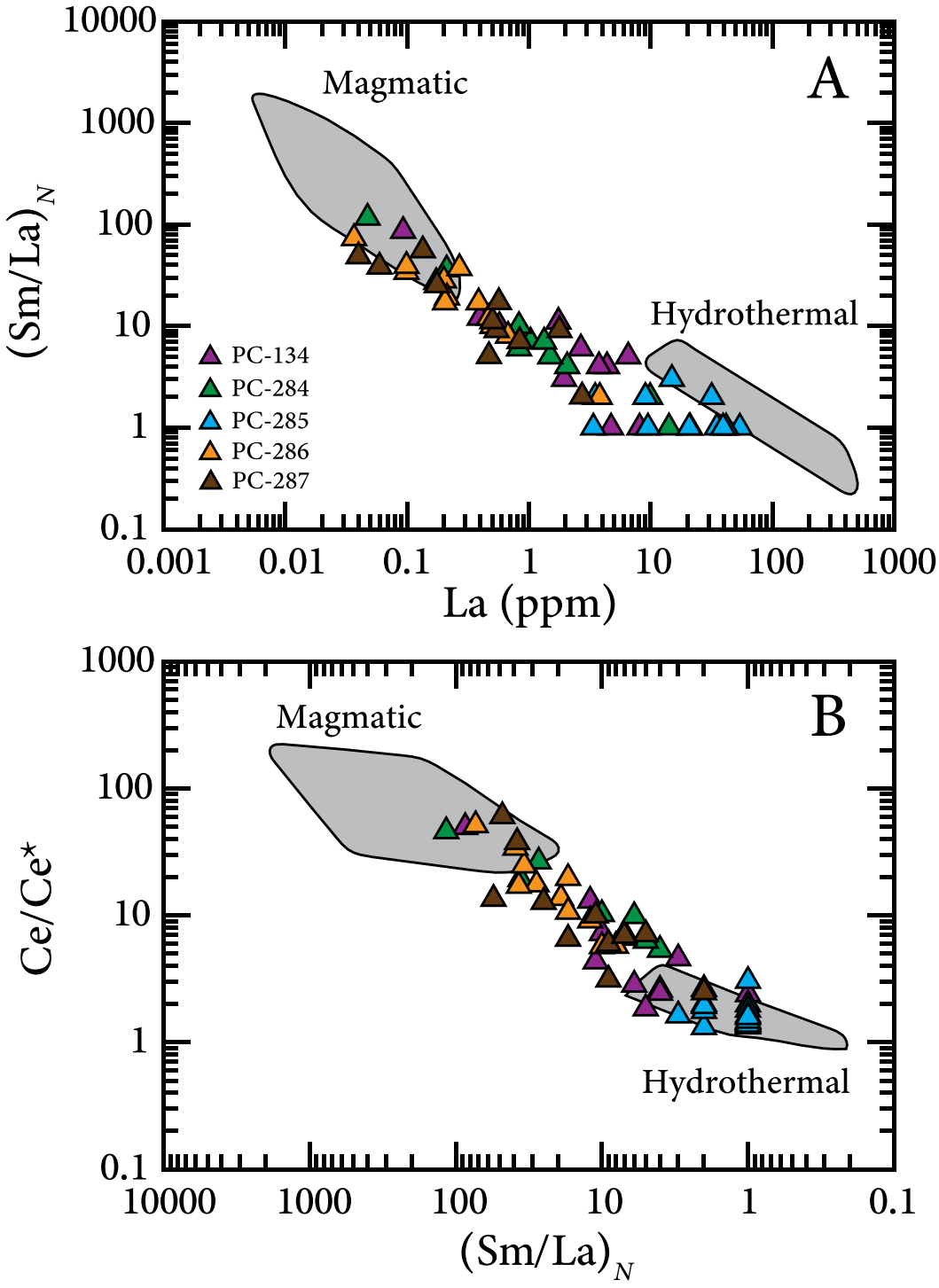

Figure 3.10: Magmatic vs. hydrothermal zircon plots. A) $(Sm/La)_N$ vs. La (ppm); B) Ce/Ce* vs. $(Sm/La)_N$. Magmatic and hydrothermal zircon fields are those defined by Hoskin (2005). Chondrite normalizing values are from Sun and McDonough (1989). Zircons displaying evidence of inclusions, as described in Section 3.4.3, are not included in these plots. Same symbols as in Figure 3.8.

3.5.2.2 Insights from zircon $\delta^{18}O$ compositions

Zircon oxygen isotope compositions have been used as an indicator to determine potential low-temperature water-rock surface interactions over time because zircon can preserve its primary $\delta^{18}O$ compositions even while subjected to high-grade metamorphism (Valley, 2003). Igneous rocks that differentiate from mantle-derived melts produce zircons with $\delta^{18}O$ values of $5.3 \pm 0.6‰$ (2σ), corresponding to "normal" mantle-like values (King et al., 1998; Valley et al., 1998). Intra-crustal recycling can cause magma to interact with supracrustal materials that experienced low-temperature hydrothermal alteration, which will produce zircon with $\delta^{18}O$ compositions that significantly deviate from the mantle value (Valley, 2003; Valley et al., 2005). Oxygen isotope fractionations are greater on or near the surface of the Earth and thus zircons inherit the $\delta^{18}O$ compositions from the altered supracrustal materials that contaminate their parental magma.

There is a slight increase in zircon $\delta^{18}O$ values over time in the multiple generations of TTGs intruding and surrounding the NGB (Figure 3.11). The mean zircon $\delta^{18}O$ compositions of both the thin band and plutonic 3.76 Ga trondhjemites plot well within the mantle zircon field whereas the average $\delta^{18}O$ value for the zircons from the 3.66 Ga tonalite is slightly higher than the mantle zircon field. Zircons from the 3.51 Ga tonalite show an average $\delta^{18}O$ value overlapping with the mantle zircon field but also display the most important variation, with a number of zircons exhibiting higher $\delta^{18}O$ values compared to the mantle zircon field. Only the youngest granitoid found in the NGB, the 3.35 Ga felsic schist (PC-134), displays zircon $\delta^{18}O$ values that are completely outside of the mantle zircon field with an average $\delta^{18}O$ value of 6.58‰. This suggests that the earliest felsic magmas were derived from a relatively pristine crustal source that did not experience significant hydrothermal alteration whereas the zircons from the 3.66 Ga to 3.35 Ga

granitoids crystallized from a melt that was sourced from supracrustal material that had experienced varying degrees of low-temperature hydrothermal alteration.

The more radiogenic Hf isotopic composition of the zircons from the 3.76 Ga TTG compared to the ≤3.66 Ga NGB granitoids has led O'Neil et al. (2013) to suggest a possible distinct crustal source for the oldest NGB TTG. This also seems to be supported by slightly lower $\delta^{18}O$ values for the 3.76 Ga zircons, although not statistically resolvable from the 3.66 Ga to 3.51 Ga TTG. Based on zircon initial Hf isotope compositions, it has been suggested that the ≤3.66 Ga TTGs were derived from mafic crust similar in age and composition to that of the Ujaraaluk unit, whereas the 3.76 Ga trondhjemites are more consistent with the derivation of a mafic rock with an age and composition similar to that of the fine-grained gneissic gabbros (O'Neil et al., 2013). The Ujaraaluk unit has been interpreted as representing a package of mafic pyroclastic deposits that experienced variable degrees of hydrothermal alteration (O'Neil et al., 2011). In comparison, the fine-grained gabbro sills are massive intrusions with limited signs of alteration. The $\delta^{18}O$ values measured here in the NGB zircons would be consistent with this interpretation that the 3.76 trondhjemites, displaying mantle-like zircon $\delta^{18}O$ compositions, were derived from a source similar to the unaltered gneissic gabbros while the younger TTG would be sourced from the hydrothermally altered Ujaraaluk unit, producing zircons with higher $\delta^{18}O$ values. The slight increase in $\delta^{18}O$ compositions with time observed in the ≤3.66 Ga zircons (Figure 3.11) would also suggest that the degree of low-temperature hydrothermal alteration of the source material increased with time to produce 3.66 Ga and 3.51 Ga TTG with more heterogeneous $\delta^{18}O$ composition overlapping the upper limit of mantle-like values, and younger 3.35 Ga felsic crust sourced from more readily hydrothermally altered supracrustal materials.

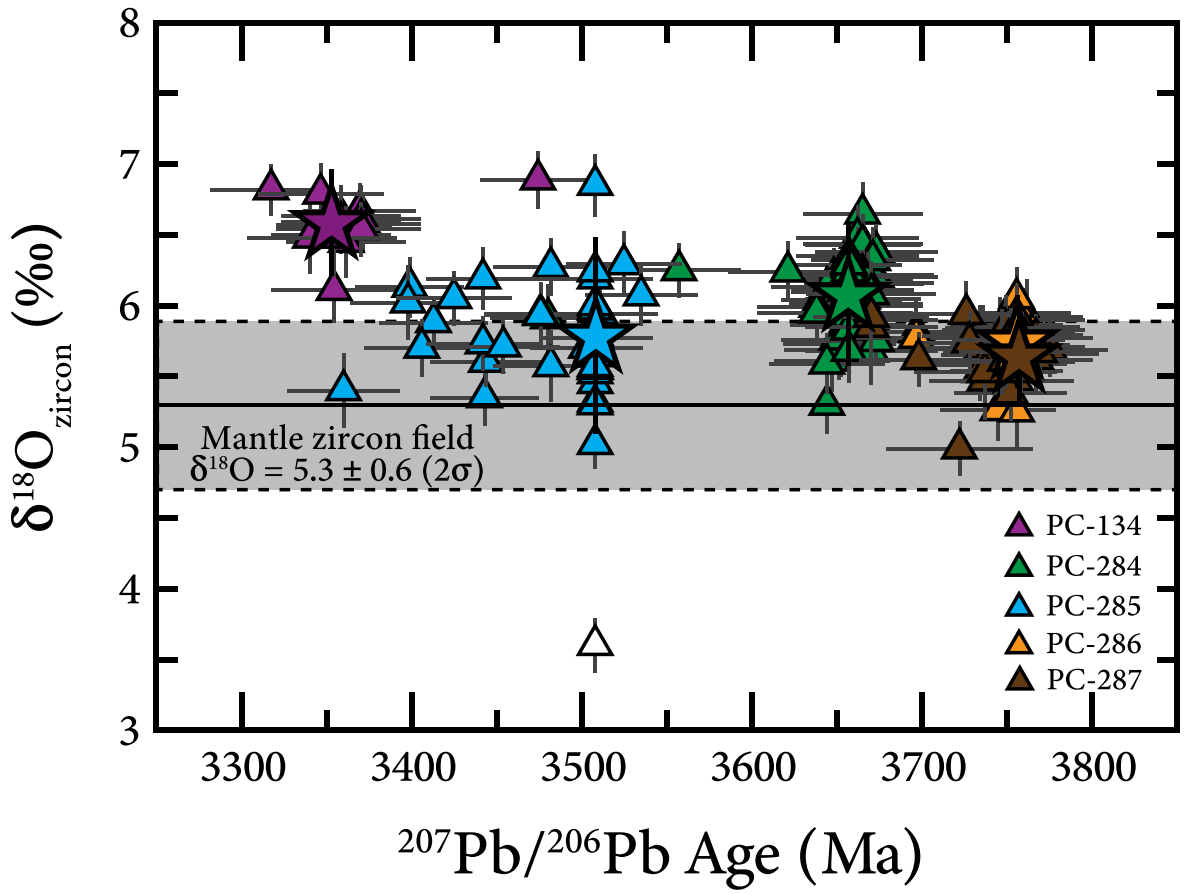

Figure 3.11: $\delta^{18}O$ zircon VSMOW values (‰) vs. $^{207}Pb/^{206}Pb$ Age (Ma). Mantle zircon field is defined by Valley et al. (1998). Same symbols as in Figure 3.8. White triangle represents an outlier analysis that was not included in the mean calculations of Table 3.3. Stars represent mean $\delta^{18}O$ zircon values (Table 3.3) for each sample plotted at the weighted mean $^{207}Pb/^{206}Pb$ age of its host rock. Zircons that had not previously been dated were also plotted at the weighted mean $^{207}Pb/^{206}Pb$ age of their host rock. $^{207}Pb/^{206}Pb$ ages are those reported in O'Neil et al. (2013). Error bars are reported as 2σ.

3.5.3 Crustal source of Hadean-Eoarchean continental crust

Zircon oxygen isotope and trace element analyses, combined with more traditional U-Pb-Hf isotope analyses, have become increasingly used over the past two decades as a way of better understanding the petrogenetic processes associated with the evolution and production of the continental crust. The combination of short-lived isotopic systems such as ^{146}Sm-^{142}Nd in host rocks and U-Pb-Hf in zircons from the oldest preserved rocks on Earth point to an early crust, predominantly mafic in composition, which served as source material to produce the felsic rocks

forming the oldest continental crust (e.g. Carlson et al., 2019). Zircon oxygen isotopic compositions have also provided a unique window into the source material of the felsic magmas crystallizing the oldest zircons on Earth from the Jack Hills. Valley et al. (2005) noted that nearly all Hadean and Archean zircons from the Jack Hills have a relatively small range of $\delta^{18}O$ values overlapping the mantle zircon field, but with some zircons displaying heavier oxygen isotopic compositions up to 7.5‰. Cavosie et al. (2005) defined a field of Archean "supracrustal zircons" with $\delta^{18}O$ values between 6.5‰ and 7.5‰, indicative of Hadean and early Archean zircons that crystallized from a felsic magma derived from the melting of crustal material that had previously experienced low-temperature hydrothermal alteration. Based on these elevated $\delta^{18}O$ values, they concluded that alteration from liquid water occurred at Earth's surface by 4200 Ma, and possibly as early as 4325 Ma, and that reworking of previously altered crust is a process that was involved in the formation of the earliest continental crust. Since then, zircons from a number of other ancient terranes have been analyzed for $\delta^{18}O$ compositions and the following section will compare the zircon oxygen isotope compositions of the Nuvvuagittuq Greenstone Belt to those of other Hadean and early Archean terranes to further understand the petrogenesis of the continental crust and highlight possible global or larger scale processes that operated during Earth's early crust formation.

Figure 3.12 compiles zircon $\delta^{18}O$ compositions for some of Earth's oldest felsic crustal rocks and the Jack Hills detrital zircons. Individual zircon $\delta^{18}O$ values are shown, as well as the average $\delta^{18}O$ value obtained for zircons separated from the same rock sample of magmatic origin (i.e. not detrital zircons) as they should have crystallized from the same magma under similar conditions. One exception is for the 4.02 Ga zircons from the Idiwhaa tonalitic gneiss of the Acasta

Gneiss Complex, which have distinct phases with different $\delta^{18}O$ compositions (Reimink et al., 2014). The average $\delta^{18}O$ values for both zircon phases are plotted at the same age for this sample.

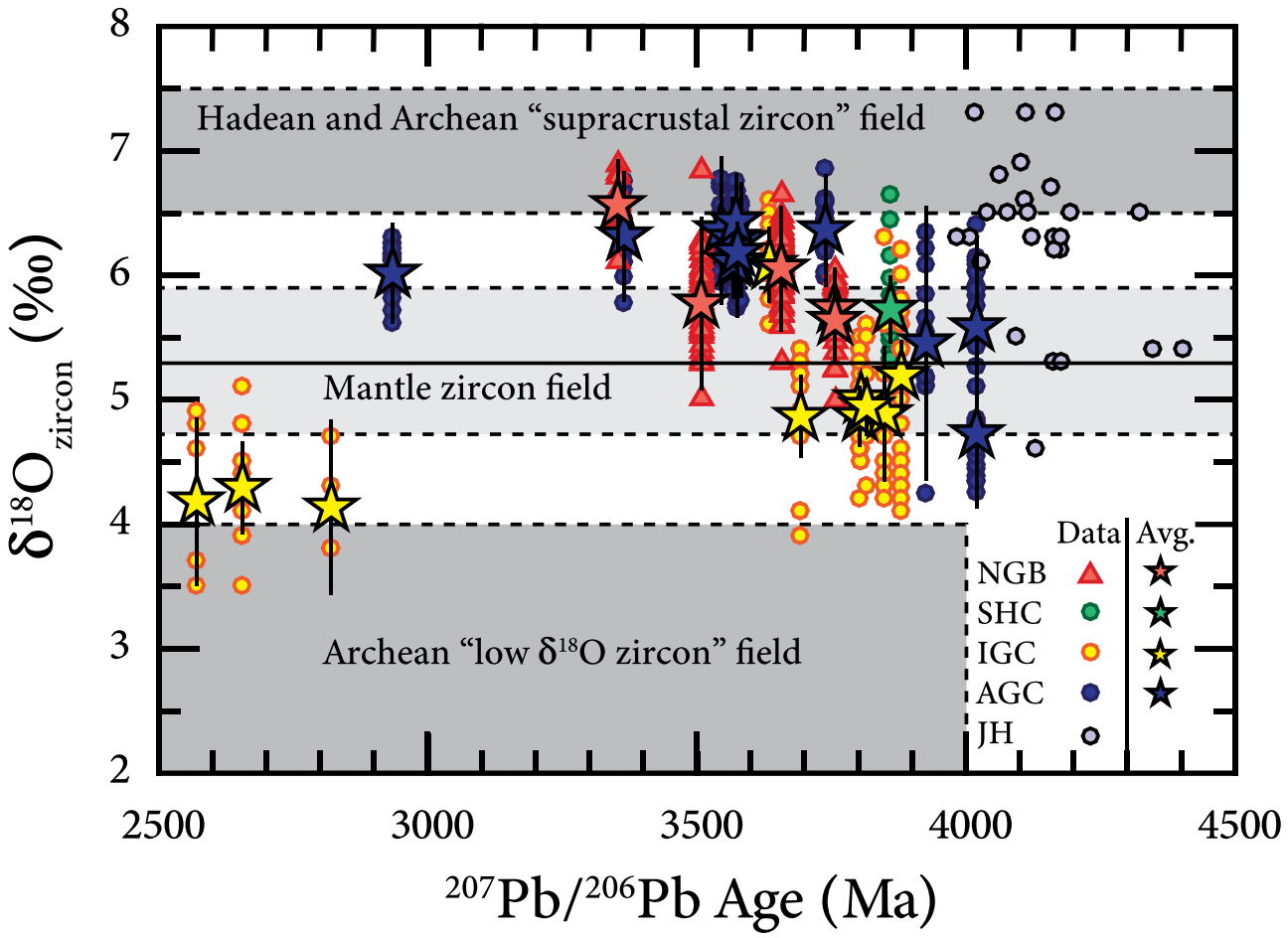

Figure 3.12: Compilation of selected oxygen isotope analyses from other Hadean and Archean zircons with 95–105% concordance. Data from: Nuvvuagittuq Greenstone Belt (this study, ages reported in O'Neil et al., 2013); Saglek-Hebron Complex (Vezinet et al., 2018); Itsaq Gneiss Complex (Hiess et al., 2009, 2011); Acasta Gneiss Complex (Reimink et al., 2014, 2016); Jack Hills zircons (Cavosie et al., 2005). Zircons were plotted at the $^{207}Pb/^{206}Pb$ age of their host rock, except for the Jack Hills zircons which were plotted according to their reported $^{207}Pb/^{206}Pb$ age. Mantle zircon field ($\delta^{18}O$ = 5.3 ± 0.6‰ (2σ)) is defined by Valley et al. (1998), Hadean and Archean "supracrustal zircon" field ($\delta^{18}O$ = 6.5–7.5‰) is defined by Cavosie et al. (2005) and Archean "low $\delta^{18}O$ zircon" field ($\delta^{18}O$ = 2.0–4.0‰) is defined by Hiess et al. (2011). Average $\delta^{18}O$ zircon values from the NGB and AGC TTGs are reported as means ± 2σ whereas data from the SHC and IGC TTGs are reported as weighted means ± 95% confidence level. Abbreviations: NGB = Nuvvuagittuq Greenstone Belt; SHC = Saglek-Hebron Complex; IGC = Itsaq Gneiss Complex; AGC = Acasta Gneiss Complex; JH = Jack Hills; Avg. = Average. Symbols: Red triangles = NGB data; Red stars = Avg. $\delta^{18}O$ zircon values for NGB granitoids; Green circles = SHC data; Green star = Avg. $\delta^{18}O$ zircon values for SHC granitoids; Yellow circles = IGC data; Yellow stars = Avg. $\delta^{18}O$ zircon values for IGC granitoids; Blue circles = AGC data; Blue stars = Avg. $\delta^{18}O$ zircon values for AGC granitoids; Grey circles = JH data.

The NGB zircon $\delta^{18}O$ compositions are consistent with the range of values from mantle-like to slightly heavier O isotopic compositions seen throughout the Hadean and Archean. However, no $\delta^{18}O$ lower than the mantle zircon value have been measured in the NGB such as is the case with some zircons from the Acasta and the Itsaq Gneiss complexes. Since these low $\delta^{18}O$ values have been interpreted as indicative of parental magmas derived from a crustal component that was hydrothermally altered by meteoric fluids at high temperatures (e.g. Hiess et al., 2011; Reimink et al., 2014), this suggests that high-temperature hydrothermalism was not an important process affecting the precursor crustal material of the NGB granitoids.

The trend seen in the Nuvvuagittuq Greenstone Belt, where the oldest felsic magmas appear to crystallize zircons with mantle-like $\delta^{18}O$ values, to later crystallize zircons with higher $\delta^{18}O$ values during younger felsic magmatic events, seems to be generally observed for other Eoarchean terranes. The oldest granitoids from the Acasta Gneiss Complex, Itsaq Gneiss Complex and the Saglek-Hebron Complex are also dominated by zircons with mantle-like to slightly lower $\delta^{18}O$ compositions. Some individual >3800 Ma zircons from the Acasta Gneiss Complex, Itsaq Gneiss Complex and the Saglek-Hebron Complex display slightly higher $\delta^{18}O$ values, even overlapping with the "supracrustal zircon" field, but with average $\delta^{18}O$ values within the mantle zircon field (Figure 3.12). The $\delta^{18}O$ values that are outside of the mantle zircon field become predominant only after ~3700 Ma. This increase, or decrease, of $\delta^{18}O$ values with time observed in multiple early terranes may suggest a similar progressive alteration of the precursor source(s) of early Archean granitoids where the first evolved crust in these areas was derived from melting of older crustal material exhibiting limited surface alteration, which then transitioned to a precursor source of felsic crust in the Paleoarchean that had experience either low-temperature hydrothermal alteration leading to $\delta^{18}O$ compositions over the mantle zircon field (e.g. Reimink et al., 2016) or

high-temperature alteration processes leading to $\delta^{18}O$ compositions below the mantle zircon field (e.g. Hiess et al., 2011). This could be consistent with the interpretation made by Hiess et al. (2011) for the Itsaq Gneiss Complex, that the emplacement of the first evolved crust may have facilitated the incorporation of fluids to produce hydrothermally altered materials that were assimilated in subsequent felsic magmatic events. If the crustal precursor source for these different generations of Hadean to Paleoarchean felsic rocks is a common long-lived mafic crust, as suggested by other isotopic tracers, at least for the NGB (O'Neil et al., 2013; O'Neil and Carlson, 2017), it would suggest that it remained at shallow depths for up to 400 million years before being subjected to low-temperature surface alteration processes.

For the Acasta Gneiss Complex, the shift to elevated zircon $\delta^{18}O$ values appears to coincide with the transition between 3600 and 3700 Ma to more radiogenic Hf compositions, suggesting the involvement of more juvenile material and a fundamental change in the source of the magmas (Bauer et al., 2017). This could suggest that the Hadean/Eoarchean and Paleoarchean felsic crust from Acasta was sourced from distinct crustal material rather than progressive alteration of a long-lived crustal source. This is however not observed for zircons from the NGB and the Itsaq Gneiss Complex, where the apparent shift to elevated zircon $\delta^{18}O$ values is not coeval with the shift in Hf isotopic compositions (Næraa et al., 2012; O'Neil et al., 2013). The transition to more juvenile Hf isotopic compositions is also observed in the Saglek-Hebron Complex at ~3200 Ma (Wasilewski et al., *submitted*), but the current limited number of $\delta^{18}O$ analyses restricted to Eoarchean zircons (Vezinet et al., 2018) does not allow to evaluate if there is a concomitant shift in Hf and O isotopic composition.

Although the few oldest (>4350 Ma) detrital zircons from the Jack Hills displayed mantle-like values to later show elevated $\delta^{18}O$ values, similar to the trend observed in most other early

terranes, Figure 3.12 suggests that the hydrothermal alteration processes affecting the precursor crust of the Jack Hills zircons and that of the other early granitoids was not coeval. The oldest zircons from the early gneissic complexes and the NGB mostly exhibit mantle-like $\delta^{18}O$ values between 4000 and 3750 Ma, and display higher, or lower, $\delta^{18}O$ values only after ~3700 Ma, whereas most 4000 Ma to 4200 Ma detrital zircons from the Jack Hills exhibit elevated $\delta^{18}O$ values. Moreover, no zircons from the early gneissic complexes yielded $\delta^{18}O$ values as high as what was measured in the Jack Hills detrital zircons. This would suggest that the crustal precursor source of the Jack Hills zircons had experienced more extensive low-temperature alteration, already in the Hadean, compared to the crustal source of the granitoids from other early terranes, which appear to have been subjected to more prominent low-temperature hydrothermal processes only after 3750 Ma. Therefore, even if alteration from liquid water occurred at Earth's surface by 4200 Ma, as evidenced from the Jack Hills zircons (Cavosie et al., 2005), it may not have been a widespread process affecting the earliest crust.

3.6 Conclusion

The oldest known evolved rocks from the Superior Province are ~3.8 Ga trondhjemites that have previously only been observed in the southwestern corner of the Nuvvuagittuq Greenstone Belt as thin intrusions or as a single plutonic sample in direct contact with the belt. New U-Pb data reported here indicates a more important extent of this Eoarchean magmatic event, with 3.76 Ga trondhjemites now identified in the central and eastern parts surrounding the NGB. However, no granitoid with a similar age of 3.76 Ga has yet to be identified within the neighbouring Ukaliq Supracrustal Belt, despite the fact that it appears to include similar lithologies to the NGB. This is

perhaps indicative that this early Archean felsic magmatic event is restricted only to the immediate surroundings of the NGB.

Zircon trace element compositions of most of the Eoarchean to Paleoarchean granitoids from the NGB display typical magmatic REE patterns and thus provide an ideal temporal suite to study the primary petrogenetic processes responsible for the formation and evolution of early continental crust production from the Superior Province. However, zircons from the NGB 3.51 Ga tonalite have unusual REE compositions, with atypical positive Eu-anomalies which may indicate some type of post-magmatic alteration. Further investigation would be required to better constrain the origin of their geochemical compositions. Regardless of the process that led to these unusual features, it did not appear to have affected the older, nor the younger, TTG in the NGB area.

Zircon $\delta^{18}O$ values slightly increase from the oldest TTGs to the youngest TTGs in the NGB. The 3.76 Ga trondhjemites display zircon $\delta^{18}O$ values consistent with the derivation of unaltered differentiated mantle melts while the ≤3.66 Ga TTGs have zircon $\delta^{18}O$ values indicating some degree of low-temperature hydrothermally altered supracrustal materials in their crustal source. This could be consistent with different precursor sources exhibiting variable degrees of alteration, such as the unaltered fine-grained gneissic gabbros and the hydrothermally altered Ujaraaluk unit, as previously proposed based on Hf isotopes. The similar trend observed on a global scale, where the first felsic magmatic event tends to crystallize zircons with mantle-like $\delta^{18}O$ values whereas younger generations of felsic magmatism tend to diverge towards higher or lower zircon $\delta^{18}O$ compositions, could suggest that a comparable process was involved in the formation of the earliest continental crust in other Hadean and Eoarchean terranes. The first evolved crust in these terranes appears to have derived from relatively unaltered older crust and the emplacement of this first evolved crust may have assisted in the transport of fluids and thus

the incorporation of altered supracrustal materials in successive felsic magmatic events. This shift to higher $\delta^{18}O$ values appears to be relatively coeval in most Hadean-Eoarchean terranes around 3750 Ma, except for the Jack Hills detrital zircons showing earlier evidence of low-temperature alteration processes.

References

Adam, J., Rushmer, T., O'Neil, J., & Francis, D. (2012). Hadean greenstones from the Nuvvuagittuq fold belt and the origin of the Earth's early continental crust. Geology, 40(4), 363–366.

Augland, L. E., & David, J. (2015). Protocrustal evolution of the Nuvvuagittuq Supracrustal Belt as determined by high precision zircon Lu-Hf and U-Pb isotope data. Earth and Planetary Science Letters, 428, 162–171.

Barker, F. (1979). Trondhjemite: Definition, environment and hypotheses of origin. In F. Barker (Ed.), Trondhjemites, Dacites and Related Rocks. Developments in Petrology, 6, Amsterdam: Elsevier, pp. 1–12.

Bauer, A. M., Fisher, C. M., Vervoort, J. D., & Bowring, S. A. (2017). Coupled zircon Lu–Hf and U–Pb isotopic analyses of the oldest terrestrial crust, the >4.03 Ga Acasta Gneiss Complex. Earth and Planetary Science Letters, 458, 37–48.

Bell, E. A., Boehnke, P., & Harrison, T. M. (2016). Recovering the primary geochemistry of Jack Hills zircons through quantitative estimates of chemical alteration. Geochimica et Cosmochimica Acta, 191, 187–202.

Black, L. P., Kamo, S. L., Allen, C. M., Davis, D. W., Aleinikoff, J. N., Valley, J. W., Mundil, R., Campbell, I. H., Korsch, R. J., Williams, I. S., & Foudoulis, C. (2004). Improved $^{206}Pb/^{238}U$ microprobe geochronology by the monitoring of a trace-element-related matrix effect; SHRIMP, ID-TIMS, ELA-ICP-MS and oxygen isotope documentation for a series of zircon standards. Chemical Geology, 205(1–2), 115–140.

Boily, M., Leclair, A., Maurice, C., Bédard, J. H., & David, J. (2009). Paleo- to Mesoarchean basement recycling and terrane definition in the Northeastern Superior Province, Québec, Canada. Precambrian Research, 168(1–2), 23–44.

Burnham, A. D., & Berry, A. J. (2012). An experimental study of trace element partitioning between zircon and melt as a function of oxygen fugacity. Geochimica et Cosmochimica Acta, 95, 196–212.

Carlson, R. W., Garçon, M., O'Neil, J., Reimink, J., & Rizo, H. (2019). The nature of Earth's first crust. Chemical Geology, 530, 119321.

Caro, G., Morino, P., Mojzsis, S. J., Cates, N. L., & Bleeker, W. (2017). Sluggish Hadean geodynamics: Evidence from coupled $^{146,147}Sm–^{142,143}Nd$ systematics in Eoarchean supracrustal rocks of the Inukjuak domain (Québec). Earth and Planetary Science Letters, 457, 23–37.

Cates, N. L., & Mojzsis, S. J. (2007). Pre-3750 Ma supracrustal rocks from the Nuvvuagittuq supracrustal belt, northern Québec. Earth and Planetary Science Letters, 255(1–2), 9–21.

Cates, N. L., & Mojzsis, S. J. (2009). Metamorphic zircon, trace elements and Neoarchean metamorphism in the ca. 3.75 Ga Nuvvuagittuq supracrustal belt, Québec (Canada). Chemical Geology, 261(1–2), 99–114.

Cates, N. L., Ziegler, K., Schmitt, A. K., & Mojzsis, S. J. (2013). Reduced, reused and recycled: Detrital zircons define a maximum age for the Eoarchean (ca. 3750-3780Ma) Nuvvuagittuq Supracrustal Belt, Québec (Canada). Earth and Planetary Science Letters, 362, 283–293.

Cavosie, A. J., Valley, J. W., & Wilde, S. A. (2005). Magmatic $\delta^{18}O$ in 4400-3900 Ma detrital zircons: A record of the alteration and recycling of crust in the Early Archean. Earth and Planetary Science Letters, 235(3–4), 663–681.

Cavosie, A. J., Valley, J. W., & Wilde, S. A. (2006). Correlated microanalysis of zircon: Trace element, $\delta^{18}O$, and U-Th-Pb isotopic constraints on the igneous origin of complex >3900 Ma detrital grains. Geochimica et Cosmochimica Acta, 70(22), 5601–5616.

Cavosie, A. J., Valley, J. W., & Wilde, S. A. (2007). The Oldest Terrestrial Mineral Record: A Review of 4400 to 4000 Ma Detrital Zircons from Jack Hills, Western Australia. In M. J. van Kranendonk, R. H. Smithies, & V. C. Bennett (Eds.), Earth's Oldest Rocks, Developments in Precambrian Geology, 15, Amsterdam: Elsevier, pp. 91–111.

Darling, J. R., Moser, D. E., Heaman, L. M., Davis, W. J., O'Neil, J., & Carlson, R. (2013). Eoarchean to neoarchean evolution of the Nuvvuagittuq Supracrustal belt: New insights from U-Pb zircon geochronology. American Journal of Science, 313(9), 844–876.

David, J., Godin, L., Stevenson, R., O'Neil, J., & Francis, D. (2009). U-Pb ages (3.8-2.7 Ga) and Nd isotope data from the newly identified Eoarchean Nuvvuagittuq supracrustal belt, superior Craton, Canada. Bulletin of the Geological Society of America, 121(1–2), 150–163.

Fu, B., Mernagh, T. P., Kita, N. T., Kemp, A. I. S., & Valley, J. W. (2009). Distinguishing magmatic zircon from hydrothermal zircon: A case study from the Gidginbung high-sulphidation Au-Ag-(Cu) deposit, SE Australia. Chemical Geology, 259(3–4), 131–142.

Greer, J., Caro, G., Cates, N. L., Tropper, P., Bleeker, W., Kelly, N. M., & Mojzsis, S. J. (2020). Widespread poly-metamorphosed Archean granitoid gneisses and supracrustal enclaves of the southern Inukjuak Domain, Québec (Canada). Lithos, 364–365.

Guitreau, M., Blichert-Toft, J., Mojzsis, S. J., Roth, A. S. G., & Bourdon, B. (2013). A legacy of Hadean silicate differentiation inferred from Hf isotopes in Eoarchean rocks of the Nuvvuagittuq supracrustal belt (Québec, Canada). Earth and Planetary Science Letters, 362, 171–181.

Hiess, J., Bennett, V. C., Nutman, A. P., & Williams, I. S. (2009). In situ U-Pb, O and Hf isotopic compositions of zircon and olivine from Eoarchaean rocks, West Greenland: New insights to making old crust. Geochimica et Cosmochimica Acta, 73(15), 4489–4516.

Hiess, J., Bennett, V. C., Nutman, A. P., & Williams, I. S. (2011). Archaean fluid-assisted crustal cannibalism recorded by low $\delta^{18}O$ and negative εHf(T) isotopic signatures of West Greenland granite zircon. Contributions to Mineralogy and Petrology, 161, 1027–1050.

Hoskin, P. W. O. (2005). Trace-element composition of hydrothermal zircon and the alteration of Hadean zircon from the Jack Hills, Australia. Geochimica et Cosmochimica Acta, 69(3), 637–648.

Hoskin, P. W. O., & Schaltegger, U. (2003). The composition of zircon and igneous and metamorphic petrogenesis. In J. M. Hanchar, & P. W. O. Hoskin (Eds.), Zircon. Reviews in Mineralogy and Geochemistry, 53, Mineralogical Society of America, Washington, D.C., pp. 27–62.

Hurai, V., Paquette, J.-L., Huraiova, M., & Konecny, P. (2010). Age of deep crustal magmatic chambers in the intra-Carpathian back-arc basin inferred from LA-ICPMS U-Th-Pb dating of zircon and monazite from igneous xenoliths in alkali basalts. Journal of Volcanology and Geothermal Research, 198, 275–287.

Jackson, S. E., Pearson, N. J., Griffin, W. L., & Belousova, E. A. (2004). The application of laser ablation-inductively coupled plasma-mass spectrometry to in situ U-Pb zircon geochronology. Chemical Geology, 211(1–2), 47–69.

Jochum, K. P., Willbold, M., Raczek, I., Stoll, B., & Herwig, K. (2005). Chemical Characterisation of the USGS Reference Glasses GSA-1G, GSC-1G, GSD-1G, GSE-1G, BCR-2G, BHVO-2G and BIR-1G Using EPMA, ID-TIMS, ID-ICP-MS and LA-ICP-MS. Geostandards and Geoanalytical Research, 29(3), 285–302.

King, E. M., Valley, J. W., Davis, D. W., & Edwards, G. R. (1998). Oxygen isotope ratios of Archean plutonic zircons from granite-greenstone belts of the Superior Province: Indicator of magmatic source. Precambrian Research, 92(4), 365–387.

Leclair, A.D. (2005). Géologie du nord-est de la Province du Supérieur, Québec. Ministère des Ressources naturelles et de la Faune, DV 2004-04, 19 pages, 1 carte (échelle 1:750 000).

Ludwig, K. R. (2001). Isoplot/Ex, version 2.49. A Geochronological Toolkit for Microsoft Excel. Berkeley Geochronological Center, Special Publication, 55 p.

Marks, N. E., Borg, L. E., Hutcheon, I. D., Jacobsen, B., & Clayton, R. N. (2014). Samarium-neodymium chronology and rubidium-strontium systematics of an Allende calcium-aluminum-rich inclusion with implications for 146Sm half-life. Earth and Planetary Science Letters, 405(1777), 15–24.

Moyen, J. F., & Martin, H. (2012). Forty years of TTG research. Lithos, 148, 312–336.

Mullen, E. K., Paquette, J. L., Tepper, J. H., & McCallum, I. S. (2018). Temporal and spatial evolution of Northern Cascade Arc magmatism revealed by LA–ICP–MS U–Pb zircon dating. Canadian Journal of Earth Sciences, 55(5), 443–462.

Murali, A. V., Parthasarathy, R., Mahadevan, T. M., & Das, M. S. (1983). Trace element characteristics, REE patterns and partition coefficients of zircons from different geological environments-A case study on Indian zircons. Geochimica et Cosmochimica Acta, 47(11), 2047–2052.

Næraa, T., Scherstén, A., Rosing, M. T., Kemp, A. I. S., Hoffmann, J. E., Kokfelt, T. F., & Whitehouse, M. J. (2012). Hafnium isotope evidence for a transition in the dynamics of continental growth 3.2 Gyr ago. Nature, 485(7400), 627–630.

O'Neil, J., Boyet, M., Carlson, R. W., & Paquette, J. L. (2013). Half a billion years of reworking of Hadean mafic crust to produce the Nuvvuagittuq Eoarchean felsic crust. Earth and Planetary Science Letters, 379, 13–25.

O'Neil, J., & Carlson, R. W. (2017). Building Archean cratons from Hadean mafic crust. Science, 355(6330), 1199–1202.

O'Neil, J., Carlson, R. W., Francis, D., & Stevenson, R. K. (2008). Neodymium-142 evidence for hadean mafic crust. Science, 321(5897), 1828–1831.

O'Neil, J., Carlson, R. W., Papineau, D., Levine, E. Y., & Francis, D. (2019). The Nuvvuagittuq Greenstone Belt: A Glimpse of Earth's earliest crust. In M. J. Van Kranendonk, V. C. Bennett, & J. E. Hoffmann (Eds.), Earth's Oldest Rocks. Amsterdam: Elsevier, pp. 349–374.

O'Neil, J., Carlson, R. W., Paquette, J. L., & Francis, D. (2012). Formation age and metamorphic history of the Nuvvuagittuq Greenstone Belt. Precambrian Research, 220–221, 23–44.

O'Neil, J., Francis, D., & Carlson, R. W. (2011). Implications of the Nuvvuagittuq Greenstone Belt for the Formation of Earth's Early Crust. Journal of Petrology, 52(5), 985–1009.

Paquette, J.-L., Piro, J.-L., Devidal, J.-L., Bosse, V., Didier, A., Sannac, S., & Abdelnour, Y. (2014). Sensitivity Enhancement in LA-ICP-MS by N2 Addition to Carrier Gas: Application to Radiometric Dating of U-Th-Bearing Minerals. Agilent ICP-MS Journal, 58, 4–5.

Pearce, N. J. G., Perkins, W. T., Westgate, J. A., Gorton, M. P., Jackson, S. E., Neal, C. R., & Chenery, S. P. (1997). A compilation of new and published major and trace element data for NIST SRM 610 and NIST SRM 612 glass reference materials. Geostandards Newsletter, 21(1), 115–144.

Peck, W. H., Valley, J. W., Wilde, S. A., & Graham, C. M. (2001). Oxygen isotope ratios and rare earth elements in 3.3 to 4.4 Ga zircons: Ion microprobe evidence for high δ18O continental crust and oceans in the early Archean. Geochimica et Cosmochimica Acta, 65(22), 4215–4229.

Percival, J. A., & Card, K.D. (1994). Geology, Lac Minto - Rivière aux Feuilles. Geological Survey of Canada; Map 1854A, scale 1/500 000.

Percival, J.A., Skulski, T. & Card, K.D. (1995). Geology, Rivière Kogaluc - Lac Qalluviartuuq region (parts of 34J and 34O). Geological Survey of Canada; Open file 3112.

Percival, J.A., Skulski, T. & Nadeau, L. (1996). Geology, Lac Couture, Quebec. Geological Survey of Canada; Open file 3315.

Percival, J.A., Skulski, T. & Nadeau, L. (1997). Reconnaissance geology of the Pelican - Nantais belt, northeastern Superior province, Quebec. Geological Survey of Canada; Open file 3525.

Rayner, N., Stern, R. A., & Carr, S. D. (2005). Grain-scale variations in trace element composition of fluid-altered zircon, Acasta Gneiss Complex, northwestern Canada. Contributions to Mineralogy and Petrology, 148(6), 721–734.

Reimink, J. R., Chacko, T., Stern, R. A., & Heaman, L. M. (2014). Earth's earliest evolved crust generated in an Iceland-like setting. Nature Geoscience, 7(7), 529–533.

Reimink, J. R., Chacko, T., Stern, R. A., & Heaman, L. M. (2016). The birth of a cratonic nucleus: Lithogeochemical evolution of the 4.02-2.94 Ga Acasta Gneiss Complex. Precambrian Research, 281, 453–472.

Reimink, J. R., Davies, J. H. F. L., Bauer, A. M., & Chacko, T. (2020). A comparison between zircons from the Acasta Gneiss Complex and the Jack Hills region. Earth and Planetary Science Letters, 531, 115975.

Roth, A. S. G., Bourdon, B., Mojzsis, S. J., Touboul, M., Sprung, P., Guitreau, M., & Blichert-Toft, J. (2013). Inherited 142Nd anomalies in Eoarchean protoliths. Earth and Planetary Science Letters, 361, 50–57.

Rubatto, D. (2002). Zircon trace element geochemistry: Partitioning with garnet and the link between U-Pb ages and metamorphism. Chemical Geology, 184(1–2), 123–138.

Schaltegger, U. (2007). Hydrothermal zircon. Elements, 3(1), 51–79.

Shannon, R. D. (1976). Revised effective ionic radii and systematic studies of interatomic distances in halides and chalcogenides. Acta Crystallographica Section A, 32(5), 751–767.

Simard, M., Parent, M., David, J., & Sharma, K. N. M. (2003). Géologie de la région de la rivière Innuksuac (34K et 34L). Ministère des Ressources naturelles, Québec; RG 2002-10, 46 pages.

Sun, S. S., & McDonough, W. F. (1989). Chemical and isotopic systematics of oceanic basalts: Implications for mantle composition and processes. Geological Society Special Publication, 42(1), 313–345.

Valley, J. W. (2003). Oxygen isotopes in zircon. In J. M. Hanchar, & P. W. O. Hoskin (Eds.), Zircon. Reviews in Mineralogy and Geochemistry, 53, Mineralogical Society of America, Washington, D.C., pp. 343–385.

Valley, J. W., Kinny, P. D., Schulze, D. J., & Spicuzza, M. J. (1998). Zircon megacrysts from kimberlite: Oxygen isotope variability among mantle melts. Contributions to Mineralogy and Petrology, 133(1–2), 1–11.

Valley, J. W., Lackey, J. S., Cavosie, A. J., Clechenko, C. C., Spicuzza, M. J., Basei, M. A. S., Bindeman, I. N., Ferreira, V. P., Sial, A. N., King, E. M., Peck, W. H., Sinha, A. K., & Wei, C. S. (2005). 4.4 billion years of crustal maturation: Oxygen isotope ratios of magmatic zircon. Contributions to Mineralogy and Petrology, 150(6), 561–580.

van Achterbergh, E., Ryan, C. G., Jackson, S. E., & Griffin, W. L. (2001). Data reduction software for LA-ICP-MS. In P. J. Sylvester (Ed.), Laser Ablation-ICPMS in the Earth Sciences, Mineralogical Association of Canada, 29, pp. 239–243.

Vezinet, A., Pearson, D. G., Thomassot, E., Stern, R. A., Sarkar, C., Luo, Y., & Fisher, C. M. (2018). Hydrothermally-altered mafic crust as source for early Earth TTG: Pb/Hf/O isotope and trace element evidence in zircon from TTG of the Eoarchean Saglek Block, N. Labrador. Earth and Planetary Science Letters, 503, 95–107.

Wasilewski, B., O'Neil, J., Rizo, H., & Paquette, J.-L. (Submitted). Petrogeochemistry, geochronology and crustal evolution of the Saglek-Hebron Complex (Northern Labrador).

Whitehouse, M. J., & Kamber, B. S. (2002). On the overabundance of light rare earth elements in terrestrial zircons and its implication for Earth's earliest magmatic differentiation. Earth and Planetary Science Letters, 204(3–4), 333–346.

Wiedenbeck, M., Allé, P., Corfu, F., Griffin, W. L., Meier, M., Oberli, F., von Quadt, A., Roddick, J. C., & Spiegel, W. (1995). Three natural zircon standards for U-Th-Pb, Lu-Hf, trace element and REE analyses. Geostandards Newsletter, 19(1), 1–23.

Wilde, S. A., Valley, J. W., Peck, W. H., & Graham, C. M. (2001). Evidence from detrital zircons for the existence of continental crust and oceans on the Earth 4.4 Gyr ago. Nature, 409(6817), 175–178.

Yui, T. F., Maki, K., Usuki, T., Lan, C. Y., Martens, U., Wu, C. M., Wu, T. W., & Liou, J. G. (2010). Genesis of Guatemala jadeitite and related fluid characteristics: Insight from zircon. Chemical Geology, 270(1–4), 45–55.

Zhong, S., Feng, C., Seltmann, R., Li, D., & Qu, H. (2018). Can magmatic zircon be distinguished from hydrothermal zircon by trace element composition? The effect of mineral inclusions on zircon trace element composition. Lithos, 314–315, 646–657.

Chapter 4

Conclusions

As one of the oldest, if not the oldest terrane preserved on Earth, the Nuvvuagittuq Greenstone Belt (NGB) presents a perfect opportunity for geoscientists to gain a glimpse of the first geological processes to have operated very early on in Earth's history. This MSc thesis has contributed to refining the geochronological constraints on the Nuvvuagittuq Greenstone Belt as well as providing a more detailed insight on the petrogenetic processes responsible for the formation of the multiple generations of granitoids in and around the belt. Over the course of this study, we have collected 53 samples during fieldwork, performed major and trace element geochemical analyses on 44 samples, whole-rock ^{147}Sm-^{143}Nd isotope analyses on 8 samples, analyzed 482 zircons for U-Pb (total of 503 measurements), 82 zircons for trace element compositions (total of 87 measurements) and 161 zircons for oxygen isotopic compositions (total of 203 measurements). A summary of the major findings from Chapters 2 and 3 are highlighted here.

1. Zircons from two compositionally evolved portions of the fine-grained gneissic gabbros resulted in U-Pb ages of 2669 and 2626 Ma. The shape and texture of these zircons are consistent with a metamorphic origin and their age is coeval with the ~2.7 Ga regional metamorphism of the Northeastern Superior Province. Zircons from a plagioclase-rich layer found within the gneissic gabbros yielded a slightly older age of 2789 Ma. Their texture and Th/U ratios may suggest that they formed by the breakdown of primary igneous baddeleyites. Their age is interpreted as indicative of the timing of the dissolution-recrystallization processes rather than constraining the age of emplacement of the fine-grained gneissic gabbros.
2. A new sampling strategy designed to constrain the age of magmatic differentiation of the gabbro sills targeted their most evolved and cumulative portions. The ^{147}Sm-^{143}Nd isochron including four homogeneous samples with variable Sm/Nd ratios, a plagioclase-

rich layer and a hornblende-rich rock interpreted as a cumulate formed from magmatic differentiation, yielded an age of 4151 ± 290 Ma. Our isotopic model has shown that the isotopic compositions of the fine-grained gneissic gabbros cannot be explained by the mixing of a superchondritic depleted source and/or of an enriched source. The isotopic compositions of the gneissic gabbros are rather explained by igneous differentiation of a depleted mantle source. This 4.1 Ga isochron is consistent with data previously obtained on more homogeneous parts of the sills and with the Sm-Nd isotopic composition of similar gabbroic rocks of the nearby Ukaliq Supracrustal Belt, suggesting that Hadean mafic rocks appear to be preserved over a larger scale of the Northeastern Superior Province than previously thought. Due to their intrusive nature in the NGB, the fine-grained gneissic gabbros put a strong minimum age constraint on the Ujaraaluk unit and support their Hadean age.

3. Two new 3.76 Ga trondhjemite locations were found in the central and eastern parts surrounding the southern limit of the Nuvvuagittuq Greenstone Belt suggesting that the extent of this 3.76 Ga magmatic event is larger than previously thought. The 3.76 Ga felsic magmatic event may be restricted to the NGB and has not yet been identified in the neighbouring Ukaliq Supracrustal Belt.
4. The 3.76 Ga, 3.66 Ga and 3.35 Ga felsic magmatic events host zircons with typical magmatic rare earth element (REE) trends indicating that they crystallized in oxidized melts that experienced plagioclase fractionation. However, zircons from the 3.51 Ga felsic magmatic event display a higher abundance of light-REE and a distinct positive Eu-anomaly which is interpreted as indicating some type of post-magmatic alteration and breakdown of plagioclase prior to zircon crystallization.

5. Zircon oxygen isotope compositions in the 3.76 Ga trondhjemites are consistent with the derivation of unaltered differentiated mantle melts. In comparison, the ≤3.66 Ga granitoids have zircon $\delta^{18}O$ compositions that slightly increase towards values higher than the mantle zircon field indicating that some minor to mild amounts of low-temperature hydrothermally altered supracrustal materials were present in their parental magmas. The zircon $\delta^{18}O$ values may suggest that the 3.76 Ga trondhjemites were derived from the fine-grained gneissic gabbros whereas the ≤3.66 Ga granitoids are partial melts of the Ujaraaluk unit. The zircon $\delta^{18}O$ trend observed in the NGB is similar to that of other Hadean and Eoarchean terranes, suggesting that similar processes may have operated on a global scale. The first evolved crust in these terranes typically displays mantle-like zircon $\delta^{18}O$ values which shift towards higher or lower $\delta^{18}O$ values in successive felsic magmatic events. This could suggest that the emplacement of the first evolved crust facilitated the transport of fluids which contributed to the incorporation of altered supracrustal materials in the crustal source of younger felsic magmatic events.

The debate regarding the age of the Nuvvuagittuq Greenstone Belt has been an ongoing issue for over the past decade. A more targeted approach reported here has helped establish robust evidence for a 4.1 Ga age for the fine-grained gneissic gabbros making them rare Hadean rocks preserved on Earth. Their intrusive nature further supports the fact that the NGB includes the oldest rocks preserved on Earth. The results of this thesis have also further hinted that the multiple generations of granitoids surrounding the belt may be intimately related to the mafic units of the NGB. Furthermore, the zircon REE and oxygen isotope compositions of these granitoids are similar to those reported in other Hadean and Eoarchean terranes, suggesting that similar processes were involved in the production and evolution of early felsic crust on a global scale.

Future work should focus on detailed chemical mapping of the zircons in the plagioclase-rich layer found within the gneissic gabbros to determine if any primary baddeleyite still remains and can be dated. As for the multiple generations of granitoids surrounding the NGB, titanium-in-zircon thermometry could be applied to potentially constrain zircon crystallization temperatures in order to determine if there are any variations throughout time. More samples of the 3.51 Ga tonalite found elsewhere throughout the Tikkerutuk Domain should also be analyzed for their zircon REE compositions to determine if the values reported here, notably the positive Eu-anomaly, are a product of post-magmatic alteration or of specific petrogenetic conditions.

Appendices

Appendix A – Supplementary information for Chapter 2

Table A.1: Samples collected during fieldwork in 2017. Coordinates are in Easting and Northing UTM NAD 27, zone 18.

Sample	Lithology	Location	Easting	Northing
PC-601	Fine-grained gneissic gabbro	Nuvvuagittuq	339794	6463499
PC-602	Fine-grained gneissic gabbro	Nuvvuagittuq	339801	6463525
PC-603	Fine-grained gneissic gabbro	Nuvvuagittuq	339794	6463441
PC-604	Hornblende-rich amphibolite in gneissic gabbro	Nuvvuagittuq	339796	6463486
PC-605	Fine-grained gneissic gabbro	Nuvvuagittuq	339737	6463735
PC-606	Fine-grained gneissic gabbro	Nuvvuagittuq	339749	6463763
PC-607	Fine-grained gneissic gabbro	Nuvvuagittuq	339742	6463737
PC-608	Fine-grained gneissic gabbro	Nuvvuagittuq	339592	6463754
PC-609	Fine-grained gneissic gabbro	Nuvvuagittuq	339595	6463789
PC-610	Fine-grained gneissic gabbro	Nuvvuagittuq	339601	6463769
PC-611	Fine-grained gneissic gabbro	Nuvvuagittuq	339619	6463758
PC-612	Fine-grained gneissic gabbro	Nuvvuagittuq	339606	6463773
PC-613	Fine-grained gneissic gabbro	Nuvvuagittuq	339622	6463744
PC-614	Fine-grained gneissic gabbro	Nuvvuagittuq	339633	6463761
PC-615	Fine-grained gneissic gabbro	Nuvvuagittuq	339787	6463729
PC-616	Fine-grained gneissic gabbro	Nuvvuagittuq	339799	6463747
PC-617	Fine-grained gneissic gabbro	Nuvvuagittuq	339802	6463751
PC-618	Plagioclase-rich layer in gneissic gabbro	Nuvvuagittuq	339821	6463780
PC-619	Fine-grained gneissic gabbro	Nuvvuagittuq	339844	6463760
PC-620	Fine-grained gneissic gabbro	Nuvvuagittuq	339857	6463777
PC-621	Fine-grained gneissic gabbro	Nuvvuagittuq	339815	6463753
PC-627	Coarse-grained undeformed gabbro	Nuvvuagittuq	339883	6465198
PC-628	Fine-grained gneissic gabbro	Nuvvuagittuq	339874	6465181
PC-629	Fine-grained gneissic gabbro	Nuvvuagittuq	339977	6465189
PC-630	Fine-grained gneissic gabbro	Nuvvuagittuq	339967	6465164
PC-631	Fine-grained gneissic gabbro	Nuvvuagittuq	339977	6465123
PC-632	Fine-grained gneissic gabbro	Nuvvuagittuq	340001	6465131
PC-633	Coarse-grained undeformed gabbro	Nuvvuagittuq	339953	6465108
PC-635	Hornblende-rich amphibolite in gneissic gabbro	Nuvvuagittuq	340043	6463214
PC-636	Coarse-grained undeformed gabbro	Nuvvuagittuq	340050	6463212
UK-001	Fine-grained gneissic gabbro	Ukaliq	342265	6466171
UK-003	Fine-grained gneissic gabbro	Ukaliq	342274	6466179

Table A.2: Chromatography column chemistry protocols for Sm-Nd isotopic analyses.

Primary Columns

Biorad columns (10 ml) filled with 2 ml AG50W-X8, 200–400 mesh

Step	Eluent	Volume
Conditioning	2 N HCl	10 ml
		10 ml
Load Sample	**2 N HCl**	**2 ml**
Rinse	2 N HCl	1 ml
		1 ml
Discard	2 N HCl	8 ml
		8 ml
Discard	2.5 N HCl	10 ml
Collect LREE	**6 N HCl**	**10 ml**
Wash	6 N HCl	10 ml
	6 N HCl	10 ml
	MQ H_2O	10 ml
	6 N HCl	10 ml
	MQ H_2O	10 ml
Store	MQ H_2O + squirt HCl	

Ln-spec resin column

Quartz columns: Eichrom Ln-spec resin 50–100 µm 300 mg, 68 mm x 4 mm

Step	Eluent	Volume
Conditioning	0.2 N HCl	3 ml
Load Sample	**0.2 N HCl**	**0.25 ml**
Rinse	0.2 N HCl	0.25 ml
Discard	0.2 N HCl	4.5 ml
Collect Nd	**0.2 N HCl**	**5.5 ml**
Rinse	0.5 N HCl	0.5 ml
Collect Sm	**0.5 N HCl**	**2.75 ml**
Wash	6 N HCl	10 ml
	MQ H_2O + squirt HCl	10 ml
Store	MQ H_2O + squirt HCl	

Table A.3: Operating conditions and instrument settings for U-Pb isotopic analyses.

Laser ablation system	
Make, Model & type	Resonetics/M-50E 193nm, Excimer
Ablation cell & volume	Laurin Cell ® two volumes cell, Laurin Technic Ltd., volume ca. 1cm^3
Laser wavelength	193 nm
Pulse width	< 4 ns
Fluence	2.5 J.cm^{-2}
Repetition rate	3 Hz
Spot size	20 µm
Sampling mode / pattern	Single spot
Carrier gas	100% He, Ar make-up gas and N_2 combined using the Squid® device from RESOlution Instruments.
Background collection	30 s
Ablation duration	60 s
Wash-out delay	30 s
Cell carrier gas flow	0.70 l/min He
ICP-MS Instrument	
Make, Model & type	Element XR SF-ICP-MS
Sample introduction	Via conventional tubing
RF power	1200 W
Make-up gas flow	0.98 l/min Ar
Detection system	Single collector secondary electron multiplier (Faraday cup)
Masses measured	204, 206, 207, 208, 232, 238
Integration time per peak	20 ms
Sensitivity / Efficiency	15 000 cps/ppm ^{238}U (47 µm, 10 Hz, 3.5 J/cm^2)
Dead time	6 ns
Data Processing	
Gas blank	30 second on-peak
Calibration strategy	GJ-1 used as primary reference material, 91500 used as secondary reference material (Quality Control)
Reference Material info	91500 (Wiedenbeck et al., 1995) GJ1 (Jackson et al., 2004)
Data processing package used / Correction for LIEF	GLITTER ® (van Achterbergh et al., 2001)
Mass discrimination	Standard-sample bracketing with ^{207}Pb/^{206}Pb and ^{206}Pb/^{238}U normalized to reference material GJ-1
Common-Pb correction, composition and uncertainty	No common-Pb correction. Analyses discarded of the age calculation when discordance >20%
Uncertainty level & propagation	Ages are quoted at 2σ absolute, propagation is by quadratic addition according to Horstwood et al. (2003). Reproducibility and age uncertainty of reference material are propagated.
Quality control / Validation	91500: Concordia age = 1064.9 ± 3.1 (2SD, MSWD = 0.47, *n* = 64)
Other information	For detailed method description see Hurai et al. (2010). For detailed laser technical description see Müller et al. (2009).

References

Horstwood, M. S. A., Foster, G. L., Parrish, R. R., Noble, S. R., & Nowell, G. M. (2003). Common-Pb corrected in situ U-Pb accessory mineral geochronology by LA-MC-ICP-MS. Journal of Analytical Atomic Spectrometry, 18(8), 837–846.

Hurai, V., Paquette, J.-L., Huraiova, M., & Konecny, P. (2010). Age of deep crustal magmatic chambers in the intra-Carpathian back-arc basin inferred from LA-ICPMS U-Th-Pb dating of zircon and monazite from igneous xenoliths in alkali basalts. Journal of Volcanology and Geothermal Research, 198, 275–287.

Jackson, S. E., Pearson, N. J., Griffin, W. L., & Belousova, E. A. (2004). The application of laser ablation-inductively coupled plasma-mass spectrometry to in situ U-Pb zircon geochronology. Chemical Geology, 211(1–2), 47–69.

Müller, W., Shelley, M., Miller, P., & Broude, S. (2009). Initial performance metrics of a new custom-designed ArF excimer LA-ICPMS system coupled to a two-volume laser-ablation cell. Journal of Analytical Atomic Spectrometry, 24(2), 209–214.

van Achterbergh, E., Ryan, C. G., Jackson, S. E., & Griffin, W. L. (2001). Data reduction software for LA-ICP-MS. In P. J. Sylvester (Ed.), Laser Ablation-ICPMS in the Earth Sciences, Mineralogical Association of Canada, 29, pp. 239–243.

Wiedenbeck, M., Allé, P., Corfu, F., Griffin, W. L., Meier, M., Oberli, F., von Quadt, A., Roddick, J. C., & Spiegel, W. (1995). Three natural zircon standards for U-Th-Pb, Lu-Hf, trace element and REE analyses. Geostandards Newsletter, 19(1), 1–23.

Figure A.1: Repeated measurements of the GJ-1 primary reference material to correct for U-Pb fractionation during laser sampling and instrumental mass discrimination.

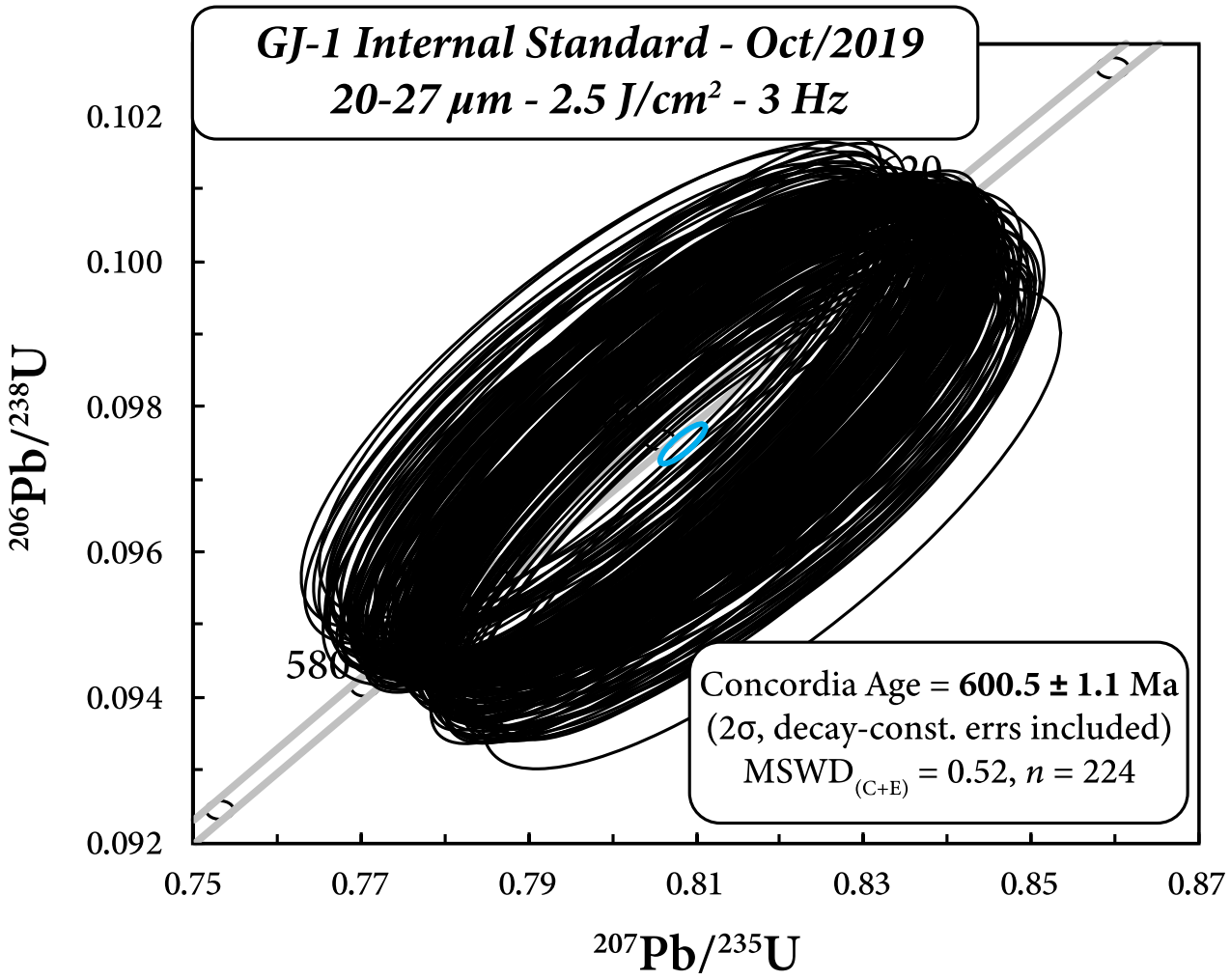

Figure A.2: Repeated measurements of the 91500 secondary reference material for reproducibility and accuracy of the corrections during U-Pb analysis.

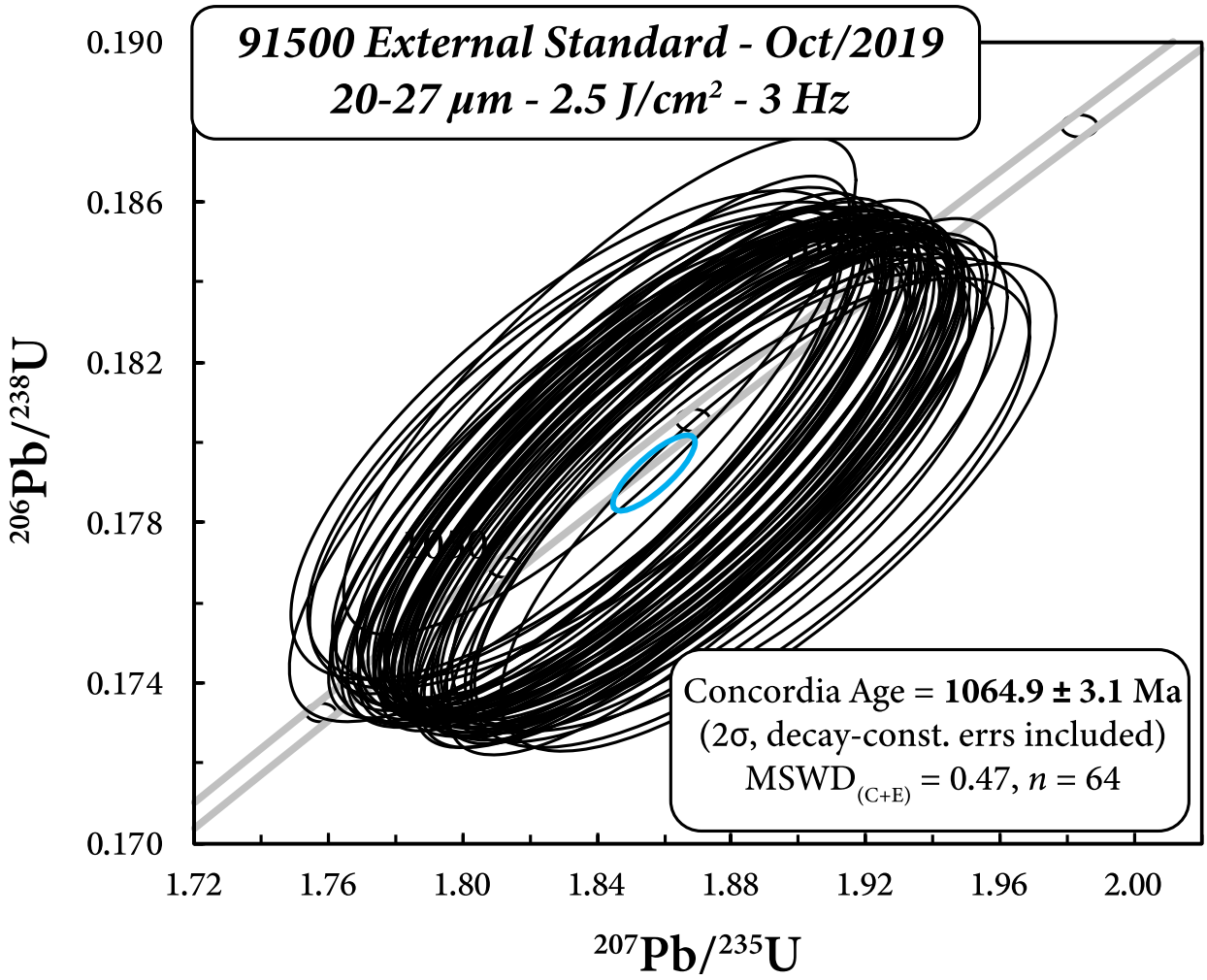

Table A.4: Whole rock major and trace element compositions of the Nuvvuagittuq (NGB) and Ukaliq (USB) gabbros. Major element concentrations (hydrous compositions) are reported in wt.% and trace element concentrations are reported in ppm. Abbreviations: GG = Fine-grained gneissic gabbro; Plag-GG = Plagioclase-rich evolved layer; Hbl-GG = Hornblende-rich cumulative rock; CG = Coarse-grained undeformed gabbro.

Sample	PC-601	PC-602	PC-603	PC-604	PC-605	PC-606	PC-607	PC-608	PC-609
Location	NGB	NGB	NGB	NGB	NGB	NGB	NGB	NGB	NGB
Lithology	GG	GG	GG	Hbl-GG	GG	GG	GG	GG	GG
SiO_2	51.49	56.22	51.07	50.90	52.26	54.83	53.67	51.22	53.03
TiO_2	0.56	0.48	0.46	0.32	0.58	0.50	0.52	0.88	0.79
Al_2O_3	15.80	16.49	17.07	6.09	15.91	14.96	15.66	9.90	10.47
Fe_2O_3	11.05	7.54	8.99	13.12	11.23	10.30	9.66	14.30	13.30
MnO	0.23	0.15	0.17	0.41	0.22	0.18	0.18	0.21	0.21
MgO	6.83	3.10	7.12	15.53	8.03	7.33	6.94	10.22	8.83
CaO	7.29	13.25	9.72	11.48	8.40	7.94	9.05	9.65	9.59
Na_2O	3.88	0.17	1.21	0.50	2.15	1.54	1.88	1.98	2.14
K_2O	0.85	0.04	1.66	0.27	0.24	0.77	0.57	0.43	0.60
P_2O_5	0.07	0.06	0.05	0.03	0.06	0.06	0.06	0.08	0.08
LOI	1.80	2.23	2.31	1.26	0.78	1.44	0.80	0.90	0.77
Sc	42.6	32.9	39.5	18.2	42.4	37.1	39.7	35.7	32.7
V	217	170	195	168	217	199	205	213	198
Cr	133	112	376	43.7	132	113	124	477	438
Co	43.2	29.2	40.0	52.6	44.0	40.6	39.2	60.9	55.0
Ni	93.5	62.3	134	73.0	88.4	80.7	82.5	126	118
Cu	11.1	183	9.62	0.92	29.0	2.07	1.22	27.1	24.6
Zn	74.1	39.1	62.8	105	94.7	70.0	67.3	92.7	84.7
Ga	14.7	15.0	14.3	8.68	14.9	14.4	14.6	13.0	13.4
Ge	1.50	0.88	1.22	1.70	1.32	1.16	1.16	1.67	1.51
Rb	20.5	0.94	48.8	4.37	4.56	20.3	12.3	5.73	7.84
Sr	86.0	161	104	3.29	89.0	76.6	88.2	66.2	111
Y	19.7	14.4	15.4	20.7	19.6	16.9	19.2	20.5	18.8
Zr	64.9	66.9	48.9	17.2	66.1	59.3	63.5	82.4	80.5
Nb	3.71	3.77	2.75	1.90	3.69	3.30	3.67	6.02	4.55
Cs	0.19	0.08	0.94	0.09	0.33	0.91	0.93	0.14	0.16
Ba	95.0	5.10	267	24.8	42.9	114	123	88.0	152
La	9.39	12.0	7.60	7.83	9.38	10.1	11.1	10.1	10.1
Ce	20.2	18.9	16.8	16.1	19.8	19.8	21.5	23.1	21.8
Pr	2.44	1.96	2.03	1.91	2.44	2.23	2.55	2.89	2.75
Nd	9.85	7.57	8.05	7.64	9.69	8.52	9.93	12.1	11.4
Sm	2.29	1.67	1.73	1.93	2.36	1.94	2.34	3.11	2.87
Eu	0.64	0.50	0.61	0.61	0.67	0.65	0.68	0.92	0.89
Gd	2.64	2.04	2.11	2.51	2.70	2.30	2.81	3.53	3.25
Tb	0.48	0.34	0.37	0.44	0.47	0.39	0.47	0.59	0.55
Dy	3.13	2.35	2.47	3.01	3.11	2.72	3.13	3.72	3.40
Ho	0.69	0.52	0.56	0.67	0.68	0.59	0.69	0.75	0.71
Er	2.10	1.55	1.65	1.91	2.04	1.78	2.02	2.11	1.90
Tm	0.33	0.25	0.26	0.30	0.33	0.28	0.32	0.31	0.29
Yb	2.17	1.62	1.72	1.91	2.15	1.90	2.08	1.89	1.83
Lu	0.33	0.26	0.26	0.28	0.33	0.29	0.32	0.28	0.26
Hf	1.81	1.81	1.38	0.54	1.81	1.69	1.82	2.24	2.17
Ta	0.30	0.33	0.27	0.18	0.25	0.28	0.29	0.32	0.34
Pb	1.10	8.29	5.07	0.60	5.99	4.29	5.83	4.01	5.18
Th	1.80	11.9	4.38	1.56	1.58	4.83	5.07	0.97	3.17
U	0.54	2.03	1.06	0.28	0.35	0.88	0.66	0.29	0.66

Table A.4 *(Continued)*

Sample	PC-610	PC-611	PC-612	PC-613	PC-614	PC-615	PC-616	PC-617	PC-618
Location	NGB	NGB	NGB	NGB	NGB	NGB	NGB	NGB	NGB
Lithology	GG	GG	GG	GG	GG	GG	GG	GG	Plag-GG
SiO_2	54.66	51.23	51.50	49.09	51.14	53.53	54.04	54.42	53.06
TiO_2	0.75	0.48	0.97	0.50	0.55	0.57	0.55	0.56	0.58
Al_2O_3	10.26	15.89	13.22	15.91	16.67	16.31	16.03	16.14	16.40
Fe_2O_3	12.81	10.50	14.85	11.51	10.33	10.60	10.99	10.32	8.92
MnO	0.20	0.17	0.26	0.18	0.16	0.20	0.20	0.19	0.17
MgO	9.39	8.51	7.54	9.14	8.05	6.59	7.43	7.22	5.24
CaO	8.99	8.46	6.98	9.11	8.37	8.60	7.69	7.68	11.56
Na_2O	1.00	1.43	1.99	1.49	2.28	2.83	2.37	2.36	1.23
K_2O	0.64	1.15	0.46	0.80	0.74	0.20	0.13	0.19	0.48
P_2O_5	0.07	0.05	0.10	0.04	0.05	0.06	0.06	0.06	0.07
LOI	1.07	1.97	0.97	1.68	1.35	0.38	0.37	0.70	2.15
Sc	30.4	43.5	29.8	47.3	45.9	43.3	41.4	42.9	43.2
V	193	258	241	272	252	221	218	223	200
Cr	412	217	47.3	233	246	139	146	142	130
Co	54.9	42.3	58.5	45.5	41.9	42.1	43.9	43.3	29.0
Ni	118	80.9	60.9	88.7	84.7	86.6	88.9	87.7	56.8
Cu	41.4	56.1	314	1.37	3.16	13.8	11.4	23.4	21.6
Zn	96.8	68.6	116	76.6	71.3	81.6	85.2	88.0	58.6
Ga	13.1	13.8	19.2	14.7	14.7	16.2	14.9	15.1	13.7
Ge	1.67	1.28	2.01	1.45	1.33	1.46	1.49	1.42	1.08
Rb	12.6	23.5	7.10	15.7	13.8	2.10	2.65	4.12	17.0
Sr	63.9	70.1	65.5	77.1	80.7	101	105	103	151
Y	17.3	16.7	24.5	15.7	15.6	20.4	17.8	19.5	14.0
Zr	76.6	41.0	116	38.9	41.1	67.9	63.5	67.7	70.5
Nb	4.18	1.87	6.01	1.98	2.11	3.78	3.64	3.83	3.88
Cs	0.37	0.74	0.30	0.84	0.78	0.08	0.12	0.20	0.22
Ba	129	128	52.2	105	90.0	37.7	35.4	42.4	53.7
La	10.4	4.86	14.6	5.01	5.31	11.2	8.75	9.03	7.52
Ce	21.2	10.7	29.5	10.5	11.3	22.8	17.0	18.2	15.2
Pr	2.58	1.35	3.73	1.27	1.38	2.69	2.01	2.19	1.86
Nd	10.6	5.72	15.8	5.34	5.58	10.6	8.18	8.93	7.57
Sm	2.56	1.49	4.04	1.44	1.42	2.38	1.96	2.22	1.85
Eu	0.88	0.51	1.04	0.54	0.52	0.68	0.52	0.57	0.59
Gd	2.95	1.94	4.47	1.81	1.84	2.71	2.36	2.57	2.04
Tb	0.52	0.36	0.73	0.34	0.35	0.48	0.42	0.45	0.37
Dy	3.08	2.54	4.45	2.38	2.40	3.28	2.88	3.09	2.45
Ho	0.63	0.59	0.92	0.54	0.55	0.74	0.64	0.67	0.53
Er	1.83	1.80	2.51	1.68	1.64	2.16	1.85	2.04	1.57
Tm	0.26	0.27	0.38	0.27	0.26	0.32	0.30	0.32	0.24
Yb	1.65	1.78	2.40	1.75	1.78	2.20	1.89	2.09	1.55
Lu	0.25	0.28	0.36	0.28	0.27	0.34	0.30	0.33	0.23
Hf	2.00	1.22	3.08	1.15	1.19	1.90	1.71	1.82	1.95
Ta	0.33	0.16	0.45	0.17	0.18	0.29	0.29	0.30	0.27
Pb	2.37	4.04	7.75	3.34	4.35	6.68	6.60	6.81	3.73
Th	3.42	1.35	6.02	0.98	1.25	2.99	2.66	2.95	3.98
U	0.71	0.35	1.33	0.29	0.27	0.67	0.60	0.76	0.97

Table A.4 *(Continued)*

Sample	PC-619	PC-620	PC-621	PC-627	PC-628	PC-629	PC-630	PC-631	PC-632
Location	NGB	NGB	NGB	NGB	NGB	NGB	NGB	NGB	NGB
Lithology	GG	GG	GG	CG	GG	GG	GG	GG	GG
SiO_2	52.30	52.74	51.92	49.13	49.86	51.17	50.84	51.50	50.82
TiO_2	0.55	0.57	0.56	0.85	0.77	0.51	0.49	0.45	0.54
Al_2O_3	15.96	16.24	16.31	16.02	14.81	15.92	16.19	15.18	16.67
Fe_2O_3	11.85	10.45	11.43	11.25	11.93	10.59	10.59	11.96	10.49
MnO	0.21	0.22	0.21	0.20	0.23	0.18	0.19	0.21	0.19
MgO	7.34	6.95	8.17	7.77	8.41	8.30	8.72	9.97	8.49
CaO	6.17	8.44	7.02	10.98	11.06	9.61	8.86	6.88	9.38
Na_2O	2.62	2.40	2.62	2.44	1.51	2.44	2.46	2.30	2.45
K_2O	1.63	0.38	0.91	0.31	0.36	0.35	0.44	0.24	0.18
P_2O_5	0.06	0.07	0.07	0.06	0.06	0.05	0.04	0.03	0.04
LOI	1.17	0.84	0.62	0.79	0.79	0.68	1.02	1.16	0.59
Sc	42.8	43.0	40.6	45.9	38.9	50.2	47.5	37.9	44.7
V	225	216	220	285	260	268	246	218	283
Cr	135	136	138	394	330	244	233	205	242
Co	45.6	41.7	45.8	50.4	46.1	41.9	41.4	48.0	42.5
Ni	88.7	83.4	89.7	130	142	83.2	84.9	85.5	85.9
Cu	9.58	38.1	3.75	14.0	67.4	1.28	1.06	1.69	0.91
Zn	92.7	73.9	88.2	86.3	89.9	77.7	82.8	94.3	78.8
Ga	16.3	15.1	15.3	15.5	14.8	14.3	13.9	13.2	15.4
Ge	1.56	1.44	1.48	1.50	1.44	1.33	1.35	1.48	1.32
Rb	58.7	10.4	29.2	5.14	7.17	7.10	12.8	8.48	3.37
Sr	67.3	60.6	104	161	96.7	84.9	89.4	72.1	69.1
Y	17.5	20.4	17.8	19.5	17.7	16.9	15.3	11.8	17.4
Zr	67.2	66.7	67.6	28.2	26.2	42.3	41.5	37.5	43.8
Nb	3.77	3.73	3.73	2.03	1.87	2.03	1.85	1.73	2.10
Cs	1.53	0.28	0.86	0.23	0.58	0.22	0.68	0.65	0.14
Ba	134	75.8	101	59.3	47.5	65.6	81.1	60.3	22.3
La	10.7	8.86	9.47	2.71	2.65	5.45	4.64	3.81	5.33
Ce	20.0	18.4	18.0	7.21	6.92	12.1	9.67	6.94	11.7
Pr	2.25	2.29	2.17	1.13	1.05	1.49	1.21	0.81	1.46
Nd	8.71	9.43	8.64	5.76	5.35	5.99	5.14	3.33	6.04
Sm	2.06	2.32	2.09	1.91	1.76	1.58	1.38	0.93	1.61
Eu	0.60	0.77	0.57	0.69	0.68	0.56	0.48	0.35	0.58
Gd	2.46	2.81	2.37	2.51	2.26	1.98	1.83	1.27	2.09
Tb	0.40	0.47	0.41	0.46	0.43	0.37	0.32	0.24	0.38
Dy	2.87	3.29	2.85	3.20	2.94	2.62	2.36	1.77	2.66
Ho	0.64	0.71	0.64	0.73	0.65	0.61	0.54	0.42	0.61
Er	1.87	2.05	1.85	2.11	1.90	1.78	1.62	1.30	1.87
Tm	0.29	0.32	0.29	0.33	0.29	0.28	0.25	0.20	0.28
Yb	1.91	2.08	1.93	2.10	1.84	1.90	1.74	1.40	1.92
Lu	0.28	0.33	0.28	0.32	0.29	0.29	0.26	0.21	0.30
Hf	1.85	1.87	1.84	1.05	0.98	1.19	1.17	1.06	1.28
Ta	0.30	0.29	0.28	0.16	0.15	0.17	0.16	0.14	0.19
Pb	5.97	4.00	5.74	8.12	5.19	5.14	7.15	6.05	8.61
Th	2.98	2.81	2.95	0.23	0.25	0.83	0.88	1.83	0.80
U	0.59	0.70	0.63	0.07	0.07	0.23	0.22	0.22	0.25

Table A.4 *(Continued)*

Sample	PC-633	PC-635	PC-636	UK-001	UK-003
Location	NGB	NGB	NGB	USB	USB
Lithology	CG	Hbl-GG	CG	GG	GG
SiO_2	48.62	44.90	47.95	51.94	48.44
TiO_2	0.80	0.99	0.74	0.76	1.03
Al_2O_3	15.14	9.92	16.85	10.45	14.83
Fe_2O_3	12.01	20.11	11.30	13.16	13.59
MnO	0.22	0.28	0.20	0.23	0.21
MgO	8.56	9.07	7.14	9.10	7.40
CaO	11.35	12.00	11.22	10.43	9.74
Na_2O	1.27	1.06	1.79	1.79	1.81
K_2O	0.77	0.63	0.85	0.90	1.39
P_2O_5	0.07	0.07	0.05	0.09	0.07
LOI	0.99	0.58	1.71	0.93	1.31
Sc	43.4	27.8	40.8	30.6	42.2
V	266	239	262	164	293
Cr	396	1825	495	839	272
Co	47.8	79.8	38.8	56.2	51.1
Ni	146	746	112	214	141
Cu	18.9	2.45	6.73	86.1	117
Zn	86.2	89.4	81.5	89.4	85.3
Ga	15.1	14.2	16.1	13.5	16.9
Ge	1.45	2.30	1.26	1.50	1.64
Rb	32.4	6.34	25.5	33.6	71.5
Sr	84.8	137	135	107	105
Y	17.9	20.1	16.8	18.2	22.5
Zr	31.2	32.6	37.4	98.3	36.8
Nb	1.86	3.35	1.91	6.07	2.37
Cs	0.98	0.09	0.64	0.19	0.56
Ba	76.8	68.8	125	103	82.1
La	2.68	3.38	3.01	11.8	3.24
Ce	7.01	9.39	7.48	25.0	8.44
Pr	1.07	1.53	1.07	3.12	1.29
Nd	5.18	7.97	5.12	12.9	6.84
Sm	1.78	2.58	1.67	2.97	2.27
Eu	0.66	0.96	0.68	0.93	0.83
Gd	2.35	3.18	2.15	3.29	2.91
Tb	0.43	0.55	0.40	0.53	0.55
Dy	2.93	3.64	2.78	3.29	3.68
Ho	0.67	0.76	0.62	0.67	0.81
Er	1.97	2.20	1.79	1.91	2.35
Tm	0.28	0.31	0.28	0.27	0.36
Yb	1.90	1.94	1.86	1.77	2.38
Lu	0.29	0.30	0.27	0.25	0.37
Hf	1.01	1.17	1.16	2.54	1.27
Ta	0.14	0.23	0.16	0.36	0.16
Pb	4.57	5.32	5.77	4.61	4.43
Th	0.33	0.25	0.38	1.71	0.28
U	0.08	0.12	0.12	0.45	0.07

Table A.5: U-Pb isotopic data of zircons from two compositionally evolved gneissic gabbros (PC-601 and PC-602) and a plagioclase-rich layer (PC-618). ρ is the error correlation coefficient.

Zircon #	Pb (ppm)	U (ppm)	Th (ppm)	Th/U	$^{207}Pb/^{235}U$ ± 2σ	$^{206}Pb/^{238}U$ ± 2σ	ρ	Ages ± 2σ		Concordance %
								$^{207}Pb/^{206}Pb$	$^{206}Pb/^{238}U$	
PC-601										
A4	377	103	687	0.15	12.9916 ± 0.3831	0.5169 ± 0.0144	0.94	2674 ± 52	2686 ± 61	100
A5	321	116	590	0.20	12.6172 ± 0.3752	0.5063 ± 0.0141	0.94	2660 ± 53	2641 ± 60	99
A6	458	246	813	0.30	12.6525 ± 0.3722	0.5068 ± 0.0141	0.94	2663 ± 52	2643 ± 60	99
A7	346	143	623	0.23	12.8548 ± 0.3792	0.5068 ± 0.0141	0.94	2689 ± 52	2643 ± 60	98
A8	431	96	795	0.12	12.8591 ± 0.3766	0.5110 ± 0.0141	0.94	2676 ± 52	2661 ± 60	99
A9	365	104	744	0.14	10.9648 ± 0.3239	0.4612 ± 0.0127	0.93	2581 ± 53	2445 ± 56	95
A10	357	96	642	0.15	12.9694 ± 0.3833	0.5179 ± 0.0143	0.93	2668 ± 53	2690 ± 61	101
A11	253	98	451	0.22	12.8566 ± 0.3812	0.5115 ± 0.0141	0.93	2674 ± 53	2663 ± 60	100
A13	310	110	556	0.20	12.8945 ± 0.3876	0.5080 ± 0.0140	0.92	2690 ± 54	2648 ± 60	98
A14	302	128	548	0.23	12.7016 ± 0.3809	0.5104 ± 0.0140	0.92	2657 ± 54	2658 ± 60	100
B2	396	135	723	0.19	12.6422 ± 0.3767	0.5106 ± 0.0140	0.92	2649 ± 54	2659 ± 60	100
B3	305	95	554	0.17	12.9147 ± 0.3865	0.5159 ± 0.0141	0.91	2667 ± 54	2682 ± 60	101
B4	334	136	601	0.23	12.8175 ± 0.3838	0.5076 ± 0.0138	0.91	2681 ± 54	2646 ± 59	99
B6	330	159	688	0.23	10.4335 ± 0.3137	0.4408 ± 0.0120	0.90	2574 ± 55	2354 ± 54	91
B7	340	104	613	0.17	12.8932 ± 0.3878	0.5126 ± 0.0139	0.90	2675 ± 55	2668 ± 59	100
B8	482	73	898	0.08	12.8410 ± 0.3851	0.5085 ± 0.0137	0.90	2682 ± 55	2650 ± 59	99
B9	324	142	580	0.24	12.8942 ± 0.3904	0.5114 ± 0.0138	0.89	2679 ± 55	2663 ± 59	99
B10	441	100	909	0.11	11.3035 ± 0.3416	0.4633 ± 0.0125	0.89	2624 ± 55	2454 ± 55	94
B11	372	116	671	0.17	12.9707 ± 0.3971	0.5171 ± 0.0140	0.88	2670 ± 56	2687 ± 59	101
B12	292	109	521	0.21	12.9214 ± 0.3945	0.5160 ± 0.0139	0.88	2668 ± 56	2682 ± 59	101
B15	358	115	651	0.18	12.9133 ± 0.3654	0.5144 ± 0.0140	0.96	2672 ± 51	2675 ± 60	100
C1	291	110	531	0.21	12.7295 ± 0.3605	0.5063 ± 0.0138	0.96	2674 ± 51	2641 ± 59	99
C2	344	153	614	0.25	12.8599 ± 0.3631	0.5145 ± 0.0140	0.96	2665 ± 51	2676 ± 60	100
C4	341	142	617	0.23	12.6909 ± 0.3594	0.5096 ± 0.0139	0.96	2658 ± 51	2655 ± 59	100
C5	339	104	623	0.17	12.7507 ± 0.3601	0.5071 ± 0.0138	0.96	2674 ± 51	2644 ± 59	99
C6	275	107	493	0.22	13.0036 ± 0.3701	0.5137 ± 0.0140	0.96	2686 ± 51	2672 ± 60	100
C7	459	97	1149	0.08	8.7908 ± 0.2491	0.3857 ± 0.0105	0.96	2511 ± 52	2103 ± 49	84
C10	358	143	657	0.22	12.4089 ± 0.3502	0.5062 ± 0.0138	0.96	2632 ± 51	2640 ± 59	100
C11	311	118	558	0.21	12.8899 ± 0.3653	0.5125 ± 0.0140	0.96	2675 ± 51	2667 ± 59	100
C12	370	123	681	0.18	12.6087 ± 0.3577	0.5049 ± 0.0137	0.96	2663 ± 51	2635 ± 59	99
C13	325	113	582	0.19	12.9802 ± 0.3672	0.5172 ± 0.0141	0.96	2671 ± 51	2687 ± 60	101
C14	273	105	492	0.21	12.8269 ± 0.3629	0.5112 ± 0.0139	0.96	2671 ± 51	2662 ± 59	100
C15	339	86	839	0.10	8.6933 ± 0.2469	0.3880 ± 0.0106	0.96	2482 ± 52	2113 ± 49	85
D1	141	37	260	0.14	12.8080 ± 0.3654	0.5074 ± 0.0138	0.96	2681 ± 52	2646 ± 59	99

Table A.5 *(Continued)*

Zircon #	Pb (ppm)	U (ppm)	Th (ppm)	Th/U	$^{207}Pb/^{235}U$ ± 2σ	$^{206}Pb/^{238}U$ ± 2σ	ρ	Ages ± 2σ $^{207}Pb/^{206}Pb$	Ages ± 2σ $^{206}Pb/^{238}U$	Concordance %
PC-601										
D2	320	111	576	0.19	12.9488 ± 0.3718	0.5139 ± 0.0140	0.95	2678 ± 52	2673 ± 60	100
D3	342	103	615	0.17	12.9105 ± 0.3650	0.5173 ± 0.0141	0.96	2662 ± 51	2688 ± 60	101
D4	338	145	608	0.24	12.8061 ± 0.3629	0.5126 ± 0.0139	0.96	2664 ± 51	2668 ± 59	100
D5	310	106	569	0.19	12.6115 ± 0.3572	0.5114 ± 0.0139	0.96	2642 ± 52	2663 ± 59	101
D7	321	151	575	0.26	12.8455 ± 0.3649	0.5119 ± 0.0139	0.96	2671 ± 52	2665 ± 59	100
D8	320	143	572	0.25	12.8810 ± 0.3655	0.5149 ± 0.0140	0.96	2666 ± 52	2678 ± 60	100
D9	314	140	556	0.25	12.9845 ± 0.3702	0.5189 ± 0.0141	0.95	2666 ± 52	2695 ± 60	101
D10	357	109	688	0.16	12.1171 ± 0.3447	0.4883 ± 0.0133	0.95	2652 ± 52	2564 ± 57	97
D11	526	113	973	0.12	12.6097 ± 0.3574	0.5165 ± 0.0140	0.96	2625 ± 52	2684 ± 60	102
D12	312	98	569	0.17	12.8630 ± 0.3678	0.5153 ± 0.0140	0.95	2662 ± 52	2679 ± 60	101
D13	283	125	508	0.24	12.8256 ± 0.3675	0.5122 ± 0.0140	0.95	2668 ± 52	2666 ± 59	100
D14	242	101	435	0.23	13.0138 ± 0.3730	0.5141 ± 0.0140	0.95	2685 ± 52	2674 ± 60	100
D15	321	109	583	0.19	12.9642 ± 0.3702	0.5141 ± 0.0140	0.95	2679 ± 52	2674 ± 59	100
E2	367	126	667	0.19	12.9065 ± 0.3692	0.5145 ± 0.0140	0.95	2671 ± 52	2676 ± 60	100
E3	339	140	612	0.23	12.8376 ± 0.3665	0.5124 ± 0.0139	0.95	2668 ± 52	2667 ± 59	100
E4	387	104	713	0.15	12.7641 ± 0.3639	0.5131 ± 0.0140	0.95	2657 ± 52	2670 ± 59	101
E5	306	111	555	0.20	12.8574 ± 0.3678	0.5129 ± 0.0140	0.95	2669 ± 52	2669 ± 59	100
E6	424	124	780	0.16	12.7393 ± 0.3652	0.5091 ± 0.0138	0.95	2666 ± 52	2653 ± 59	99
E7	343	150	616	0.24	12.8232 ± 0.3679	0.5124 ± 0.0139	0.95	2667 ± 52	2667 ± 59	100
E8	313	119	564	0.21	12.8334 ± 0.3694	0.5149 ± 0.0140	0.95	2660 ± 52	2677 ± 60	101
E10	342	91	625	0.15	12.8811 ± 0.3724	0.5147 ± 0.0140	0.94	2667 ± 52	2677 ± 60	100
E11	335	111	614	0.18	12.5844 ± 0.3603	0.5099 ± 0.0138	0.95	2644 ± 52	2656 ± 59	100
E12	242	104	434	0.24	12.8486 ± 0.3717	0.5133 ± 0.0140	0.94	2667 ± 52	2671 ± 60	100
E13	350	149	628	0.24	12.9238 ± 0.3720	0.5155 ± 0.0140	0.94	2670 ± 52	2680 ± 60	100
E14	261	95	483	0.20	12.6091 ± 0.3633	0.5078 ± 0.0138	0.94	2654 ± 52	2647 ± 59	100
F3	343	145	617	0.23	12.9172 ± 0.3718	0.5155 ± 0.0140	0.94	2669 ± 52	2680 ± 60	100
F4	356	170	643	0.26	12.6422 ± 0.3650	0.5087 ± 0.0138	0.94	2655 ± 52	2651 ± 59	100
F5	453	94	984	0.10	10.7420 ± 0.3118	0.4444 ± 0.0121	0.94	2609 ± 53	2370 ± 54	91
F8	379	131	697	0.19	12.7917 ± 0.3694	0.5092 ± 0.0138	0.94	2673 ± 52	2653 ± 59	99
F9	422	94	779	0.12	12.8697 ± 0.3705	0.5159 ± 0.0140	0.94	2661 ± 52	2682 ± 60	101
F10	312	116	570	0.20	12.7164 ± 0.3696	0.5105 ± 0.0139	0.94	2659 ± 53	2659 ± 59	100
F11	381	151	722	0.21	12.2472 ± 0.3555	0.4903 ± 0.0133	0.94	2663 ± 53	2572 ± 58	97
F12	377	133	683	0.19	12.8298 ± 0.3723	0.5140 ± 0.0140	0.94	2662 ± 53	2674 ± 59	100
F13	381	215	669	0.32	12.8359 ± 0.3731	0.5140 ± 0.0140	0.94	2663 ± 53	2674 ± 59	100

Table A.5 *(Continued)*

Zircon #	Pb (ppm)	U (ppm)	Th (ppm)	Th/U	$^{207}Pb/^{235}U$ ± 2σ	$^{206}Pb/^{238}U$ ± 2σ	ρ	Ages ± 2σ $^{207}Pb/^{206}Pb$	Ages ± 2σ $^{206}Pb/^{238}U$	Concordance %
PC-601										
F15	337	104	612	0.17	12.7050 ± 0.3704	0.5184 ± 0.0141	0.93	2632 ± 53	2692 ± 60	102
G1	290	118	527	0.22	12.8624 ± 0.3762	0.5096 ± 0.0139	0.93	2681 ± 53	2655 ± 59	99
G2	326	123	593	0.21	12.9158 ± 0.3789	0.5106 ± 0.0139	0.93	2684 ± 53	2659 ± 59	99
G3	360	134	651	0.21	12.9210 ± 0.3765	0.5139 ± 0.0140	0.93	2674 ± 53	2673 ± 59	100
G4	362	103	667	0.15	12.8288 ± 0.3741	0.5116 ± 0.0139	0.93	2670 ± 53	2663 ± 59	100
G5	300	116	541	0.21	12.9759 ± 0.3786	0.5130 ± 0.0139	0.93	2684 ± 53	2670 ± 59	99
G6	270	105	489	0.21	12.8632 ± 0.3790	0.5134 ± 0.0140	0.92	2668 ± 53	2671 ± 60	100
G7	443	108	815	0.13	12.8126 ± 0.3745	0.5151 ± 0.0140	0.93	2656 ± 53	2679 ± 59	101
G8	358	178	638	0.28	12.7744 ± 0.3749	0.5128 ± 0.0139	0.92	2659 ± 53	2669 ± 59	100
G10	399	149	727	0.21	12.7166 ± 0.3733	0.5118 ± 0.0139	0.92	2655 ± 53	2664 ± 59	100
G11	348	123	632	0.19	12.8816 ± 0.3795	0.5132 ± 0.0140	0.92	2671 ± 53	2670 ± 59	100
G12	317	142	566	0.25	12.9236 ± 0.3804	0.5130 ± 0.0140	0.92	2678 ± 53	2669 ± 59	100
G13	373	197	658	0.30	12.9267 ± 0.3794	0.5144 ± 0.0140	0.92	2673 ± 53	2675 ± 59	100
G15	272	123	488	0.25	12.8458 ± 0.3812	0.5109 ± 0.0139	0.92	2674 ± 54	2661 ± 59	99
H1	378	75	913	0.08	9.1261 ± 0.2702	0.3995 ± 0.0109	0.92	2514 ± 54	2167 ± 50	86
H2	276	110	632	0.17	9.3114 ± 0.2756	0.4089 ± 0.0111	0.92	2509 ± 54	2210 ± 51	88
H3	257	110	633	0.17	9.0499 ± 0.2683	0.3804 ± 0.0103	0.92	2582 ± 54	2078 ± 48	80
H4	344	107	759	0.14	9.8749 ± 0.2925	0.4272 ± 0.0116	0.92	2534 ± 54	2293 ± 52	91
H5	301	104	544	0.19	12.8900 ± 0.3845	0.5125 ± 0.0140	0.91	2675 ± 54	2667 ± 59	100
H6	495	183	913	0.20	12.2862 ± 0.3657	0.5029 ± 0.0137	0.91	2627 ± 54	2626 ± 59	100
H7	459	215	859	0.25	11.9431 ± 0.3562	0.4888 ± 0.0133	0.91	2627 ± 54	2565 ± 57	98
H9	326	117	588	0.20	12.9441 ± 0.3879	0.5102 ± 0.0139	0.91	2689 ± 54	2658 ± 59	99
H10	369	109	672	0.16	12.7578 ± 0.3805	0.5112 ± 0.0139	0.91	2662 ± 54	2662 ± 59	100
H11	425	140	845	0.17	11.3768 ± 0.3406	0.4723 ± 0.0128	0.91	2603 ± 55	2494 ± 56	96
H12	308	97	563	0.17	12.9121 ± 0.3864	0.5103 ± 0.0139	0.91	2685 ± 54	2658 ± 59	99
H13	446	127	968	0.13	10.2142 ± 0.3060	0.4384 ± 0.0119	0.91	2548 ± 55	2343 ± 53	92
H15	412	206	730	0.28	12.8006 ± 0.3837	0.5136 ± 0.0140	0.91	2660 ± 54	2672 ± 59	100
PC-602										
A1	430	117	835	0.14	11.7028 ± 0.3200	0.4877 ± 0.0128	0.96	2597 ± 52	2561 ± 55	99
A2	488	135	1075	0.13	10.0267 ± 0.2745	0.4342 ± 0.0113	0.95	2533 ± 52	2325 ± 51	92
A3	407	77	779	0.10	12.1247 ± 0.3318	0.4993 ± 0.0131	0.96	2617 ± 52	2611 ± 56	100
A4	408	124	928	0.13	9.7639 ± 0.2682	0.4182 ± 0.0109	0.95	2551 ± 52	2252 ± 50	88
A5	395	113	1043	0.11	8.0027 ± 0.2198	0.3634 ± 0.0095	0.95	2453 ± 53	1998 ± 45	81

Table A.5 *(Continued)*

Zircon #	Pb (ppm)	U (ppm)	Th (ppm)	Th/U	$^{207}Pb/^{235}U$ ± 2σ	$^{206}Pb/^{238}U$ ± 2σ	ρ	Ages ± 2σ $^{207}Pb/^{206}Pb$	Ages ± 2σ $^{206}Pb/^{238}U$	Concordance %
PC-602										
A6	157	354	195	1.81	12.6823 ± 0.3517	0.5001 ± 0.0131	0.95	2688 ± 52	2614 ± 56	97
A8	365	78	716	0.11	11.6238 ± 0.3202	0.4867 ± 0.0127	0.95	2589 ± 52	2557 ± 55	99
A10	470	140	956	0.15	11.0998 ± 0.3049	0.4636 ± 0.0121	0.95	2593 ± 52	2456 ± 53	95
A11	464	135	1081	0.12	9.5246 ± 0.2632	0.4085 ± 0.0107	0.95	2549 ± 53	2208 ± 49	87
A13	357	97	680	0.14	11.9790 ± 0.3298	0.4966 ± 0.0130	0.95	2605 ± 52	2599 ± 56	100
B1	336	73	811	0.09	9.0774 ± 0.2492	0.3999 ± 0.0104	0.95	2504 ± 53	2169 ± 48	87
B2	293	88	563	0.16	12.0891 ± 0.3325	0.4875 ± 0.0128	0.95	2651 ± 52	2560 ± 55	97
B3	354	88	800	0.11	9.8812 ± 0.2714	0.4239 ± 0.0111	0.95	2548 ± 52	2278 ± 50	89
B5	415	122	999	0.12	9.1244 ± 0.2517	0.3996 ± 0.0104	0.95	2514 ± 53	2167 ± 48	86
B6	391	108	725	0.15	12.5291 ± 0.3449	0.5082 ± 0.0133	0.95	2642 ± 52	2649 ± 57	100
B8	499	125	1168	0.11	9.4180 ± 0.2609	0.4106 ± 0.0107	0.94	2521 ± 53	2218 ± 49	88
B9	329	92	608	0.15	12.5348 ± 0.3460	0.5060 ± 0.0132	0.95	2650 ± 52	2639 ± 57	100
B10	334	107	607	0.18	12.7127 ± 0.3518	0.5102 ± 0.0134	0.95	2659 ± 52	2658 ± 57	100
B12	465	97	973	0.10	10.9606 ± 0.3033	0.4558 ± 0.0119	0.94	2600 ± 52	2421 ± 53	93
C2	429	122	956	0.13	9.9368 ± 0.2750	0.4267 ± 0.0111	0.94	2547 ± 53	2291 ± 50	90
C3	295	77	615	0.12	10.8032 ± 0.3004	0.4544 ± 0.0119	0.94	2581 ± 53	2415 ± 53	94
C5	460	118	853	0.14	12.6156 ± 0.3498	0.5071 ± 0.0132	0.94	2657 ± 52	2644 ± 57	100
C7	443	111	1033	0.11	9.4575 ± 0.2639	0.4087 ± 0.0107	0.94	2536 ± 53	2209 ± 49	87
C8	486	104	1195	0.09	8.8805 ± 0.2500	0.3934 ± 0.0103	0.93	2494 ± 54	2138 ± 48	86
C10	466	101	1008	0.10	10.3935 ± 0.2923	0.4441 ± 0.0116	0.93	2555 ± 53	2369 ± 52	93
C12	127	6	247	0.02	12.4842 ± 0.3608	0.5013 ± 0.0132	0.91	2658 ± 54	2619 ± 57	99
C14	435	134	1001	0.13	9.5587 ± 0.2685	0.4130 ± 0.0108	0.93	2536 ± 53	2229 ± 49	88
D3	313	103	574	0.18	12.4342 ± 0.3492	0.5083 ± 0.0133	0.93	2629 ± 53	2649 ± 57	101
D4	373	101	709	0.14	12.0256 ± 0.3387	0.4972 ± 0.0130	0.93	2610 ± 53	2602 ± 56	100
D5	359	127	659	0.19	12.4200 ± 0.3498	0.5063 ± 0.0132	0.93	2633 ± 53	2641 ± 57	100
D7	346	85	823	0.10	9.2679 ± 0.2615	0.4054 ± 0.0106	0.93	2516 ± 54	2194 ± 49	87
D8	488	91	1130	0.08	9.7023 ± 0.2752	0.4178 ± 0.0110	0.92	2542 ± 54	2251 ± 50	89
D9	848	134	1613	0.08	12.4673 ± 0.3517	0.5050 ± 0.0132	0.93	2644 ± 53	2635 ± 57	100
E1	451	127	1105	0.11	8.7597 ± 0.2486	0.3940 ± 0.0103	0.92	2469 ± 54	2141 ± 48	87
E2	474	146	899	0.16	12.0848 ± 0.3432	0.4974 ± 0.0130	0.92	2617 ± 53	2603 ± 56	99
E3	378	133	926	0.14	8.6421 ± 0.2465	0.3882 ± 0.0101	0.92	2471 ± 54	2114 ± 47	86
E4	603	168	1364	0.12	9.8027 ± 0.2801	0.4219 ± 0.0110	0.92	2543 ± 54	2269 ± 50	89
E5	231	53	449	0.12	11.9141 ± 0.3442	0.4893 ± 0.0128	0.91	2621 ± 54	2568 ± 56	98
E7	250	70	486	0.14	11.8998 ± 0.3429	0.4819 ± 0.0126	0.91	2644 ± 54	2536 ± 55	96

Table A.5 *(Continued)*

Zircon #	Pb (ppm)	U (ppm)	Th (ppm)	Th/U	$^{207}Pb/^{235}U$ ± 2σ	$^{206}Pb/^{238}U$ ± 2σ	ρ	Ages ± 2σ $^{207}Pb/^{206}Pb$	Ages ± 2σ $^{206}Pb/^{238}U$	Concordance %
PC-602										
E10	328	120	652	0.18	11.4600 ± 0.3322	0.4677 ± 0.0123	0.91	2631 ± 54	2473 ± 54	94
E12	553	241	1252	0.19	9.7179 ± 0.2808	0.4159 ± 0.0109	0.91	2552 ± 55	2242 ± 50	88
F1	567	165	1169	0.14	11.0271 ± 0.3199	0.4614 ± 0.0121	0.90	2590 ± 55	2446 ± 53	94
F2	412	91	838	0.11	11.4313 ± 0.3296	0.4698 ± 0.0123	0.91	2620 ± 54	2483 ± 54	95
F3	382	120	726	0.16	12.1001 ± 0.3518	0.4962 ± 0.0130	0.90	2623 ± 54	2597 ± 56	99
F4	585	155	1282	0.12	10.3158 ± 0.3003	0.4364 ± 0.0114	0.90	2572 ± 55	2335 ± 51	91
F5	355	121	653	0.19	12.6552 ± 0.3701	0.5080 ± 0.0133	0.90	2659 ± 55	2648 ± 57	100
F6	377	141	782	0.18	10.8968 ± 0.3186	0.4528 ± 0.0119	0.90	2601 ± 55	2408 ± 53	93
F7	507	100	1337	0.07	8.1091 ± 0.2376	0.3703 ± 0.0097	0.90	2443 ± 56	2031 ± 46	83
F8	675	199	1587	0.13	9.2651 ± 0.2717	0.4056 ± 0.0107	0.90	2514 ± 55	2195 ± 49	87
F12	347	119	805	0.15	9.3186 ± 0.2734	0.4059 ± 0.0107	0.89	2523 ± 55	2196 ± 49	87
G1	355	163	640	0.25	12.6347 ± 0.3752	0.5057 ± 0.0133	0.89	2664 ± 55	2638 ± 57	99
G2	491	146	945	0.15	11.8654 ± 0.3504	0.4885 ± 0.0128	0.89	2617 ± 55	2564 ± 55	98
G3	618	174	1488	0.12	9.0348 ± 0.2687	0.3997 ± 0.0105	0.88	2496 ± 56	2168 ± 48	87
G5	580	205	1423	0.14	8.7288 ± 0.2597	0.3896 ± 0.0102	0.88	2482 ± 56	2121 ± 47	85
G6	663	207	1558	0.13	9.2162 ± 0.2762	0.4070 ± 0.0107	0.88	2500 ± 57	2201 ± 49	88
G11	528	124	1202	0.10	9.6511 ± 0.2792	0.4250 ± 0.0113	0.92	2504 ± 54	2283 ± 51	91
H4	489	129	1087	0.12	9.9991 ± 0.2992	0.4272 ± 0.0113	0.88	2555 ± 56	2293 ± 51	90
H5	321	92	601	0.15	12.2555 ± 0.3682	0.5005 ± 0.0133	0.88	2630 ± 56	2616 ± 57	99
H6	446	105	1002	0.10	9.7125 ± 0.2933	0.4249 ± 0.0112	0.87	2515 ± 57	2283 ± 51	91
H7	490	106	936	0.11	12.2706 ± 0.3725	0.5003 ± 0.0132	0.87	2633 ± 56	2615 ± 57	99
H10	619	166	1421	0.12	9.6024 ± 0.2966	0.4178 ± 0.0110	0.85	2525 ± 58	2250 ± 50	89
H11	517	168	970	0.17	12.1681 ± 0.3800	0.4997 ± 0.0132	0.85	2621 ± 58	2613 ± 57	100
PC-618										
A1	66	114	100	1.14	11.8336 ± 0.3676	0.4566 ± 0.0124	0.87	2724 ± 57	2425 ± 55	89
A2	3.7	0.01	6.9	0.002	13.9915 ± 0.6136	0.5235 ± 0.0165	0.72	2775 ± 77	2714 ± 70	98
A3	62	107	98	1.09	11.7790 ± 0.3759	0.4607 ± 0.0126	0.86	2702 ± 58	2443 ± 56	90
A3	42	84	59	1.44	12.3757 ± 0.4072	0.4818 ± 0.0133	0.84	2710 ± 60	2535 ± 58	94
A4	19	0.22	35	0.006	14.1529 ± 0.4625	0.5268 ± 0.0146	0.85	2784 ± 59	2728 ± 61	98
A7	21	26	35	0.74	12.6254 ± 0.4268	0.4839 ± 0.0135	0.83	2735 ± 61	2544 ± 59	93
A8	7.7	0.37	14	0.026	14.0911 ± 0.5573	0.5321 ± 0.0159	0.76	2760 ± 70	2750 ± 67	100
A9	18	21	29	0.75	13.0067 ± 0.4527	0.4924 ± 0.0139	0.81	2756 ± 62	2581 ± 60	94
A10	18	11	33	0.34	12.4463 ± 0.4233	0.4741 ± 0.0132	0.82	2746 ± 61	2501 ± 58	91

Table A.5 *(Continued)*

Zircon #	Pb (ppm)	U (ppm)	Th (ppm)	Th/U	$^{207}Pb/^{235}U$ ± 2σ	$^{206}Pb/^{238}U$ ± 2σ	ρ	Ages ± 2σ $^{207}Pb/^{206}Pb$	Ages ± 2σ $^{206}Pb/^{238}U$	Concordance %
PC-618										
A11	15	0.04	28	0.001	13.9814 ± 0.4728	0.5294 ± 0.0148	0.82	2756 ± 61	2739 ± 62	99
A12	14	0.45	25	0.018	14.1633 ± 0.5112	0.5360 ± 0.0153	0.79	2756 ± 64	2767 ± 64	100
B2	46	87	77	1.13	11.3028 ± 0.3552	0.4419 ± 0.0119	0.86	2703 ± 57	2359 ± 53	87
B3	15	9.9	26	0.38	12.8438 ± 0.4747	0.4864 ± 0.0140	0.78	2755 ± 66	2555 ± 61	93
B4	83	0.42	149	0.003	14.4520 ± 0.4708	0.5479 ± 0.0150	0.84	2753 ± 59	2816 ± 62	102
B7	18	19	29	0.67	13.1483 ± 0.4706	0.4972 ± 0.0140	0.79	2758 ± 64	2602 ± 60	94
B8	19	15	34	0.44	12.7819 ± 0.4518	0.4856 ± 0.0136	0.79	2750 ± 63	2552 ± 59	93
B10	41	67	65	1.02	12.1584 ± 0.4176	0.4649 ± 0.0128	0.80	2740 ± 62	2461 ± 57	90
B11	7.3	1.6	13	0.12	13.1512 ± 0.8345	0.4948 ± 0.0194	0.62	2766 ± 109	2591 ± 84	94
B12	26	5.4	52	0.10	12.1357 ± 0.4405	0.4638 ± 0.0131	0.78	2740 ± 65	2457 ± 58	90
B13	6	0.09	10	0.008	14.2292 ± 0.6425	0.5273 ± 0.0167	0.70	2791 ± 79	2730 ± 70	98
B14	56	0.83	101	0.008	14.0763 ± 0.4938	0.5379 ± 0.0149	0.79	2740 ± 63	2775 ± 63	101
C1	53	80	93	0.86	11.0326 ± 0.4013	0.4299 ± 0.0121	0.77	2708 ± 65	2305 ± 54	85
C2	50	42	94	0.45	11.4584 ± 0.4093	0.4470 ± 0.0124	0.78	2707 ± 64	2382 ± 55	88
C3	11	7.4	19	0.39	12.7465 ± 0.5541	0.4633 ± 0.0142	0.71	2822 ± 76	2454 ± 63	87
C4	51	71	81	0.87	12.2949 ± 0.4361	0.4750 ± 0.0131	0.78	2722 ± 64	2506 ± 57	92
C5	23	23	40	0.58	12.0940 ± 0.4581	0.4629 ± 0.0132	0.75	2738 ± 68	2452 ± 58	90
C6	28	32	45	0.70	12.5270 ± 0.4467	0.4786 ± 0.0132	0.77	2741 ± 64	2521 ± 58	92
C7	25	77	25	3.04	12.8950 ± 0.4898	0.4895 ± 0.0139	0.75	2751 ± 68	2568 ± 60	93
C8	53	107	82	1.30	11.6105 ± 0.3636	0.4477 ± 0.0127	0.90	2725 ± 55	2385 ± 56	88
C9	119	0.76	228	0.003	13.2224 ± 0.3879	0.5077 ± 0.0141	0.94	2732 ± 52	2647 ± 60	97
C10	5.6	0.01	10	0.001	14.4968 ± 0.5451	0.5320 ± 0.0162	0.81	2807 ± 65	2750 ± 68	98
C11	8.3	5.4	15	0.37	13.0895 ± 0.5012	0.4739 ± 0.0145	0.80	2829 ± 66	2500 ± 63	88
C12	47	126	64	1.97	11.8691 ± 0.3696	0.4586 ± 0.0129	0.91	2722 ± 55	2433 ± 57	89
E1	50	63	85	0.74	12.1584 ± 0.3687	0.4743 ± 0.0133	0.92	2706 ± 54	2502 ± 58	92
E2	6.7	2.1	12	0.18	13.9319 ± 0.5664	0.5090 ± 0.0160	0.77	2814 ± 70	2652 ± 68	94
E3	19	4.0	35	0.12	13.8350 ± 0.4505	0.5053 ± 0.0145	0.88	2814 ± 57	2636 ± 62	94
E4	19	20	31	0.66	13.2465 ± 0.4310	0.5055 ± 0.0145	0.88	2743 ± 57	2637 ± 62	96
E5	1.4	0.07	2.5	0.028	14.6416 ± 0.7195	0.5430 ± 0.0188	0.70	2789 ± 84	2796 ± 78	100
E6	29	0.7	54	0.013	13.4106 ± 0.4391	0.5114 ± 0.0146	0.87	2744 ± 58	2663 ± 62	97
E8	12	8.7	20	0.44	12.9107 ± 0.4533	0.4926 ± 0.0145	0.84	2743 ± 62	2582 ± 62	94
E9	34	34	56	0.60	12.7630 ± 0.4097	0.4936 ± 0.0140	0.88	2721 ± 57	2586 ± 61	95
E10	17	5.7	30	0.19	13.5864 ± 0.4535	0.5060 ± 0.0146	0.86	2782 ± 59	2640 ± 62	95
E11	15	38	17	2.30	13.5215 ± 0.5309	0.5060 ± 0.0155	0.78	2775 ± 68	2639 ± 67	95

Table A.5 *(Continued)*

Zircon #	Pb (ppm)	U (ppm)	Th (ppm)	Th/U	$^{207}Pb/^{235}U$ ± 2σ	$^{206}Pb/^{238}U$ ± 2σ	ρ	Ages ± 2σ		Concordance %
								$^{207}Pb/^{206}Pb$	$^{206}Pb/^{238}U$	
PC-618										
F1	3.5	0.009	6.5	0.001	13.7281 ± 0.5239	0.5258 ± 0.0159	0.79	2737 ± 66	2724 ± 67	100
F7	30	35	51	0.68	11.8223 ± 0.3817	0.4576 ± 0.0130	0.88	2719 ± 57	2429 ± 57	89
F8	11	9.1	18	0.51	14.5354 ± 0.5272	0.5288 ± 0.0158	0.82	2821 ± 63	2736 ± 66	97
F9	63	111	100	1.11	11.6866 ± 0.3654	0.4505 ± 0.0126	0.90	2726 ± 55	2397 ± 56	88
F11	45	100	63	1.60	12.0358 ± 0.3850	0.4682 ± 0.0132	0.88	2711 ± 57	2476 ± 58	91
G2	28	20	52	0.38	11.9333 ± 0.3856	0.4641 ± 0.0131	0.88	2711 ± 57	2458 ± 58	91
G3	39	32	71	0.45	11.8934 ± 0.3650	0.4635 ± 0.0129	0.91	2708 ± 55	2455 ± 57	91
G4	9.2	4.7	16	0.30	13.7588 ± 0.4862	0.5028 ± 0.0147	0.83	2813 ± 62	2626 ± 63	93
G6	24	18	42	0.41	12.7937 ± 0.4210	0.4930 ± 0.0140	0.86	2727 ± 58	2583 ± 61	95
G7	14	10	22	0.46	13.9639 ± 0.4847	0.5106 ± 0.0148	0.84	2813 ± 61	2659 ± 63	95
G8	16	10	27	0.36	13.0535 ± 0.4583	0.4988 ± 0.0145	0.83	2740 ± 62	2609 ± 62	95
G9	12	4.6	22	0.20	13.0191 ± 0.5135	0.4695 ± 0.0144	0.78	2835 ± 68	2482 ± 63	88
G12	12	7.0	20	0.34	13.9142 ± 0.4790	0.5075 ± 0.0146	0.84	2817 ± 60	2646 ± 63	94

Appendix B – Supplementary information for Chapter 3

Table B.1: Samples collected during fieldwork in 2017. Coordinates are in Easting and Northing UTM NAD 27, zone 18.

Sample	Lithology	Location	Easting	Northing
PC-622	Trondhjemite	Southeast of Nuvvuagittuq	341924	6462414
PC-623	Granodiorite	Southeast of Nuvvuagittuq	341950	6462461
PC-625A	Granodiorite	South of Nuvvuagittuq, bordering the Hudson Bay	340869	6462451
PC-625B	Granodiorite	South of Nuvvuagittuq, bordering the Hudson Bay	340869	6462451
PC-626	Tonalite	South of Nuvvuagittuq	340516	6462899
PC-634	Granodiorite	Northwest corner of Nuvvuagittuq	339589	6465310
PC-638	Trondhjemite	Bordering Nuvvuagittuq to the south	340196	6463527
PC-639	Trondhjemite	Bordering Nuvvuagittuq to the south	340195	6463303
PC-642	Granite	West of Nuvvuagittuq	339214	6464217
PC-643	Pegmatite	Intruding the gneissic gabbro sills of Nuvvuagittuq	339766	6463731
PC-648	Granite	Northeast of Nuvvuagittuq, near the big lake	341423	6465140
UK-002	Tonalite	Intruding the hornblende-amphibolites of Ukaliq	342263	6466200

Table B.2: Detection limits and dwell times of measured masses during zircon trace element LA-ICP-MS analyses. Detection limits are reported at 99% confidence based on primary reference material NIST 612.

Mass	Detection limit (ppm)	Dwell times (ms)
^{29}Si	160.4178	0.005
^{31}P	25.36381	0.005
^{47}Ti	0.533104	0.02
^{49}Ti	0.730604	0.03
^{56}Fe	2.935970	0.005
^{89}Y	0.010058	0.01
^{91}Zr	0.227714	0.005
^{139}La	0.008683	0.02
^{140}Ce	0.012131	0.02
^{141}Pr	0.006574	0.02
^{146}Nd	0.037425	0.02
^{147}Sm	0.042531	0.02
^{151}Eu	0.013418	0.02
^{157}Gd	0.045846	0.02
^{159}Tb	0.006751	0.02
^{163}Dy	0.029042	0.02
^{165}Ho	0.007359	0.02
^{167}Er	0.032026	0.02
^{169}Tm	0.007433	0.02
^{173}Yb	0.049878	0.02
^{175}Lu	0.008170	0.02
^{177}Hf	0.036064	0.03
^{232}Th	0.018766	0.01
^{235}U	5.808209	0.02
^{238}U	0.015325	0.01

Figure B.1: Weighted mean diagram of the TEM-2 zircon reference material used for SIMS oxygen isotope analyses in zircon. The black horizontal bar represents the mean value of the run and dashed lines are the 2σ-mean error. The red horizontal bar represents the accepted value from Black et al. (2004). Vertical error bars are reported in 2σ.

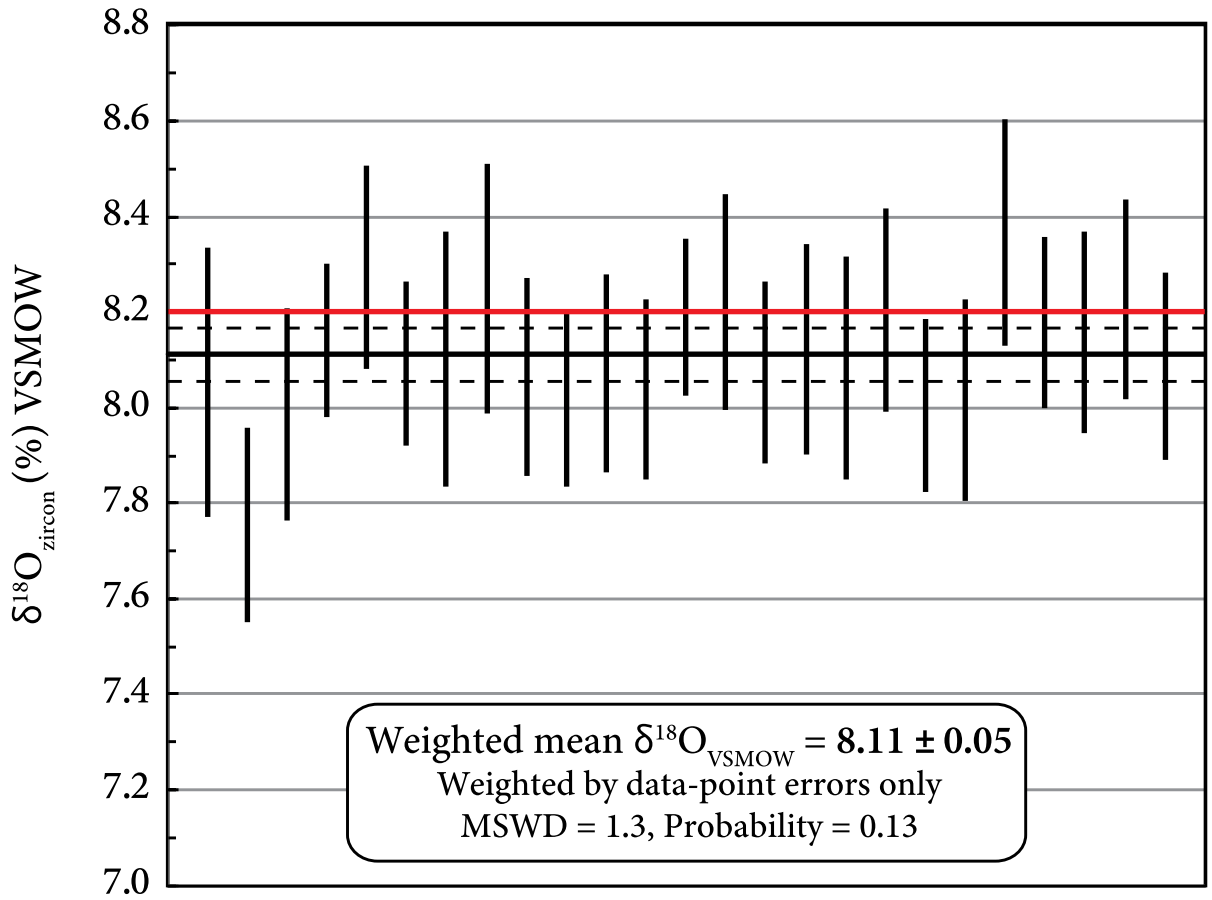

Table B.3: Operating conditions and instrument settings for U-Pb isotopic analyses.

Laser ablation system	
Make, Model & type	Resonetics/M-50E 193nm, Excimer
Ablation cell & volume	Laurin Cell ® two volumes cell, Laurin Technic Ltd., volume ca. 1cm^3
Laser wavelength	193 nm
Pulse width	< 4 ns
Fluence	2.5 J.cm^{-2}
Repetition rate	3 Hz
Spot size	20 µm (UK-002), 27 µm (PC-622, PC-638)
Sampling mode / pattern	Single spot
Carrier gas	100% He, Ar make-up gas and N_2 combined using the Squid® device from RESOlution Instruments.
Background collection	30 s
Ablation duration	60 s
Wash-out delay	30 s
Cell carrier gas flow	0.70 l/min He
ICP-MS Instrument	
Make, Model & type	Element XR SF-ICP-MS
Sample introduction	Via conventional tubing
RF power	1200 W
Make-up gas flow	0.98 l/min Ar
Detection system	Single collector secondary electron multiplier (Faraday cup)
Masses measured	204, 206, 207, 208, 232, 238
Integration time per peak	20 ms
Sensitivity / Efficiency	15 000 cps/ppm ^{238}U (47 µm, 10 Hz, 3.5 J/cm^2)
Dead time	6 ns
Data Processing	
Gas blank	30 second on-peak
Calibration strategy	GJ-1 used as primary reference material, 91500 used as secondary reference material (Quality Control)
Reference Material info	91500 (Wiedenbeck et al., 1995) GJ1 (Jackson et al., 2004)
Data processing package used / Correction for LIEF	GLITTER ® (van Achterbergh et al., 2001)
Mass discrimination	Standard-sample bracketing with ^{207}Pb/^{206}Pb and ^{206}Pb/^{238}U normalized to reference material GJ-1
Common-Pb correction, composition and uncertainty	No common-Pb correction. Analyses discarded of the age calculation when discordance >20%
Uncertainty level & propagation	Ages are quoted at 2σ absolute, propagation is by quadratic addition according to Horstwood et al. (2003). Reproducibility and age uncertainty of reference material are propagated.
Quality control / Validation	91500: Concordia age = 1064.9 ± 3.1 (2SD, MSWD = 0.47, *n* = 64)
Other information	For detailed method description see Hurai et al. (2010). For detailed laser technical description see Müller et al. (2009).

References

Horstwood, M. S. A., Foster, G. L., Parrish, R. R., Noble, S. R., & Nowell, G. M. (2003). Common-Pb corrected in situ U-Pb accessory mineral geochronology by LA-MC-ICP-MS. Journal of Analytical Atomic Spectrometry, 18(8), 837–846.

Hurai, V., Paquette, J.-L., Huraiova, M., & Konecny, P. (2010). Age of deep crustal magmatic chambers in the intra-Carpathian back-arc basin inferred from LA-ICPMS U-Th-Pb dating of zircon and monazite from igneous xenoliths in alkali basalts. Journal of Volcanology and Geothermal Research, 198, 275–287.

Jackson, S. E., Pearson, N. J., Griffin, W. L., & Belousova, E. A. (2004). The application of laser ablation-inductively coupled plasma-mass spectrometry to in situ U-Pb zircon geochronology. Chemical Geology, 211(1–2), 47–69.

Müller, W., Shelley, M., Miller, P., & Broude, S. (2009). Initial performance metrics of a new custom-designed ArF excimer LA-ICPMS system coupled to a two-volume laser-ablation cell. Journal of Analytical Atomic Spectrometry, 24(2), 209–214.

van Achterbergh, E., Ryan, C. G., Jackson, S. E., & Griffin, W. L. (2001). Data reduction software for LA-ICP-MS. In P. J. Sylvester (Ed.), Laser Ablation-ICPMS in the Earth Sciences, Mineralogical Association of Canada, 29, pp. 239–243.

Wiedenbeck, M., Allé, P., Corfu, F., Griffin, W. L., Meier, M., Oberli, F., von Quadt, A., Roddick, J. C., & Spiegel, W. (1995). Three natural zircon standards for U-Th-Pb, Lu-Hf, trace element and REE analyses. Geostandards Newsletter, 19(1), 1–23.

Figure B.2: Repeated measurements of the GJ-1 primary reference material to correct for U-Pb fractionation during laser sampling and instrumental mass discrimination.

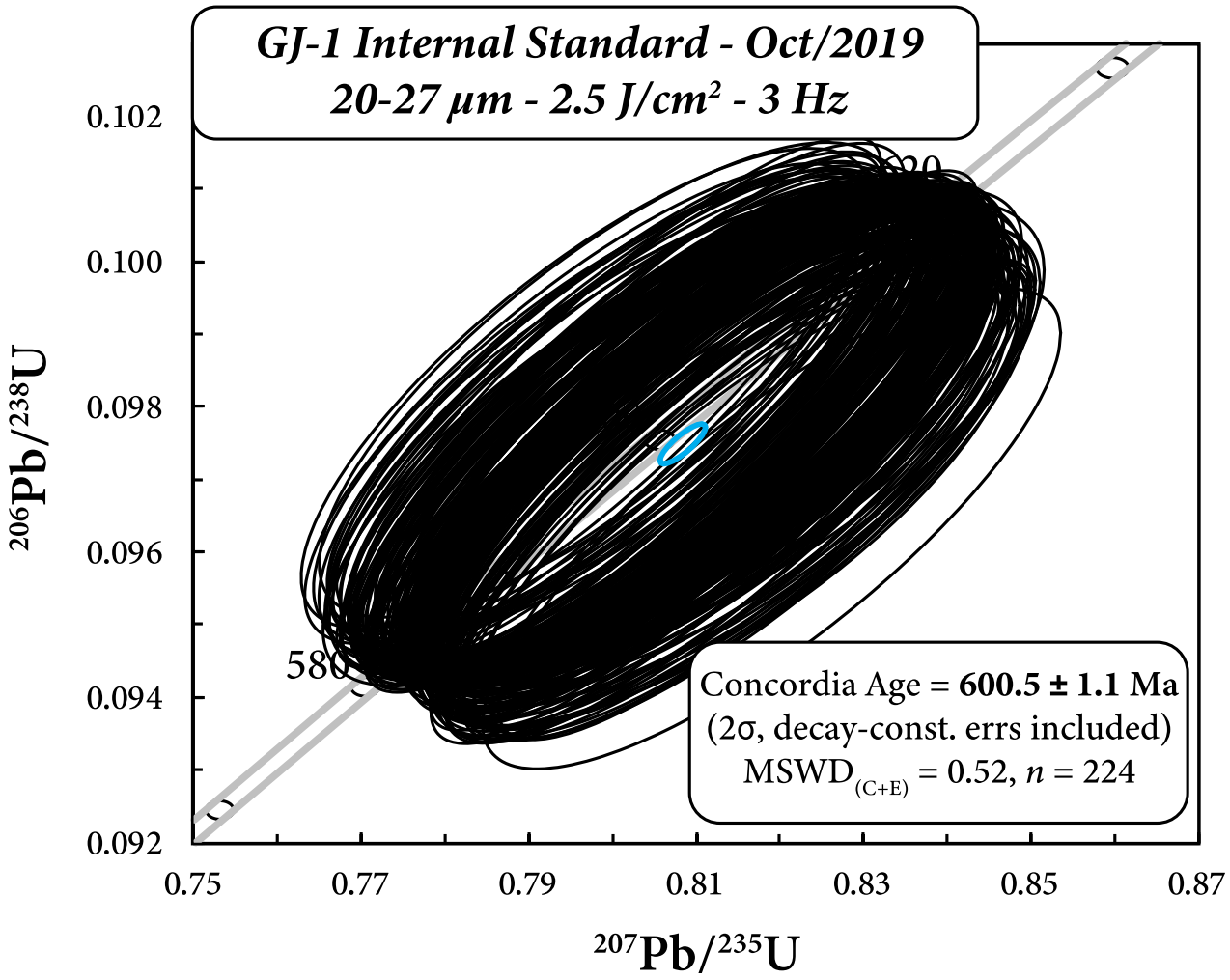

Figure B.3: Repeated measurements of the 91500 secondary reference material for reproducibility and accuracy of the corrections during U-Pb analysis.

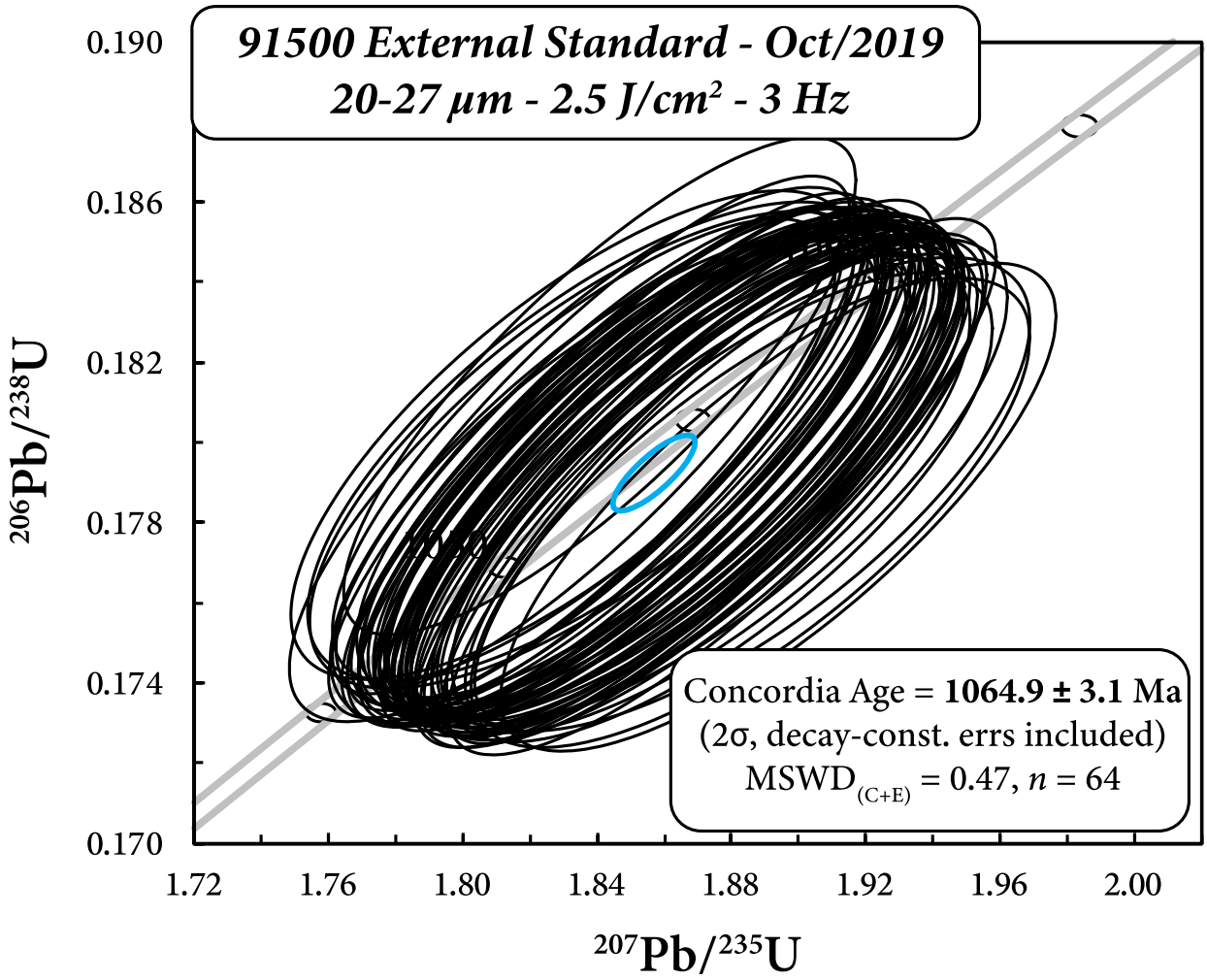

Table B.4: Whole rock major and trace element compositions of the Nuvvuagittuq (NGB) and Ukaliq (USB) granitoids and pegmatite. Major element concentrations (hydrous compositions) are reported in wt.% and trace element concentrations are reported in ppm.

Sample	PC-622	PC-623	PC-625A	PC-625B	PC-626	PC-634
Location	NGB	NGB	NGB	NGB	NGB	NGB
Lithology	Trondhjemite	Granodiorite	Granodiorite	Granodiorite	Tonalite	Granodiorite
SiO_2	65.29	60.25	73.22	70.48	65.23	65.52
TiO_2	16.52	16.00	13.77	14.10	17.03	15.77
Al_2O_3	4.55	7.66	2.32	3.78	3.94	4.34
Fe_2O_3	0.07	0.12	0.05	0.06	0.06	0.07
MnO	2.78	3.83	1.04	1.09	2.02	2.21
MgO	1.85	2.66	2.85	2.23	3.03	3.96
CaO	4.68	2.96	3.58	3.63	4.89	3.74
Na_2O	2.26	3.64	2.22	3.30	2.27	2.46
K_2O	0.44	0.82	0.24	0.41	0.47	0.44
P_2O_5	0.02	0.28	0.00	0.03	0.09	0.10
LOI	1.37	1.60	0.48	0.67	0.80	1.27
Sc	6.37	14.2	3.70	6.61	6.52	8.65
V	55.2	117	26.1	29.7	55.1	64.8
Cr	20.3	52.4	25.4	8.56	23.9	28.6
Co	10.7	22.6	6.23	5.62	9.09	11.2
Ni	19.5	35.1	10.8	3.37	20.3	23.4
Cu	3.45	48.8	41.1	17.4	2.10	7.40
Zn	45.4	79.4	35.5	34.0	49.0	47.0
Ga	20.8	20.0	14.2	16.2	21.9	19.1
Ge	0.95	1.52	0.71	1.01	1.08	0.95
Rb	93.7	173	75.6	107	88.8	74.5
Sr	188	148	112	122	267	288
Y	7.79	21.8	13.0	15.1	8.53	12.2
Zr	120	177	154	276	110	148
Nb	5.82	8.87	4.70	9.12	4.89	6.86
Cs	3.19	4.11	2.46	3.13	1.85	1.05
Ba	402	294	426	737	389	672
La	20.7	37.0	42.4	48.4	22.4	31.7
Ce	38.6	73.7	78.7	81.3	41.1	57.1
Pr	4.26	8.22	7.82	8.09	4.51	6.12
Nd	15.5	30.0	24.8	26.7	16.1	21.3
Sm	2.74	5.07	3.60	4.29	2.80	3.52
Eu	0.77	1.48	0.76	1.13	0.97	0.99
Gd	2.34	4.79	3.54	4.12	2.54	3.27
Tb	0.29	0.64	0.43	0.53	0.31	0.41
Dy	1.41	3.68	2.25	2.77	1.58	2.21
Ho	0.26	0.75	0.45	0.52	0.30	0.42
Er	0.70	2.13	1.29	1.49	0.81	1.21
Tm	0.10	0.32	0.18	0.21	0.11	0.18
Yb	0.63	2.07	1.03	1.38	0.73	1.12
Lu	0.10	0.30	0.15	0.21	0.11	0.16
Hf	3.09	4.16	4.38	6.08	2.88	3.78
Ta	0.78	0.67	0.34	1.14	0.45	0.43
Pb	10.9	6.30	18.7	14.7	8.08	15.9
Th	7.22	6.09	21.3	16.2	4.94	9.00
U	1.10	1.67	3.01	2.72	0.65	0.76

Table B.4 *(Continued)*

Sample	PC-638	PC-639	PC-642	PC-643	PC-648	UK-002
Location	NGB	NGB	NGB	NGB	NGB	USB
Lithology	Trondhjemite	Trondhjemite	Granite	Pegmatite	Granite	Tonalite
SiO_2	68.94	71.14	73.70	74.16	72.53	68.74
TiO_2	15.79	14.54	12.82	13.69	14.81	15.18
Al_2O_3	3.05	2.79	2.26	0.05	1.24	4.00
Fe_2O_3	0.05	0.03	0.03	0.00	0.01	0.04
MnO	1.60	1.50	0.50	0.00	0.41	1.61
MgO	2.20	1.36	1.40	0.14	2.34	3.53
CaO	4.76	4.88	2.51	1.92	4.38	3.71
Na_2O	2.04	2.10	5.68	9.82	3.00	1.73
K_2O	0.37	0.30	0.34	0.01	0.13	0.37
P_2O_5	0.10	0.08	0.07	0.00	0.03	0.07
LOI	0.97	1.06	0.50	0.10	0.88	0.89
Sc	4.47	3.03	4.68	0.04	0.61	6.62
V	36.7	25.6	13.4	0.39	12.5	48.6
Cr	23.0	14.9	10.9	4.82	6.19	22.3
Co	6.43	5.78	3.12	0.02	2.23	9.89
Ni	11.9	10.3	2.98	0.10	1.34	28.1
Cu	10.9	2.89	16.5	0.32	2.53	4.15
Zn	35.6	30.6	15.5	0.15	20.1	41.3
Ga	20.6	18.5	16.4	10.4	18.3	16.9
Ge	0.94	0.91	0.97	0.19	0.54	1.18
Rb	101	83.6	275	292	79.8	133
Sr	229	143	104	29.4	405	221
Y	5.34	3.36	37.0	1.05	1.40	5.69
Zr	136	134	355	1.48	99.0	144
Nb	4.82	4.69	21.0	0.61	1.15	7.67
Cs	2.35	1.95	1.34	1.03	0.22	2.08
Ba	438	510	615	120	830	222
La	25.8	24.5	78.2	2.31	13.2	38.5
Ce	45.5	40.7	150	2.81	22.7	67.4
Pr	4.78	4.00	14.8	0.27	2.25	6.79
Nd	16.3	12.9	47.7	0.84	7.24	22.4
Sm	2.53	1.78	7.72	0.17	0.91	3.17
Eu	0.83	0.64	0.88	0.30	0.73	0.72
Gd	2.20	1.54	7.67	0.16	0.76	2.74
Tb	0.23	0.15	1.02	0.02	0.07	0.28
Dy	1.04	0.63	5.94	0.14	0.27	1.21
Ho	0.18	0.11	1.17	0.03	0.05	0.23
Er	0.48	0.31	3.49	0.11	0.14	0.56
Tm	0.06	0.04	0.52	0.02	0.02	0.07
Yb	0.41	0.27	3.40	0.14	0.13	0.40
Lu	0.06	0.05	0.50	0.02	0.02	0.07
Hf	3.52	3.78	9.82	0.10	2.80	3.92
Ta	0.42	0.34	1.89	0.03	0.11	0.74
Pb	7.37	15.3	20.8	147	26.9	18.3
Th	8.15	11.1	41.1	1.20	29.6	17.8
U	1.65	2.51	3.88	0.22	0.62	1.55

Table B.5: U-Pb isotopic data of zircons from two Nuvvuagittuq trondhjemites (PC-622 and PC-638) and the Ukaliq tonalite (UK-002). ρ is the error correlation coefficient. Abbreviations: C = Core; R = Rim.

Spot #	Pb (ppm)	U (ppm)	Th (ppm)	Th/U	$^{207}Pb/^{235}U$ ± 2σ	$^{206}Pb/^{238}U$ ± 2σ	ρ	Ages ± 2σ		Concordance %
								$^{207}Pb/^{206}Pb$	$^{206}Pb/^{238}U$	
PC-622										
A1	108	62	105	0.59	38.2559 ± 1.0931	0.7739 ± 0.0215	0.97	3743 ± 47	3695 ± 78	99
A2-C	119	119	107	1.11	35.7716 ± 1.0225	0.7667 ± 0.0213	0.97	3655 ± 47	3669 ± 78	100
A2-R	86	65	86	0.75	33.9315 ± 0.9779	0.7406 ± 0.0206	0.97	3628 ± 48	3573 ± 76	98
A3	259	235	238	0.99	37.3905 ± 1.0663	0.7692 ± 0.0213	0.97	3718 ± 47	3678 ± 78	99
A5	147	114	135	0.85	39.0594 ± 1.1154	0.7859 ± 0.0218	0.97	3752 ± 47	3739 ± 79	100
A6	168	146	152	0.96	38.9444 ± 1.1120	0.7818 ± 0.0217	0.97	3755 ± 47	3724 ± 78	99
A7	111	79	101	0.78	39.7509 ± 1.1385	0.7952 ± 0.0221	0.97	3760 ± 47	3772 ± 79	100
A8	143	51	144	0.35	39.1932 ± 1.1234	0.7903 ± 0.0219	0.97	3748 ± 47	3754 ± 79	100
A9	109	68	102	0.67	39.1914 ± 1.1258	0.7915 ± 0.0220	0.97	3746 ± 47	3759 ± 79	100
A10-C	218	73	229	0.32	37.4460 ± 1.0700	0.7622 ± 0.0211	0.97	3734 ± 47	3652 ± 77	98
A10-R	114	52	114	0.46	38.3031 ± 1.1014	0.7795 ± 0.0217	0.97	3734 ± 47	3715 ± 78	99
A11	108	71	111	0.64	35.8308 ± 1.0345	0.7241 ± 0.0202	0.96	3745 ± 47	3512 ± 75	94
A12	140	83	133	0.62	39.3356 ± 1.1310	0.7889 ± 0.0219	0.97	3757 ± 47	3749 ± 79	100
A13	219	188	199	0.95	38.5923 ± 1.1063	0.7814 ± 0.0216	0.97	3742 ± 47	3722 ± 78	99
A14	229	202	223	0.91	36.1795 ± 1.0512	0.7299 ± 0.0203	0.96	3748 ± 48	3533 ± 76	94
A15	203	221	173	1.28	39.4350 ± 1.1354	0.7882 ± 0.0219	0.96	3762 ± 47	3747 ± 79	100
B1	206	143	199	0.72	37.5792 ± 1.0813	0.7625 ± 0.0212	0.96	3739 ± 47	3653 ± 77	98
B2	196	146	184	0.79	37.8696 ± 1.0908	0.7699 ± 0.0214	0.96	3736 ± 47	3680 ± 78	99
B3	113	80	102	0.78	40.3692 ± 1.1671	0.7995 ± 0.0222	0.96	3776 ± 47	3787 ± 80	100
B4	98	63	91	0.69	39.5111 ± 1.1449	0.7923 ± 0.0220	0.96	3757 ± 47	3762 ± 79	100
B5	140	76	134	0.57	39.3275 ± 1.1420	0.7909 ± 0.0220	0.96	3752 ± 47	3757 ± 79	100
B6	140	88	142	0.62	36.2727 ± 1.0494	0.7329 ± 0.0203	0.96	3745 ± 47	3544 ± 76	95
B7	139	111	135	0.83	37.1261 ± 1.0747	0.7470 ± 0.0207	0.96	3752 ± 47	3597 ± 76	96
B9	139	89	130	0.68	39.4610 ± 1.1488	0.7915 ± 0.0220	0.95	3756 ± 48	3759 ± 79	100
B10	156	122	142	0.85	38.9866 ± 1.1356	0.7880 ± 0.0219	0.95	3745 ± 48	3746 ± 79	100
B11	180	140	168	0.84	38.1486 ± 1.1100	0.7717 ± 0.0214	0.95	3744 ± 48	3687 ± 78	98
B12	57	27	55	0.49	38.9583 ± 1.1546	0.7892 ± 0.0221	0.94	3741 ± 48	3750 ± 80	100
B13	224	155	209	0.74	39.0022 ± 1.1354	0.7895 ± 0.0219	0.95	3742 ± 48	3751 ± 79	100
C2	98	70	102	0.68	34.7061 ± 1.0424	0.7151 ± 0.0201	0.94	3716 ± 49	3478 ± 76	94
C4	95	54	89	0.61	39.9337 ± 1.1775	0.7916 ± 0.0220	0.94	3774 ± 48	3759 ± 79	100
C5	157	112	144	0.78	39.6970 ± 1.1684	0.7897 ± 0.0219	0.94	3769 ± 48	3752 ± 79	100
C6	216	211	187	1.13	39.2811 ± 1.1532	0.7927 ± 0.0219	0.94	3747 ± 48	3763 ± 79	100
C9	93	56	88	0.63	39.7966 ± 1.1904	0.7905 ± 0.0221	0.94	3771 ± 49	3755 ± 80	100
C10	124	103	120	0.86	37.0082 ± 1.1004	0.7442 ± 0.0207	0.94	3753 ± 49	3586 ± 77	96

Table B.5 *(Continued)*

Spot #	Pb (ppm)	U (ppm)	Th (ppm)	Th/U	$^{207}Pb/^{235}U$ ± 2σ	$^{206}Pb/^{238}U$ ± 2σ	ρ	Ages ± 2σ $^{207}Pb/^{206}Pb$	Ages ± 2σ $^{206}Pb/^{238}U$	Concordance %
PC-622										
C12	192	146	174	0.84	39.2605 ± 1.1647	0.7900 ± 0.0219	0.94	3752 ± 49	3753 ± 79	100
C13	469	366	454	0.81	36.7857 ± 1.0875	0.7589 ± 0.0210	0.94	3714 ± 48	3640 ± 77	98
C14	157	113	145	0.78	39.9196 ± 1.1842	0.7945 ± 0.0220	0.93	3768 ± 48	3769 ± 79	100
D2	168	124	156	0.80	38.4631 ± 1.1459	0.7826 ± 0.0217	0.93	3735 ± 49	3727 ± 78	100
D4	111	57	113	0.51	36.2068 ± 1.0883	0.7562 ± 0.0210	0.93	3695 ± 49	3630 ± 77	98
D6	120	71	119	0.60	36.7138 ± 1.0547	0.7429 ± 0.0206	0.97	3743 ± 47	3581 ± 76	96
D7	124	67	123	0.54	37.2000 ± 1.0622	0.7494 ± 0.0207	0.97	3750 ± 47	3605 ± 76	96
D8	114	61	113	0.54	37.5654 ± 1.0691	0.7596 ± 0.0210	0.97	3744 ± 47	3643 ± 77	97
D9	74	38	71	0.54	39.2299 ± 1.1268	0.7866 ± 0.0218	0.97	3757 ± 47	3741 ± 79	100
D10	112	59	109	0.54	37.2329 ± 1.0692	0.7667 ± 0.0213	0.97	3716 ± 47	3669 ± 78	99
D11	197	120	182	0.66	39.3750 ± 1.1189	0.7918 ± 0.0218	0.97	3752 ± 47	3760 ± 79	100
D12	129	86	118	0.72	38.8382 ± 1.1058	0.7823 ± 0.0216	0.97	3750 ± 47	3725 ± 78	99
D14	96	60	88	0.68	39.3788 ± 1.1280	0.7857 ± 0.0218	0.97	3764 ± 47	3738 ± 79	99
D15	109	58	102	0.57	39.5398 ± 1.1243	0.7922 ± 0.0218	0.97	3758 ± 47	3761 ± 79	100
E2	181	112	178	0.63	36.9239 ± 1.0548	0.7480 ± 0.0207	0.97	3741 ± 47	3600 ± 76	96
E3	235	185	228	0.81	35.6544 ± 1.0166	0.7334 ± 0.0203	0.97	3718 ± 47	3546 ± 75	95
E5	132	89	119	0.75	39.2158 ± 1.1153	0.7920 ± 0.0218	0.97	3746 ± 47	3761 ± 79	100
E6	184	131	167	0.78	38.6759 ± 1.1020	0.7854 ± 0.0217	0.97	3737 ± 47	3737 ± 78	100
E7	292	184	298	0.62	33.7462 ± 0.9592	0.7343 ± 0.0202	0.97	3632 ± 47	3549 ± 75	98
E8-C	148	82	158	0.52	32.3543 ± 0.9218	0.7124 ± 0.0197	0.97	3614 ± 47	3467 ± 74	96
E8-R	101	32	101	0.31	39.4365 ± 1.1225	0.7943 ± 0.0219	0.97	3750 ± 47	3769 ± 79	100
E9	222	181	219	0.82	35.3610 ± 1.0072	0.7213 ± 0.0199	0.97	3731 ± 47	3501 ± 74	94
E10	169	98	161	0.61	39.2404 ± 1.1169	0.7889 ± 0.0218	0.97	3753 ± 47	3749 ± 78	100
E11	133	34	156	0.22	30.4830 ± 0.8686	0.7243 ± 0.0200	0.97	3497 ± 48	3512 ± 75	100
E12	84	55	86	0.64	34.3460 ± 0.9815	0.7399 ± 0.0204	0.96	3647 ± 47	3570 ± 76	98
E13	154	83	148	0.56	39.2752 ± 1.1179	0.7902 ± 0.0218	0.97	3752 ± 47	3754 ± 78	100
E14	62	37	59	0.62	39.7160 ± 1.1497	0.7913 ± 0.0220	0.96	3766 ± 48	3758 ± 79	100
E15	102	55	102	0.54	38.1409 ± 1.1030	0.7608 ± 0.0211	0.96	3765 ± 48	3647 ± 77	97
F1	101	62	94	0.66	40.0883 ± 1.1531	0.7951 ± 0.0220	0.96	3773 ± 47	3771 ± 79	100
F3	251	194	257	0.75	33.5581 ± 0.9580	0.7201 ± 0.0198	0.96	3653 ± 47	3497 ± 74	96
F5	162	108	161	0.67	34.2177 ± 0.9811	0.7540 ± 0.0208	0.96	3613 ± 48	3622 ± 76	100
F6	173	143	154	0.93	39.3121 ± 1.1314	0.7927 ± 0.0219	0.96	3748 ± 47	3763 ± 79	100
F7	304	246	297	0.83	36.4671 ± 1.0436	0.7397 ± 0.0204	0.96	3739 ± 47	3570 ± 75	95
F8	177	113	165	0.69	39.5741 ± 1.1309	0.7929 ± 0.0218	0.96	3758 ± 47	3764 ± 78	100

Table B.5 *(Continued)*

Spot #	Pb (ppm)	U (ppm)	Th (ppm)	Th/U	$^{207}Pb/^{235}U$ ± 2σ	$^{206}Pb/^{238}U$ ± 2σ	ρ	Ages ± 2σ $^{207}Pb/^{206}Pb$	Ages ± 2σ $^{206}Pb/^{238}U$	Concordance %
PC-622										
F9	222	175	202	0.86	38.7335 ± 1.1045	0.7873 ± 0.0216	0.96	3736 ± 47	3744 ± 78	100
F10	201	159	183	0.87	39.2361 ± 1.1224	0.7842 ± 0.0216	0.96	3762 ± 47	3732 ± 78	99
F11	279	244	249	0.98	39.3732 ± 1.1254	0.7891 ± 0.0217	0.96	3757 ± 47	3750 ± 78	100
F12	132	71	124	0.57	40.4503 ± 1.1683	0.7937 ± 0.0219	0.96	3790 ± 47	3766 ± 79	99
F13	286	262	249	1.05	38.8341 ± 1.1116	0.7952 ± 0.0219	0.96	3725 ± 47	3772 ± 79	101
F14	187	154	168	0.92	39.7222 ± 1.1399	0.7898 ± 0.0218	0.96	3770 ± 47	3752 ± 78	100
F15	102	58	96	0.60	39.9945 ± 1.1566	0.7957 ± 0.0220	0.96	3769 ± 48	3774 ± 79	100
G1	267	244	253	0.96	36.3570 ± 1.0457	0.7387 ± 0.0203	0.96	3737 ± 47	3566 ± 75	95
G2	153	97	143	0.68	39.8708 ± 1.1484	0.7974 ± 0.0220	0.96	3761 ± 47	3780 ± 79	101
G5	224	182	209	0.87	37.9422 ± 1.0900	0.7621 ± 0.0209	0.96	3754 ± 47	3652 ± 77	97
G8	127	87	118	0.74	39.2970 ± 1.1370	0.7914 ± 0.0218	0.95	3750 ± 48	3758 ± 78	100
G9	149	131	156	0.84	33.1445 ± 0.9675	0.6687 ± 0.0185	0.95	3747 ± 48	3301 ± 71	88
G11	64	37	65	0.58	35.8762 ± 1.0630	0.7489 ± 0.0209	0.94	3696 ± 49	3604 ± 77	98
G12	246	209	250	0.83	33.9187 ± 0.9869	0.7102 ± 0.0196	0.95	3691 ± 48	3459 ± 74	94
G13	166	110	156	0.71	39.1707 ± 1.1354	0.7912 ± 0.0218	0.95	3746 ± 48	3758 ± 78	100
G14	279	230	262	0.88	37.8585 ± 1.0959	0.7631 ± 0.0210	0.95	3749 ± 48	3655 ± 77	98
G15	218	174	197	0.88	39.8535 ± 1.1600	0.7871 ± 0.0217	0.95	3780 ± 48	3743 ± 78	99
H1	104	67	103	0.65	36.4542 ± 1.0611	0.7539 ± 0.0208	0.95	3710 ± 48	3622 ± 76	98
H2	306	260	288	0.90	36.9212 ± 1.0697	0.7470 ± 0.0205	0.95	3743 ± 48	3596 ± 76	96
H3	90	53	84	0.63	40.0069 ± 1.1709	0.7938 ± 0.0219	0.94	3773 ± 48	3767 ± 79	100
H4	115	73	120	0.61	34.4381 ± 1.0147	0.7279 ± 0.0202	0.94	3677 ± 49	3525 ± 75	96
H5	201	132	202	0.66	34.9044 ± 1.0181	0.7489 ± 0.0206	0.94	3654 ± 48	3603 ± 76	99
H6	165	100	156	0.65	39.2278 ± 1.1431	0.7897 ± 0.0217	0.94	3751 ± 48	3752 ± 78	100
H7	161	98	151	0.65	39.5897 ± 1.1567	0.7939 ± 0.0219	0.94	3757 ± 48	3767 ± 79	100
H8	105	57	105	0.54	36.5841 ± 1.0725	0.7597 ± 0.0209	0.94	3704 ± 48	3643 ± 77	98
H9	138	93	129	0.72	39.1028 ± 1.1461	0.7907 ± 0.0218	0.94	3744 ± 48	3756 ± 78	100
H10	158	118	157	0.75	35.8564 ± 1.0559	0.7380 ± 0.0204	0.94	3717 ± 49	3563 ± 76	96
H12	263	206	251	0.82	37.4034 ± 1.0979	0.7558 ± 0.0208	0.94	3745 ± 48	3629 ± 76	97
H13	202	146	185	0.79	39.7802 ± 1.1713	0.7898 ± 0.0218	0.94	3772 ± 48	3753 ± 78	99
H15	205	163	194	0.84	38.0948 ± 1.1233	0.7606 ± 0.0210	0.93	3763 ± 48	3647 ± 77	97
PC-638										
A2	147	80	140	0.58	39.0334 ± 1.1738	0.7836 ± 0.0227	0.96	3755 ± 47	3730 ± 82	99
A4	83	37	79	0.47	39.2280 ± 1.1960	0.7898 ± 0.0229	0.95	3751 ± 48	3753 ± 83	100

Table B.5 *(Continued)*

Spot #	Pb (ppm)	U (ppm)	Th (ppm)	Th/U	$^{207}Pb/^{235}U$ ± 2σ	$^{206}Pb/^{238}U$ ± 2σ	ρ	Ages ± 2σ $^{207}Pb/^{206}Pb$	Ages ± 2σ $^{206}Pb/^{238}U$	Concordance %
PC-638										
A6	131	100	118	0.85	39.5596 ± 1.2090	0.7897 ± 0.0228	0.94	3764 ± 48	3752 ± 82	100
A8	171	108	158	0.68	39.4556 ± 1.2137	0.7902 ± 0.0228	0.95	3759 ± 49	3754 ± 82	97
A9	176	132	154	0.86	39.6669 ± 1.2239	0.7934 ± 0.0229	0.95	3761 ± 49	3765 ± 82	99
A10	120	59	114	0.51	39.4311 ± 1.2285	0.7881 ± 0.0228	0.95	3762 ± 49	3746 ± 82	95
A11	134	61	130	0.47	39.2455 ± 1.2323	0.7868 ± 0.0228	0.95	3757 ± 50	3742 ± 82	87
A12	98	42	97	0.43	39.3343 ± 1.2367	0.7825 ± 0.0227	0.95	3769 ± 50	3726 ± 82	100
A13	208	121	193	0.62	38.9732 ± 1.2273	0.7873 ± 0.0228	0.95	3746 ± 50	3743 ± 82	87
A14	128	84	118	0.71	39.0890 ± 1.1515	0.7866 ± 0.0227	0.95	3751 ± 46	3741 ± 82	97
A15	152	70	146	0.48	39.3566 ± 1.1615	0.7910 ± 0.0228	0.95	3753 ± 47	3757 ± 82	89
B1	184	151	180	0.84	35.8995 ± 1.0598	0.7254 ± 0.0209	0.95	3745 ± 47	3516 ± 78	86
B2	185	112	172	0.65	39.0629 ± 1.1515	0.7902 ± 0.0228	0.95	3744 ± 47	3754 ± 82	100
B4	87	37	84	0.44	39.3033 ± 1.1668	0.7904 ± 0.0229	0.94	3753 ± 47	3755 ± 82	88
B6	183	126	166	0.76	39.5446 ± 1.1621	0.7890 ± 0.0227	0.95	3764 ± 46	3750 ± 82	100
B7	139	74	132	0.56	38.8485 ± 1.1515	0.7792 ± 0.0225	0.95	3756 ± 47	3714 ± 81	100
B8	263	196	238	0.83	38.9144 ± 1.1433	0.7890 ± 0.0227	0.94	3740 ± 47	3750 ± 82	93
B9	219	111	219	0.51	36.9271 ± 1.0892	0.7643 ± 0.0220	0.94	3709 ± 47	3660 ± 80	90
B10	243	177	218	0.81	39.3754 ± 1.1610	0.7923 ± 0.0228	0.94	3752 ± 47	3761 ± 82	94
B13	172	120	157	0.76	38.7514 ± 1.1508	0.7871 ± 0.0227	0.94	3737 ± 47	3743 ± 82	100
B14	216	80	218	0.37	38.3216 ± 1.1272	0.7823 ± 0.0224	0.94	3730 ± 47	3726 ± 81	87
B15	80	41	77	0.53	39.0079 ± 1.1634	0.7910 ± 0.0229	0.93	3740 ± 47	3757 ± 82	86
C1	122	59	119	0.49	38.9843 ± 1.1563	0.7740 ± 0.0223	0.93	3772 ± 47	3695 ± 81	93
C3	129	71	123	0.58	39.1125 ± 1.1666	0.7840 ± 0.0226	0.91	3757 ± 47	3732 ± 82	99
C4	117	54	112	0.49	39.7721 ± 1.1813	0.7933 ± 0.0228	0.93	3765 ± 47	3765 ± 82	88
C5	166	103	154	0.67	39.1510 ± 1.1547	0.7926 ± 0.0227	0.93	3742 ± 47	3763 ± 82	101
C7	143	97	133	0.72	38.4511 ± 1.1389	0.7765 ± 0.0223	0.93	3746 ± 47	3704 ± 81	100
C9	160	114	151	0.76	38.0216 ± 1.1257	0.7763 ± 0.0223	0.93	3729 ± 47	3704 ± 81	100
C10	120	90	112	0.80	38.6411 ± 1.1394	0.7849 ± 0.0224	0.93	3737 ± 47	3735 ± 81	87
C11	170	129	157	0.82	38.7765 ± 1.1410	0.7753 ± 0.0221	0.92	3761 ± 47	3700 ± 80	89
C12	194	132	181	0.73	38.9173 ± 1.1533	0.7837 ± 0.0224	0.93	3750 ± 47	3731 ± 81	100
C13	70	37	71	0.52	35.1812 ± 1.0441	0.7530 ± 0.0216	0.92	3657 ± 48	3619 ± 79	87
C15	106	68	100	0.68	39.5673 ± 1.1744	0.7892 ± 0.0226	0.92	3765 ± 47	3750 ± 81	99
D1	120	71	114	0.62	39.5627 ± 1.1738	0.7969 ± 0.0228	0.92	3750 ± 47	3778 ± 82	86
D4-C	107	68	100	0.68	38.8571 ± 1.1552	0.7859 ± 0.0225	0.92	3744 ± 47	3738 ± 81	89
D4-R	158	104	150	0.69	38.3334 ± 1.1384	0.7770 ± 0.0222	0.91	3740 ± 47	3706 ± 81	98

Table B.5 *(Continued)*

Spot #	Pb (ppm)	U (ppm)	Th (ppm)	Th/U	$^{207}Pb/^{235}U$ ± 2σ	$^{206}Pb/^{238}U$ ± 2σ	ρ	Ages ± 2σ $^{207}Pb/^{206}Pb$	Ages ± 2σ $^{206}Pb/^{238}U$	Concordance %
PC-638										
D5	229	157	217	0.72	38.6675 ± 1.1405	0.7744 ± 0.0221	0.91	3759 ± 47	3697 ± 80	96
D6	114	65	108	0.60	39.6464 ± 1.1821	0.7924 ± 0.0227	0.96	3762 ± 48	3762 ± 82	100
D7	141	81	136	0.60	39.5143 ± 1.1786	0.7795 ± 0.0223	0.96	3782 ± 47	3715 ± 81	98
D8	87	45	86	0.52	38.8395 ± 1.1633	0.7725 ± 0.0221	0.96	3769 ± 48	3690 ± 81	98
D9	69	34	67	0.51	39.2084 ± 1.1812	0.7802 ± 0.0224	0.95	3768 ± 48	3718 ± 81	99
D11	139	91	131	0.69	39.1858 ± 1.1622	0.7899 ± 0.0225	0.96	3749 ± 47	3753 ± 81	100
D12	213	134	196	0.68	39.2197 ± 1.1621	0.7908 ± 0.0225	0.96	3748 ± 47	3756 ± 81	100
D13	77	33	75	0.44	39.1152 ± 1.1756	0.7759 ± 0.0222	0.95	3773 ± 48	3702 ± 81	98
D14	102	60	97	0.62	38.9565 ± 1.1611	0.7851 ± 0.0224	0.96	3749 ± 48	3736 ± 81	100
D15	105	50	102	0.49	39.2114 ± 1.1723	0.7788 ± 0.0222	0.95	3771 ± 48	3713 ± 80	98
E1	156	89	157	0.57	36.6111 ± 1.0916	0.7379 ± 0.0210	0.95	3749 ± 48	3563 ± 78	95
E2	106	56	101	0.55	38.8356 ± 1.1627	0.7860 ± 0.0224	0.95	3743 ± 48	3739 ± 81	100
E3	382	361	337	1.07	37.6922 ± 1.1174	0.7742 ± 0.0219	0.96	3720 ± 48	3696 ± 80	99
E4	373	380	320	1.19	38.6223 ± 1.1469	0.7844 ± 0.0222	0.95	3737 ± 48	3733 ± 80	100
E5-C	275	189	255	0.74	38.8938 ± 1.1561	0.7869 ± 0.0223	0.95	3743 ± 48	3742 ± 80	100
E5-R	171	86	164	0.53	39.0782 ± 1.1736	0.7843 ± 0.0223	0.95	3756 ± 48	3732 ± 81	99
E6	56	29	55	0.52	39.0895 ± 1.1739	0.7832 ± 0.0223	0.95	3758 ± 48	3729 ± 81	99
E9	135	87	127	0.68	39.3498 ± 1.1820	0.7915 ± 0.0225	0.95	3752 ± 48	3759 ± 81	100
E10	210	255	322	0.79	13.5898 ± 0.4093	0.5213 ± 0.0148	0.94	2734 ± 52	2705 ± 63	99
E11	149	71	148	0.48	38.5666 ± 1.1582	0.7791 ± 0.0221	0.94	3746 ± 48	3714 ± 80	99
E12	162	127	147	0.86	39.3767 ± 1.1808	0.7890 ± 0.0223	0.94	3758 ± 48	3750 ± 80	100
E13-C	90	46	86	0.53	39.4192 ± 1.1903	0.7902 ± 0.0224	0.94	3757 ± 48	3754 ± 81	100
E13-R	110	36	109	0.33	39.5016 ± 1.1996	0.7917 ± 0.0226	0.94	3758 ± 49	3759 ± 81	100
E14	130	73	121	0.60	39.4204 ± 1.1477	0.7886 ± 0.0224	0.97	3760 ± 47	3748 ± 81	100
E15	171	118	168	0.70	36.0907 ± 1.0427	0.7331 ± 0.0207	0.98	3737 ± 47	3545 ± 77	95
F1	170	126	158	0.80	38.5632 ± 1.1156	0.7844 ± 0.0221	0.98	3735 ± 47	3733 ± 80	100
F2	239	170	220	0.77	38.1788 ± 1.1048	0.7814 ± 0.0221	0.98	3726 ± 47	3722 ± 80	100
F6-C	54	25	52	0.48	39.0166 ± 1.1527	0.7891 ± 0.0225	0.97	3744 ± 47	3750 ± 81	100
F6-R	100	73	105	0.69	34.2207 ± 0.9924	0.6888 ± 0.0194	0.97	3751 ± 47	3378 ± 74	90
F8	144	105	132	0.80	39.0928 ± 1.1389	0.7806 ± 0.0221	0.97	3763 ± 47	3719 ± 80	99
F10	117	97	120	0.81	36.2531 ± 1.0519	0.7274 ± 0.0205	0.97	3756 ± 47	3524 ± 77	94
F11	131	80	122	0.65	38.6612 ± 1.1255	0.7875 ± 0.0222	0.97	3733 ± 47	3744 ± 80	100
F12	270	220	246	0.90	38.8424 ± 1.1251	0.7849 ± 0.0221	0.97	3745 ± 47	3735 ± 80	100
F13	98	71	90	0.80	39.3662 ± 1.1459	0.7884 ± 0.0222	0.97	3759 ± 47	3747 ± 80	100

Table B.5 *(Continued)*

Spot #	Pb (ppm)	U (ppm)	Th (ppm)	Th/U	$^{207}Pb/^{235}U$ ± 2σ	$^{206}Pb/^{238}U$ ± 2σ	ρ	Ages ± 2σ $^{207}Pb/^{206}Pb$	Ages ± 2σ $^{206}Pb/^{238}U$	Concordance %
PC-638										
F14	82	38	79	0.48	39.2898 ± 1.1647	0.7872 ± 0.0224	0.96	3758 ± 48	3743 ± 81	100
F15	176	115	166	0.69	39.1149 ± 1.1399	0.7854 ± 0.0221	0.97	3755 ± 47	3737 ± 80	100
G1	119	83	112	0.74	37.7110 ± 1.1057	0.7691 ± 0.0218	0.96	3731 ± 47	3677 ± 79	99
G2	88	64	92	0.70	33.2513 ± 0.9835	0.6957 ± 0.0197	0.96	3692 ± 48	3404 ± 75	92
G3	157	107	144	0.74	39.2496 ± 1.1457	0.7894 ± 0.0223	0.97	3752 ± 47	3751 ± 80	100
G4	68	37	64	0.57	39.6139 ± 1.1742	0.7918 ± 0.0225	0.96	3762 ± 48	3760 ± 81	100
G5-C	139	106	124	0.86	39.4798 ± 1.1538	0.7913 ± 0.0223	0.96	3758 ± 47	3758 ± 80	100
G5-R	102	52	99	0.53	39.3832 ± 1.1627	0.7877 ± 0.0223	0.96	3761 ± 48	3745 ± 80	100
G6	138	121	124	0.97	39.4246 ± 1.1545	0.7906 ± 0.0223	0.96	3757 ± 47	3755 ± 80	100
G7	212	162	195	0.83	38.9955 ± 1.1408	0.7898 ± 0.0222	0.96	3742 ± 47	3752 ± 80	100
G8	132	102	121	0.85	39.3550 ± 1.1641	0.7836 ± 0.0222	0.96	3768 ± 48	3730 ± 80	99
G9	126	112	115	0.97	39.2993 ± 1.1537	0.7871 ± 0.0221	0.96	3758 ± 47	3743 ± 80	100
G10	171	150	152	0.99	39.3998 ± 1.1612	0.7896 ± 0.0222	0.96	3758 ± 48	3752 ± 80	100
G11	201	133	187	0.71	39.1114 ± 1.1509	0.7911 ± 0.0223	0.96	3744 ± 48	3757 ± 80	100
G12	279	198	259	0.77	39.1738 ± 1.1487	0.7899 ± 0.0222	0.96	3748 ± 47	3753 ± 80	100
G15	459	490	405	1.21	37.9894 ± 1.1171	0.7735 ± 0.0217	0.95	3734 ± 48	3693 ± 79	99
H1	254	227	237	0.96	36.7612 ± 1.0865	0.7559 ± 0.0213	0.95	3719 ± 48	3629 ± 78	98
H2	284	275	267	1.03	36.8875 ± 1.0894	0.7494 ± 0.0210	0.95	3737 ± 48	3605 ± 77	96
H3	214	168	212	0.79	35.6026 ± 1.0511	0.7317 ± 0.0205	0.95	3719 ± 48	3540 ± 76	95
H5	89	46	85	0.55	39.9842 ± 1.1898	0.7951 ± 0.0224	0.95	3769 ± 48	3772 ± 80	100
H7	153	79	144	0.55	39.2134 ± 1.1664	0.7886 ± 0.0222	0.95	3752 ± 48	3748 ± 80	100
H9	221	162	197	0.82	39.8081 ± 1.1869	0.7894 ± 0.0222	0.94	3774 ± 48	3751 ± 80	99
H11	124	66	116	0.57	39.6019 ± 1.1866	0.7930 ± 0.0223	0.94	3759 ± 49	3764 ± 80	100
H12	129	83	119	0.70	39.8587 ± 1.2121	0.7867 ± 0.0223	0.93	3781 ± 49	3741 ± 80	99
H13	306	259	271	0.95	39.3960 ± 1.1766	0.7896 ± 0.0221	0.94	3757 ± 48	3752 ± 80	100
UK-002										
A1	531	230	880	0.26	12.1061 ± 0.3528	0.5009 ± 0.0141	0.97	2609 ± 51	2618 ± 61	100
A3-R	585	214	1064	0.20	12.4216 ± 0.3628	0.5064 ± 0.0143	0.97	2633 ± 51	2641 ± 61	100
A4	576	208	1068	0.19	12.0413 ± 0.3520	0.4973 ± 0.0140	0.97	2612 ± 51	2602 ± 60	100
A5	422	150	769	0.19	12.5490 ± 0.3665	0.5046 ± 0.0143	0.97	2656 ± 51	2634 ± 61	99
A6-C	148	83	142	0.58	36.1377 ± 1.0594	0.7687 ± 0.0218	0.97	3667 ± 47	3676 ± 79	100
A6-R	420	137	720	0.19	12.7907 ± 0.3737	0.5082 ± 0.0143	0.97	2676 ± 51	2649 ± 61	99
A7	600	222	1087	0.20	12.4851 ± 0.3641	0.5079 ± 0.0143	0.97	2637 ± 51	2648 ± 61	100

Table B.5 *(Continued)*

Spot #	Pb (ppm)	U (ppm)	Th (ppm)	Th/U	$^{207}Pb/^{235}U$ ± 2σ	$^{206}Pb/^{238}U$ ± 2σ	ρ	Ages ± 2σ $^{207}Pb/^{206}Pb$	Ages ± 2σ $^{206}Pb/^{238}U$	Concordance %
UK-002										
A8	717	311	1502	0.21	9.9187 ± 0.2896	0.4334 ± 0.0122	0.96	2517 ± 52	2321 ± 55	92
A9	749	315	1484	0.21	10.8405 ± 0.3168	0.4713 ± 0.0133	0.97	2526 ± 52	2489 ± 58	99
A11	592	222	1084	0.21	12.4515 ± 0.3634	0.5038 ± 0.0142	0.97	2646 ± 51	2630 ± 61	99
A12	799	369	1810	0.20	8.6160 ± 0.2515	0.3975 ± 0.0112	0.96	2426 ± 52	2157 ± 52	89
A13	553	206	1032	0.20	11.5709 ± 0.3376	0.4842 ± 0.0136	0.96	2590 ± 52	2545 ± 59	98
A15	443	101	840	0.12	11.9436 ± 0.3494	0.4961 ± 0.0140	0.96	2602 ± 52	2597 ± 60	100
B1	335	106	616	0.17	12.7635 ± 0.3737	0.5031 ± 0.0142	0.96	2689 ± 51	2627 ± 61	98
B2	760	322	1491	0.22	10.9949 ± 0.3204	0.4705 ± 0.0132	0.96	2552 ± 52	2486 ± 58	97
B3	738	261	1380	0.19	12.0817 ± 0.3524	0.4946 ± 0.0139	0.96	2626 ± 52	2590 ± 60	99
B4	631	245	1222	0.20	10.6844 ± 0.3118	0.4639 ± 0.0130	0.96	2528 ± 52	2457 ± 57	97
B5	553	203	1044	0.19	11.7448 ± 0.3428	0.4892 ± 0.0137	0.96	2598 ± 52	2567 ± 59	99
B6	838	352	1598	0.22	11.1855 ± 0.3269	0.4845 ± 0.0136	0.96	2532 ± 52	2547 ± 59	101
B7	995	376	1932	0.19	11.2107 ± 0.3269	0.4720 ± 0.0132	0.96	2580 ± 52	2492 ± 58	97
B8	545	200	1029	0.19	11.6880 ± 0.3413	0.4893 ± 0.0137	0.96	2589 ± 52	2567 ± 59	99
B9-R	402	112	742	0.15	12.4868 ± 0.3655	0.5074 ± 0.0143	0.96	2639 ± 52	2645 ± 61	100
B10	633	243	1169	0.21	11.9900 ± 0.3511	0.5000 ± 0.0140	0.96	2595 ± 52	2614 ± 60	101
B12	247	68	453	0.15	12.7845 ± 0.3764	0.5102 ± 0.0143	0.95	2669 ± 52	2658 ± 61	100
B13	766	269	1556	0.17	10.4430 ± 0.3057	0.4600 ± 0.0129	0.96	2504 ± 53	2440 ± 57	97
B15	891	382	1765	0.22	9.6012 ± 0.2812	0.4285 ± 0.0120	0.96	2482 ± 53	2299 ± 54	93
C1-C	144	56	106	0.53	30.3208 ± 0.9040	0.7231 ± 0.0204	0.95	3491 ± 49	3508 ± 76	100
C1-R	858	249	1293	0.19	10.9288 ± 0.3201	0.4736 ± 0.0132	0.95	2531 ± 52	2499 ± 58	99
C2	451	162	762	0.21	12.7265 ± 0.3752	0.5066 ± 0.0142	0.95	2673 ± 52	2642 ± 61	99
C3	748	272	1412	0.19	11.7148 ± 0.3439	0.4922 ± 0.0138	0.95	2583 ± 52	2580 ± 59	100
C4	654	228	1209	0.19	12.1351 ± 0.3571	0.5030 ± 0.0141	0.95	2606 ± 52	2627 ± 60	101
C5	908	430	2008	0.21	9.1690 ± 0.2699	0.4216 ± 0.0118	0.95	2432 ± 53	2268 ± 53	93
C6	434	153	787	0.19	12.6635 ± 0.3743	0.5086 ± 0.0142	0.95	2658 ± 52	2651 ± 61	100
C7	473	327	462	0.71	33.8732 ± 0.9982	0.7525 ± 0.0211	0.95	3601 ± 48	3617 ± 77	100
C8	840	379	1815	0.21	8.8346 ± 0.2605	0.4061 ± 0.0113	0.95	2432 ± 53	2197 ± 52	90
C10-C1	558	174	760	0.23	23.0942 ± 0.6826	0.6251 ± 0.0175	0.95	3294 ± 50	3130 ± 69	95
C10-C2	106	55	106	0.52	35.0806 ± 1.0430	0.7616 ± 0.0214	0.94	3636 ± 49	3650 ± 78	100
C11	671	225	1276	0.18	11.3158 ± 0.3348	0.4764 ± 0.0133	0.94	2580 ± 53	2512 ± 58	97
C12	580	212	1096	0.19	11.1786 ± 0.3306	0.4796 ± 0.0134	0.94	2548 ± 53	2525 ± 58	99
C13	525	197	923	0.21	12.2049 ± 0.3617	0.5008 ± 0.0140	0.94	2622 ± 53	2617 ± 60	100
C14	799	291	1486	0.20	12.0045 ± 0.3554	0.4995 ± 0.0139	0.94	2599 ± 53	2611 ± 60	100

Table B.5 *(Continued)*

Spot #	Pb (ppm)	U (ppm)	Th (ppm)	Th/U	$^{207}Pb/^{235}U$ ± 2σ	$^{206}Pb/^{238}U$ ± 2σ	ρ	Ages ± 2σ $^{207}Pb/^{206}Pb$	Ages ± 2σ $^{206}Pb/^{238}U$	Concordance %
UK-002										
C15	429	166	780	0.21	12.4951 ± 0.3725	0.5054 ± 0.0141	0.94	2646 ± 53	2637 ± 60	100
D1	499	181	915	0.20	12.3617 ± 0.3673	0.5031 ± 0.0140	0.94	2636 ± 53	2627 ± 60	100
D2	569	197	1040	0.19	12.4733 ± 0.3707	0.5063 ± 0.0141	0.94	2640 ± 53	2641 ± 60	100
D3	970	338	1766	0.19	12.5275 ± 0.3725	0.5053 ± 0.0141	0.94	2651 ± 53	2637 ± 60	99
D4	656	272	1478	0.18	9.2826 ± 0.2771	0.4144 ± 0.0116	0.93	2481 ± 54	2235 ± 53	90
D5-C1	139	130	134	0.97	34.5201 ± 1.0342	0.7434 ± 0.0208	0.93	3648 ± 49	3583 ± 77	98
D5-C2	156	92	153	0.60	34.6753 ± 1.0454	0.7485 ± 0.0210	0.93	3645 ± 49	3602 ± 77	99
D6	737	279	1423	0.20	11.1453 ± 0.3323	0.4803 ± 0.0134	0.93	2541 ± 54	2529 ± 58	100
D7	685	257	1244	0.21	12.3424 ± 0.3688	0.5047 ± 0.0140	0.93	2628 ± 53	2634 ± 60	100
D8	588	231	1149	0.20	11.1592 ± 0.3337	0.4713 ± 0.0131	0.93	2575 ± 54	2489 ± 57	97
D9	843	318	1676	0.19	11.0059 ± 0.3290	0.4643 ± 0.0129	0.93	2577 ± 54	2458 ± 57	95
D10-R	642	258	1255	0.21	11.1982 ± 0.3353	0.4727 ± 0.0131	0.93	2575 ± 54	2495 ± 58	97
D11-C	273	147	278	0.53	34.3999 ± 1.0360	0.7403 ± 0.0206	0.93	3649 ± 49	3572 ± 77	98
D11-R	610	230	1133	0.20	12.2141 ± 0.3671	0.4975 ± 0.0138	0.92	2635 ± 54	2603 ± 60	99
D10-C	204	127	177	0.72	33.6181 ± 1.0145	0.7412 ± 0.0207	0.92	3612 ± 50	3575 ± 77	99
D12	593	450	2065	0.22	4.5189 ± 0.1306	0.2724 ± 0.0076	0.96	1961 ± 55	1553 ± 38	79
E3	412	342	370	0.92	34.1009 ± 0.9844	0.7522 ± 0.0209	0.96	3611 ± 47	3616 ± 77	100
E5	746	371	1697	0.22	8.4863 ± 0.2450	0.4046 ± 0.0113	0.96	2370 ± 53	2190 ± 52	92
E6	94	62	96	0.65	34.0451 ± 1.0020	0.7243 ± 0.0204	0.96	3667 ± 48	3512 ± 76	96
E8	264	176	277	0.64	27.4040 ± 0.7970	0.6675 ± 0.0186	0.96	3458 ± 48	3296 ± 72	95
E10-C	664	658	589	1.12	33.5728 ± 0.9687	0.7379 ± 0.0205	0.96	3617 ± 47	3563 ± 76	98
E10-R	570	214	1077	0.20	11.7960 ± 0.3407	0.4914 ± 0.0137	0.96	2597 ± 52	2577 ± 59	99
E12-C	91	47	94	0.50	33.7705 ± 0.9852	0.7413 ± 0.0207	0.96	3619 ± 48	3575 ± 77	99
E12-R	984	391	1832	0.21	11.8506 ± 0.3430	0.4980 ± 0.0138	0.96	2583 ± 52	2605 ± 60	101
E13	617	218	1161	0.19	11.1630 ± 0.3227	0.4817 ± 0.0134	0.96	2539 ± 52	2535 ± 58	100
F3	751	599	2182	0.27	5.9319 ± 0.1726	0.3189 ± 0.0089	0.95	2163 ± 54	1784 ± 43	82
F5-C1	273	124	209	0.60	35.6610 ± 1.0399	0.7577 ± 0.0212	0.96	3669 ± 48	3636 ± 78	99
F5-C2	180	73	133	0.55	35.4616 ± 1.0370	0.7615 ± 0.0213	0.96	3652 ± 48	3650 ± 78	100
F5-R	552	207	1029	0.20	11.9892 ± 0.3476	0.4976 ± 0.0138	0.96	2604 ± 52	2603 ± 59	100
F13	330	186	447	0.42	18.8174 ± 0.5494	0.5415 ± 0.0151	0.95	3198 ± 50	2790 ± 63	87
F14	287	113	181	0.63	25.1697 ± 0.7361	0.6682 ± 0.0186	0.95	3324 ± 49	3299 ± 72	99
F15	679	269	1319	0.20	11.1177 ± 0.3239	0.4795 ± 0.0133	0.95	2539 ± 52	2525 ± 58	99
G1	766	355	1795	0.20	8.1395 ± 0.2369	0.3884 ± 0.0108	0.95	2368 ± 53	2115 ± 50	89
G2	1278	468	1688	0.28	7.9282 ± 0.2309	0.3849 ± 0.0107	0.95	2339 ± 54	2099 ± 50	90

Table B.5 *(Continued)*

Spot #	Pb (ppm)	U (ppm)	Th (ppm)	Th/U	$^{207}Pb/^{235}U$ ± 2σ	$^{206}Pb/^{238}U$ ± 2σ	ρ	Ages ± 2σ $^{207}Pb/^{206}Pb$	Ages ± 2σ $^{206}Pb/^{238}U$	Concordance %
UK-002										
G4-C	211	146	151	0.96	33.3021 ± 0.9899	0.7257 ± 0.0204	0.94	3630 ± 49	3517 ± 76	97
G4-R	765	273	1444	0.19	11.7061 ± 0.3417	0.4923 ± 0.0137	0.95	2582 ± 52	2581 ± 59	100
G5	558	448	1846	0.24	5.1842 ± 0.1527	0.2818 ± 0.0078	0.94	2144 ± 55	1600 ± 39	75
G7	99	47	100	0.46	35.5897 ± 1.0679	0.7574 ± 0.0213	0.94	3666 ± 49	3635 ± 78	99
G8	722	279	1516	0.18	10.0556 ± 0.2961	0.4472 ± 0.0124	0.94	2488 ± 53	2383 ± 55	96
G9	800	382	1781	0.21	6.3811 ± 0.1882	0.3300 ± 0.0092	0.94	2230 ± 55	1838 ± 44	82
G10	1033	490	2019	0.24	11.0727 ± 0.3269	0.4704 ± 0.0131	0.94	2565 ± 53	2485 ± 57	97
G11	706	388	1772	0.22	6.0713 ± 0.1794	0.3227 ± 0.0089	0.94	2182 ± 55	1803 ± 44	83
G13	306	218	274	0.80	34.2405 ± 1.0166	0.7524 ± 0.0209	0.94	3617 ± 49	3617 ± 77	100
G14	299	263	277	0.95	33.9486 ± 1.0123	0.7414 ± 0.0207	0.94	3627 ± 49	3576 ± 76	99
G14	229	123	226	0.55	35.2330 ± 1.0539	0.7586 ± 0.0212	0.93	3648 ± 49	3639 ± 78	100
G15	630	293	1521	0.19	7.9413 ± 0.2358	0.3829 ± 0.0106	0.93	2351 ± 54	2090 ± 50	89
H3-C	591	234	563	0.42	24.6011 ± 0.7388	0.6489 ± 0.0181	0.93	3334 ± 50	3224 ± 71	97
H3-R	535	189	979	0.19	12.2879 ± 0.3681	0.5022 ± 0.0140	0.93	2629 ± 53	2623 ± 60	100
H6	701	273	1614	0.17	6.0819 ± 0.1826	0.3151 ± 0.0088	0.93	2227 ± 56	1766 ± 43	79
H6	444	166	813	0.20	12.4205 ± 0.3745	0.5038 ± 0.0140	0.92	2642 ± 54	2630 ± 60	100
H7	675	255	1536	0.17	7.2015 ± 0.2170	0.3584 ± 0.0100	0.92	2296 ± 56	1975 ± 47	86
H8	601	371	1548	0.24	6.9456 ± 0.2095	0.3429 ± 0.0095	0.92	2310 ± 56	1901 ± 46	82
H10	244	109	284	0.38	24.9799 ± 0.7707	0.6616 ± 0.0186	0.91	3328 ± 52	3273 ± 72	98
H11	584	201	1109	0.18	11.7114 ± 0.3547	0.4905 ± 0.0136	0.92	2588 ± 54	2573 ± 59	99
H13	557	202	1017	0.20	12.5337 ± 0.3806	0.5067 ± 0.0141	0.91	2647 ± 54	2643 ± 60	100
H15	494	194	945	0.21	11.3959 ± 0.3475	0.4801 ± 0.0133	0.91	2579 ± 55	2528 ± 58	98

Table B.6: Trace element data of zircons from five granitoid samples surrounding and locally intruding the Nuvvuagittuq Greenstone Belt. Trace element concentrations are reported in ppm. Zircon $^{207}Pb/^{206}Pb$ ages are from O'Neil et al. (2013). Abbreviations: C = Core; R = Rim; BDL = Below detection limit.

Sample	**PC-134**													
Lithology	**Felsic schist**													
Zircon #	7	11	14	18-C	18-R	28	46	53	57	59	81	97	98	102
Age (Ma)	3369	3358	3353	3371	3371	3354	3352	3474	3361	3370	3317	3340	3346	3354
Si	152853	152853	152853	152853	152853	152853	152853	152853	152853	152853	152853	152853	152853	152853
P	159	221	184	168	195	191	239	455	200	290	277	317	213	80.9
^{47}Ti	1891	1976	1781	1975	1887	2225	2224	1924	1836	2042	2029	1430	2015	2086
^{49}Ti	12.4	22.4	17.0	12.4	25.6	574.8	15.4	15.8	42.5	12.1	12.9	25.4	16.1	742.7
Fe	212	200	148	26.5	25.1	7989	195	326	3879	75.7	28.6	144	35.1	14591
Y	660	1377	675	1196	744	929	1574	1889	1455	988	744	678	1484	644
Zr	471475	487099	440768	488444	448747	429478	560033	467420	425216	488031	490919	358576	488348	329239
La	0.40	4.39	1.95	2.68	4.74	1.24	1.75	3.77	1.00	0.09	0.58	8.11	6.55	2.70
Ce	17.4	35.0	17.3	27.0	24.2	32.7	27.0	32.0	30.9	26.9	16.6	28.8	41.5	24.8
Pr	0.27	2.51	0.45	2.04	1.32	0.83	1.34	2.73	0.97	0.19	0.56	2.95	4.69	1.97
Nd	2.44	17.1	2.85	13.2	6.16	5.36	11.5	16.3	8.25	2.89	4.34	14.1	32.0	12.3
Sm	3.02	11.9	3.38	11.0	4.23	4.90	12.0	10.4	9.03	5.17	3.82	5.51	19.2	6.63
Eu	0.24	1.50	0.37	0.97	0.37	0.39	0.99	2.14	0.50	0.31	0.36	0.68	1.93	0.75
Gd	13.5	37.8	16.4	33.6	17.8	19.2	46.2	38.6	38.5	21.3	16.8	16.8	49.4	16.8
Tb	4.5	11.2	4.86	10.1	5.68	6.47	13.2	13.3	11.9	7.03	5.48	5.04	13.5	5.22
Dy	53.3	124	57.1	110	64.4	77.3	145	165	134	81.0	60.7	57.4	145	59.7
Ho	20.3	44.3	20.8	38.6	24.0	29.3	50.3	62.8	49.9	30.5	23.1	21.2	48.8	21.4
Er	96.4	196	95.3	172	111	141	215	303	238	148	105	95.0	209	95.4
Tm	19.8	38.9	19.4	34.5	21.2	28.3	43.3	62.1	45.8	30.6	21.5	18.5	41.2	18.7
Yb	181	339	180	305	196	255	380	569	417	281	196	167	359	174
Lu	35.1	62.8	34.3	53.3	37.5	50.5	69.4	104	71.0	52.3	37.5	31.5	62.3	32.0
Hf	9736	9274	8470	9531	8854	10537	10923	10689	8907	10292	9606	6802	8947	7072
Th	81.7	85.4	63.6	105	71.0	168	99.3	311	244	172	44.3	82.4	98.5	59.6
^{235}U	298	284	218	486	227	658	321	2464	779	600	177	296	472	334
^{238}U	85.4	87.4	61.3	153	58.7	212	92.7	731	222	180	51.9	84.1	138	101

Table B.6 *(Continued)*

Sample	PC-284													
Lithology	Tonalite													
Zircon #	4	7	12	17	23	24	26	29	47	56	57	58	64	71
Age (Ma)	3655	3652	3670	3651	3480	3647	3650	3644	3659	3672	3557	3665	3662	3665
Si	152856	152855	152855	152855	152855	152855	152855	152855	152855	152855	152855	152855	152854	152854
P	199	228	324	174	319	233	378	262	247	495	256	387	210	148
^{47}Ti	2131	1990	2142	2103	1951	2073	2024	2105	2299	2036	2066	2062	1977	2032
^{49}Ti	9.02	22.5	8.34	8.12	13.3	8.94	8.49	7.72	10.9	7.76	11.9	8.71	16.4	14.0
Fe	42.2	522	62.8	87.4	54.6	33.9	32.7	136	1194	130	52.5	5190	979	874
Y	630	679	778	667	989	723	818	919	700	685	922	800	719	556
Zr	435201	465802	477826	470048	418380	470722	445829	461099	467183	449262	451199	444788	427054	431843
La	1.03	9.39	0.83	0.17	0.21	0.83	0.05	14.2	0.74	2.07	1.50	2.93	1.18	11.9
Ce	27.0	72.0	30.7	19.9	21.1	22.3	15.0	47.7	26.9	36.8	33.9	31.3	26.9	58.1
Pr	0.82	8.09	0.66	0.20	0.34	0.37	0.14	2.46	0.60	1.39	1.17	1.71	1.04	6.47
Nd	5.82	55.6	5.65	2.10	3.73	2.80	2.04	10.9	4.12	8.62	6.99	11.4	7.99	36.4
Sm	4.49	25.7	5.3	3.04	4.88	3.35	3.56	4.78	4.45	5.42	4.91	6.98	6.09	13.6
Eu	1.10	5.20	1.28	0.61	1.20	0.58	1.09	0.90	1.13	1.06	1.14	1.23	1.24	2.47
Gd	14.7	36.4	19.1	13.1	19.3	14.7	19.0	20.2	16.8	16.6	18.4	21.5	18.6	22.6
Tb	4.17	6.40	5.53	4.30	6.61	4.82	6.04	6.61	5.22	4.71	6.04	6.46	5.42	4.71
Dy	49.9	58.2	65.4	52.5	81.1	60.7	73.5	79.4	62.1	57.3	74.8	70.3	63.5	48.6
Ho	20.9	20.4	25.7	21.3	33.2	22.9	28.1	30.7	25.6	22.5	30.4	27.4	24.0	17.7
Er	111	88.4	124	106	167	108	131	145	119	106	156	128	113	81.5
Tm	26.1	19.0	27.6	23.8	35.1	24.2	27.5	31.1	24.1	23.7	34.6	25.8	23.1	16.9
Yb	255	184	266	236	345	242	261	299	219	231	345	250	229	167
Lu	53.6	37.4	53.4	48.9	71.4	45.4	51.9	58.7	44.8	47.8	73.4	51.0	45.6	34.8
Hf	9386	9182	8904	9089	7856	9184	8335	9193	8966	9415	9059	8586	8931	9004
Th	121	204	168	97.4	101	95.0	79.7	131	94.4	242	126	97.0	104	100
^{235}U	480	650	581	423	429	405	257	540	381	640	570	566	401	370
^{238}U	174	230	191	134	152	142	95.8	171	128	235	191	209	135	118

Table B.6 *(Continued)*

Sample	PC-284			PC-285											
Lithology	Tonalite			Tonalite											
Zircon #	87	89	90	4-R	4-C1	4-C2	10	11	18	21	31	27	42	52
Age (Ma)	3673	3671	3668	3413	3413	3413	3443	3399	3360	3444	3509	3341	3484	3398
Si	152854	152854	152854	152854	152854	152854	152854	152854	152854	152854	152854	152854	152854	152854
P	263	249	256	511	221	271	404	267	449	134	306	346	155	397
^{47}Ti	2498	2023	2133	1909	2792	2023	2248	2131	1957	1830	2001	1988	2056	2147
^{49}Ti	593	9.66	17.4	6.31	136	11.5	14.6	14.5	9.99	13.7	75.4	11.1	13.5	8.57
Fe	6456	114	227	2548	4168	327	526	827	1316	1339	3271	572	663	867
Y	692	726	812	815	806	713	1939	730	1713	568	1221	911	946	1239
Zr	416666	432345	483791	401376	553968	408164	450423	409030	409048	386859	398743	425263	415644	436618
La	1.98	1.34	9.94	8.67	65.7	54.1	15.0	41.8	51.1	36.6	8.79	31.8	35.0	9.06
Ce	28.4	35.9	58.6	47.5	173	225	84.9	199	120	98.1	51.9	129	149	51.8
Pr	2.00	1.32	5.23	5.60	20.9	31.9	11.0	28.8	7.09	11.7	4.70	18.2	20.5	5.74
Nd	13.7	9.23	27.3	27.6	68.2	148	63.9	136	23.4	45.5	20.0	101	103	29.2
Sm	8.21	5.87	11.5	6.95	9.43	25.2	31.2	30.0	8.67	5.53	6.54	32.5	26.5	10.6
Eu	1.86	1.25	2.44	4.98	33.5	22.8	8.98	35.3	49.0	5.32	4.82	34.6	102	10.5
Gd	18.3	17.0	24.8	16.8	13.6	35.3	72.3	36.4	34.4	10.4	18.9	47.3	37.8	29.8
Tb	5.00	4.78	6.32	4.94	3.58	6.51	18.0	6.92	11.6	2.93	6.39	7.93	7.68	8.91
Dy	60.5	60.0	72.4	63.1	46.9	66.8	199	68.0	151	38.1	89.4	75.1	79.3	112
Ho	23.6	23.9	25.8	26.6	23.9	24.4	72.1	23.7	59.5	17.2	39.1	28.0	29.5	42.9
Er	112	115	118	129	146	108	316	116	277	92.3	200	129	144	199
Tm	23.8	25.5	25.9	28.0	37.4	21.7	61.6	23.7	55.7	21.8	45.6	27.1	33.0	40.5
Yb	233	259	260	274	436	199	562	242	540	237	470	270	344	384
Lu	50.3	54.5	49.6	58.8	111	41.6	101	50.0	106	52.3	98.0	56.2	74.7	76.9
Hf	8560	9810	8650	8877	14743	8214	8907	10958	8763	8810	10253	9752	10739	9020
Th	81.7	264	113	156	984	369	332	192	432	199	385	186	248	216
^{235}U	465	1156	485	1189	3582	829	1438	1903	2469	2344	3891	1653	2432	1297
^{238}U	164	385	168	402	1284	276	521	637	829	793	1317	572	816	461

Table B.6 *(Continued)*

Sample	PC-285											PC-286		
Lithology	Tonalite											Trondhjemite		
Zircon #	54	55	56	58	61	65	70	74	81	96	102	1	2	10
Age (Ma)	3525	3511	3482	3425	3508	3406	3442	3503	3535	3454	3476	3763	3755	3750
Si	152854	152854	152854	152854	152854	152854	152854	152854	152854	152854	152854	152853	152853	152853
P	279	311	164	1326	114	283	154	484	149	437	277	125	227	129
^{47}Ti	2148	2025	2252	2091	1942	2086	2097	2165	2072	1985	2091	1914	1967	1890
^{49}Ti	15.7	12.7	4.80	9.44	2.42	10.2	11.3	27.0	28.9	28.2	158	5.69	7.17	14.4
Fe	153	1890	304	885	231	377	1417	1075	1360	3381	3905	16.2	23.9	520
Y	1532	1174	637	959	437	964	1090	1402	411	1837	970	593	719	609
Zr	444105	433364	450559	403462	416600	436323	428241	407261	410992	404943	392368	453318	458890	447111
La	39.3	20.8	3.51	1.52	5.37	9.53	3.39	21.2	20.8	11.8	47.5	BDL	0.20	6.80
Ce	167	96.4	23.6	20.0	16.7	52.4	24.6	113	99.7	70.2	167	19.5	18.3	43.0
Pr	19.7	12.2	2.60	0.47	0.80	5.32	1.17	13.8	11.7	6.02	20.4	0.09	0.33	7.62
Nd	98.8	76.1	12.9	2.74	2.48	21.8	5.04	69.3	46.1	23.8	79.9	1.24	3.29	54.2
Sm	26.7	29.98	4.91	2.4	1.17	5.28	3.24	17.42	11.04	10.02	13.22	2.47	3.66	25.05
Eu	35.0	17.8	3.65	0.38	3.01	3.53	1.18	22.8	14.9	9.85	45.0	0.67	0.89	2.52
Gd	55.9	50.5	15.8	12.6	4.97	18.9	16.7	37.6	17.3	41.6	26.3	12.0	16.4	38.6
Tb	13.8	10.5	4.68	4.84	2.03	6.27	6.18	10.7	3.78	13.4	7.03	3.81	5.13	7.48
Dy	156	110	56.0	67.9	28.9	81.7	80.1	127	36.4	157	81.2	46.0	58.5	61.6
Ho	54.6	40.8	21.7	29.4	13.1	32.8	33.9	48.5	13.4	57.8	31.6	18.4	23.5	19.6
Er	232	184	104	163	73.5	155	176	229	63.1	285	162	94.0	112	87.1
Tm	44.3	37.6	21.6	39.0	17.9	31.6	40.4	45.7	14.0	60.0	34.9	20.6	24.6	17.8
Yb	414	360	215	403	198	313	417	419	146	567	357	209	234	175
Lu	77.5	69.9	41.5	89.0	46.0	63.9	87.7	82.9	30.9	113	76.6	45.9	51.0	36.1
Hf	8141	8507	10396	9950	10731	8672	10344	8758	9638	8443	9690	9372	9138	10352
Th	145	267	96.7	295	117	166	319	436	67.6	540	208	115	132	107
^{235}U	614	1481	834	2569	1303	1030	2296	2318	732	2244	1515	477	528	494
^{238}U	218	538	289	892	436	360	810	824	253	812	535	144	151	143

Table B.6 *(Continued)*

Sample	PC-286												
Lithology	Trondhjemite												
Zircon #	20	23	39	40	45	46	60	66	82	90	92	98	119
Age (Ma)	3756	3760	3761	3745	3746	3697	3740	3735	3754	3762	3750	3752	3761
Si	152853	152853	152853	152853	152853	152853	152853	152853	152853	152853	152853	152853	152853
P	144	160	161	4469	195	136	173	208	174	277	130	7888	240
^{47}Ti	1837	1983	1764	2040	1987	1861	1947	1944	1977	1877	1871	2204	1851
^{49}Ti	5.45	5.13	5.4	7.22	7.85	3.45	5.35	6.77	4.81	6.86	5.4	6.48	6.82
Fe	24.9	27.9	26.4	122	23.3	11.9	13.8	24.6	27.9	194	27.0	314	40.1
Y	467	797	417	301	665	350	457	393	503	620	353	312	453
Zr	424327	473104	417267	447409	469312	433173	447029	457229	446740	425092	436313	488883	401272
La	0.04	0.27	0.21	8.34	0.39	0.10	0.21	0.68	3.82	0.47	0.50	23.7	0.10
Ce	10.3	22.4	13.8	42.9	19.2	9.66	13.7	14.9	20.6	19.0	10.9	74.8	17.9
Pr	0.07	0.39	0.29	5.15	0.51	0.09	0.14	0.60	0.97	0.56	0.44	8.52	0.17
Nd	0.95	5.18	2.43	27.2	4.80	1.26	1.67	4.82	5.67	4.83	3.77	43.1	1.83
Sm	1.73	6.45	2.57	8.00	4.31	2.17	2.24	3.52	5.15	3.51	3.12	11.0	2.52
Eu	0.58	2.05	0.61	1.16	1.00	0.66	0.67	0.69	1.39	0.74	0.48	1.62	0.75
Gd	8.74	24.4	9.44	11.5	16.1	9.51	11.1	10.4	17.9	13.7	9.14	14.8	11.2
Tb	2.98	7.02	2.97	2.94	4.89	2.82	3.37	2.95	4.71	4.30	2.71	3.23	3.50
Dy	36.3	74.0	33.9	29.2	55.5	29.3	39.3	33.2	49.1	49.5	28.9	31.0	38.9
Ho	15.1	26.4	13.2	10.3	21.5	11.0	14.7	12.8	17.0	20.3	11.0	10.9	14.6
Er	74.8	122	64.2	47.4	104	54.0	74.3	63.3	79.5	100	53.4	51.7	70.4
Tm	16.0	25.6	14.0	10.5	22.5	11.0	16.4	14.0	17.9	21.1	11.5	11.3	15.1
Yb	154	254	143	106	222	106	163	146	181	209	113	111	145
Lu	38.5	50.9	30.4	20.4	47.1	22.3	33.3	31.6	31.4	46.0	24.5	23.0	33.1
Hf	8263	9722	8564	9060	9248	9640	9417	10354	8849	8529	9198	10942	8515
Th	59.3	173	77.9	70.0	123	48.9	73.6	83.0	95.2	100	46.3	70.4	134
^{235}U	274	571	360	335	505	184	378	355	389	428	218	363	519
^{238}U	80.7	163	102	88.7	140	56.0	97.6	102	112	124	59.9	100	141

Table B.6 *(Continued)*

Sample	PC-287													
Lithology	Trondhjemite band													
Zircon #	2	3	10	14	17	18	20	37	47	49-C	49-R	53	54	78
Age (Ma)	3770	3725	3755	3734	3745	3736	3747	3752	3670	3775	3775	3737	3767	3776
Si	152853	152853	152853	152853	152853	152853	152853	152853	152853	152853	152853	152853	152853	152853
P	156	222	817	149	342	154	247	328	202	782	386	212	471	470
^{47}Ti	2004	1986	2003	2075	2188	1866	2115	1827	1785	2008	1867	2124	2251	1957
^{49}Ti	13.7	9.04	2.11	3.51	12.2	3.16	56.0	13.1	40.2	13.0	5.86	13.5	272	18.2
Fe	41.6	119	73.5	50.5	70.3	50.5	794	139	913	80.3	33.8	189	2672	789
Y	374	491	444	382	1059	274	576	261	307	632	537	579	726	492
Zr	466616	472551	454377	468055	524254	436669	467389	417484	407708	463271	426422	483523	447474	443091
La	0.18	0.55	1.45	0.06	0.14	0.04	9.25	0.47	0.47	0.35	0.50	0.57	2.01	5.03
Ce	12.2	14.5	14.9	11.5	9.96	11.0	65.2	11.9	10.0	17.3	13.0	17.4	24.4	53.5
Pr	0.31	0.65	0.98	0.10	0.25	0.05	11.6	0.36	0.56	0.46	0.21	0.75	2.70	6.09
Nd	2.57	4.69	6.29	1.03	2.78	0.52	73.7	2.64	3.43	4.18	2.48	6.20	18.4	39.7
Sm	2.84	3.3	4.09	1.45	4.77	1.25	32.6	1.57	2.51	3.58	3.41	6.32	11.4	15.5
Eu	0.81	1.09	1.01	0.42	1.61	0.29	4.82	0.45	0.67	0.89	0.79	1.42	2.42	2.52
Gd	10.7	12.6	12.2	8.82	22.4	5.98	49.0	6.45	9.03	14.9	17.6	19.7	26.6	25.0
Tb	3.10	3.98	3.48	2.66	8.00	1.97	8.67	1.93	2.54	4.65	4.89	5.51	6.60	5.13
Dy	33.6	42.7	38.4	32.3	92.5	23.6	65.6	21.7	26.7	54.2	51.5	56.2	65.1	45.5
Ho	12.4	16.2	14.3	12.4	34.3	8.61	17.7	7.88	9.62	20.5	18.0	19.5	22.9	14.8
Er	58.9	76.7	69.4	60.5	163	43.1	71.6	41.8	48.1	97.2	83.4	88.5	115	71.4
Tm	13.3	16.0	14.9	13.5	36.4	9.54	14.1	8.96	10.5	21.7	17.0	18.1	26.1	15.3
Yb	133	154	154	133	357	96.5	134	92.9	105	212	160	178	253	149
Lu	26.9	32.8	32.8	28.3	66.6	22.3	24.9	21.3	22.8	44.0	34.2	35.9	51.0	34.0
Hf	9741	9329	11355	11990	8443	11295	11041	10393	8592	8703	10174	10568	10068	10979
Th	53.8	90.4	66.7	94.1	129	87.0	129	69.8	30.1	95.7	107	95.6	127	77.1
^{235}U	278	549	676	670	906	614	1193	373	246	420	617	405	1310	638
^{238}U	78.0	160	183	195	241	161	301	102	57.8	121	162	112	339	157

Table B.6 *(Continued)*

Sample	PC-287			
Lithology	Trondhjemite band			
Zircon #	84	88-C	88-R	97
Age (Ma)	3749	3747	3747	3737
Si	152853	152853	152853	152853
P	302	288	258	3657
^{47}Ti	1994	2047	1889	2018
^{49}Ti	10.8	19.1	3.80	12.4
Fe	122	134	91.7	252
Y	415	683	446	770
Zr	457547	457347	396693	455981
La	0.84	1.79	2.75	11.2
Ce	19.6	25.1	17.7	40.8
Pr	0.58	2.2	1.12	3.17
Nd	5.79	15.9	5.04	15.1
Sm	3.98	10.6	2.78	7.23
Eu	0.80	2.12	0.41	1.06
Gd	10.5	27.1	9.64	22.6
Tb	3.05	6.83	3.09	6.56
Dy	34.8	67.3	35.4	70.0
Ho	13.3	23.2	14.5	25.0
Er	62.7	105	72.0	115
Tm	14.8	22.0	16.5	24.7
Yb	150	222	160	238
Lu	32.8	43.5	36.4	47.5
Hf	9814	9215	10290	10642
Th	91.7	130	89.3	170
^{235}U	510	592	943	1563
^{238}U	129	153	245	412

Table B.7: Oxygen isotopic data of zircons from five granitoid samples surrounding and locally intruding the Nuvvuagittuq Greenstone Belt. Zircon $^{207}Pb/^{206}Pb$ ages are from O'Neil et al. (2013). Additional zircons that were analyzed for their oxygen isotope compositions but had not been previously analyzed for U-Pb are identified by zircon# starting with "E". Abbreviations: C = Core; R = Rim; F = Fragment.

Sample	Lithology	Zircon #	Age (Ma)	$^{18}O/^{16}O$	$\delta^{18}O_{VSMOW}$ (‰)	2σ (‰)
PC-134	Felsic schist	7	3369	0.00201858	6.67	0.18
PC-134	Felsic schist	11-F1	3358	0.00201849	6.63	0.21
PC-134	Felsic schist	11-F2	3358	0.00201842	6.59	0.21
PC-134	Felsic schist	18	3371	0.00201839	6.58	0.19
PC-134	Felsic schist	28-F1	3354	0.00201838	6.57	0.19
PC-134	Felsic schist	28-F2	3354	0.00201832	6.54	0.21
PC-134	Felsic schist	46	3352	0.00201824	6.50	0.18
PC-134	Felsic schist	53	3474	0.00201902	6.89	0.19
PC-134	Felsic schist	57-F	3361	0.00201813	6.45	0.24
PC-134	Felsic schist	59-F1	3370	0.00201846	6.61	0.23
PC-134	Felsic schist	59-F2	3370	0.00201831	6.54	0.18
PC-134	Felsic schist	81	3317	0.00201888	6.82	0.17
PC-134	Felsic schist	97	3340	0.00201819	6.48	0.24
PC-134	Felsic schist	98-F	3346	0.00201882	6.79	0.20
PC-134	Felsic schist	102-F1	3354	0.00201745	6.11	0.22
PC-134	Felsic schist	102-F2	3354	0.00201820	6.48	0.26
PC-284	Tonalite	4-F	3655	0.00201727	6.02	0.21
PC-284	Tonalite	7-F	3652	0.00201662	5.69	0.18
PC-284	Tonalite	12-F1	3670	0.00201694	5.85	0.21
PC-284	Tonalite	12-F2	3670	0.00201702	5.90	0.20
PC-284	Tonalite	12-F3	3670	0.00201659	5.68	0.23
PC-284	Tonalite	17-F	3651	0.00201670	5.73	0.24
PC-284	Tonalite	23	3480	0.00201705	5.91	0.23
PC-284	Tonalite	24	3647	0.00201645	5.61	0.21
PC-284	Tonalite	26	3650	0.00201676	5.76	0.21
PC-284	Tonalite	29-C	3644	0.00201583	5.30	0.19
PC-284	Tonalite	29-R	3644	0.00201640	5.59	0.20
PC-284	Tonalite	47-F1	3659	0.00201713	5.95	0.19
PC-284	Tonalite	47-F2	3659	0.00201760	6.18	0.18
PC-284	Tonalite	47B	3666	0.00201753	6.15	0.20
PC-284	Tonalite	56	3672	0.00201756	6.16	0.21
PC-284	Tonalite	57	3557	0.00201774	6.25	0.18
PC-284	Tonalite	58-F1	3665	0.00201723	6.00	0.19
PC-284	Tonalite	58-F2	3665	0.00201852	6.65	0.21
PC-284	Tonalite	58-F3	3665	0.00201812	6.44	0.19
PC-284	Tonalite	64-F1	3662	0.00201819	6.48	0.22

Table B.7 *(Continued)*

Sample	Lithology	Zircon #	Age (Ma)	$^{18}O/^{16}O$	$\delta^{18}O_{VSMOW}$ (‰)	2σ (‰)
PC-284	Tonalite	64-F2	3662	0.00201793	6.35	0.19
PC-284	Tonalite	71-F1	3665	0.00201733	6.05	0.21
PC-284	Tonalite	71-F2	3665	0.00201809	6.43	0.18
PC-284	Tonalite	87-C	3673	0.00201799	6.38	0.18
PC-284	Tonalite	87-R	3673	0.00201762	6.20	0.22
PC-284	Tonalite	89-F1	3671	0.00201768	6.22	0.23
PC-284	Tonalite	89-F2	3671	0.00201786	6.32	0.22
PC-284	Tonalite	90-F	3668	0.00201755	6.16	0.20
PC-284	Tonalite	14-C	3648	0.00201764	6.20	0.19
PC-284	Tonalite	14-R	3655	0.00201781	6.29	0.19
PC-284	Tonalite	16	3644	0.00201749	6.13	0.16
PC-284	Tonalite	20	3621	0.00201771	6.24	0.20
PC-284	Tonalite	27-F	3656	0.00201694	5.86	0.19
PC-284	Tonalite	41	3652	0.00201732	6.04	0.20
PC-284	Tonalite	61-C	3659	0.00201745	6.11	0.16
PC-284	Tonalite	61-R	3659	0.00201743	6.10	0.21
PC-284	Tonalite	84-F1	3665	0.00201725	6.01	0.19
PC-284	Tonalite	84-F2	3665	0.00201767	6.22	0.16
PC-284	Tonalite	44-C	3638	0.00201720	5.99	0.23
PC-284	Tonalite	44-R	3638	0.00201713	5.95	0.19
PC-284	Tonalite	80-F	3673	0.00201674	5.75	0.15
PC-284	Tonalite	91-C	N/A	0.00201734	6.05	0.26
PC-284	Tonalite	91-R	N/A	0.00201762	6.20	0.18
PC-284	Tonalite	99	3670	0.00201739	6.08	0.22
PC-284	Tonalite	E1	N/A	0.00201692	5.84	0.21
PC-284	Tonalite	E2	N/A	0.00201777	6.27	0.24
PC-284	Tonalite	E3	N/A	0.00201784	6.30	0.23
PC-284	Tonalite	E4	N/A	0.00201750	6.13	0.20
PC-284	Tonalite	E5	N/A	0.00201747	6.12	0.18
PC-284	Tonalite	E6-C	N/A	0.00201735	6.06	0.18
PC-284	Tonalite	E6-R	N/A	0.00201753	6.15	0.24
PC-284	Tonalite	E7	N/A	0.00201791	6.34	0.24
PC-284	Tonalite	E8	N/A	0.00201738	6.08	0.23
PC-284	Tonalite	E9	N/A	0.00201706	5.92	0.16
PC-284	Tonalite	E10	N/A	0.00201740	6.08	0.22
PC-284	Tonalite	E11	N/A	0.00201689	5.83	0.23
PC-284	Tonalite	E12	N/A	0.00201749	6.13	0.22
PC-284	Tonalite	E13	N/A	0.00201734	6.05	0.16
PC-284	Tonalite	E14	N/A	0.00201781	6.29	0.24

Table B.7 *(Continued)*

Sample	Lithology	Zircon #	Age (Ma)	$^{18}O/^{16}O$	$\delta^{18}O_{VSMOW}$ (‰)	2σ (‰)
PC-284	Tonalite	E15-C	N/A	0.00201770	6.24	0.18
PC-284	Tonalite	E15-R	N/A	0.00201659	5.68	0.21
PC-284	Tonalite	E116	N/A	0.00201729	6.03	0.17
PC-284	Tonalite	E117	N/A	0.00201781	6.29	0.21
PC-285	Tonalite	4	3413	0.00201697	5.87	0.15
PC-285	Tonalite	10	3443	0.00201590	5.34	0.19
PC-285	Tonalite	11	3399	0.00201748	6.12	0.20
PC-285	Tonalite	18	3360	0.00201601	5.39	0.25
PC-285	Tonalite	21	3444	0.00201641	5.59	0.16
PC-285	Tonalite	31	3509	0.00201676	5.76	0.22
PC-285	Tonalite	52	3398	0.00201725	6.01	0.25
PC-285	Tonalite	54	3525	0.00201778	6.28	0.22
PC-285	Tonalite	55-F	3511	0.00201709	5.93	0.19
PC-285	Tonalite	56-F1	3482	0.00201634	5.56	0.24
PC-285	Tonalite	56-F2	3482	0.00201775	6.26	0.19
PC-285	Tonalite	58	3425	0.00201730	6.04	0.18
PC-285	Tonalite	61-F	3508	0.00201759	6.18	0.18
PC-285	Tonalite	65	3406	0.00201661	5.69	0.19
PC-285	Tonalite	70-C	3442	0.00201667	5.72	0.18
PC-285	Tonalite	70-R	3442	0.00201758	6.18	0.21
PC-285	Tonalite	74	3503	0.00201661	5.69	0.21
PC-285	Tonalite	81	3535	0.00201735	6.06	0.20
PC-285	Tonalite	96	3454	0.00201662	5.70	0.18
PC-285	Tonalite	102-F1	3476	0.00201708	5.93	0.19
PC-285	Tonalite	102-F2	3476	0.00201707	5.92	0.22
PC-285	Tonalite	E101	N/A	0.00201632	5.54	0.16
PC-285	Tonalite	E102	N/A	0.00201679	5.78	0.21
PC-285	Tonalite	E103-C	N/A	0.00201239	3.59	0.18
PC-285	Tonalite	E103-R	N/A	0.00201661	5.69	0.22
PC-285	Tonalite	E104	N/A	0.00201892	6.84	0.21
PC-285	Tonalite	E105	N/A	0.00201663	5.70	0.18
PC-285	Tonalite	E107	N/A	0.00201663	5.70	0.26
PC-285	Tonalite	E108	N/A	0.00201668	5.72	0.17
PC-285	Tonalite	E109	N/A	0.00201585	5.31	0.21
PC-285	Tonalite	E110	N/A	0.00201696	5.87	0.22
PC-285	Tonalite	E111	N/A	0.00201611	5.44	0.16
PC-285	Tonalite	E112	N/A	0.00201581	5.29	0.24
PC-285	Tonalite	E114	N/A	0.00201716	5.96	0.15
PC-285	Tonalite	E115	N/A	0.00201524	5.01	0.16

Table B.7 *(Continued)*

Sample	Lithology	Zircon #	Age (Ma)	$^{18}O/^{16}O$	$\delta^{18}O_{VSMOW}$ (‰)	2σ (‰)
PC-285	Tonalite	E116	N/A	0.00201770	6.23	0.17
PC-285	Tonalite	E117	N/A	0.00201625	5.51	0.21
PC-285	Tonalite	E118	N/A	0.00201631	5.54	0.19
PC-285	Tonalite	E119	N/A	0.00201650	5.63	0.17
PC-285	Tonalite	E120	N/A	0.00201721	5.99	0.23
PC-285	Tonalite	E121	N/A	0.00201635	5.56	0.22
PC-286	Trondhjemite	1	3763	0.00201663	5.70	0.20
PC-286	Trondhjemite	2	3755	0.00201711	5.94	0.17
PC-286	Trondhjemite	10-F	3750	0.00201664	5.71	0.17
PC-286	Trondhjemite	20	3756	0.00201684	5.81	0.17
PC-286	Trondhjemite	23-C	3750	0.00201690	5.84	0.21
PC-286	Trondhjemite	23-R	3750	0.00201705	5.91	0.19
PC-286	Trondhjemite	39	3761	0.00201678	5.78	0.23
PC-286	Trondhjemite	40-F	3745	0.00201572	5.25	0.20
PC-286	Trondhjemite	45-F	3746	0.00201687	5.82	0.22
PC-286	Trondhjemite	46-F1	3697	0.00201684	5.80	0.23
PC-286	Trondhjemite	46-F2	3697	0.00201675	5.76	0.19
PC-286	Trondhjemite	60-F	3740	0.00201638	5.57	0.19
PC-286	Trondhjemite	66	3735	0.00201659	5.68	0.21
PC-286	Trondhjemite	82-F	3754	0.00201665	5.71	0.16
PC-286	Trondhjemite	90-F	3762	0.00201705	5.91	0.25
PC-286	Trondhjemite	92-F1	3750	0.00201693	5.85	0.16
PC-286	Trondhjemite	92-F2	3750	0.00201629	5.53	0.23
PC-286	Trondhjemite	98-F	3752	0.00201652	5.65	0.16
PC-286	Trondhjemite	119-C	3761	0.00201701	5.89	0.18
PC-286	Trondhjemite	119-R	3761	0.00201686	5.82	0.20
PC-286	Trondhjemite	E101	N/A	0.00201661	5.69	0.21
PC-286	Trondhjemite	E102	N/A	0.00201658	5.68	0.18
PC-286	Trondhjemite	E103	N/A	0.00201719	5.98	0.27
PC-286	Trondhjemite	E104	N/A	0.00201652	5.64	0.16
PC-286	Trondhjemite	E105	N/A	0.00201706	5.91	0.18
PC-286	Trondhjemite	E106	N/A	0.00201678	5.78	0.22
PC-286	Trondhjemite	E107	N/A	0.00201668	5.73	0.27
PC-286	Trondhjemite	E108	N/A	0.00201690	5.83	0.21
PC-286	Trondhjemite	E109-C	N/A	0.00201685	5.81	0.15
PC-286	Trondhjemite	E109-R	N/A	0.00201692	5.84	0.20
PC-286	Trondhjemite	E110	N/A	0.00201680	5.79	0.22
PC-286	Trondhjemite	E111	N/A	0.00201691	5.84	0.24
PC-286	Trondhjemite	E112	N/A	0.00201655	5.66	0.20

Table B.7 *(Continued)*

Sample	Lithology	Zircon #	Age (Ma)	$^{18}O/^{16}O$	$\delta^{18}O_{VSMOW}$ (‰)	2σ (‰)
PC-286	Trondhjemite	E113	N/A	0.00201731	6.04	0.18
PC-286	Trondhjemite	E114	N/A	0.00201571	5.24	0.24
PC-286	Trondhjemite	E115	N/A	0.00201659	5.68	0.19
PC-286	Trondhjemite	E116	N/A	0.00201705	5.91	0.17
PC-286	Trondhjemite	E117	N/A	0.00201670	5.73	0.16
PC-286	Trondhjemite	E118	N/A	0.00201678	5.78	0.21
PC-286	Trondhjemite	E119-C	N/A	0.00201689	5.83	0.20
PC-286	Trondhjemite	E119-R	N/A	0.00201644	5.61	0.22
PC-286	Trondhjemite	E120	N/A	0.00201704	5.91	0.22
PC-286	Trondhjemite	E121	N/A	0.00201695	5.86	0.20
PC-286	Trondhjemite	E122	N/A	0.00201686	5.82	0.20
PC-286	Trondhjemite	E123	N/A	0.00201660	5.68	0.26
PC-286	Trondhjemite	E124	N/A	0.00201656	5.67	0.18
PC-286	Trondhjemite	E125-C	N/A	0.00201689	5.83	0.17
PC-286	Trondhjemite	E125-R	N/A	0.00201644	5.61	0.19
PC-286	Trondhjemite	E126	N/A	0.00201644	5.61	0.15
PC-287	Trondhjemite band	2	3770	0.00201655	5.66	0.18
PC-287	Trondhjemite band	10-F1	3755	0.00201665	5.71	0.16
PC-287	Trondhjemite band	10-F2	3755	0.00201617	5.47	0.17
PC-287	Trondhjemite band	14-F1	3734	0.00201681	5.79	0.20
PC-287	Trondhjemite band	14-F2	3734	0.00201630	5.53	0.19
PC-287	Trondhjemite band	17	3745	0.00201652	5.65	0.26
PC-287	Trondhjemite band	18	3736	0.00201662	5.70	0.29
PC-287	Trondhjemite band	20-F	3747	0.00201642	5.60	0.17
PC-287	Trondhjemite band	37-F1	3752	0.00201641	5.59	0.22
PC-287	Trondhjemite band	37-F2	3752	0.00201598	5.38	0.18
PC-287	Trondhjemite band	37-F3	3752	0.00201681	5.79	0.18
PC-287	Trondhjemite band	47	3670	0.00201692	5.85	0.22
PC-287	Trondhjemite band	47-F	3670	0.00201707	5.92	0.21
PC-287	Trondhjemite band	49	3775	0.00201661	5.69	0.18
PC-287	Trondhjemite band	53-F	3737	0.00201617	5.47	0.26
PC-287	Trondhjemite band	54-F1	3767	0.00201678	5.77	0.16
PC-287	Trondhjemite band	54-F2	3767	0.00201647	5.62	0.22
PC-287	Trondhjemite band	84	3749	0.00201692	5.84	0.22
PC-287	Trondhjemite band	88-F	3747	0.00201657	5.67	0.29
PC-287	Trondhjemite band	1-F	3726	0.00201711	5.94	0.22
PC-287	Trondhjemite band	97-F1	3737	0.00201642	5.60	0.25
PC-287	Trondhjemite band	97-F2	3737	0.00201629	5.53	0.24
PC-287	Trondhjemite band	19	3728	0.00201671	5.74	0.21

Table B.7 *(Continued)*

Sample	Lithology	Zircon #	Age (Ma)	$^{18}O/^{16}O$	$\delta^{18}O_{VSMOW}$ (‰)	2σ (‰)
PC-287	Trondhjemite band	41-C	N/A	0.00201664	5.70	0.18
PC-287	Trondhjemite band	41-R	N/A	0.00201630	5.53	0.22
PC-287	Trondhjemite band	42	3758	0.00201643	5.60	0.20
PC-287	Trondhjemite band	45	3751	0.00201675	5.76	0.19
PC-287	Trondhjemite band	93	3749	0.00201644	5.61	0.18
PC-287	Trondhjemite band	21	3769	0.00201658	5.67	0.19
PC-287	Trondhjemite band	59-C	3756	0.00201658	5.67	0.20
PC-287	Trondhjemite band	59-R	3756	0.00201656	5.67	0.19
PC-287	Trondhjemite band	83	3698	0.00201648	5.62	0.18
PC-287	Trondhjemite band	98	3722	0.00201520	4.99	0.18